Title

Electrical Characterization and Conductance Enhancement of DNA Origami Nanowires for DNA-Based Electronics

Author

Marrs, Jonathan

Publication Date

2023

Peer reviewed|Thesis/dissertation

Electrical Characterization and Conductance Enhancement of DNA Origami Nanowires for DNA-Based Electronics

By

JONATHAN MARRS
DISSERTATION

Submitted in partial satisfaction of the requirements for the degree of

DOCTOR OF PHILOSOPHY

in

Electrical and Computer Engineering

in the

OFFICE OF GRADUATE STUDIES

of the

UNIVERSITY OF CALIFORNIA

DAVIS

Approved:

_____

Joshua Hihath, Chair

_____

Erkin Șeker

_____

David Doty

Committee in Charge

2023

Dedication

To my wife,

for being my best friend and partner in life.

To my parents,

for their unwavering love and support.

To my dog,

for her loyalty and companionship.

Acknowledgments

My academic journey provided me with the opportunity to spend a lot of enjoyable and memorable time at the University of California, Davis (UC Davis). I completed my Bachelor of Science (B.S.) degree, my Master of Science (M.S.) degree, and now my Doctor of Philosophy (Ph.D.) degree—all at UC Davis. This academic hat trick allowed me to meet many different UC Davis faculty members and colleagues who instructed, advised, and helped me over the years. During my academic adventure as both a student and a researcher, UC Davis has felt like a home to me, and the Department of Electrical and Computer Engineering has felt like a family. I am grateful that I had the privilege of receiving a high-quality college/graduate education and was able to interact with so many smart and talented people at UC Davis.

First and foremost, I would like to thank Professor Joshua Hihath for being an excellent advisor and for honing my skills as a scientist and engineer. I am grateful to Professor Hihath for allowing me to join his research group and for letting me pursue very interesting and fulfilling research on nanotechnology, molecular electronics, and DNA origami nanowires. Throughout my time in graduate school, Professor Hihath was always patient, kind, thorough, professional, helpful, and was an endless source of knowledge for guiding me with my research. I am also very thankful for Professor Hihath obtaining research grants, financially supporting me as a graduate student researcher, and ensuring that our research group had the resources and equipment that we needed to complete our research projects successfully. His resourcefulness, positive attitude, and intellectual prowess made our research group meetings very enjoyable and productive.

I would also like to thank Professor Erkin Seker, whose nanofabrication and nanotechnology courses, advice, and laboratory equipment were extremely helpful to me for completing my research. I also appreciate Professor Seker providing insight into what it is like to

work as a professor in academia and introducing me to the process of writing research proposals and applying for research grants. I greatly benefitted from his teaching and resources.

Professor David Doty provided much-appreciated advice on DNA nanotechnology and gave useful feedback on my dissertation manuscript. DNA origami is a relatively new technology, so I am thankful to have benefitted from Professor Doty's rare expertise on this novel subject.

It was a pleasure to share a graduate student office space in Kemper Hall with the other graduate students and research group members of the Hihath Research Group and the Seker Research Group. They made my academic journey much more fun and successful by providing comradery and support. There are too many people to name individually, but I will cherish the many interactions that I had with all my fellow graduate student peers and cohort. I am thankful for the interesting and useful conversations that we had, and the experience that we shared.

My parents, Ross Marrs and Kris Marrs, were essential in igniting my interest in STEM at an early age and raising me to have curiosity, think critically, and try to understand how the world works. I am thankful for them guiding me towards a fulfilling education and career in science and engineering. I am grateful for their strong support, encouragement, and devotion to my family.

Finally, I would like to thank my wife, Kimberly Marrs. Pursuing a Ph.D. is a massive endeavor, and I couldn't have done it without her love, support, dedication, and sacrifice. She agreed to completely uproot her life by changing her job and moving to Davis with me to enable my dream of obtaining a Ph.D. in Electrical Engineering. I am very lucky to have her in my life.

Abstract

Exploring the structural and electrical properties of DNA origami nanowires is an important endeavor for the advancement of DNA nanotechnology and DNA nanoelectronics. Highly conductive DNA origami nanowires are a desirable target for creating low-cost, self-assembled, nanoelectronic devices and circuits. In this work, the structure-dependent and moisture-dependent electrical conductance of DNA origami nanowires is systematically investigated. Silicon nitride (Si_3N_4) on silicon semiconductor chips with gold electrodes are used for collecting electrical conductance measurements of DNA origami nanowires, which are found to be more electrically conductive on Si_3N_4 substrates treated with a monolayer of hexamethyldisilazane (HMDS) (~10^{13} ohms) than on native Si_3N_4 substrates without HMDS (~10^{14} ohms). Atomic force microscopy (AFM) measurements of the height of DNA origami nanowires on mica and Si_3N_4 substrates reveal that DNA origami nanowires are ~1.6 nm taller on HMDS-treated substrates than on the untreated ones indicating that the DNA origami nanowires undergo increased structural deformation when deposited onto untreated substrates, causing a decrease in electrical conductivity. Another study indicates that the same DNA origami nanowires are more electrically conductive (~10^{12} ohms) in ambient/humid conditions. Finally, we demonstrate that DNA origami nanowires are more electrically conductive in aqueous conditions than under dry conditions in air. These studies highlight the importance of understanding and controlling the interface conditions and environmental factors that affect the electrical conductance of DNA origami nanowires, while also revealing the potential of DNA origami nanowires to be used as sensors and electronic devices.

Table of Contents

List of Acronyms

10HB NW	10-Helix Bundle Pentamer (5-mer) DNA Origami Nanowire
14HB NW	14-Helix Bundle Dimer DNA Origami Nanowire
16HB NW	16-Helix Bundle Dimer DNA Origami Nanowire
6HB NW	6-Helix Bundle Dimer DNA Origami Nanowire
A	Adenine
AFM	Atomic Force Microscopy
C	Cytosine
DNA	Deoxyribonucleic Acid
DNA NWs	Deoxyribonucleic Acid Origami Nanowires
dsDNA	Double-Stranded Deoxyribonucleic Acid
EAC	Electrode Array Chip
EtBr	Ethidium Bromide
G	Guanine
HOMO	Highest Occupied Molecular Orbital
HMDS	Hexamethyldisilazane
LPCVD	Low-Pressure Chemical Vapor Deposition
LUMO	Lowest Unoccupied Molecular Orbital
PBS	Phosphate-Buffered Saline
PDMS	Polydimethylsiloxane
PECVD	Plasma-Enhanced Chemical Vapor Deposition
PI	Propidium Iodide
SEM	Scanning Electron Microscopy

Si	Silicon
Si_3N_4	Silicon Nitride
ssDNA	Single-Stranded Deoxyribonucleic Acid
T	Thymine
TEM	Transmission Electron Microscopy

List of Figures

List of Tables

List of Publications

1. J. Marrs, Q. Lu, V. Pan, Y. Ke, and J. Hihath, "Structure-dependent electrical conductance of DNA origami nanowires," *ChemBioChem*, vol. 24, no. 2, 2022.

2. J. Marrs, T. Ghomian, L. Domulevicz, C. McCold, and J. Hihath, "Gold Nanoparticle Synthesis," *Journal of Visualized Experiments*, no. 173, 2021.

3. Z. Li, L. Mejía, J. Marrs, H. Jeong, J. Hihath, and I. Franco, "Understanding the conductance dispersion of single-molecule junctions," *The Journal of Physical Chemistry C*, vol. 125, no. 6, pp. 3406–3414, 2020.

Chapter 1: Introduction

Deoxyribonucleic acid (DNA) origami is a novel type of DNA nanotechnology that has the potential to dramatically improve the capability, performance, scalability, and customizability of nanoelectronic devices. DNA origami consists of a long single-stranded DNA "scaffold" coupled with short single-stranded DNA "staples" that hybridize with specific nucleic acid sequences in the scaffold strand. By combining DNA origami scaffold strands with specially designed DNA staple strands, a plethora of different self-assembled DNA nanostructures can be created that are securely held together as bundles of folded double-stranded DNA. Due to their nanoscale size, it is highly enticing to use these folded DNA origami bundles as nanowires for creating extremely scalable electronic circuits. However, the intrinsic electrical conductivity of DNA origami nanowires (DNA NWs) has not yet been established, and DNA itself appears to be a poor electrical conductor. Hence, there is now a need to determine the electrical conductivity of DNA NWs, and a desire to enhance the electrical conductivity of DNA NWs. Another key objective is to control the location and orientation of the DNA NWs when depositing them onto a substrate, so that the DNA NWs can be incorporated with other nanodevices to create integrated circuits. Therefore, to unlock the full potential of DNA nanotechnology for the field of nanoelectronics, there is a compelling opportunity to evaluate DNA NWs as electrical conductors, to enhance their electrical conductivity, as well as to control the location and orientation of the DNA NWs on a substrate during deposition. Solving these questions and challenges for DNA NWs could enable high-capability, low-power, high-density, and customizable DNA nanoelectronic devices, thereby ushering in a new technology paradigm of DNA-based electronics.

1.1 Dissertation Objectives

The overall goal of this dissertation is to utilize novel DNA nanotechnologies such as DNA origami to enhance the capabilities of electronic devices. The fundamental objective of this dissertation is to evaluate the electrical conductivity of DNA origami nanowires (DNA NWs), to understand the structure-dependent and moisture-dependent electrical conductivity of DNA NWs, to enhance the electrical conductivity of the DNA NWs, and to control the location and orientation of the DNA NWs during deposition onto a substrate. There are many problems facing the conventional top-down semiconductor fabrication paradigm, as scaling to ever-smaller nodes is getting increasingly difficult, complicated, and expensive. However, many of the issues with traditional top-down semiconductor device scaling could be avoided by utilizing a bottom-up fabrication approach. For example, it is very challenging to use lithography to make devices that are ~5 nm in size, whereas DNA is naturally only a couple nanometers thick. It is also very difficult to enhance the electrical conductivity of very small lithographically defined devices through doping, whereas DNA can be doped or electrically enhanced before deposition. Furthermore, it is challenging to make dense three-dimensional structures that are lithographically defined with conventional nanofabrication, but such dense 3D structures could be achieved with DNA origami. As a tradeoff, it is difficult to control the location and orientation of the DNA during deposition. The rationale for pursuing this project is that by using DNA NWs for electronic devices while using intercalators or another means to enhance the electrical conductivity of the DNA, it should be possible to improve the capability, performance, scalability, and customizability of nanoelectronic devices. To realize these goals, the following objectives are addressed:

1 – Electrical Characterization of DNA Origami Nanowires

The first objective is to characterize the intrinsic electrical conductivity of DNA origami nanowires (DNA NWs) to evaluate their potential use in DNA-based electronics. The intrinsic electrical conductivity of DNA NWs is characterized by microfabricating Electrode Array Chips (EACs) with arrays of gold electrodes that are separated by different gap sizes (1 micron, 750 nm, 625 nm, 500 nm, 250 nm) to be used as test substrates, depositing DNA NWs onto the chips, imaging the DNA NWs on the chips using fluorescence microscopy, and finally by acquiring resistance measurements for the devices that have DNA NWs bridging the gold electrodes. This electrical characterization establishes the resistance vs. distance/length of DNA NWs, and this baseline resistance helps to reveal the potential of DNA NWs to be used in DNA-based electronics.

2 – Structure-Dependent Electrical Conductance of DNA Origami Nanowires

The next objective is to study the structure-dependent electrical conductance of DNA NWs to understand how the interaction of DNA NWs with the substrates they are deposited on can affect their electrical conductivity. This information is important for identifying substrates and surface treatments that facilitate DNA-based electronics.

3 – Conductance Enhancement of DNA Origami Nanowires

The next objective is to enhance the electrical conductivity of DNA NWs to improve their utility in DNA-based electronics. The electrical conductivity of DNA NWs can be increased by using a couple different strategies, such as doping the DNA with intercalators or fluorescent dyes, and keeping the DNA in a wet or buffered environment. Some of the intercalators or fluorescent dyes that are studied with the DNA NWs include ethidium bromide (EtBr), propidium iodide (PI),

acridine orange (AO), DAPI, Hoechst 33258, Hoechst 33342, and a relatively new family of dyes known as the Miami series (green, red, yellow, orange). These intercalators have been selected because they are all soluble in water and should readily intercalate with DNA NWs in an aqueous solution without leaving behind a chemical residue on the chip that could adversely affect the electrical measurements. The intercalators also have different DNA binding modes and different energy levels/gaps that should enhance the electrical conductivity of DNA. Furthermore, these intercalating dyes can also be used as fluorescent tags that provide separate/orthogonal channels for imaging the DNA NWs on each test chip using fluorescence microscopy. Non-fluorescent DNA intercalators may also increase the electrical conductivity of DNA, so some of these non-fluorescent intercalators (e.g., anthraquinone neomycin) are tested as well. After imaging the DNA NWs on the chip and determining where DNA NWs are bridging gold electrodes, the electrical resistivity of the DNA NW devices is measured and compared to evaluate the effectiveness of each strategy for modulating the electrical conductivity of DNA NWs.

4 – Controlled Deposition of DNA Origami Nanowires

Another objective is to selectively deposit DNA NWs in controlled regions on test substrates. The motivation behind this objective is to do a proof of concept and establish a framework for attracting/repelling DNA NWs to eventually control the deposition of DNA NWs for forming nanoelectronic devices and electronic circuits with high yield. This goal is primarily aimed at depositing DNA NWs themselves as circuit elements, but an ancillary strategy could be to use DNA origami as a host/carrier for delivering circuit elements, electronic components, or other device elements such as carbon nanotubes.

The work described here is expected to improve the cost, performance, density, scalability, functionalization, and overall capability of nanoelectronic devices. The broader impact of this research is that it has the potential to make electronic devices such as memories much cheaper and even more powerful with ultra-high-density data storage, thereby potentially enabling a myriad of different applications and technologies that require large amounts of data; including the internet of things, blockchain, cloud computing, machine learning, and artificial intelligence.

1.2 Significance – Scaling Nanoelectronics Beyond the Conventional Limit

The significance of these dissertation objectives is that DNA origami can solve several problems that are impeding the advancement of nanoelectronics. One of these problems is the scalability of nanoelectronic devices. Conventional 2-dimensional (2D) photolithography process techniques are limited by the smallest feature size that they can generate, which is related to the wavelength of the ultraviolet light that is used and other fabrication process parameters. The 7 nm node is currently in production, with the 5 nm node set to begin production within the next few years [1]. While some advancements such as extreme ultraviolet (EUV) technology could make it feasible to reach the 5 nm node or even the 3 nm node, there are fundamental physical limitations and quantum mechanical effects that begin to dominate as feature sizes approach the atomic limit, such as current leakage caused by quantum mechanical tunneling through thin gate oxides, and meanwhile ever-more sophisticated and expensive lithography methods are beginning to make the production of smaller feature sizes economically impractical [2]. EUV technology has been on the horizon for over a decade and has yet to substantially materialize. This overpromised and underdelivered technology has been wrought with immense challenges, many delays and

unexpected additional expenses and complexities that make the technology impractical or prohibitively expensive. Ultimately, such top-down photolithography techniques lack molecular precision, molecular self-assembly, and self-recognition, and leave much more to be desired. Fortunately, DNA origami is a bottom-up fabrication technology that does provide molecular precision, molecular self-assembly, and self-recognition capabilities for creating nanostructures in a very scalable manner; and DNA is only ~2 nm in diameter, which makes it much smaller than the smallest features that any conventional photolithography process is currently able to achieve [3].

Another significant challenge facing nanofabrication and nanoelectronics is the goal of 3-dimensional (3D) integration. Conventional integrated circuits remain primarily 2-dimensional (2D) or planar rather than 3D. However, the density of devices on integrated circuits would vastly increase while the precious space on silicon chips would be much better utilized if devices were stacked in 3D in addition to being arrayed horizontally in 2D, especially if monolithic integration in 3D could be achieved [4]. 3D integration is a feature that could be enabled by DNA origami, as nanoelectronic devices that are made from DNA origami could be synthesized easily, quickly, and inexpensively in 3D using a bottom-up and massively-parallel self-assembly approach; thereby avoiding the complications, many fabrications steps, long fabrication times, and great expenses of fabricating 3D devices layer-by-layer with a conventional top-down lithographic approach [5].

Overall, the challenges facing nanoelectronics stem from the fact that it is increasingly difficult to create and integrate high-quality ultra-nanoscale devices using only a top-down fabrication approach with traditional semiconductor process technology. Traditional lithography is becoming ever-more challenging, complex, and expensive as semiconductor fabrication capabilities advance towards smaller technology nodes. Even as progress is made towards

achieving smaller nodes, there are fundamental physical limits (such as quantum mechanical tunneling) that will eventually prevent further scaling. The same limits that make scaling in 2D very challenging will also make scaling difficult in 3D. Therefore, at some point it will no longer be feasible to use only top-down fabrication technology for creating nanoscale devices, and it will instead make more economic and pragmatic sense to start using bottom-up self-assembly technology for creating nanoscale devices. DNA origami and DNA nanotechnology provide one such potential solution that could couple bottom-up molecular self-assembly with top-down nanofabrication; thereby allowing nanoelectronics to scale beyond the conventional limit.

1.3 Innovation – Bottom-Up DNA Origami with Top-Down Nanofabrication

DNA origami solves many of the challenges of nanoelectronics in new and innovative ways. The primary challenges of nanoelectronics are to create ultra-nanoscale devices that are high-quality with nanoscale precision, with a large device packing density, that can be mass-produced in a cheap and scalable manner, with high yield and high volume/throughput. Now that Moore's law is coming to an end, it is necessary to get creative and invent a new paradigm of biologically inspired nanoelectronic devices, circuits, and architectures that are implemented with recently emerging technologies such as DNA origami [6]. Perhaps the most notable aspect of DNA origami as opposed to many other forms of nanotechnology is that it employs a bottom-up approach rather than a top-down approach for synthesizing and manipulating nanostructures [7]. In this dissertation, bottom-up nanotechnology (the synthesis of DNA origami nanowires) is integrated with top-down nanotechnology (the nanofabrication of a semiconductor/silicon chip known as the Electrode Array Chip (EAC); which is used as the test substrate). This synergy

between bottom-up and top-down nanotechnology exploits numerous advantages of each fabrication paradigm while combining them in a way to create new capabilities that don't exist independently in either fabrication strategy. For example, it is possible to leverage the well-established economies of scale and industrial production capacity that already exists for conventional top-down semiconductor microfabrication/nanofabrication in order to create the vast majority of the microchip, while the capabilities of such chips can be greatly extended and made more cost effective, efficient, and precise in specific/targeted critical applications (e.g., for critical features smaller than 100 nm) by integrating them with ultra-nanoscale nanoelectronic devices that are created using a massively parallel and molecularly precise bottom-up approach. This allows for the creation of relatively cheap and scalable yet powerful and ultra-dense nanoelectronic devices that would otherwise be nearly impossible or too expensive and complicated to create using only conventional top-down nanofabrication or only bottom-up nanofabrication.

Another innovative aspect of DNA origami is that the DNA origami structure itself can be designed and self-assembled into almost any arbitrary/custom shape, at the molecular level, with very high accuracy [8]. This is a very useful property that has important implications for the field of nanoelectronics, in which high-integrity and high-precision nanoscale devices are fabricated; because it enables unprecedented control over the structure and morphology of the DNA nanostructure, which can be designed into precisely engineered shapes and sizes with nearly atomic precision [9]. For example, by changing the width, height, and length of a DNA origami nanowire, the resistivity of the nanowire can be altered, due to the creation of more conductive pathways or longer/shorter conductive pathways, similar to how the resistance of a conventional resistor depends upon its own morphology. DNA also has programmable molecular self-assembly, molecular self-recognition properties, and long-term stability. DNA can also be functionalized

with both organic and inorganic modifiers; such as DNA intercalators, carbon nanotubes, graphene nanoribbons, conductive polymers, gold nanoparticles, fluorescent dyes, and thiols [10]. The extreme versatility of DNA origami makes it an excellent material for designing a myriad of different nanoelectronic devices.

Now that the significance and innovative aspects of DNA origami have been established, it seems clear that DNA origami has many potential benefits that could be leveraged for advancing nanoelectronics. With this motivation in mind, it is now necessary to review some background information and fundamental concepts to create an intellectual framework of topics that are germane to this dissertation. After the background information is covered, the subsequent chapters cover the comprehensive research approach/strategy and experimental results for each of the dissertation objectives. Overall, this dissertation focuses on the topic of DNA origami nanowires (DNA NWs), as they are the most fundamental and important circuit elements for enabling DNA nanoelectronics.

Chapter 2: Background

Life in this modern computer age seems to be inextricably linked to electronics. It is very likely that you have a smartphone in your pocket right now, and that you are reading this dissertation on a laptop or a personal computer; none of which existed just decades ago. Our modern lives in the digital age wouldn't be possible without the steady progression of ever-more capable electronic devices. Moore's law is a remarkable semiconductor industry trend in which the number of transistors on a chip doubles every 18-24 months, thereby substantially increasing the capability and/or lowering the cost of microchips on a regular basis [11]. This technological miracle is the cornerstone of the semiconductor industry and gives rise to the ubiquitous electronic devices that enhance everyday life for billions of people around the world [12]. However, the conventional top-down semiconductor fabrication paradigm that enables Moore's law now faces serious challenges and fundamental limits that need to be resolved in order for the scaling and performance enhancements to continue [13]. Coincidentally, alongside the explosive growth in computing power, there is an equally impressive trend of exponential improvement that is occurring in genomics and deoxyribonucleic acid (DNA) technology, which could ultimately lay the foundation for extending the exponential scaling of nanoelectronics even further.

2.1 Deoxyribonucleic Acid (DNA)

Deoxyribonucleic acid (DNA) is a long double-helix molecule that is comprised of many nucleotides that are connected by a sugar-phosphate backbone, with each nucleotide containing one of four types of nitrogen bases: adenine (A), thymine (T), guanine (G) and cytosine (C) [14]. DNA is best-known for encoding the instructions of life for creating living organisms. Due to its

critical role in biological processes, DNA is a subject of intense study and scientific discovery, and therefore new applications and technologies are continually emerging for DNA.

The DNA revolution was launched in 1953 when Watson and Crick discovered the structure of DNA, igniting a scientific odyssey to harness the full potential of the double helix molecule [15]. A major milestone in this quest to unlock the secrets of the molecule of life was reached decades later in 2003 at the culmination of the Human Genome Project, which took ~13 years at a cost of ~$3-billion to sequence the ~3 billion base pairs of the human genome for the first time [16], [17]. Using state-of-the-art technology, it now takes only ~24 hours to sequence an entire human genome at a cost of less than ~$1,000 [18]. Even after these great strides in technological progress, the rate of genome sequencing continues to increase, while the cost of genome sequencing continues to decrease. Such dramatic improvements in sequencing cost and speed are nucleating a renaissance in DNA technology by creating an increasingly sophisticated tapestry of DNA-based discoveries, techniques, and applications.

The advancement of DNA technology is now bolstered by the contemporary ascension of synthetic biology. It is now not only possible to sequence whole genomes, but also to design and synthesize entirely new synthetic DNA strands with precise sequences specified down to each individual nucleotide. In fact, synthetic biology has been used to create new synthetic lifeforms [19]. This newfound ability to design and synthesize novel DNA sequences, along with the ability to functionalize DNA with a wide variety of both organic and inorganic modifiers and linkers, forms a very intriguing platform for designing and building a vast array of DNA-based nanoscale systems. The potential applications of such DNA-based nanoscale systems are quickly expanding beyond the realm of molecular biology, making it clear that we have just scratched the surface of what is possible in this nascent field of DNA nanotechnology.

2.2 DNA Nanotechnology

In 1960, Richard Feynman famously envisioned a future in which it would be possible to precisely manipulate matter at the nanoscale, which kindled the field of nanotechnology [20]. Remarkably, that future is arriving, as it is now possible to use DNA to precisely manipulate matter at the nanoscale. The field of DNA nanotechnology emerged in 1982 when a researcher named Nadrian Seeman invented nucleic acid junctions and lattices that consist of strands of DNA hybridized into a cross shape with four ends, instead of the natural DNA structure of individual linear DNA strands that have only two ends [21]. This technique of making synthetic DNA structures was later extended to create DNA crystals formed by repeating two-dimensional DNA tiles [22]. DNA nanotechnology now encompasses a wide set of technologies that use DNA to manipulate or create new objects and fulfill useful functions at the nanoscale [23]. One of the features that makes DNA nanotechnology promising is molecular self-assembly, which enables bottom-up nanofabrication [24]. There are many potential applications of DNA nanotechnology; not only in molecular biology, but also in the material world [25]. One of the foundational DNA nanotechnologies that underpins many of these potential applications is DNA origami.

2.3 DNA Origami

DNA origami is one of the flagship technologies of DNA nanotechnology. DNA origami was invented by Paul Rothemund at Caltech in 2006 [26]. The foundational principle of DNA origami is the molecular folding of a long single scaffold strand of DNA (often the M13mp18 scaffold strand, with 7,249 bases) by using short custom-designed DNA staple strands that

hybridize with the long DNA scaffold strand in specific locations to fold and hold the scaffold strand in the designed shape. DNA origami is a structural DNA nanotechnology that can be used to synthesize and create an enormous variety of DNA nanostructures such as DNA wires, DNA nanopores, and even DNA smiley faces [27]. These DNA nanostructures have been designed and synthesized in one, two, or three dimensions [28]; in twisted or curved topologies [29], [30]; and structured into a variety of polyhedrons [31]. Larger structures can be formed using origami tiles or unit cells that can connect together in repeating patterns [32], which has resulted in DNA origami systems up to the gigadalton scale [33]. As the DNA origami technology is improving, the yields are increasing while the costs are decreasing, and it is now estimated that 1 gram of DNA origami can be produced for only $200 [34], [35]. These expanding capabilities in DNA nanotechnology are enabling new applications where low cost, high scalability, and nanoscale precision are needed.

DNA origami provides unprecedented opportunities for designing hybrid nanomaterials from the bottom-up by allowing nanoscale precision assembly, integration, and functionalization with many degrees of design freedom [36]. In fact, DNA origami allows for nanomaterials to be placed precisely in a regularly repeating pattern with a pitch of only ~3.4-3.6 nm along the DNA strand, while the DNA duplex has a diameter of only ~2 nm [37]. Therefore, DNA origami could very well become an indispensable tool in the field of nanoelectronics, wherein the goal is to create very small and very precise nanoscale electronic devices with specifically engineered properties. DNA origami is a state-of-the-art technology that is now ripe for innovation and is poised to disrupt the nanoelectronics industry, particularly if this nascent technology can be utilized to create electrically conductive DNA origami nanowires.

2.4 DNA Origami Nanowires (DNA NWs)

One potential application of DNA nanotechnology and DNA origami is to create DNA nanostructures that could be useful for making nanoelectronic devices. Perhaps the most important and fundamental DNA nanostructures that would enable DNA-based nanoelectronics are DNA origami nanowires (DNA NWs). Due to the inherent design flexibility of DNA origami, these DNA NWs can be designed to have a wide variety of arbitrary lengths, widths, and heights. DNA NWs can be designed to contain pores, channels, and other geometric features and patterns embedded into the design of the wire. DNA origami is also very durable and is able to survive a wide range of environmental conditions and chemical environments [38], [39]. DNA origami structures have been functionalized with a wide range of other molecules, biomarkers, fluorescent dyes, and inorganic materials such as gold nanoparticles [40], [41], [42], [43], [44], [45], [46]. These versatile design parameters that encompass DNA origami provide a unique repertoire for designing DNA NWs that could enable applications such as DNA nanoelectronics.

For such DNA NWs to be useful as circuit elements for the field of nanoelectronics, the DNA NWs must be electrically characterized to determine their electrical conductivity and establish their baseline resistance. DNA NWs are relatively new nanostructures, and initial research studies have reported a wide range of electrical resistance values for DNA origami, which leaves a research gap that needs to be filled for the field of DNA nanoelectronics to progress further. Although DNA NWs have not been fully electrically characterized, there have been some studies on the electrical conductivity of single-stranded DNA (ssDNA) and double-stranded DNA (dsDNA), which may serve as a foundation for understanding the potential of DNA NWs to be used in DNA nanoelectronics.

2.5 DNA Nanoelectronics

The field of DNA nanoelectronics has primarily focused on measuring the electrical conductivity of short double-stranded DNA (dsDNA) duplexes [47], [48]. The study of DNA as an electrically conductive material was initiated by Eley and Spivey in 1962, when they concluded that DNA was electrically conductive due to the overlapping of the π-electron orbitals of the aromatic bases along the axis of the DNA helix [49]. The π-electron orbitals of the DNA bases include the highest occupied molecular orbital (HOMO) and the lowest unoccupied molecular orbital (LUMO), which are perpendicular to the molecular plane [47]. The overlapping of these orbitals between each adjacent base in the stack allows the DNA to be a one-dimensional conductor, or a molecular wire. However, DNA can be an insulator, semiconductor, or conductor; depending on various factors such as the nucleotide/base sequence of the DNA, the structure of the DNA, the experimental environment, and the measurement methods [47]. The two primary mechanisms of charge transfer/transport in DNA are unistep coherent tunneling (also known as superexchange) and multistep incoherent hopping [50]. Charge migration in DNA can also be due to a combination of coherent tunneling and incoherent hopping, or due to band-like motion [51].

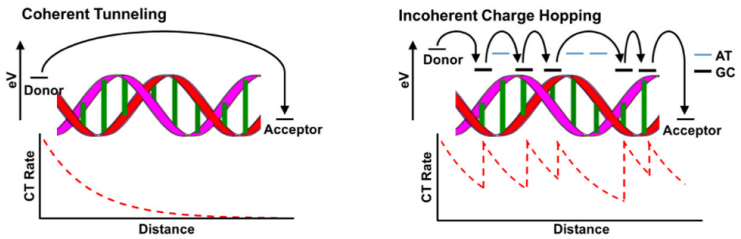

Figure 2.1. Coherent Tunneling vs. Incoherent Charge Hopping [52]

These charge migration mechanisms have different dependencies on parameters such as distance, nucleotide (or base pair) sequence, molecular structure/morphology, and applied voltage.

Single-stranded DNA (ssDNA) does not appear to mediate charge transport over long molecular distances, whereas double-stranded DNA (dsDNA) can mediate charge transport over long molecular distances; depending upon the effective coupling, structure and dynamics of the DNA base pair π-stack [53]. The charge migration mechanism that dominates in DNA at long distances (>100 Å) is incoherent charge hopping, as the efficacy of coherent tunneling or superexchange decreases exponentially with increasing distance [54]. The sequence of the nucleotides or base pairs also affects the charge migration mechanism. A multitude of experiments have confirmed that charge transport in DNA occurs through the base pair π-stack, rather than through the sugar-phosphate backbone of the DNA, and that the tunneling and hopping charge transport mechanisms that account for charge migration in DNA are sensitive to the sequence-dependent conformation and dynamical variations that affect coupling within the DNA base pair π-stacked array [55]. Hole migration occurs predominantly via short-range incoherent hopping between guanine (G) bases in irregular sequences/stacks of dsDNA that contain combinations of guanine-cytosine (G-C) and adenine-thymine (A-T) base pairs, whereas hole migration occurs predominantly via band-like motion in regular sequences/stacks of dsDNA that contain only guanine-cytosine (G-C) base pairs [56]. A-T base pairs act as barriers that inhibit the electrical conductivity of dsDNA because they have high ionization potential, high flexibility, and poor stacking dynamics; whereas G-C base pairs act as electrical conduits that promote the electrical conductivity of dsDNA because they have low ionization potential, low flexibility, and good stacking dynamics (sufficient overlap of the base pair π-stack electronic orbitals) [57]. DNA that is rich in guanine-cytosine (G-C) content tends to have higher electrical conductivity because guanine (G) has the lowest ionization potential of all the natural nucleotides [58]. The anchoring groups that connect the DNA to the electrodes also affect the DNA electrical conductivity [59].

Environmental conditions can also affect the electrical conductivity of DNA. Electrical conduction in DNA could be temperature dependent due to the enhancement of electron localization by strong thermal structural fluctuations in the DNA; with nearest neighbor hopping occurring at high temperatures, and variable range hopping occurring at low temperatures [60]. The electrical conductivity of DNA also depends upon the humidity of the test environment, as the current flow across the DNA at atmospheric pressure with a relative humidity of 40% or higher is mainly attributed to ionic conduction (due to the movement of ions across the adsorbed water molecules on the DNA), rather than electrical conduction through the base pair stack of the DNA itself [61]. In an ambient atmosphere with a relative humidity ~50%, water molecules and counterions in the hydration shell around the DNA contribute significantly to the conductivity; and after the DNA has an extended exposure under a vacuum or dry nitrogen environment with a relative humidity <20%, the conductivity decreases significantly [62]. The presence or absence of water/humidity also affects the structure of the DNA; which transitions from its standard/biological B-form to its unnatural A-form as the amount of water decreases below 13 water molecules per nucleotide, and the hydrophobic base pairs in the core of the DNA begin to twist and separate from each other, creating a less effective overlap/alignment of the base pair π-stack, which decreases the electrical conductivity of the DNA [63]. The interaction between DNA and the underlying substrate that it is deposited on (e.g., silicon nitride, silicon dioxide, mica) is another key parameter that affects the conducting or insulating properties of the DNA molecule, and this DNA-substrate interaction is objectively detectable as the thickness of the DNA decreases to ½ – ¼ the native DNA thickness after it is deposited onto the substrate; however, the DNA-substrate interaction can be mitigated by depositing a polymer film (e.g., by glow discharge of pentylamine vapor to form an NH_3^+ monolayer on the substrate), thereby decreasing the

hydrophilicity of the substrate and preserving the native height and conductive properties of the DNA molecule [64].

Various DNA nanoelectronics experiments have been done to attempt to measure the electrical conductivity of ssDNA and/or dsDNA. One of the first DNA nanoelectronics experiments demonstrated that a few DNA molecules associated into ropes that were at least 600 nm long were as conductive as a good semiconductor, with resistance values on the order of 1 MΩ [65]. Another DNA nanoelectronics experiment demonstrated that dsDNA with a length of ~10 nm behaved as an insulator or a large-bandgap semiconductor, with a current less than 1 pA when a low bias of a few volts or less was applied, but an increase in the current was observed at higher biases [66]. Long-range charge transport has been confirmed in dsDNA over a distance of 34 nm, or 100 base pairs [67]. However, electrical conductivity in individual DNA molecules longer than 40 nm has not yet been observed [68]. These DNA electrical conductance experiments had fixed/immobile environments such as semiconductor and metal test substrates, whereas other experiments had dynamic/mobile environments such as break junctions.

Dynamic molecular electronics experiments often use the single-molecule break junction (SMBJ) approach to measure the electrical conductivity of DNA or RNA [69], [70]. Scanning probe microscopy (SPM) techniques such as atomic force microscopy (AFM) or scanning tunneling microscopy (STM) are often used to perform such SMBJ measurements. STM break junction (STM-BJ) experiments have shown that the electrical conductance of DNA depends upon both the sequence and length of the DNA; with G:C-rich DNA being more conductive than A:T-rich DNA, with shorter DNA strands being more conductive than longer DNA strands, with an exponential length dependence across A:T regions due to the tunneling/superexchange charge transport mechanism, and with a linear length dependence across G:C regions due to the hopping

charge transport mechanism [71]. The STM-BJ technique has been used to experimentally demonstrate that alteration of a single base pair in the sequence of a dsDNA helix can affect the electrical conductance of the DNA by as much as an order of magnitude [72]. Another STM-BJ experimental study shows that changing the structural conformation of the DNA (e.g., transitioning from the naturally-wound B-form structure to the tightly-wound A-form structure) can affect the electrical conductance of the DNA by about one order of magnitude [73]. The fact that DNA can exhibit extensive changes in its electronic properties when it is subjected to various dynamic environments and/or it is structurally/compositionally/chemically modified is encouraging because it demonstrates a diverse repertoire of strategies for achieving high electrical conductivity in DNA. However, because the properties and characteristics of DNA can be modulated by such a large set of design parameters, this also highlights a need for understanding the electronic/structural integrity and durability of DNA under various environmental conditions.

There is ample evidence that electronic conduction can occur in DNA, yet such evidence must be coupled with a practical understanding of the electronic/structural durability and integrity of DNA when it is subjected to a broad range of environmental conditions. Some studies have shown that DNA is more robust and durable than one might expect. For example, it has been reported that the electrical conductivity of DNA can actually improve as the temperature increases from 4 °C – 40 °C as the number/concentration and energy of carriers increase due to thermal excitation, and then the electrical conductivity may begin to decrease as the temperature exceeds ~40 °C as lattice vibration in the bases and phonon scattering begin to dominate by decreasing the carrier mobility, but the DNA still appears to exhibit some electrical conductivity up to the DNA melting point (75 °C – 120 °C) [74], [75]. DNA may become more conductive at moderate temperatures above room temperature, and the structure of DNA appears to remain intact at fairly

high temperatures, making DNA suitable for many potential electronics applications. The electrical conductivity of DNA is also affected by UV light, as the base pairs and phosphate groups are damaged, thereby inhibiting charge hopping and electron tunneling, and increasing the electrical impedance. The damage to the DNA is dependent upon the intensity, duration, and wavelength of the incident UV light. Decreases in the electrical conductivity of DNA are observed with a UV-C radiant exposure as low as 1.2 J/cm^2, with destruction of the DNA and high impedance occurring at a UV-C radiant exposure of ~5 J/cm^2 or a UV-A radiant exposure of ~40 J/cm^2 [74], [75]. DNA is fairly durable when exposed to low or moderate fluences of UV light, making DNA suitable for many potential electronics applications, especially when the DNA is shielded or encapsulated to protect the DNA from UV light. Overall, DNA appears to be fairly robust when subjected to a wide range of environmental conditions.

To reinforce all of the experimental results for DNA as an electronic material, models and computational studies have shown that electrical conduction can occur in double-stranded DNA as long as 30 nm, that natural/intrinsic DNA is a poor electrical conductor, and that the electrical conductivity of DNA can be affected by various factors; such as the shape/morphology and molecular environment, the metal-molecule contact (e.g., gold-thiol bond), and the content and sequence/order of the nucleotides in the DNA molecule (DNA that is rich in G:C nucleotides is more conductive than DNA that is rich in A:T nucleotides) [76]. Another model shows that charge hopping in DNA is due to hole migration and localization on guanine (G) bases, with higher charge transfer efficiencies (and therefore higher electrical conductivity) occurring in guanine-rich DNA [77]. This model is reinforced by another that proposes the thermally induced hopping mechanism for long-range charge transport in DNA, in which the dominant charge migration mechanism switches from superexchange to hopping as the number of A-T bases in the bridge between

guanine (G) bases exceeds 4 bases [78]. These results all indicate that DNA is a versatile material with many parameters that could be engineered to exhibit desirable electronic properties in designed structures such as DNA origami. While some electronic studies have been performed on ssDNA and dsDNA, relatively few studies have been performed on DNA origami.

Initial investigations on how native/intrinsic DNA origami could be used to create a conductive pathway and form an electrical wire have returned mixed results. The intrinsic electrical conductivity of DNA NWs, as well as methods to enhance the electrical conductivity of such DNA NWs, are unsettled topics that remain fundamental knowledge gaps in the research fields of DNA nanotechnology and molecular electronics. One of the studies that has been done on the electrical properties of DNA origami found that triangular DNA origami nanostructures (~90 nm per side) had a high impedance of ~20 GΩ [79]. Another study found that ~90 nm long rectangular DNA origami nanostructures had a lower impedance of ~70 MΩ, which was attributed to both electronic conduction and ionic conduction [80]. Clearly, the studies that have been performed report a wide range of electrical conductance values for DNA origami. There appears to be a multitude of different factors that could affect the electrical conductivity of DNA origami, making it an excellent candidate for further studies. While some of the studies have focused on native/intrinsic DNA origami, others have focused on modified/extrinsic DNA origami.

Some preliminary studies have been done to understand how to use DNA origami as a template for depositing, synthesizing, or otherwise creating conductive structures with metals and other inorganic materials attached to the DNA origami template. DNA origami has been used to precisely place gold nanoparticles along the DNA structure, which have been used to nucleate/seed the growth of gold nanowires along the DNA nanowire template [81]. DNA has also been used as a template for the seeding and growth of conductive silver nanowires [82]. In such cases, the DNA

itself is not the active electrical pathway, but the gold/silver/metal nanowire that was seeded by the DNA is the electrical pathway. For example, in one study, a coulomb blockade of gold nanoparticles was formed to make a single electron transistor on a DNA origami template [83]. While such metal nanowires can be highly electrically conductive, they can also be low-yield and are less suitable to being stoichiometrically modulated by chemical doping (e.g., with DNA intercalation). Ideally, DNA intercalators could allow for the precisely controlled design and engineering of long-range (> 100 nm) electrically conductive DNA NWs.

2.6 DNA Intercalators

DNA intercalators are molecules that bind to specific regions of DNA. Some DNA intercalators can be used to enhance the electrical conductivity of DNA, like how chemical dopants/impurities such as phosphorous and boron can be used to enhance the electrical conductivity of semiconductors such as silicon. Moreover, many DNA intercalators are used as fluorescent dyes or nucleic acid stains that allow the DNA to be visualized and imaged with fluorescence microscopy. There are several different types of nucleic acid stains/dyes, which differ in their molecular/chemical makeup, and can differ in how they bind to DNA. There are a few different DNA binding modes; as the dyes can bind/intercalate between the base pairs of the DNA, bind to the minor groove of the DNA, bind to the major groove of the DNA, bind externally to the DNA, or bind/intercalate to multiple regions between base pairs of the DNA. Some examples of intercalating dyes include ethidium bromide (EtBr) and propidium iodide (PI). Some examples of minor-groove binders include DAPI and the Hoechst dyes (e.g., Hoechst 33258, Hoechst 33342). An example of an external binder is acridine orange (AO). Fluorescent dyes such as nucleic acid stains typically have one or more characteristic excitation peaks and emission peaks; which

respectively define the most efficient energies or wavelengths for the absorption of highly energetic (shorter wavelength) photons, and the emission of less energetic (longer wavelength) photons. Fluorescence microscopy makes use of the characteristic excitation/emission peaks and specific binding properties of fluorescent dyes to selectively excite and image certain areas of interest within a sample, such as DNA within the nucleus of a cell.

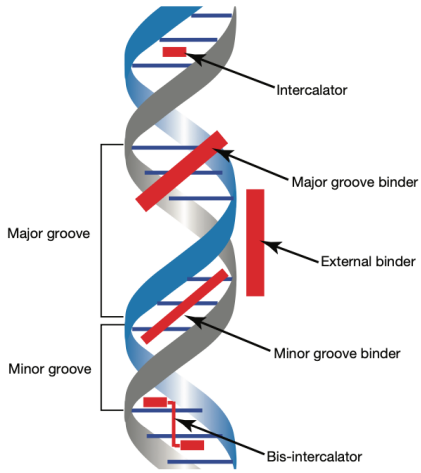

Figure 2.2. Schematic Diagram Showing the Different Binding Modes of Dyes to DNA [84]

The most common DNA binding mode is intercalation into the base pair stack at the core of the DNA, and DNA intercalation typically occurs with cationic molecules with planar aromatic rings [85]. One of the most popular and well-established DNA intercalators is ethidium bromide (EtBr), which intercalates between the aromatic base pairs of the DNA with little to no sequence preference, and after binding to the DNA exhibits a ~20-fold enhanced/brighter orange (605 nm) emission fluorescence when exposed to the appropriate excitation wavelength of light (~300 nm) [86]. Ethidium bromide is very inexpensive and is therefore often used for staining DNA in conventional molecular biology procedures such as agarose gel electrophoresis. Propidium iodide (PI) is another intercalating agent that is very similar to ethidium bromide with a nitrogen-

containing ring structure at its core, and PI binds roughly once per 4-5 base pairs with no sequence preference [87]. SYBR Green I (SG) is another common intercalating dye, with an excitation wavelength of 485 nm and an emission wavelength of 524 nm, and is primarily an intercalator but can exhibit some minor groove binding at high concentrations [88]. GelRed is yet another example of an intercalator [89]. One of the mechanisms by which DNA intercalators can enhance the electrical conductivity of DNA is by assisting with the stacking or overlapping of the π-electron orbitals between the aromatic base pairs of the DNA.

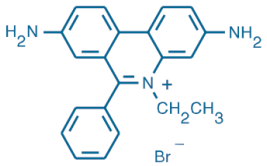

Ethidium Bromide (EtBr) [84]

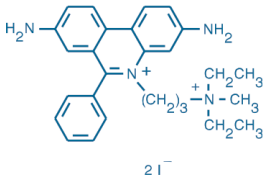

Propidium Iodide (PI) [84]

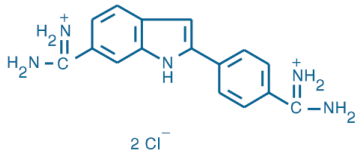

DAPI [84]

Figure 2.3. Common DNA Dyes/Stains

The second most common DNA binding mode is minor groove binding. Minor groove binding molecules are typically curved and/or somewhat flexible, which allows them to follow the minor groove of the dsDNA. DAPI is a blue fluorescent dye with an excitation peak of 358 nm and an emission peak of 461 nm, and binds strongly to A-T rich regions of the minor groove of dsDNA [87]. Hoechst 33258 (H 33258), Hoechst 33342 (H 33342), and Hoechst 34580 (H 34580) are blue fluorescent dyes, similar to DAPI, that preferentially bind to A-T rich regions of the minor groove of dsDNA; after binding to DNA they exhibit a ~30-fold increase in fluorescence at their blue (~460 nm) emission peak when exposed to UV light at their excitation peak (~360 nm) [87].

Other DNA intercalators are not as widely used in molecular biology as fluorescent dyes or nucleic acid stains. For example, there are some DNA intercalators that are not traditionally

used as nucleic acid stains nor fluorescent dyes, but nonetheless still bind to DNA and have the potential to enhance the electrical conductivity of the DNA. DNA intercalators such as these include anthraquinone-neomycin adduct (DPA 561) [90]. There are also some novel DNA intercalators or novel DNA fluorescent dyes that are not yet widely used and are still being studied or characterized, as they were recently created in the laboratory. These include the Miami Series of dyes (Red, Orange, Yellow, Green) [91], [92], [93]. Metallointercalators are another less-common type of DNA intercalator which π-stack with unbroken DNA base pairs after entering via the major groove [94]. Long-range (~10-20 base pair) charge transfer has been confirmed through the DNA base pair stack after being doped with metallointercalators [95]. Clearly there is a wide variety of different intercalators, each with their own properties and unique attributes. Together, these intercalators provide a versatile repertoire for engineering DNA origami with desirable properties such as enhanced electrical conductivity and fluorescence.

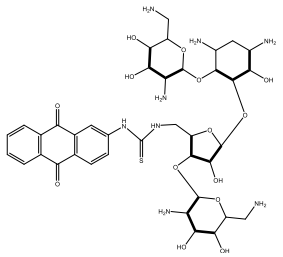

Figure 2.4. Anthraquinone-Neomycin Adduct (DPA 561)

Overall, DNA intercalators provide a very promising mechanism for potentially enhancing the electrical conductivity of DNA. DNA intercalators that also act as fluorescent dyes or nucleic acid stains serve another useful purpose as they facilitate the fluorescence microscopy imaging of DNA. Therefore, DNA intercalators and fluorescent dyes should play an important role in both the electrical enhancement and the imaging of DNA origami, which are important capabilities for the

implementation of DNA NWs in nanoelectronic devices. However, another key capability for utilizing DNA NWs in nanoelectronics is not only to enhance the electrical conductivity of the DNA origami and image it with fluorescence microscopy, but also to selectively deposit the DNA NWs and control the location and orientation of the DNA NWs as they adhere to the underlying substrate.

2.7 DNA Origami Deposition

The deposition of DNA origami onto substrates is an important factor for utilizing DNA NWs in nanoelectronic devices. Toward this goal, a variety of different strategies have been developed for depositing DNA or DNA origami onto substrates such as semiconductor chips/wafers and metal electrodes. Perhaps the most simple and imprecise method is to use a micropipette to apply some DNA origami solution onto an untreated substrate and then allow the solution to incubate on the substrate/chip for an extended period of time. Eventually, some of the DNA origami structures will settle out of the solution and onto the surface of the substrate/chip, in a random location and with a random orientation. Given a high enough concentration of DNA origami, it is likely that some DNA origami will eventually settle in the general area where it is desired on the substrate/chip, possibly with the correct orientation. This method could be called "spray and pray" due to the random and chaotic nature of the deposition process, with little to no control over the final location and orientation of the DNA origami on the substrate.

Other DNA origami deposition/adhesion methods include chemical/molecular strategies, such as forming self-assembled monolayers (SAMs) and other surface treatments on the substrate that either selectively attract or repel the DNA origami nanostructures. One example of this type of chemical strategy is to use a carboxylic acid-terminated self-assembled monolayer (SAM), such as 11-mercaptoundecanoic acid (MUA), to concentrate and chelate positive magnesium (Mg^{2+}) cations at the gold surface to attract the negative phosphate backbone of the DNA origami nanostructure; a technique that has been used to selectively immobilize DNA origami nanostructures onto gold surfaces [96]. Other chemical/molecular surface treatments for the selective deposition of DNA origami include hexamethyldisilazane (HMDS) which is hydrophobic and repels DNA origami, and (3-aminopropyl)triethoxysilane (APTES) which is positively

charged and attracts the negatively charged phosphate backbone of DNA origami. The ion concentration and composition of the buffer solution is also very important, as divalent cations such as magnesium (Mg^{2+}) have been demonstrated to play a primary role in the adhesion of DNA origami nanostructures on substrates such as mica, while monovalent cations such as sodium (Na^{+}) have been demonstrated to play a primary role in the surface diffusion of DNA origami nanostructures along substrates such as mica [97]. It is possible to achieve high-yield DNA origami adhesion to an SiO_2 substrate with a buffer that has a low magnesium (Mg^{2+}) ion concentration; but the magnesium ion concentration (for forming Mg^{2+} bridges between the DNA origami and the substrate) and pH level (for ionizing silanols) of the buffer, the DNA origami nanostructure concentration, and the incubation time after deposition all play important roles in the binding of DNA origami nanostructures to SiO_2 substrates; with maximum DNA-substrate binding observed at ~35 mM Mg^{2+}, 110 pM DNA origami, pH 8.35, and 60 minute incubation; and smoother substrate surfaces may further allow for such relatively low-magnesium concentrations as smooth surfaces facilitate a greater number of Mg^{2+} bridges between DNA origami and ionized silanols [98]. DNA origami is stable in very-low-magnesium (~10 μM) buffers, which is beneficial in DNA nanoelectronics because having less magnesium reduces the amount of ionic conduction along the DNA [99]. It is also possible to achieve DNA origami nanostructure deposition/adhesion without any magnesium ions (Mg^{2+}), through the conversion of surface silanols into positively charged amino groups ($–NH^{3+}$) using a silanization agent such as aminopropyl silatrane, which makes the surface of the SiO_2 substrate positively charged in order to attract the negatively charged phosphate backbone of the DNA, and which is much less prone to aggregation than (3-aminopropyl)triethoxysilane (APTES) [98]. Alternatively, the surface silanols that are created when the SiO_2 or Si_3N_4 substrate undergoes an O_2 plasma etch can be converted to carboxylate

groups by incubating the substrate in a disodium carboxyethylsilanetriol silanization buffer followed by sonication in deionized (DI) water, and the resulting carboxylate group binding sites can be used to enable DNA origami binding with a low Mg^{2+} concentration (15 mM) [100].

In addition to chemical/molecular surface treatments, an ancillary strategy is to use lithographic patterning methods to activate or modulate specific regions of surface-treated substrates to selectively deposit DNA origami. For example, electron-beam lithography or photolithography and dry oxidative etching can be used to create small nanoscale features (with the approximate size and shape of the DNA origami nanostructures) in photoresist to form targeted hydrophilic binding sites on substrates such as SiO_2 that are pre-treated with hydrophobic hexamethyldisilazane (HMDS) to form a trimethylsilyl (TMS) monolayer; allowing DNA origami nanostructures in a ~100 mM $MgCl_2$ buffer to specifically bind with high selectivity, orientation accuracy, and yield to the lithographically patterned hydrophilic regions where the TMS has been removed by an O_2 plasma etch [101]. Subsequently, the substrate can be treated with a series of 50% - 90% ethanol-in-water solutions to wash away the buffer solution from the SiO_2 substrate and then can be allowed to dry under ambient conditions to leave behind the DNA origami adhered onto the clean and dry SiO_2 substrate; because a combination of ethanol and water is more effective than pure water at washing the substrate while not removing the DNA origami [102]. A similar lithographic technique was used to create anchor lines and pads that were patterned with electron beam lithography in photoresist to create a mask for depositing a cationic (3-aminopropyl)triethoxysilane (APTES) monolayer that was chemically attached to the underlying silicon substrate, and after DNA origami solution was applied to the substrate and the DNA origami nanostructures had bound to the APTES regions, the substrate was subsequently washed with buffer/water and imaged in air, proving the existence of a strong binding interaction between

the DNA nanostructure and the patterned anchor pad of at least -43 kJ/mol [103]. It is very important to thoroughly clean the silicon chip to decontaminate it and reduce surface roughness before applying the APTES, and to wash the substrate thoroughly with DI water after incubating the DNA origami on the substrate, as excess salt in the buffer can cause undesirable condensed deposits of salts and buffer residues if they are not washed away [104].

Aside from photolithography and electron-beam lithography techniques, nanoimprint lithography has also been used to pattern nanoscale features/indentations into a layer of polymethylmethacrylate (PMMA) resist over a hydrophobic HMDS monolayer on an SiO_2 substrate that was subsequently oxygen plasma etched to create hydrophilic regions of exposed SiO_2 where the deposited DNA origami nanostructures were attracted to and adhered, as DNA origami is attracted to hydrophilic surfaces or positively charged substrates such as SiO_2, especially when the DNA origami is in a highly-concentrated (~125 mM) magnesium ion (Mg^{2+}) buffer [105]. Another method is to do dielectrophoretic trapping of DNA origami. Dielectrophoresis (DEP) is a technique in which the manipulation or movement of a dielectric/polarizable particle (e.g., DNA origami) is controlled using a nonuniform/AC electric field, which can be used to trap a particle between two gold electrodes, as has been demonstrated with DNA origami nanostructures that were modified with thiols to assist with bonding to gold electrodes [106].

Another DNA origami deposition method is to use chemical modifiers/linkers such as thiols (–SH) on DNA to assist with the bonding of DNA origami to gold [107], [108]. By attaching thiols to the DNA origami and using covalent gold-thiol (gold-sulfur) bonds to assist with the binding of DNA origami to gold electrodes, while a hydrophobic HMDS monolayer is used to repel DNA origami from areas of the SiO_2 substrate where there are no gold electrodes, high-

magnesium buffers can be avoided; which is beneficial for applications such as DNA nanoelectronics in which parasitic ionic conduction may not be desired [109]. The number of thiols that are connected to each DNA origami nanostructure is important for increasing the efficacy of attachment of the DNA origami nanostructures to gold. At least two covalent thiol-gold bonds at each end of the DNA origami nanostructure are necessary for effective attachment, and four covalent thiol-gold bonds at each binding site improves the efficacy of attachment even further, as a single covalent thiol-gold bond is evidently insufficient for binding DNA origami nanostructures to gold [110].

Chapter 3: Design and Assembly of DNA Origami Nanowires (DNA NWs)

3.1 Introduction

This chapter contains information about the design and assembly of the DNA origami nanowires (DNA NWs). This includes the design and methods for the preparation of a few different types of DNA NWs. The first DNA NW design that is covered is the DNA origami 10-helix bundle 5-mer nanowire (10HB NW), which was the initial DNA NW design that was used for most of the experiments in this dissertation due to its longer length (~1.25 μm). Another DNA NW design that will be discussed is the DNA origami 6-helix bundle dimer nanowire (6HB NW), which is shorter in length but easier to assemble. Finally, two other DNA NW designs will be covered: the DNA origami 14-helix bundle dimer nanowire (14HB NW), and the DNA origami 16-helix bundle dimer nanowire (16HB NW). Each of these nanowire designs have slightly different lengths and widths, which make them appropriate for different applications or device sizes. However, their assembly processes are similar. The DNA NWs are all assembled using a standard DNA origami folding technique that was pioneered by Paul Rothemund [26].

3.2 Design and Assembly of DNA Origami 6HB Dimer / 10HB 5-mer NWs

The DNA origami nanowires (DNA NWs) that are initially studied in this dissertation were designed and assembled by my collaborators, Yonggang Ke and Victor Pan at Georgia Tech and Emory University. One of the DNA NW designs that is utilized in this dissertation is the 10-helix

bundle folded structure. The basic design of this DNA NW is a DNA origami monomer nanowire that is folded into a double-barrel tube shape. The basic monomer unit can be designed to connect with other monomers to form polymers such as a 5-mer, consisting of 5 connected monomer segments. This hierarchical design strategy allows for DNA NWs to be designed with almost any desired length, width, and thickness on the nanoscale. This DNA origami 10-helix bundle 5-mer nanowire (10HB NW) design is 1.25 µm long and 10 nm wide, as it is composed of 5 separate monomer segments that are connected in series and are each 250 nm long and 10 nm wide. Each end of the 1.25 µm DNA NW contains 5 thiols, which form a strong bond with gold for increasing the electrical conductivity of the DNA NW. To assist with imaging the DNA NWs using fluorescence microscopy, there are 120 equally spaced Alexa 488 fluorophores along the 1.25 µm long DNA origami 5-mer nanowire. In addition to the DNA origami monomer nanowire and the 5-mer nanowire, my collaborators also designed a similar type of DNA NW that has a 6-helix bundle structure. This 6-helix bundle dimer nanowire (6HB NW) is ~800 nm long, consisting of two connected ~400 nm long monomers folded into a ~5 nm wide single-barrel tube shape.

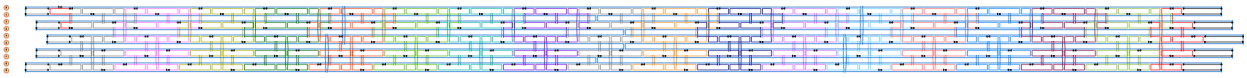

Figure 3.1. Design Schematic of DNA Origami 10-Helix Bundle Monomer (Colored Strands are Staple Strands)

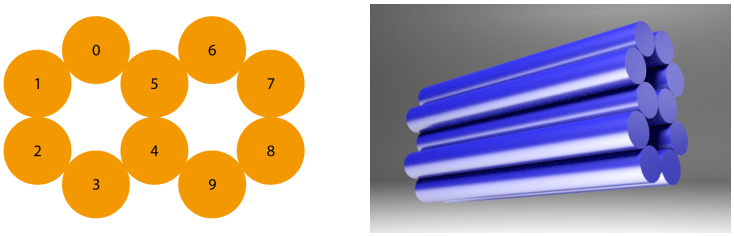

Figure 3.2. 10-Helix Bundle Folded Structure (Left); 3D Rendering of DNA Monomer (Right)

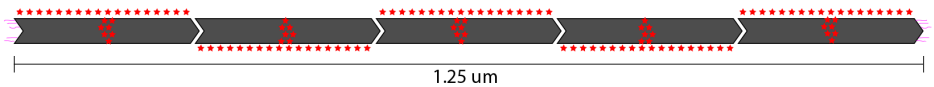

Figure 3.3. Block Diagram of DNA Origami 5-mer Nanowire (Consisting of 5 Monomers)

(Purple Lines are Thiol-terminated Strands, Red Stars are Alexa 488 Fluorophores)

Transmission Electron Microscope (TEM) Images:

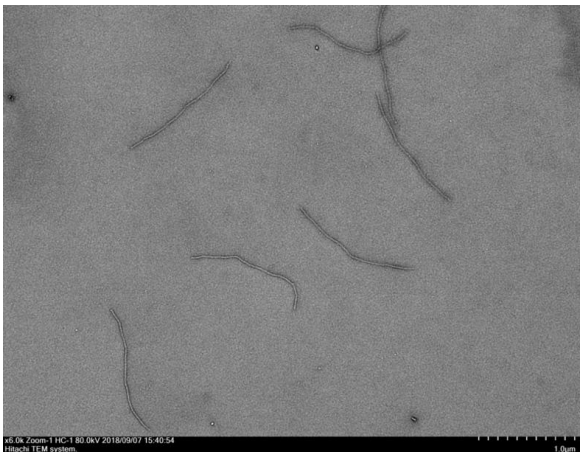

Figure 3.4. Transmission Electron Microscopy (TEM) Image of DNA Origami 10HB 5-mer Nanowires

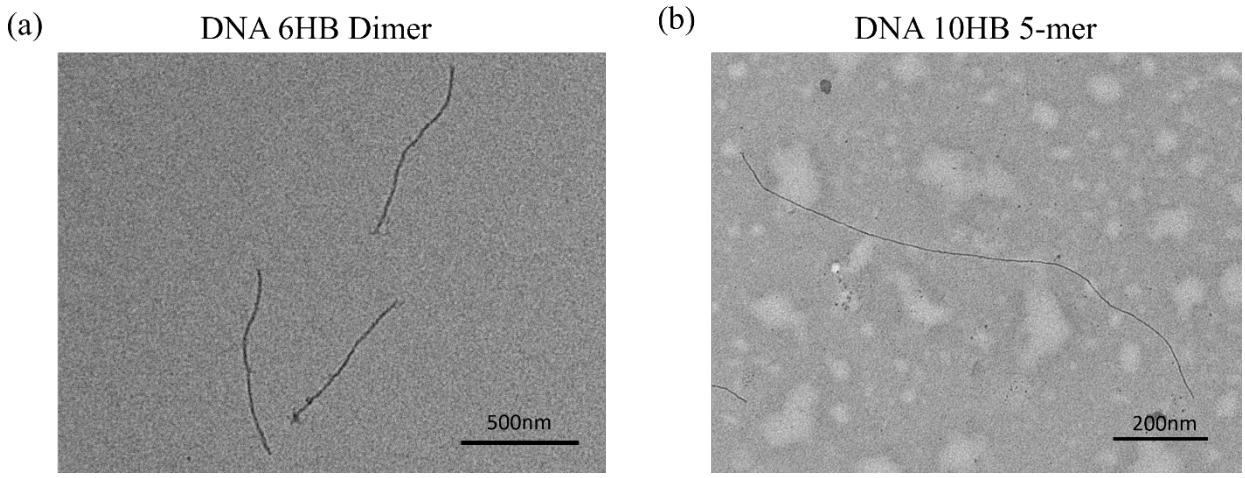

Figure 3.5. Transmission Electron Microscope (TEM) Images of DNA NWs. a) 6HB NW; b) 10HB NW.

Transmission Electron Microscope (TEM) images of DNA NWs are displayed in **Figure 3.5**, with the 6HB NW shown on the left, and the 10HB NW shown on the right. These TEM images reveal the nanoscale structure of the DNA NWs and help to confirm proper folding and assembly of the DNA NWs. All the DN NWs have the expected linear shape and expected lengths.

3.3 Design and Assembly of DNA Origami 14HB Dimer / 16HB Dimer NWs

Other types of DNA NWs that are studied in this dissertation are the DNA origami 14-helix bundle (14HB) dimer nanowire (14HB NW) and the DNA origami 16-helix bundle (16HB) dimer nanowire (16HB NW). The 14HB NW consists of two monomer units that are each ~227 nm in length, making the total length of the 14HB NW dimer ~454 nm. The 16HB NW consists of two monomer units that are each ~169 nm in length, making the total length of the 16HB NW dimer ~338 nm. Therefore, the 14HB NW is slightly longer but narrower, while the 16HB NW is slightly shorter but wider. The 14HB NW and the 16HB NW are designed to bridge gold electrodes with gap sizes less than ~500 nm, whereas the 6HB NW and the 10HB NW are designed to bridge gold electrodes with gap sizes greater than ~500 nm.

To facilitate the attachment of the DNA NWs to gold electrodes, the 14HB NW is designed to include 6 thiols on each end of the DNA NW, while the 16HB NW is designed to include 8 thiols on each end of the DNA NW. The thiols can be reduced by adding 100x molar excess of TCEP to the DNA NW solution, allowing the thiols to form a strong covalent bond with gold. To aid visualization of the DNA NWs during fluorescence microscopy, Alexa 488 fluorophores are also added to the DNA NWs. The 14HB NW includes 50 Alexa 488 fluorophores per monomer, or 100 Alexa 488 fluorophores per dimer. The 16HB NW includes 18 Alexa 488 fluorophores per monomer, or 36 Alexa 488 fluorophores per dimer.

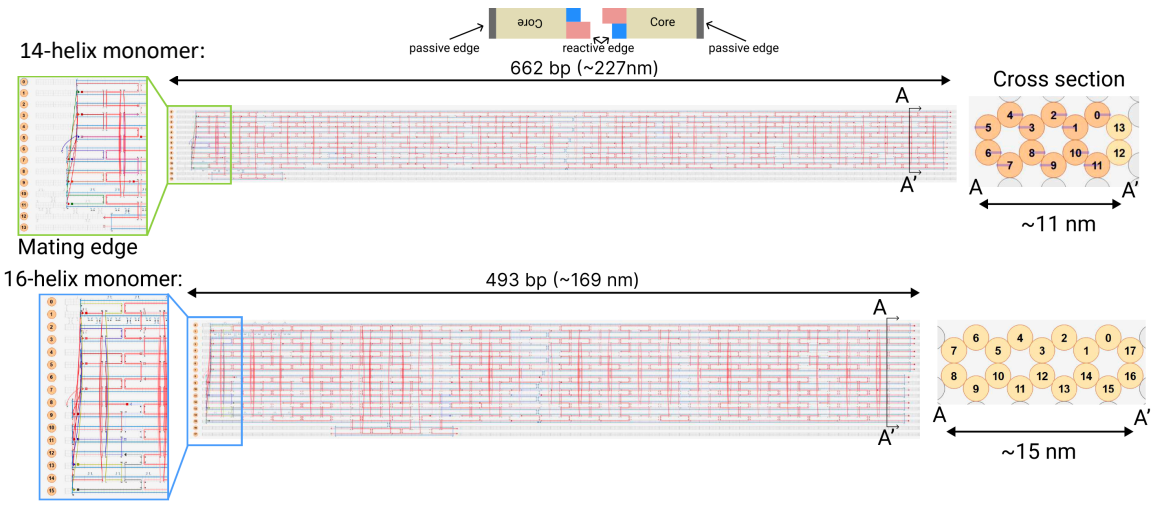

Figure 3.6. DNA Origami Nanowire Dimer Designs Based on DNA Origami 14-Helix Bundle Monomer and DNA Origami 16-Helix Bundle Monomer. (Two monomers of the same type are combined to form a dimer for each nanowire. By exploiting an asymmetry inherent in the honeycomb lattice, monomer polymerization is self-limiting by only needing one "reactive edge", which interacts with itself.)

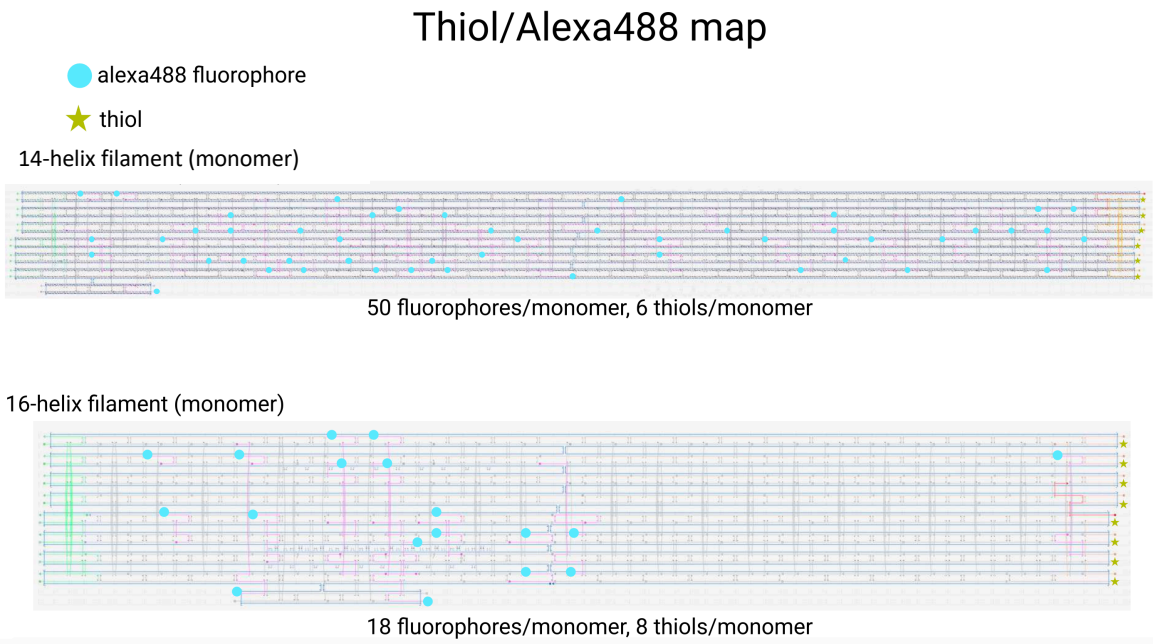

Figure 3.7. Thiol and Alexa 488 Map for DNA Origami 14-Helix Bundle Monomer and DNA Origami 16-Helix Bundle Monomer. (Two monomers of the same type are combined to form a dimer for each nanowire. Blue dots are the Alexa 488 fluorophores. Stars on the right ends are thiols.)

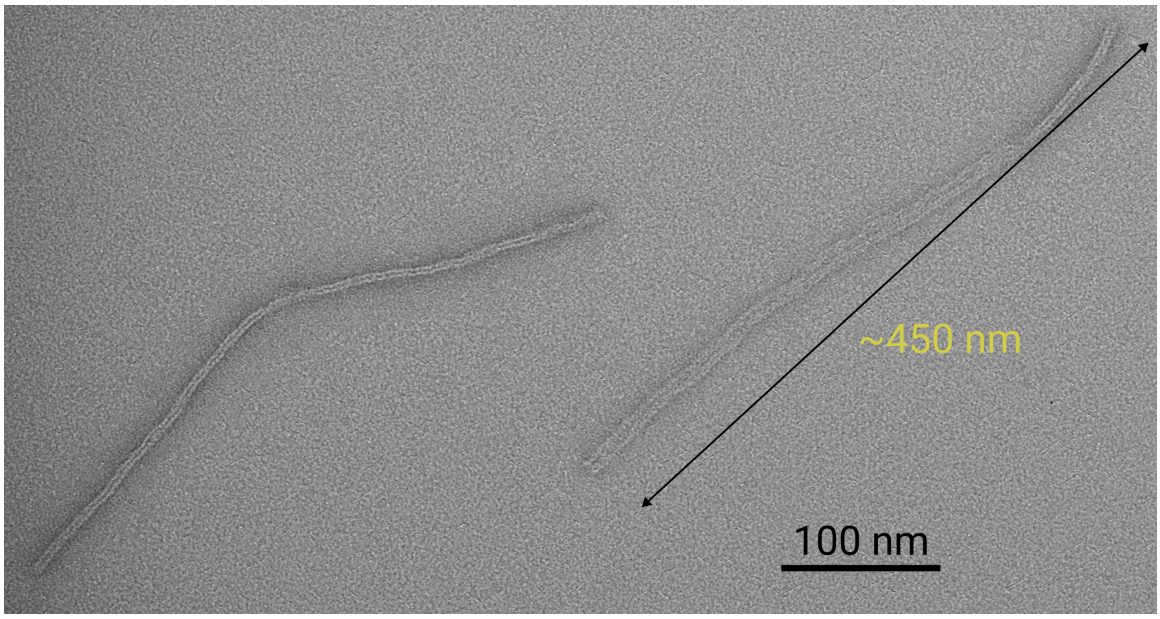

Figure 3.8. Transmission Electron Microscopy (TEM) Image of DNA Origami 14-Helix Bundle Dimer Nanowire (14HB NW)

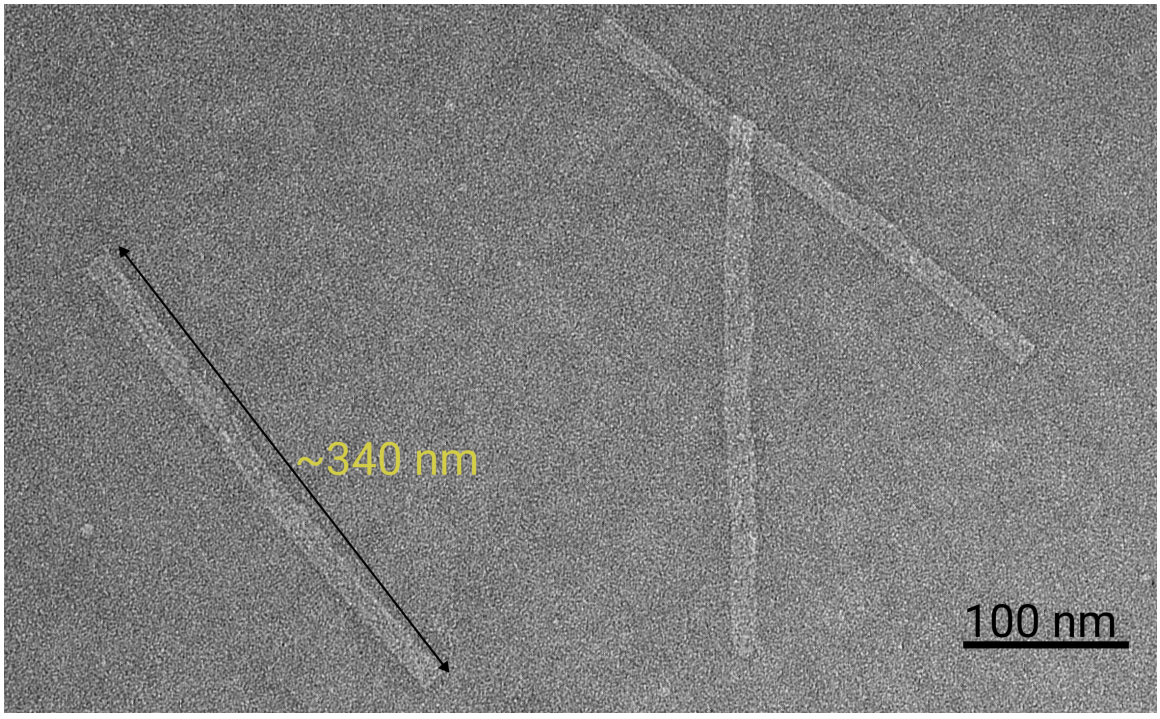

Figure 3.9. Transmission Electron Microscopy (TEM) Image of DNA Origami 16-Helix Bundle Dimer Nanowire (16HB NW)

3.4 Conclusion

In conclusion, the design and assembly of the DNA NWs were completed successfully. The four types of DNA NWs that are studied in this dissertation are the 6HB dimer, 10HB 5-mer, 14HB dimer, and 16HB dimer. This variety of different widths and lengths of DNA NWs provides a wide range of design parameters to test and evaluate the electrical performance of DNA NWs in different conditions. In particular, the different lengths of the DNA NWs make them ideal for designing electrical devices of different sizes, where the length of the DNA NW can be selected to match the size of the electrical device (e.g., a sub-micron gap between two gold electrodes). The inclusion of thiols on both ends of the DNA NWs assists with forming bonds and electrical connections with gold electrodes. Furthermore, the inclusion of Alexa 488 fluorophores along the length of each DNA NW assists with imaging each DNA NW during fluorescence microscopy. Altogether, the dimensions and properties of these DNA NWs make them promising targets for exploring the electrical performance of DNA NWs.

Chapter 4: Design and Fabrication of the Electrode Array Chip (EAC)

4.1 Introduction

This chapter covers the design and fabrication of a semiconductor chip known as the Electrode Array Chip (EAC), which is used as substrate for electrical measurements of the DNA origami nanowires (DNA NWs). Due to the extremely small size and unique properties of the DNA NWs, it was necessary to design a semiconductor microchip with submicron features for electrically measuring the DNA NWs. The microchip also needed a large density of devices to enable data collection. By fabricating a custom-designed semiconductor chip with gold electrodes and nanogaps that are similar in size to the DNA NWs, it is possible to form electrical junctions with the deposited DNA NWs and collect electrical measurements on these nanowires. Therefore, this chapter aims to provide a comprehensive overview of the EAC design and fabrication results.

4.2 Design of the Electrode Array Chip (EAC)

The experimental substrate that is used to electrically measure the DNA origami nanowires (DNA NWs) is a custom-designed microchip referred to as the Electrode Array Chip (EAC). The EAC is designed using a software program called L-Edit, which enables the design of photomasks that are then ordered from an external vendor and utilized for the photolithography process in the cleanroom. The EAC is microfabricated from a ~300 nm thick low-pressure chemical vapor deposition (LPCVD) silicon nitride (Si_3N_4) film on a silicon (Si) wafer, which is used as a substrate to pattern and deposit arrays of ~50 nm thick gold electrodes that are separated by small (micron or submicron) gaps. Each device on the chip contains 14 pairs of gold electrodes that are separated

by these small gaps. There are 5 types of devices, which have different gap sizes: 1 micron, 750 nm, 625 nm, 500 nm, and 250 nm. There are 10 devices of each gap size on the chip, so with the 5 different types/sizes of devices, there are a total of 50 devices on each chip. Since each device has 14 pairs of gold electrodes, there are up to 700 pairs of gold electrodes on each chip that can be used for electrical measurements.

There are two layers of the EAC that are patterned using photolithography. The first layer consists of the ~50 nm thick gold electrodes on the ~300 nm thick LPCVD Si_3N_4. On top of the first layer of the chip there is a second layer of ~100 nm thick Si_3N_4 which is deposited with plasma-enhanced chemical vapor deposition (PECVD). This top Si_3N_4 layer is used to encapsulate and protect most of the area of the gold electrodes from the DNA NW solution that will be deposited onto the chip. There are small openings or windows in the ~100 nm thick PECVD Si_3N_4 encapsulation layer that allow the DNA NWs to be deposited onto the device areas, where the DNA NWs are desired to bridge the gold electrodes. The gold contact pads are also exposed to allow for contact with electrical measurement probes.

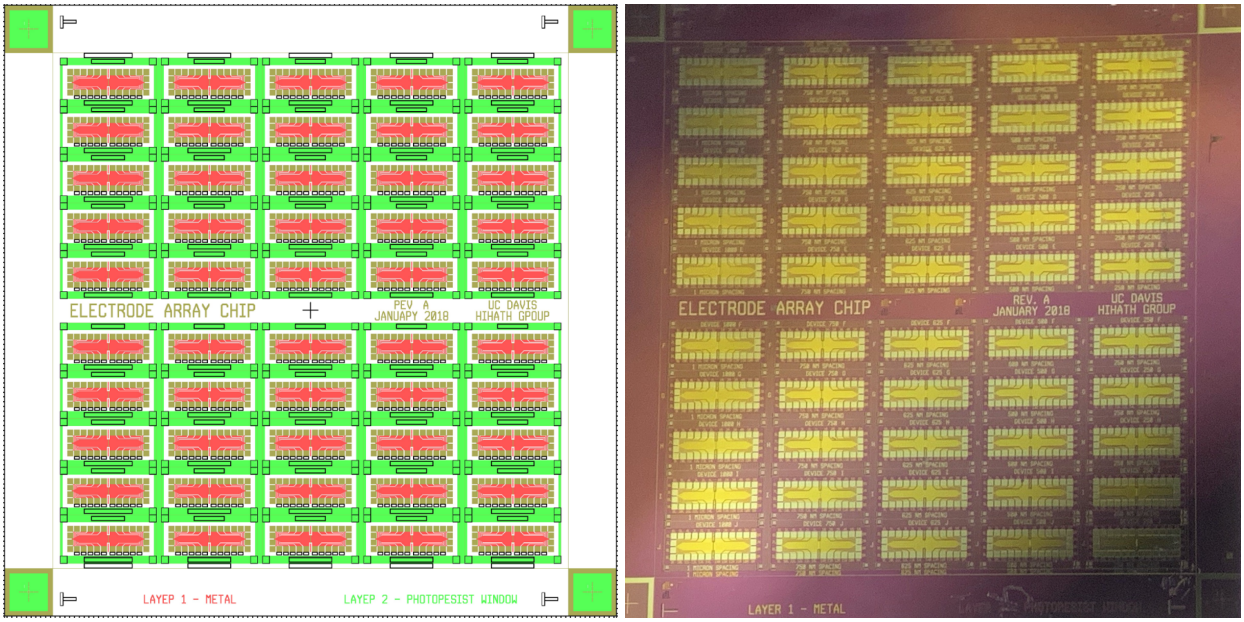

Figure 4.1. Electrode Array Chip (EAC) Design (Left) and Microfabrication (Right)

Figure 4.1 shows the design (left) and microfabrication (right) of the EAC. The image on the left shows the design of the two layers/masks of the EAC that are patterned using photolithography. The areas that are colored red indicate the pattern for mask layer 1, where the gold electrodes are formed/deposited; and the areas that are colored green indicate the pattern for mask layer 2, where windows/holes/openings are formed/etched in the ~100 nm PECVD silicon nitride (Si_3N_4) encapsulation layer. In addition to the devices that are used to measure the electrical resistance/conductance of the DNA NWs, there are also some alignment markers/fiducials and labels that are patterned onto the chip. The image on the right shows a finished microfabricated EAC chip, with the patterned gold electrodes (yellow) and silicon nitride (purple).

4.3 Fabrication of the Electrode Array Chip (EAC)

Fabrication of the Electrode Array Chip (EAC):

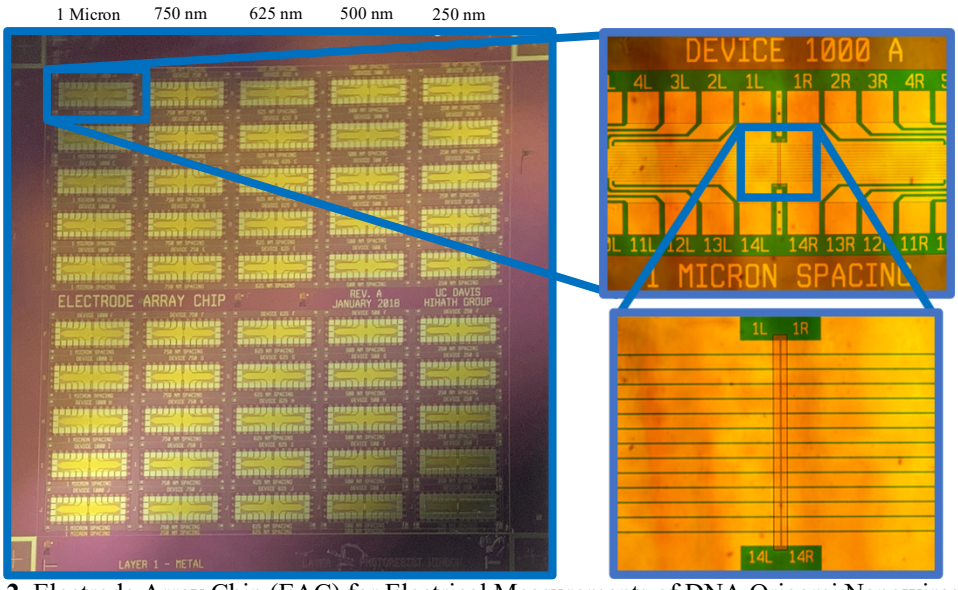

Figure 4.2. Electrode Array Chip (EAC) for Electrical Measurements of DNA Origami Nanowires (DNA NWs)

Figure 4.2 shows the Electrode Array Chip (EAC) after the fabrication process is complete. The EAC is ~1 cm x ~1 cm in size. There are 50 different devices on the chip. Each device has an array of 14 pairs of gold electrodes. These gold electrodes are separated by a gap spacing of 1 of 5 different gap sizes: 1 micron, 750 nm, 625 nm, 500 nm, 250 nm. The devices are organized into 5 separate columns of 10 devices each, with each column having one of the designated gap spacings. In principle, this design allows for the electrical resistance of DNA NWs to be measured with lengths ranging from 1 micron (or longer) down to 250 nanometers.

The EAC was successfully fabricated. As shown in **Figure 4.2**, the EAC consists of a silicon nitride (Si_3N_4) substrate, gold electrodes, and a ~100 nm silicon nitride (Si_3N_4) encapsulation window layer with windows/holes in it to allow for the deposition of DNA NWs in the desired device areas so that the DNA NWs can make electrical contact with the gold electrodes and bridge the silicon nitride gaps between the gold electrodes; as well as to allow for electrical test probes to connect with the gold contact pads. The yield is very good (>90%) for the 1 μm, 750 nm, and 625 nm gap devices, while the yield for the 500 nm and 250 nm gap devices is low (<50%). However, the yield improved somewhat with each new EAC wafer fabrication run/iteration, especially by tuning the exposure time. A detailed process flow for the fabrication of the Electrode Array Chip (EAC) is included in the Appendix.

Examples of Electrode Array Chip (EAC) devices with different gap sizes (1 μm, 750 nm, 625 nm, 500 nm, 250 nm) both before and after the formation of the ~100 nm silicon nitride (Si_3N_4) encapsulation layer are shown below in **Figure 4.3**, with both 10x and 150x magnification images. The images of the devices are organized in different rows, ordered by their gap size. **Figure 4.4** shows examples of photolithography resolution marks, demonstrating the optical resolution and the limits of the microfabrication process.

Before Si_3N_4 Encapsulation		After Si_3N_4 Encapsulation	
10x Magnification	150x Magnification	10x Magnification	150x Magnification

1 μm Gap Devices

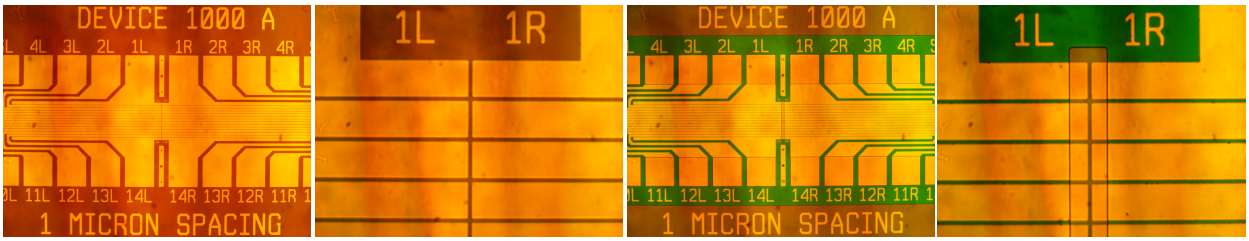

750 nm Gap Devices

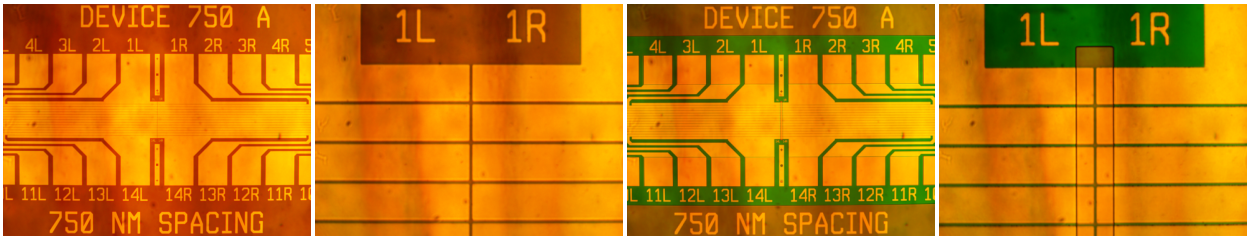

625 nm Gap Devices

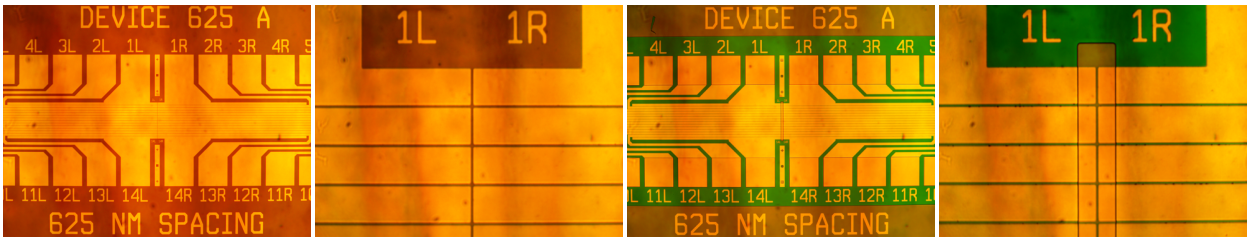

500 nm Gap Devices

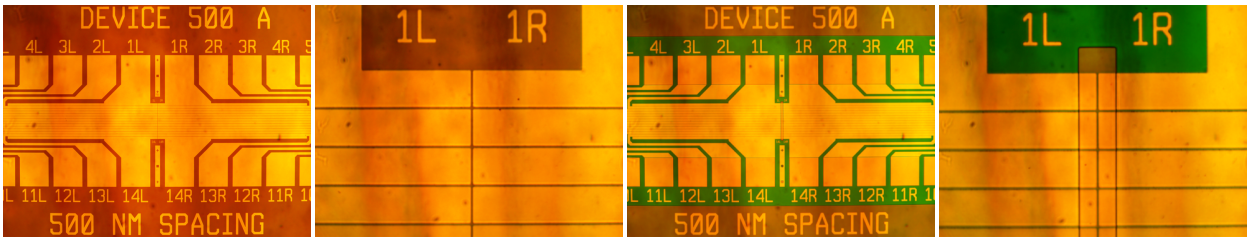

250 nm Gap Devices

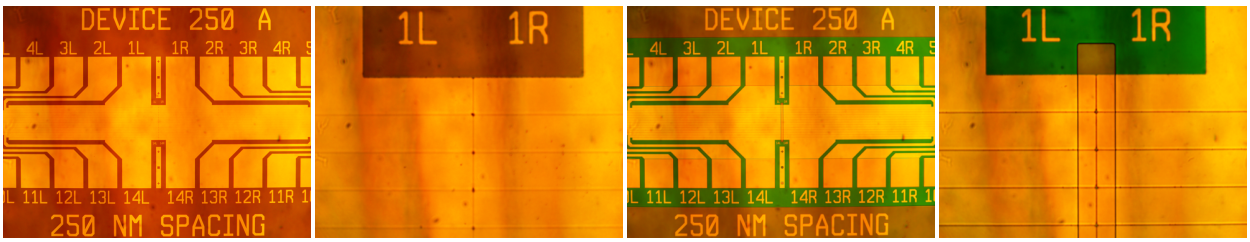

Figure 4.3. Examples of EAC Devices with Different Gap Sizes Before (Left) and After (Right) Si_3N_4 Encapsulation

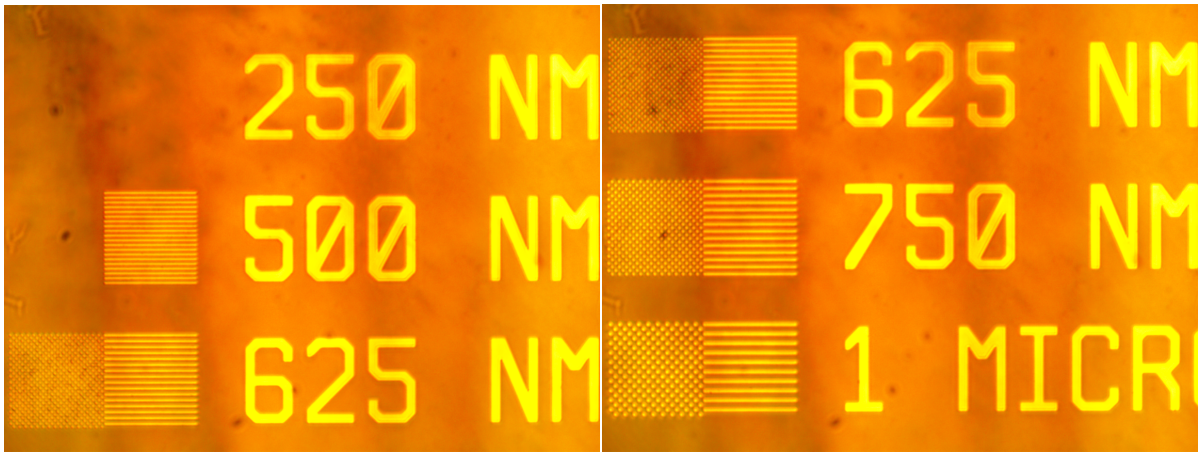

Figure 4.4. Photolithography Resolution Marks for 250 nm, 500 nm, and 625 nm Features (Left) Photolithography Resolution Marks for 625 nm, 750 nm, and 1 μm Features (Right)

4.4 Conclusion

In conclusion, the design and fabrication of the Electrode Array Chip (EAC) was successful, and the fabrication yield of the EAC improved over time. The yield steadily increased with each new EAC wafer fabrication run, by tweaking and improving process parameters with each new fabrication process iteration. Improvements in the yield have been achieved by utilizing a lift-off resist layer (LOL1000) underneath the photoresist layer to assist with the lift-off process for forming the gold electrodes, as well as optimizing the photoresist exposure time and development time. Further improvements in the yield could be achieved by continued optimization of the fabrication parameters, such as the photoresist exposure time and development time, the photoresist soft baking and post exposure baking time and temperature, and the plasma etching parameters. It is possible to reliably achieve 1 μm, 750 nm, and 625 nm gap devices with very high yield (>90%). Meanwhile, 500 nm and 250 nm gap devices still suffer from relatively poor yield (<50%). Some photolithography resolution results for an EAC wafer microfabrication run are shown below.

Chapter 5: Electrical Characterization of DNA Origami Nanowires (DNA NWs)

This chapter contains the introduction, methods, results, discussion, and conclusion for the fluorescence microscopy imaging and electrical characterization of DNA origami nanowires (DNA NWs). The initial electrical measurements indicate that the ~1 μm long DNA NWs have an electrical resistance of ~1E12 ohms (~1 teraohm) in ambient humid conditions.

5.1 Introduction

In this chapter, we will discuss the techniques used to image and electrically measure DNA origami nanowires (DNA NWs). As presented previously, DNA NWs are a type of nanostructure that are created using the technique of DNA origami, in which a long single strand of DNA is folded into a specific shape using a set of shorter complementary DNA staple strands. These DNA origami nanostructures have the potential to be used as nanowires in electronics and sensors due to their theoretical ability to conduct electricity. However, accurately measuring the electrical conductance of DNA NWs can be challenging due to their small size and the need to maintain their structural integrity during the measurement process. Therefore, we will explore the methods and results for imaging and electrically measuring the DNA NWs under various environmental/experimental conditions to gain an understanding of the baseline/intrinsic conductance of DNA NWs.

5.2 Methods

The goal of this objective is to characterize the intrinsic electrical conductivity of DNA NWs to evaluate their potential use in DNA-based electronics. To this end, the experimental design and methods that pertain to this objective are laid out in this section. After the DNA NWs are assembled and prepared, and after the Electrode Array Chips (EACs) are microfabricated, a sample can then be prepared for imaging and electrical characterization. A quick overview of the process for preparing an EAC sample with DNA NWs for imaging and electrical characterization is as follows. First, the EAC is cleaned with a ~1-minute O_2 plasma etch just prior to DNA NW solution deposition. Next, the DNA NW solution is applied to the EAC and allowed to incubate on the chip for a while. The EAC can then be washed to remove excess salt/buffer solution if desired. The deposited DNA NWs are then imaged on the EAC with fluorescence microscopy. The EAC can then vacuum dried to remove water and prevent contamination of DNA NWs for dry measurements or kept wet for wet measurements. Finally, the DNA NWs are electrically measured using a probe station. A detailed overview of this DNA NW EAC sample preparation process is discussed next.

5.2.1 Depositing DNA NWs onto the EAC

A new clean 50 mL conical centrifuge tube is filled with ~40-50 mL of ultrapure 18.2 megaohm-cm DI water (DI H_2O). This DI water is then bubbled with nitrogen gas for at least ~1 hour to flush out the oxygen that is adsorbed in the water. The nitrogen bubbling is accomplished using a flint glass pipette tip connected to the lab's nitrogen supply line via a hose that is supported by a stand with a clamp while the tip is immersed in the DI water. The 50 mL conical centrifuge tube is supported by a test tube rack. The oxygen is removed from the DI water because oxygen

can oxidize the Alexa 488 fluorophores and/or fluorescent dyes/intercalators, thereby reducing their brightness. The nitrogen-bubbled DI water is then used to make diluted solutions of DNA NWs and intercalators, and to wash and incubate the EAC.

The DNA NW sample preparation procedure is performed in a darkroom with only low-energy red lights turned on (like the conditions used for developing film), to prevent photobleaching of the Alexa 488 fluorophores and fluorescent dyes/intercalators. The ~100 pM DNA NW stock solution is gently pipetted up and down a few times to disperse the nanowires in the stock solution microcentrifuge tube, and then 3-5 μL of the DNA NW solution is pipetted into a new clean 1.5 mL microcentrifuge tube. If DNA pre-intercalation is being performed, then 15-17 μL of the intercalator solution (e.g., ethidium bromide) is pipetted into the same microcentrifuge tube. If pre-intercalation is not being performed, then 15-17 μL of nitrogen-bubbled ultrapure 18.2 megaohm-cm DI water (DI H_2O) or buffer is combined instead. There should be about 20 μL of combined solution in the microcentrifuge tube. The 20 μL combined solution is pipetted up and down several times to mix it all together. The microcentrifuge tube with this combined solution is then sealed with parafilm to prevent the solution from evaporating, wrapped with aluminum foil to block out the light, and left upright in a test tube holder in the dark to incubate. The solution is allowed to incubate in the microcentrifuge tube for at least 1 hour.

After the DNA pre-intercalation incubation, the 20 μL mixed solution is deposited onto the Electrode Array Chip (EAC). The solution is pipetted up and down on the chip several times to disperse it around the chip. The chip, which is mounted to a microscope slide with a piece of double-sided copper tape, is placed on top of a ~1 cm thick piece of PDMS that is located in a Petri dish that is partially filled with ~25 mL of DI H_2O to prevent evaporation of the solution. Nitrogen gas is gently flown into the Petri dish before closing the lid, and then nitrogen gas is purged around

the Petri dish (e.g., in a desiccator) during incubation to keep the atmosphere inert and preserve the fluorophore brightness. Aluminum foil is placed over the Petri dish to protect the DNA NW solution from light to prevent it from photobleaching. A test tube rack is placed on top of the Petri dish lid to weigh it down and keep it sealed. The solution is allowed to incubate on the chip in the dark for 1 hour – overnight.

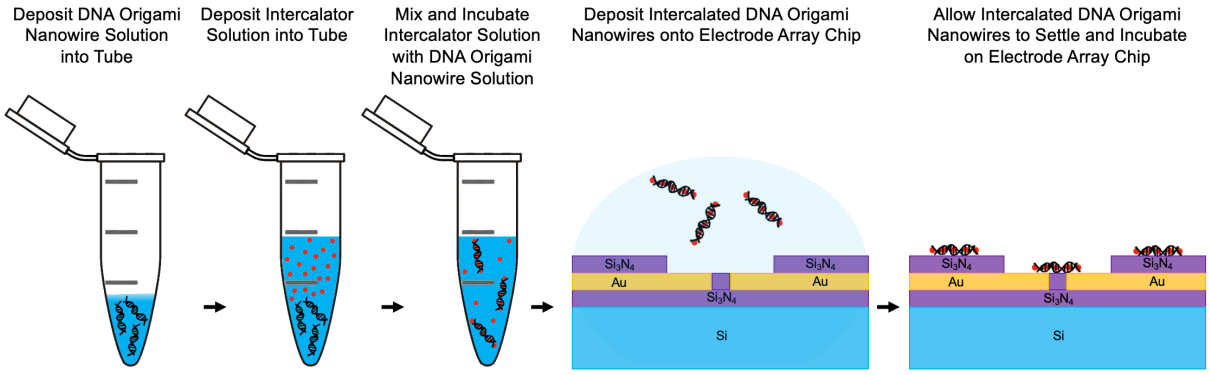

Figure 5.1. Preparation and Deposition of Intercalated DNA Origami Nanowire Solution on EAC

Depending on the experiment being performed, it may be desirable to reduce the amount of buffer or salt/ion concentration in the sample solution. If less buffer is desired in the sample solution to prevent salt residue, the sample solution can be diluted, and the chip can be washed. After the on-chip incubation, 40 µL of nitrogen-bubbled ultrapure 18.2 megaohm-cm DI H_2O can be applied to the chip using a micropipette. A coverslip is gently blown with nitrogen to dust it off, rinsed with isopropanol, gently blown dry with nitrogen, and then placed on top of the chip. After ~5 minutes, a Texwipe is used to wick away the excess buffer solution, the coverslip is removed, and an additional 40 µL of nitrogen-bubbled ultrapure 18.2 megaohm-cm DI H_2O is applied to the chip using a micropipette. A new small square coverslip (#1.5H High-Precision, ~0.17 mm thick, 18mm x 18mm) is gently blown with nitrogen to dust it off, rinsed with

isopropanol, gently blown dry with nitrogen, and then placed on top of the chip. After ~5 minutes, a Texwipe is used to wick away the excess solution again, and an additional 40 μL of nitrogen-bubbled ultrapure 18.2 megaohm-cm DI H_2O is applied to the chip using a micropipette, under the edge of the coverslip. If the initial buffer concentration is desired instead of diluting the sample solution or washing the chip, a coverslip can be applied to the chip right after sample incubation.

5.2.2 Imaging the DNA NWs on the EAC with Fluorescence Microscopy

The chip is then transported, in a Petri dish wrapped with aluminum foil to block out the light and prevent photobleaching of the fluorophores, to a lab where the fluorescence microscope is located. A microcentrifuge tube with nitrogen-bubbled ultrapure 18.2 megaohm-cm DI water and a micropipette with a 10 μL pipette tip are also brought, for rewetting the chip. Alternatively, a microcentrifuge tube with buffer could be brought for rewetting the chip to maintain the original buffer concentration. Tweezers are also brought for lifting the coverslip and for removing the coverslip.

There should be ~40 μL of DI H_2O / buffer / intercalator / DNA NW solution that was previously deposited onto the chip to keep the chip wet and prevent the Alexa 488 fluorophores from drying out and oxidizing. This excess liquid is beneficial for increasing the amount of time that the chip can be imaged before rewetting the chip. The coverslip should be held in place and stick to the chip because of the surface tension of the solution. If necessary, some of the excess solution can be wicked away using a Texwipe to prevent the coverslip from falling off the chip when inverted. Wicking away the solution helps with coverslip adhesion. However, wicking away the excess solution is usually not necessary if there is no more than ~40 μL of solution on the chip. Upon inverting the microscope slide, the coverslip should stay on the chip. The final coverslip should always be a small high-precision cover slip (#1.5H High-Precision, ~0.17 mm thick, 18mm

x 18mm) for better resolution and better adhesion. It should also be ensured that there are no air bubbles between the chip and coverslip.

The DNA NWs are then imaged on the Electrode Array Chip using fluorescence microscopy. The microscope used is a ZEISS Axio Observer inverted fluorescence microscope configured for epifluorescence with a 100x objective with oil immersion. For the fluorescence microscope imaging settings, a gain of 3x and a 5-10 second exposure time is used, and this makes it possible to visualize the DNA NWs with the Alexa 488 fluorophores and/or a fluorescent dye such as ethidium bromide (EtBr). Nitrogen-bubbled ultrapure 18.2 megaohm-cm DI water or buffer can be added to the chip as necessary during the imaging process to rewet and rinse the chip. However, adding water to the chip may reduce the brightness of the Alexa 488 fluorophores as it may expose them to oxygen. The Alexa 488 fluorophores seem to quickly become oxidized or get dimmer if the fluorophores are exposed to oxygen, so it is important to keep the DNA NWs wet rather than allowing them to dry out and get exposed to air. However, excessive washing with DI water an remove the DNA NWs from the chip. Therefore, it is best to image the DNA NWs as quickly as possible and use buffer to rewet the chip if salt ions or salt residue from the buffer are negligible for the future electrical measurements.

After the imaging is complete with the fluorescence microscope, 20-40 μL of nitrogen-bubbled ultrapure 18.2 megaohm-cm DI water or buffer can be applied to the chip under the edge of the coverslip to make it easier to remove the coverslip from the chip. Optionally, some of the applied solution can then be wicked away using a Texwipe to wash away some of the remaining salt/buffer residue again. The square coverslip is then removed from the chip using tweezers. The chip is then removed from the microscope slide and copper tape without breaking the chip, again using tweezers.

Fluorescence Microscope Images of Individual DNA Origami 10HB 5-mer Nanowires on EAC:

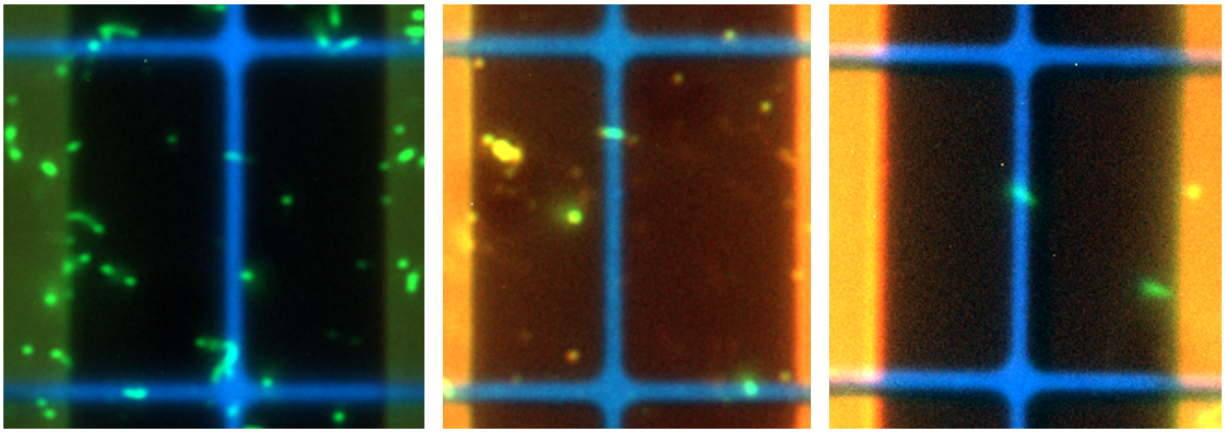

Figure 5.2. Fluorescence Microscope Images of Individual 10HB NWs Bridging 1 Micron Gaps of EAC Devices. Individual ~1.25 μm long DNA origami 10HB 5-mer nanowires (10HB NWs) are shown in green. ~1 μm wide electrically insulating silicon nitride gaps of the EAC are shown in blue. The exposed pairs of gold electrodes (that form an electrical connection with the 10HB NWs) of the EAC are shown in black.

The three separate zoomed-in fluorescence images displayed above in **Figure 5.2** show individual DNA origami 10HB 5-mer nanowires (10HB NWs) (shown in green) that are each ~1.25 μm long and are each crossing ~1 μm wide electrically insulating silicon nitride gaps (shown in blue) of electrical devices on the Electrode Array Chip (EAC). These 10HB NWs each form an electrical connection with a pair of gold electrodes (shown in black). The zoomed-in fluorescence images provide visual confirmation of the 10HB NWs forming an electrical connection with a pair of gold electrodes, helping to confirm the validity of the electrical measurements. The fluorescence images of the 10HB NWs on the 1 μm gap devices of the EAC were acquired with a ZEISS Axio Observer inverted fluorescence microscope configured for epifluorescence with a 100x objective with oil immersion, using a #1.5H High-Precision coverslip (~0.17 mm thick, 18 mm x 18 mm), with a gain of 3x and a 5-10 second exposure time for the imaging settings.

5.2.3 Electrical Characterization of DNA NWs on the EAC

If electrical measurements will be performed on the chip under wet/buffered conditions, the chip can be electrically measured directly after imaging the DNA NWs on the chip. However, if electrical measurements will be performed on the chip under dry conditions, then the chip is first vacuum dried in a vacuum desiccator for at least 1 day – 1 week. This is done to remove water from the sample and dry out the DNA NWs and the chip, as well as to prevent contamination of the chip before the electrical measurements are acquired. The procedure for electrical characterization of DNA NWs is then carried out. This includes the electrical measurements of DNA NWs that were imaged and found to be bridging gold electrode pairs in the device area of the EAC. Similarly, electrical measurements of blank or buffered samples in a dry vs. wet state may also be performed as control experiments. In some instances, further imaging/measurement techniques such as atomic force microscopy (AFM) or scanning electron microscopy (SEM) may be used to confirm the presence of DNA NWs on EAC devices.

A probe station is used to collect electrical measurements of DNA NWs on the EAC. After the chip is imaged with fluorescence microscopy to identify the locations where the DNA NWs are bridging the gold electrodes, electrical measurements are collected by performing a current-voltage (IV) sweep on each device to determine the resistance values of the DNA NWs, either in a wet state directly after the imaging process, or in a dry state after the chip is vacuum dried to remove any residual water. The IV sweep voltage should typically be kept under 1 volt (e.g., 500 mV) to prevent potential hydrolysis and electrochemical reactions with the water/buffer, especially when doing electrical measurements under wet conditions. These electrical measurements reveal the conductance/resistance of the DNA NWs, which have Alexa 488 fluorophores and thiols attached to them. Ideally, the DNA NWs should be long enough to bridge most devices on the

EAC regardless of the electrode gap size (1 μm gaps, 750 nm gaps, 625 nm gaps, 500 nm gaps, and 250 nm gaps).

There are two tungsten-tipped probes in the probe station that are maneuvered to make electrical contact with the gold contact pads for the left electrode and right electrode of whichever electrode pair of a DNA NW EAC device is being measured at a given moment. These two probes are connected to a National Instruments input/output junction box via BNC connectors and shielded cables, which allows the inputs and outputs to be collected and controlled by a LabVIEW program on a computer. One of the two probes is used to apply an output voltage/bias from an output terminal of the LabVIEW junction box. The other probe carries the input current that results from the voltage applied to the DNA NW device, and this current is amplified and converted to a voltage with a transimpedance amplifier (TIA) (with an adjustable/swappable feedback resistor that is used to set the gain) that is connected to an input terminal of the LabVIEW junction box. The metal housing/enclosure for the transimpedance amplifier box is grounded to a DC regulated power supply ground terminal (connected to earth ground), which greatly helps to suppress electrical noise in the IV curve measurements.

After a diamond scribe is used to scratch away some silicon nitride in the corner of the chip to break through the silicon nitride insulator and expose the conductive silicon body underneath, some Galinstan (liquid metal) is applied to the same corner of the chip to make a good electrical connection with the silicon body of the chip. A third tungsten-tipped probe is then maneuvered to make electrical contact with the Galinstan in the scratched area on the corner of the chip with exposed silicon to make electrical contact with the silicon body. This third probe is connected to both ground terminals on a DC regulated power supply to ground out the silicon chip to suppress electrical noise during the very sensitive electrical resistance measurements. The metal

lid/enclosure of the probe station is closed to further shield the chip and probes from radiofrequency (RF) energy and electrical noise during the measurements.

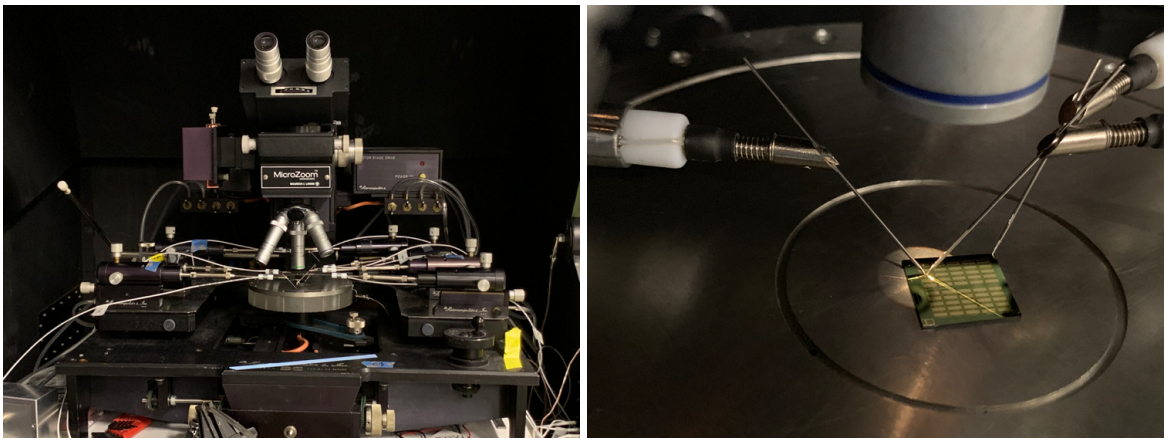

Figure 5.3. Probe Station (Left); EAC in Probe Station (Right)

The data is acquired with a LabVIEW program that controls the output sweep voltage and reads in the input current, which is converted to a voltage by a transimpedance amplifier with a feedback resistor that is used to set the appropriate gain. The resulting IV sweep ".dat" data files that are generated by the LabVIEW program are then processed and analyzed by a MATLAB program; and the processed data can then be plotted with Python, in Excel, or in OriginPro.

Control experiments are performed using very similar techniques as regular experiments to collect electrical measurements with the EAC under different experimental conditions (e.g., blank chip, chip with buffer without DNA, wet vs. dry conditions). These control experiments are done to establish baseline resistance values, and to prove that the electrical measurements of DNA NWs are valid measurements of DNA NWs rather than something else such as the buffer/salt solution or a blank EAC. The experimental procedures for control experiments are essentially the same as DNA NW experiments except they lack the application of DNA NW material.

Optionally, the DNA NWs on the EAC can be imaged with other imaging techniques (other than fluorescence microscopy) such as atomic force microscopy (AFM) or scanning electron microscopy (SEM). AFM is non-destructive to the DNA NWs, so damaging the sample is less likely with AFM imaging, although the sample can get dirty/contaminated during the long time it takes to acquire images. SEM is destructive to the DNA NWs, as it essentially burns up the organic DNA, so it destroys the possibility of further electrical measurements, and should be done only after all electrical measurements are collected.

5.3 Results and Discussion

Fluorescence Microscopy Images of DNA Origami 5-mer Wires on Electrode Array Chip (EAC):

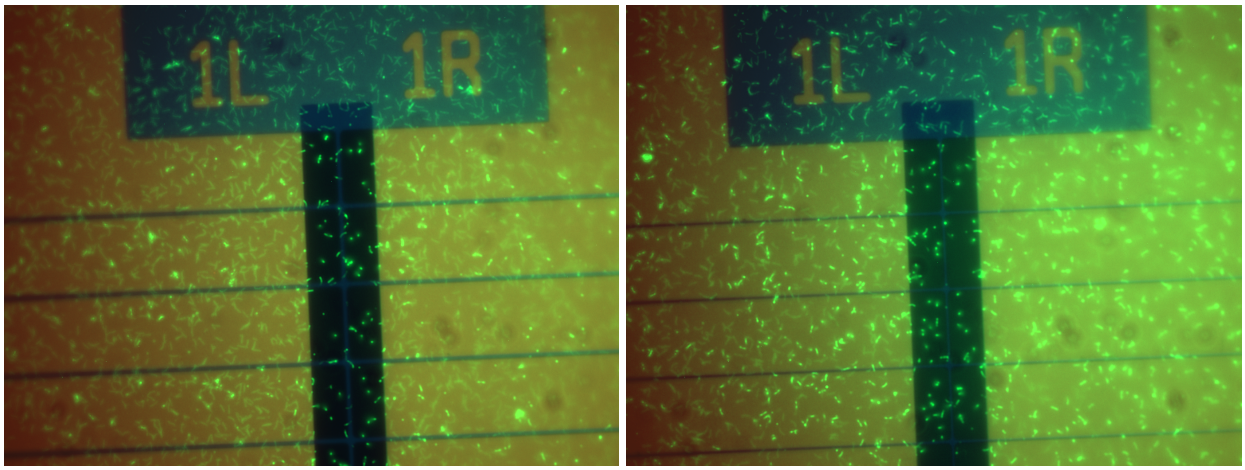

Figure 5.4. DNA Origami 5-mer Wires (Glowing Green Due to Alexa 488 Fluorophores) Are Observed Bridging 1 μm Gaps (Left) and 750 nm Gaps (Right) Between Gold Electrodes

Figure 5.4 above shows fluorescence microscopy images of DNA NWs (glowing green due to the Alexa 488 fluorophores attached to the DNA NWs) on an Electrode Array Chip (EAC), which confirm that the DNA NWs have successfully been deposited onto the EAC. The DNA NWs (green) can be seen bridging the silicon nitride gaps (blue) between gold electrodes (black).

Atomic Force Microscopy (AFM) Images of DNA Origami 5-mer Nanowires on EAC:

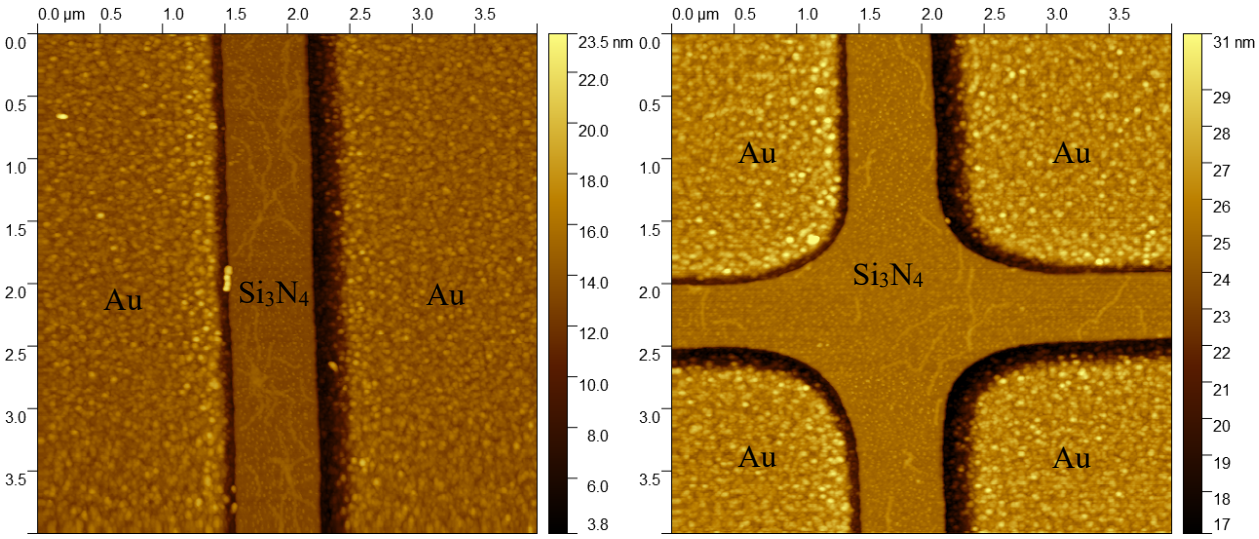

Figure 5.5. AFM Images of DNA Origami 5-mer Nanowires Bridging Gold Electrodes on EAC in Bundles of DNA Nanowires (Left) and Individual DNA Nanowires (Right)

Atomic force microscopy (AFM) images, as shown above in **Figure 5.5**, also confirm the successful deposition of DNA NWs on the EAC, with DNA NWs visibly bridging the gold electrodes, either as bundles of DNA NWs (left) or as individual DNA NWs (right). Both fluorescence microscopy and AFM can be used to verify the presence of DNA NWs on the EAC and can confirm the proper bridging of the DNA NWs across the silicon nitride (Si_3N_4) gaps to form electrical connections between the gold (Au) electrodes. These fluorescence microscopy images and AFM images of the DNA NWs on the EAC are used to confirm the validity of the electrical measurements and electrical resistance values for devices with DNA NWs deposited on them. Next, we will look at some examples of electrical measurements or resistance values for these DNA NWs.

Resistance Values for DNA Origami 5-mer Wires on EAC (SiO_2, No HMDS, Not Vacuum Dried):

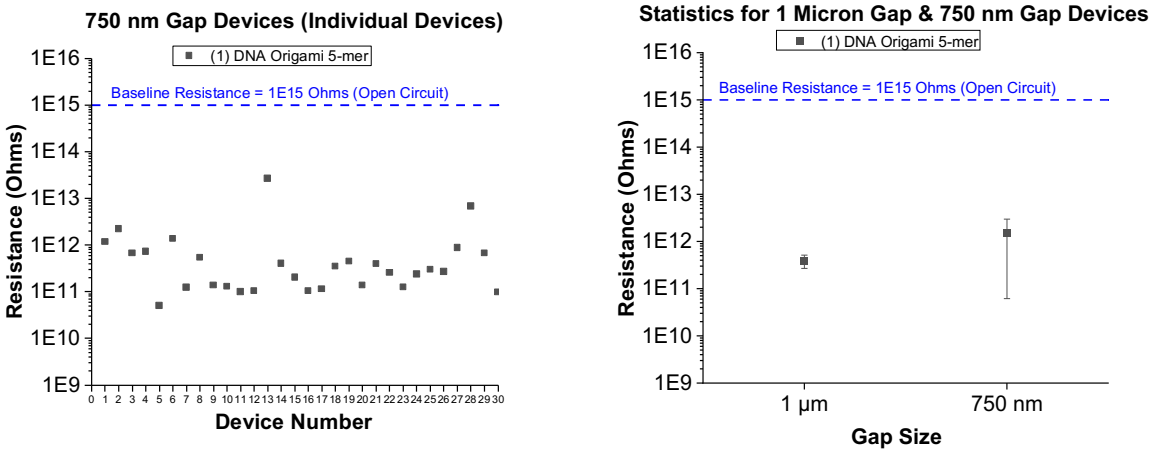

Figure 5.6. Resistance Values for DNA Origami 5-mer Nanowires (Individual Devices)

(Left: Individual 750 nm Gap Devices, Right: Statistics for Individual 1 µm and 750 nm Devices)
(SiO_2 Substrate, No HMDS Surface Pre-Treatment, Not Vacuum Dried)

Fluorescence Microscopy Image of DNA Origami 5-mer Nanowires on Electrode Array Chip:

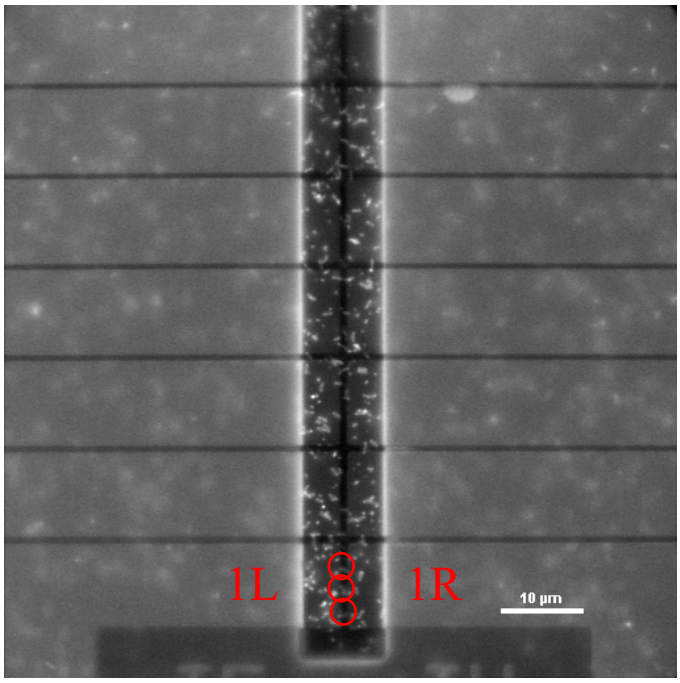

Figure 5.7. Fluorescence Microscopy Image Showing DNA Origami 5-mer Nanowires (Glowing Due to Alexa 488 Fluorophores) Bridging 1 µm Gaps Between Gold Electrodes in Multiple Locations

These resistance measurements in **Figure 5.6** show some individual resistance value measurements (left) and the statistical averages of the values (right) for some 1 μm and 750 nm gap devices. These DNA NWs are less electrically resistive (or more electrically conductive) (~1E11 ohms – ~1E12 ohms) than the baseline resistance measurements of a blank EAC (~1E15 ohms), further verifying the presence of DNA NWs on the EAC, and indicating that DNA NWs can be electrically conductive. It should be noted that these electrical resistance values are acquired in ambient conditions in which the DNA NW solution/buffer has evaporated, but the sample has not been vacuum-dried. Therefore, the sample may still be somewhat moist due to the ambient humidity and residual solution/buffer. The presence of DNA NWs on the chip is also confirmed by fluorescence microscopy images, as shown in **Figure 5.7** in which the DNA NWs are visibly bridging the 1 μm gaps between gold electrodes. Next, we will look at a control experiment involving short individual DNA origami monomer segments to further verify these results.

Control Experiment with DNA Origami Monomer Nanowires (Si_3N_4, No HMDS, Vacuum Dried):

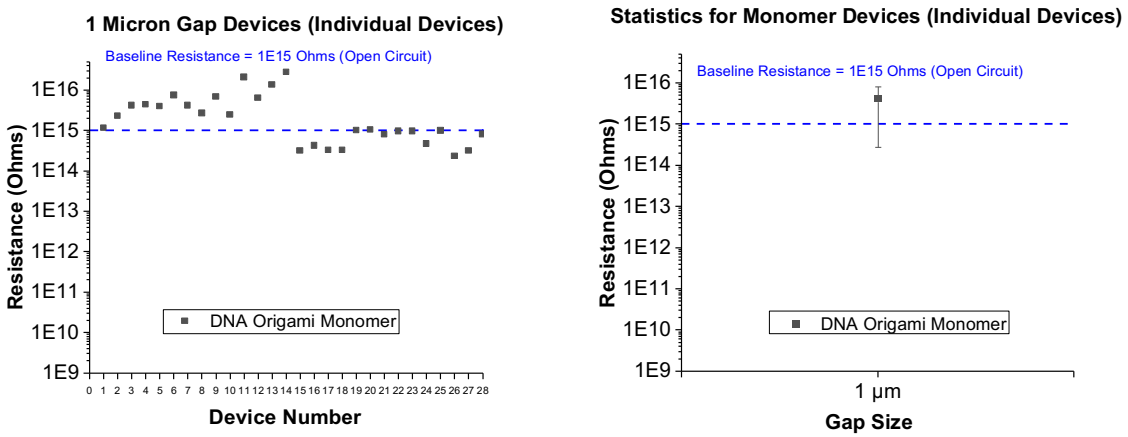

Figure 5.8. Resistance Values (Left) and Statistics (Right) for DNA Origami Monomer Nanowires (~250 nm Long) on 1 µm Gap Devices (Si_3N_4 Substrate, No HMDS Surface Pre-Treatment, Vacuum Dried)

These resistance measurements and statistics shown in **Figure 5.8** indicate that the DNA origami monomer nanowires (which are ~250 nm long) that are deposited onto 1 µm gap devices are highly resistive (~1E15 ohms, equivalent to an open circuit), as the ~250 nm long DNA origami monomer nanowires are not long enough to bridge the sets of gold electrodes that are separated by 1 µm gaps, preventing closed electrical circuits from forming. This control experiment indicates that the electrical resistance values (~1E12 ohms) that are measured for the ~1.25 µm long DNA origami 10-helix bundle 5-mer nanowires (10HB NWs) are primarily due to the electrical conductivity of the DNA origami 10-helix bundle 5-mer nanowires themselves, rather than something else in the experimental environment/setup (e.g., the buffer or the EAC) causing the increased electrical conductivity. Next, we will look at another control experiment involving the buffer solution.

Buffer Control Experiment (0.5x TBE, 10 mM Mg^{2+}) (Si_3N_4, No HMDS, Not Vacuum Dried):

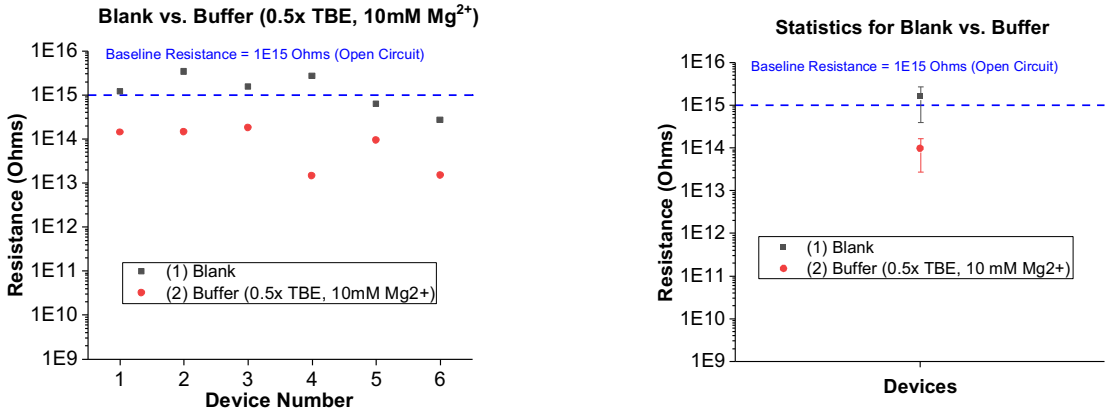

Figure 5.9. Resistance and Statistics for DNA Origami Nanowire Buffer (0.5x TBE, 10 mM Mg^{2+}) (Si_3N_4 Substrate, No HMDS Surface Pre-Treatment, Not Vacuum Dried)

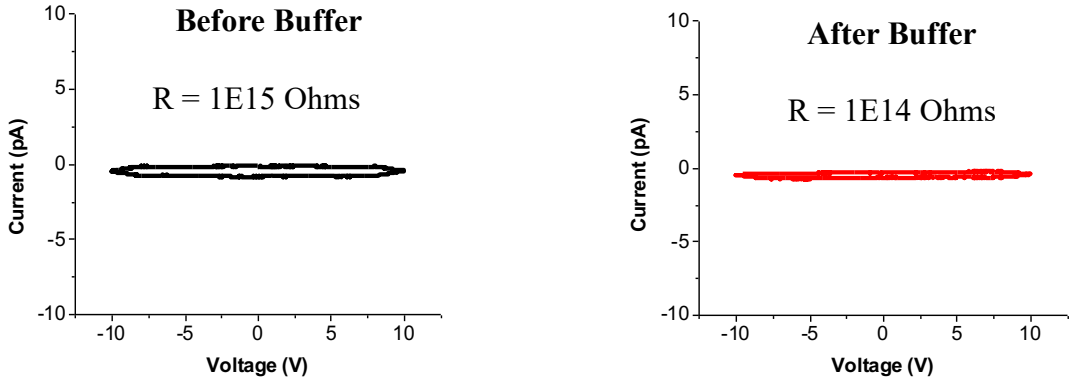

Figure 5.10. IV Curves for DNA Origami Nanowire Buffer (0.5x TBE, 10 mM Mg^{2+}) on EAC vs. Blank EAC (Si_3N_4 Substrate, No HMDS Surface Pre-Treatment, Not Vacuum Dried)

The resistance measurements and statistics (shown above) for a control experiment with the DNA origami buffer solution (0.5X TBE, 10 mM Mg^{2+}), which does not contain any DNA NWs, indicate that the buffer is highly resistive (~1E14 ohms), although the buffer is slightly less resistive than a blank Electrode Array Chip (EAC) (~1E15 ohms). This control experiment indicates that the electrical resistance values (~1E12 ohms) that are measured for the ~1.25 µm long DNA origami 5-mer nanowires are due to the electrical conductivity of the DNA origami 10HB 5-mer nanowires themselves, rather than to the buffer.

Effects of Environment on DNA Origami Nanowires:

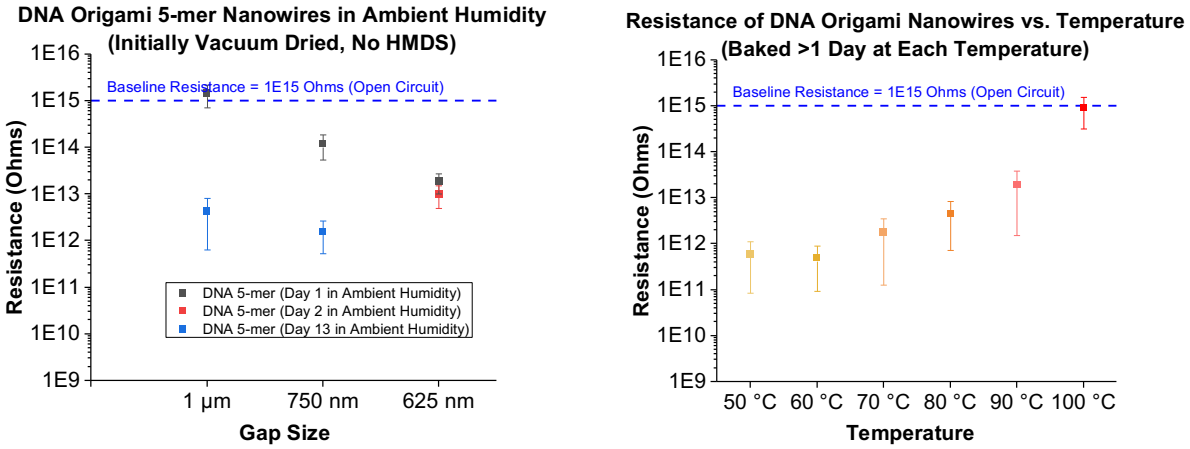

Figure 5.11. Effects of Humidity (Left) and Temperature (Right) on DNA Origami Nanowires

The electrical conductance of DNA NWs that are initially vacuum dried will increase over time as they are exposed to ambient humidity. Elevated temperatures will decrease the electrical conductance of DNA NWs as the temperature increases. These results highlight the importance of water and the importance of the physical structure of DNA NWs for preserving/increasing the electrical conductance of DNA NWs. These environmental sensitivities could be beneficial for some applications as they may allow DNA NWs to be used as humidity and temperature sensors. However, these results also raise questions as to whether the electrical conductivity of the DNA NWs is primarily due to electronic conduction through the DNA NWs themselves or is instead due to ionic conduction of salt ions through the water that is adsorbed onto the DNA NWs. Due to the greater electrical conductivity of DNA NWs in the presence of water/humidity, it seems that water plays an important role in the electrical conductivity of DNA NWs, either through ionic conduction or by affecting the physical structure of the DNA NWs. Therefore, after acquiring these initial results that were collected in an ambient (not vacuum dried) environment, I decided to start vacuum drying the chips prior to collecting electrical measurements, to remove the moisture from the chip and mitigate the effects of water on the electrical conductance of the DNA NWs.

5.4 Conclusion

In conclusion, DNA nanowires have shown promising potential as a material for use in electronics and sensors due to their ability to conduct electricity. However, further research is needed to fully characterize the electrical properties of DNA nanowires and optimize their use in these applications. The electrical measurements of the DNA NWs presented in this study indicate that the DNA NWs are not very conductive at only ~1E12 ohms (~1 teraohm), but that they exhibit some sensitivity to their environment/surroundings, such humidity/moisture vs. dryness. This environmental/experimental sensitivity may provide a vector that could be used to modify or enhance the electrical properties of the DNA NWs. The initial electrical conductivity measurements have provided valuable insights into the behavior of DNA nanowires under various conditions, but more work is needed to fully characterize their performance and increase their electrical conductivity. Overall, the electrical properties of DNA nanowires represent a significant area of active research with the potential to lead to exciting advances in the fields of nanotechnology and electronics. Given that the DNA NWs appear to be sensitive to their environment, it is sensible to further investigate how the structure and electrical properties of DNA NWs are affected by their environment.

Chapter 6: Structure-Dependent Electrical Conductance of DNA Origami Nanowires

Exploring the structural and electrical properties of DNA origami nanowires is an important endeavor for the advancement of DNA nanotechnology and DNA nanoelectronics. Highly conductive DNA origami nanowires are a desirable target for creating low-cost self-assembled nanoelectronic devices and circuits. In this work, the structure-dependent electrical conductance of DNA origami nanowires is investigated. A silicon nitride (Si_3N_4) on silicon semiconductor chip with gold electrodes is used for collecting electrical conductance measurements of DNA origami nanowires, which are found to be an order of magnitude less electrically resistive on Si_3N_4 substrates treated with a monolayer of hexamethyldisilazane (HMDS) (~10^{13} ohms) than on native Si_3N_4 substrates without HMDS (~10^{14} ohms). Atomic force microscopy (AFM) measurements of the height of DNA origami nanowires on mica and Si_3N_4 substrates reveal that DNA origami nanowires are ~1.6 nm taller on HMDS-treated substrates than on the untreated ones indicating that the DNA origami nanowires undergo increased structural deformation when deposited onto untreated substrates, causing a decrease in electrical conductivity. This study highlights the importance of understanding and controlling the interface conditions that affect the structure of DNA and thereby affect the electrical conductance of DNA origami nanowires.

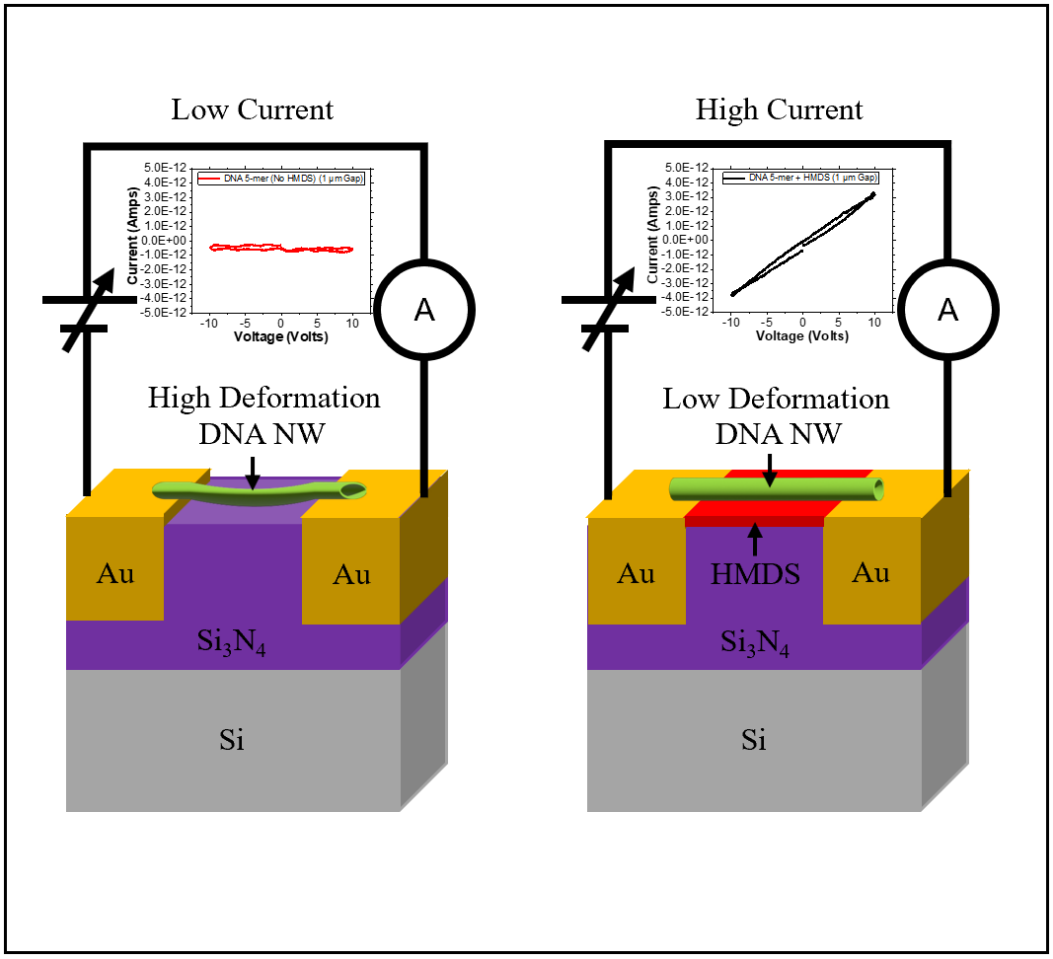

Figure 6.1. Summary of Experimental Results. (Left) A High-Deformation DNA Origami Nanowire (DNA NW) on an Untreated Si_3N_4 Substrate Produces Low Current; (Right) A Low-Deformation DNA Origami Nanowire (DNA NW) on an HMDS-Treated Si_3N_4 Substrate Produces High Current.

6.1 Introduction

Deoxyribonucleic acid (DNA) origami is a novel type of DNA nanotechnology that has the potential to dramatically improve the capability, performance, scalability, and customizability of nanoelectronic devices. The foundational principle of DNA origami is the molecular folding of a long single scaffold strand of DNA (often the M13mp18 scaffold strand, with 7,249 bases) by using short custom-designed DNA staple strands that hybridize with the long DNA scaffold strand in specific locations to fold and hold the scaffold strand in the designed shape [26]. DNA origami is a structural DNA nanotechnology that can be used to synthesize and create an enormous variety of DNA nanostructures such as DNA wires, DNA nanopores, and even DNA smiley faces [27]. These DNA nanostructures have been designed and synthesized in one, two, or three dimensions [28]; in twisted or curved topologies [29], [30]; and structured into a variety of polyhedrons [31]. Larger structures can be formed using origami tiles or unit cells that can connect together in repeating patterns [32], which has resulted in systems up to the gigadalton scale [33]. As the DNA origami technology is improving, the yields are increasing while the costs are decreasing, and it is now estimated that 1 gram of DNA origami can be produced for only $200 [34], [35]. These expanding capabilities in DNA nanotechnology are enabling new applications where low cost, high scalability, and nanoscale precision are needed.

DNA origami provides unprecedented opportunities for designing hybrid nanomaterials from the bottom-up by allowing nanoscale precision assembly, integration, and functionalization with many degrees of design freedom [36]. In fact, DNA origami allows for nanomaterials to be placed precisely in a regularly repeating pattern with a pitch of only ~3.4-3.6 nm along the DNA strand, while the DNA duplex has a diameter of only ~2 nm [37]. DNA origami is also very durable and is able to survive a wide range of environmental conditions and chemical environments [38],

[39]. DNA origami structures have been functionalized with a wide range of other molecules, biomarkers, fluorescent dyes, and inorganic materials such as gold nanoparticles [40], [41], [42], [43], [44], [45], [46]. These versatile design parameters that encompass DNA origami provide a unique repertoire for designing DNA origami nanowires (DNA NWs) that could enable applications such as DNA nanoelectronics.

The field of DNA nanoelectronics has primarily focused on measuring the electrical conductivity of short double-stranded DNA (dsDNA) duplexes [47], [48]. These studies indicate that dsDNA is able to transport charges effectively for short duplexes (up to ~10 nm), but that it is incredibly sensitive to a variety of factors including the sequence, conformation/morphology, local environment, the metal-molecule contact (e.g., gold-thiol bond), and substrate interactions [76], [111], [63]. These variables can have a profound effect on the charge transport properties of dsDNA, changing the conductance over many orders of magnitude [112], [113]. These results all indicate that DNA is a versatile material with many parameters that could be engineered to exhibit desirable electronic properties in designed structures such as DNA origami.

Similar to dsDNA duplexes, initial studies of DNA origami systems have yielded resistance values that have varied over a wide range (~70 MΩ - ~20 GΩ) [79], [80]. Given this variability, it is likely that many of the confounding variables identified in the study of dsDNA could also affect the electrical conductivity of DNA origami. Due to the many potential advantages that DNA origami could provide for nanoelectronics and the variety of factors that affect the electrical conductivity of DNA origami, this study seeks to begin examining how these environmental factors impact the electrical properties of DNA origami. In particular, we will focus on structure-dependent changes in the electrical conductance of DNA NWs due to interactions with the

substrate, as these structures are the most fundamental and important circuit elements required for enabling DNA nanoelectronics.

To examine the structure-dependent electrical conductance of DNA NWs, this paper studies the structural and electrical properties of DNA NWs, as overviewed in **Figure 6.2**. The DNA NWs that are utilized in this paper are custom-designed and assembled using standard DNA origami synthesis/folding techniques [23], [3], [98]. The two DNA NW designs that are used in this study are a 6-helix bundle dimer nanowire (6HB NW), and a 10-helix bundle pentamer (5-mer) nanowire (10HB NW). The 6HB NW (Figure 6.2a) is ~800 nm long, consisting of two connected ~400 nm long monomers folded into a ~5 nm wide single-barrel tube shape. The 10HB NW (Figure 6.2b) is ~1.25 μm long and consists of five connected ~250 nm long monomers folded into a ~10 nm wide double-barrel tube shape. Each end of both DNA NWs contains 5 thiols to assist with the binding to the gold electrodes [107], [108], [109], [110]. To assist with imaging the DNA NWs using fluorescence microscopy, the DNA NWs are modified to include Alexa 488 fluorophores attached along the length of the DNA NWs. For example, there are ~120 equally spaced Alexa 488 fluorophores along the ~1.25 μm long 10HB NW which emit green fluorescence upon excitation, as shown in Figure 6.2f. The fluorescence images allow for identification of the precise locations where the DNA NWs are deposited onto the substrate/chip used for electrical measurements, known as the Electrode Array Chip (EAC). A device of the EAC is shown in Figure 6.2e, with gold electrodes separated by 1 μm silicon nitride (Si_3N_4) gaps where the DNA NWs can be deposited and form electrical connections between the gold electrodes. As shown in Figure 6.2c and Figure 6.2d, a hexamethyldisilazane (HMDS) surface treatment can optionally be applied to change the surface properties of the substrate. This HMDS surface treatment can affect the properties of the DNA NW, such as its height/thickness and electrical conductivity. In this study,

atomic force microscopy (AFM) and electrical measurements are utilized to observe that an HMDS surface treatment increases the height/thickness of DNA NWs and increases their electrical conductivity.

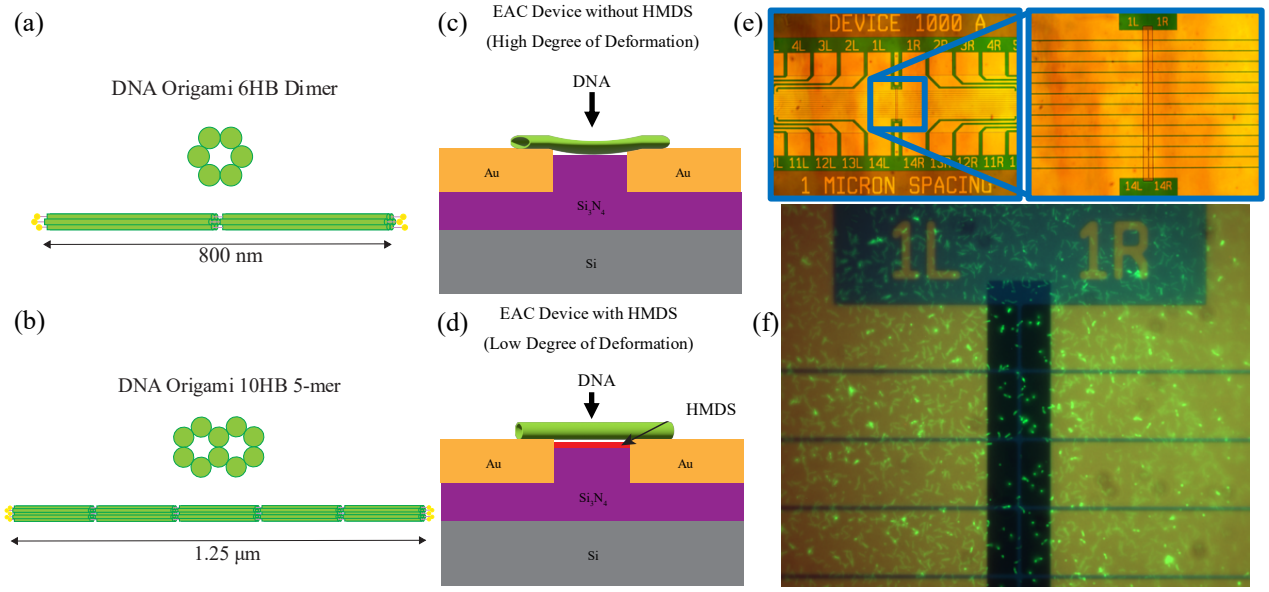

Figure 6.2. Overview of Experiment. (a) DNA Origami 6-Helix Bundle (6HB) Dimer Nanowire (6HB NW) Folded Structure and Nanowire Diagram; (b) DNA Origami 10-Helix Bundle (10HB) 5-mer Nanowire (10HB NW) Folded Structure and Nanowire Diagram; (c) Cutaway Profile of Electrode Array Chip Device without HMDS and with DNA Deformed on the Surface; (d) Cutaway Profile of Electrode Array Chip Device with HMDS and with DNA Structure Intact; (e) Electrode Array Chip (EAC) Device for Electrical Measurements of DNA Origami Nanowires (DNA NWs); (f) Fluorescence Microscopy Image of 10HB NWs Bridging Gold Electrodes with 1 µm Gaps on EAC.

6.2 Results and Discussion

6.2.1 Atomic Force Microscopy (AFM) Measurements of DNA NWs on Substrates

AFM is used to acquire images and topographical data of the 6HB NWs and 10HB NWs on mica and Si_3N_4 substrates with and without HMDS surface treatments. This topographical data is used to measure the height and structural properties of DNA NWs under these different surface conditions. All the AFM images and data are acquired with in-air imaging conditions. **Figure 6.3** displays some individual examples of the AFM imaging results and topological data for the DNA NWs. Figure 6.3a shows an example AFM image of a 6HB NW on mica. Figure 6.3b shows examples of individual perpendicular trace profiles of 6HB NWs for the different surface conditions (mica with HMDS, mica without HMDS, Si_3N_4 with HMDS, Si_3N_4 without HMDS). Figure 6.3c shows an example AFM image of a 10HB NW on Si_3N_4. Figure 6.3d shows examples of individual perpendicular trace profiles of 10HB NWs for the different surface conditions. For both the 10HB NW and the 6HB NW, and for both the mica and Si_3N_4 substrates, the DNA NWs appear to be taller when an HMDS surface treatment is applied to the substrate.

AFM height data for the DNA NWs with different surface conditions are displayed in **Figure 6.6**. This figure shows the individual DNA NW height data (10 nanowires per system) on the left, and the statistical/average DNA NW height data on the right. Data for the 6HB NW is shown on top, and data for the 10HB NW is shown on the bottom. When comparing the average data, the results are similar for the 6HB NW and the 10HB NW data, demonstrating a consistent effect across different DNA NW designs/structures. Data is displayed both for DNA NWs on substrates without HMDS (red data) and with HMDS (black data). Figure 6.6a shows AFM data for the height measurements of individual 6HB NWs with the different surface conditions. Figure 6.6b displays statistical results for the AFM data, showing the average height of the 6HB NWs for

each surface condition. Figure 6.6c shows AFM data for the height measurements of individual 10HB NWs with the different surface conditions. Figure 6.6d displays statistical results for the AFM data, showing the average height of the 10HB NWs for each surface condition. The AFM height measurement data indicates that for both the 6HB NWs and the 10 HB NWs, and for both the mica substrate as well as the Si_3N_4 substrate, the height of the DNA NWs is taller when the substrate is treated with HMDS (black data) and is shorter when not treated with HMDS (red data). The HMDS surface treatment appears to make a more significant difference in height for the Si_3N_4 substrate.

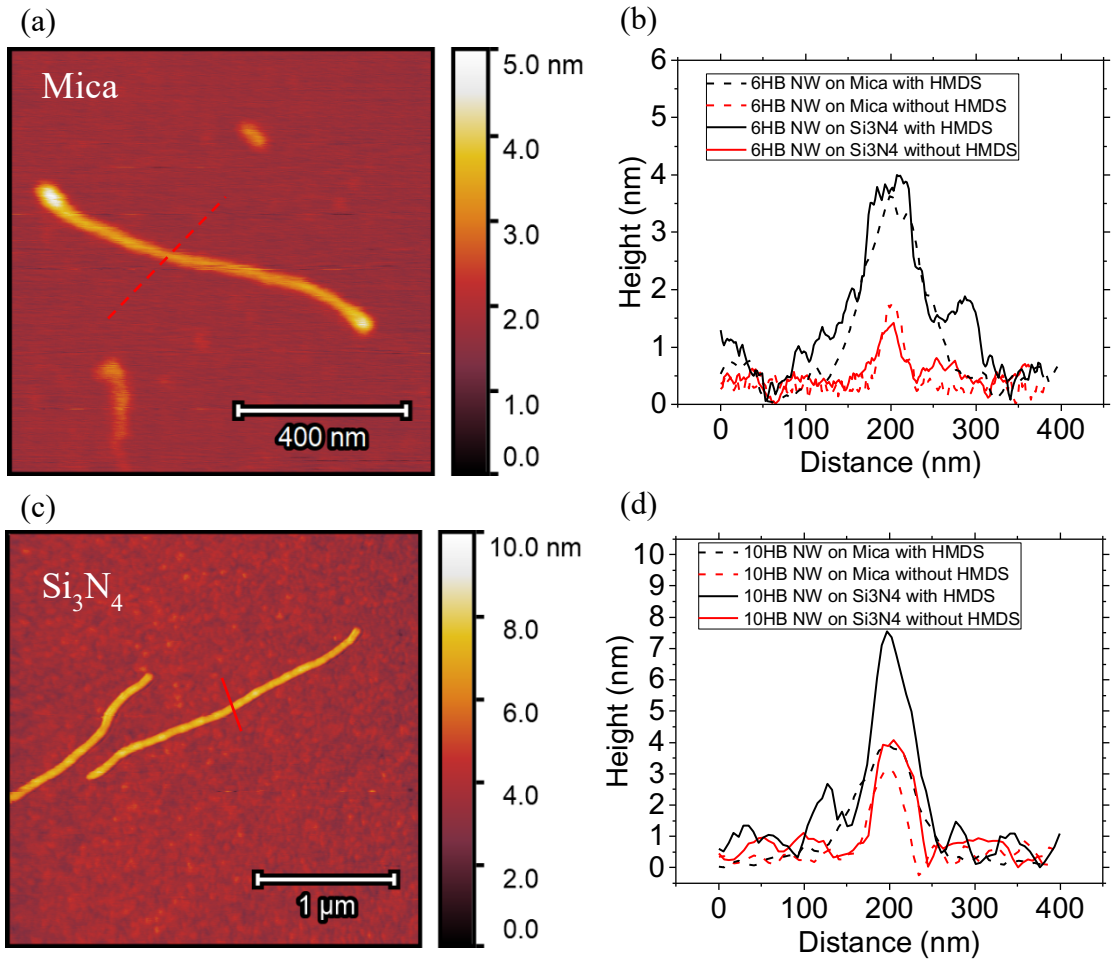

Figure 6.3. AFM Results for Height of DNA NWs on Substrates. a) AFM Image of 6HB NW on Mica without HMDS; b) Trace Profiles of Measurements of Height of 6HB NW on Substrates (Mica with HMDS, Mica without HMDS, Si_3N_4 with HMDS, Si_3N_4 without HMDS); c) AFM Image of 10HB NW on Si_3N_4 without HMDS; d) Trace Profiles of Measurements of Height of 10HB NW on Substrates (Mica with HMDS, Mica without HMDS, Si_3N_4 with HMDS, Si_3N_4 without HMDS). Trace profiles correspond to line sections taken perpendicular to the DNA NW and are used to acquire the DNA NW height data. Additional details including individual AFM images and separate trace profiles for each combination of nanowire, substrate, and surface treatment are shown in **Figure 6.4** and **Figure 6.5**.

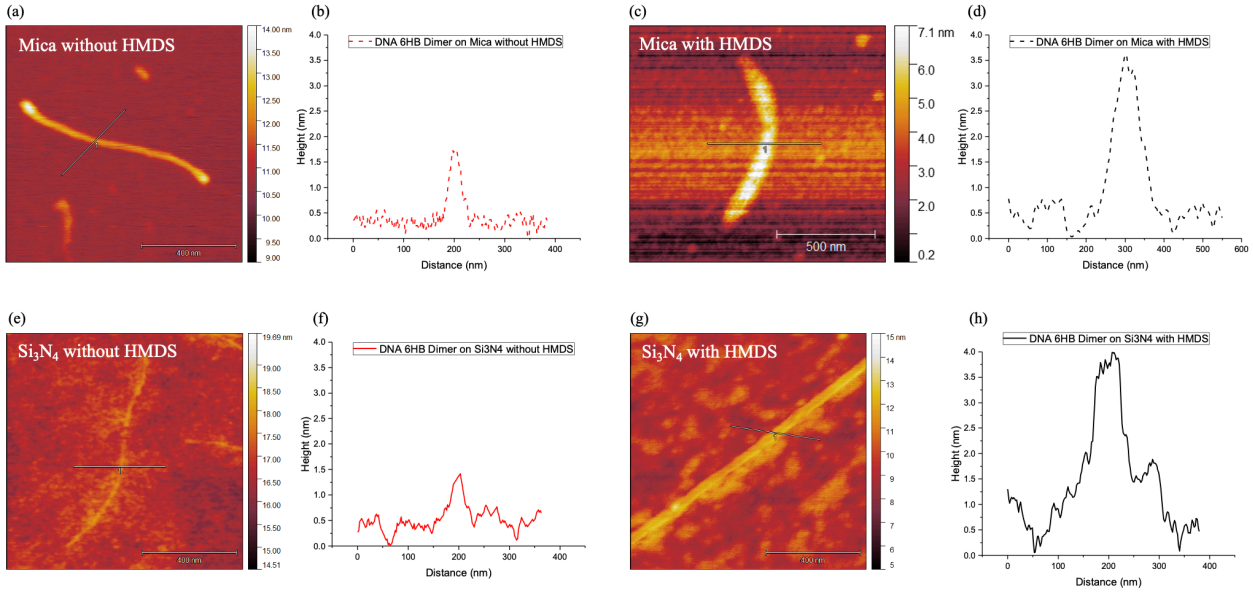

Figure 6.4. AFM Images and Trace Profiles for 6HB NWs on Substrates (Mica and Si_3N_4) without and with HMDS. a) AFM Image of 6HB NW on Mica without HMDS; b) AFM Trace Profile of 6HB NW on Mica without HMDS; c) AFM Image of 6HB NW on Mica with HMDS; d) AFM Trace Profile of 6HB NW on Mica with HMDS; e) AFM Image of 6HB NW on Si_3N_4 without HMDS; f) AFM Trace Profile of 6HB NW on Si_3N_4 without HMDS; g) AFM Image of 6HB NW on Si_3N_4 with HMDS; h) AFM Trace Profile of 6HB NW on Si_3N_4 with HMDS.

Examples of individual AFM images and trace profiles for 6HB NWs on substrates with and without HMDS is shown in **Figure 6.4**, which indicates that 6HB NWs are taller on HMDS-treated substrates than on untreated substrates. An HMDS surface treatment appears to be effective at reducing the structural/height deformation of 6HB NWs on both mica substrates and Si_3N_4 substrates.

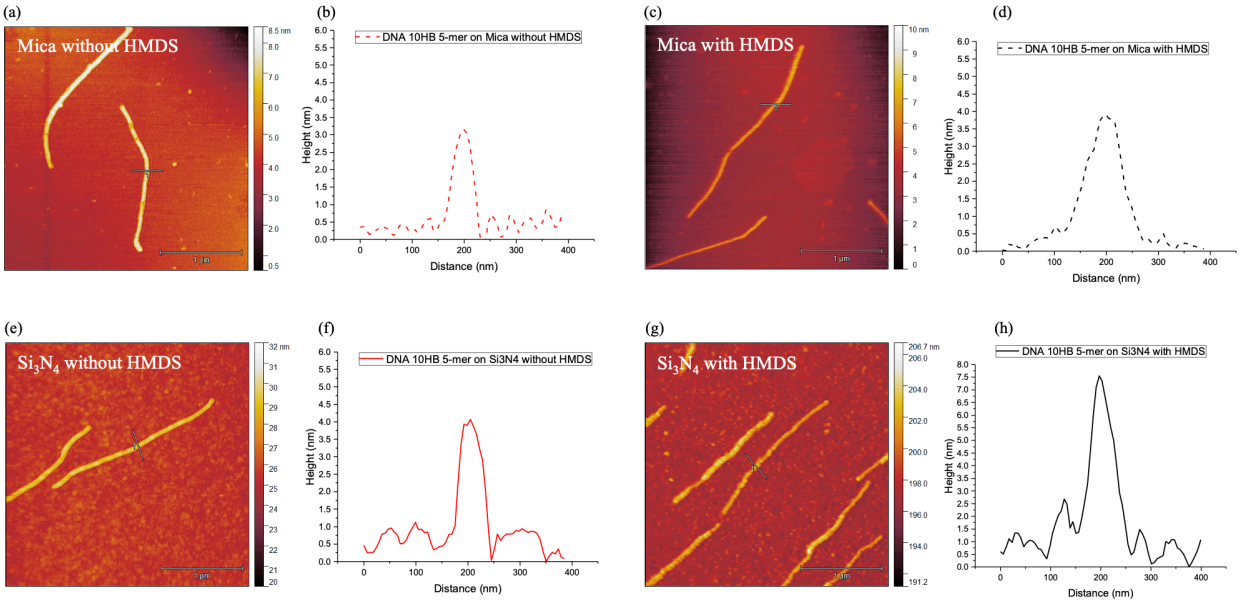

Figure 6.5. AFM Images and Trace Profiles for 10HB NWs on Substrates (Mica and Si_3N_4) without and with HMDS. a) AFM Image of 10HB NW on Mica without HMDS; b) AFM Trace Profile of 10HB NW on Mica without HMDS; c) AFM Image of 10HB NW on Mica with HMDS; d) AFM Trace Profile of 10HB NW on Mica with HMDS; e) AFM Image of 10HB NW on Si_3N_4 without HMDS; f) AFM Trace Profile of 10HB NW on Si_3N_4 without HMDS; g) AFM Image of 10HB NW on Si_3N_4 with HMDS; h) AFM Trace Profile of 10HB NW on Si_3N_4 with HMDS.

Examples of individual AFM images and trace profiles for 10HB NWs on substrates with and without HMDS are shown in **Figure 6.5**, which indicates that 10HB NWs are taller on HMDS-treated substrates than on untreated substrates. An HMDS surface treatment appears to be effective at reducing the structural/height deformation of 10HB NWs on both mica substrates and Si_3N_4 substrates.

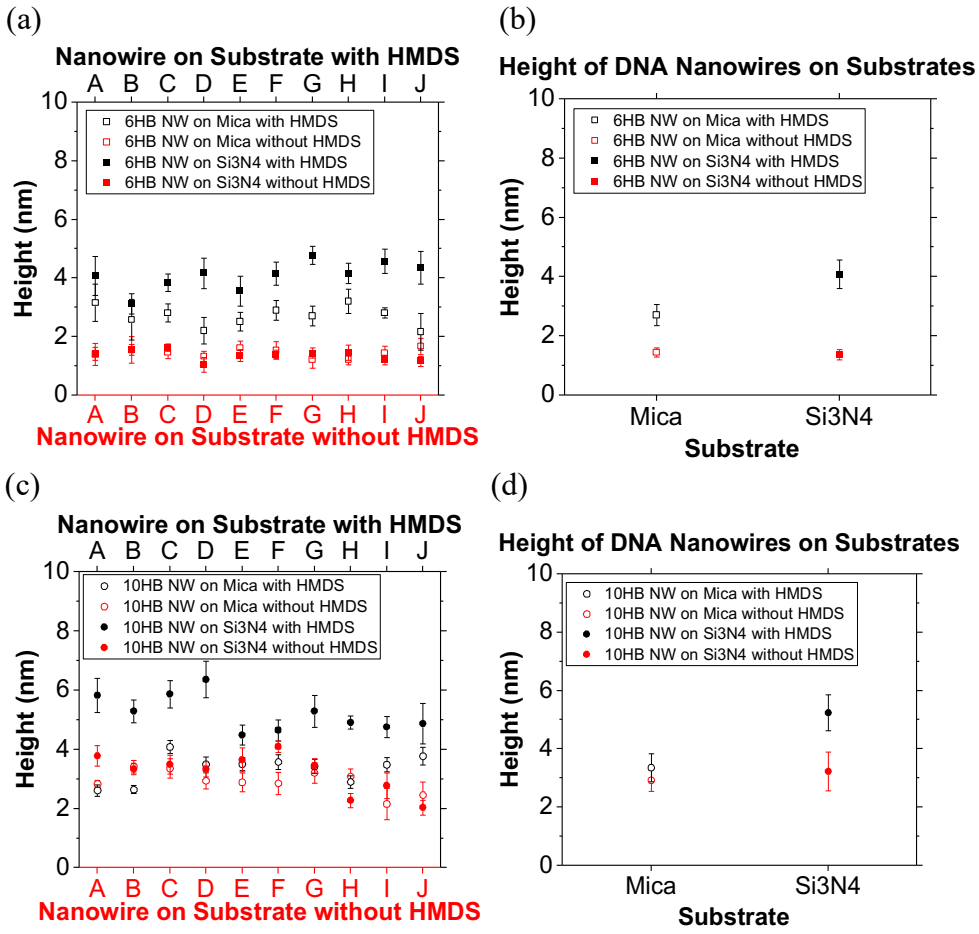

Figure 6.6. Statistical Measurement of DNA NW Heights with and without HMDS. a) Individual Nanowire Height Data for 6HB NWs; b) Statistics for 6HB NW Height Data; c) Individual Nanowire Height Data for 10HB NWs; d) Statistics for 10HB NW Height Data. Note that each letter A-J denotes a different nanowire for each condition.

The AFM height measurement data shows that the DNA NWs (6HB NWs and 10HB NWs) are taller on substrates (mica and Si_3N_4) that are treated with HMDS and are shorter on substrates without HMDS. A summary of the AFM average height measurements for the DNA NWs is shown in **Table 6.1**. The measurements from the AFM studies indicate that the structure of DNA NWs is strongly affected by their interaction with substrate surfaces. The height of these DNA NWs is reduced by 1 to 2 nm when deposited onto the untreated substrates. This deformation in the height of the DNA can be explained by a combination of electrostatic forces and van der Waals forces [114], [115]. More generally, this DNA height dependency on different substrates under different surface conditions may be described as DNA-substrate interactions [116]. DNA is negatively charged due to its sugar-phosphate backbone and its structure is sensitive to electrostatic charges such as surface charge [117], [118], [119]. However, passivating the surface of the Si_3N_4 substrate with chemical/molecular monolayers such as HMDS may help to mitigate the interaction between the DNA NW and the substrate as the chemical monolayer increases the distance between the DNA NW and the substrate and changes the surface chemistry or surface charge density of the interface. HMDS converts the surface properties of substrates such as Si_3N_4 from hydrophilic to hydrophobic. The cumulative effect of these different modifications to the surface properties of HMDS-treated substrates could explain why HMDS evidently reduces the extent of the DNA NW structure/height deformation.

Table 6.1. Summary of Atomic Force Microscopy (AFM) Results for Average Height Measurements of 6HB NWs and 10HB NWs on Substrates with and without HMDS.

DNA Nanowire	Substrate	With or Without HMDS	Average Height [nm]
DNA 6HB Dimer	Mica	without HMDS	1.4 +/-0.2
DNA 6HB Dimer	Mica	with HMDS	2.7 +/-0.4
DNA 6HB Dimer	Si_3N_4	without HMDS	1.4 +/-0.2
DNA 6HB Dimer	Si_3N_4	with HMDS	4.1 +/-0.5
DNA 10HB 5-mer	Mica	without HMDS	2.9 +/-0.4
DNA 10HB 5-mer	Mica	with HMDS	3.4 +/-0.5
DNA 10HB 5-mer	Si_3N_4	without HMDS	3.2 +/-0.7
DNA 10HB 5-mer	Si_3N_4	with HMDS	5.2 +/-0.6

6.2.2 Electrical Measurements of DNA NWs on EAC

Finally, to examine the effects of this mechanical deformation on the electrical properties of the DNA NWs we measure the I-V characteristics of the DNA NWs without HMDS and with HMDS as shown in **Figure 6.7**. These resistance measurement results show that the electrical resistance of vacuum dried 10HB NWs without HMDS on Si_3N_4 is very high, between 10^{14} and 10^{15} ohms, which is similar to values obtained on blank samples, as seen in **Figure 6.8**. When HMDS is applied to the Si_3N_4 substrate/chip and the DNA NWs are deposited onto the chip, these resistance measurements and statistics show that the 10HB NWs are more electrically conductive (between 10^{12} and 10^{13} ohms). The high electrical resistance of the 10HB NWs without HMDS appears to be caused by the deformation in the structure or height of the DNA NW. The results from the AFM study show that DNA NWs get deformed on substrates such as Si_3N_4 and mica that are not treated with HMDS, and that treating these substrates with HMDS can mitigate DNA NW deformation. It has previously been demonstrated that the electrical properties of DNA are acutely sensitive to the structure of the duplex [56], [53]; and in this case, it appears that deforming the structure of the DNA NW reduces the electrical conductivity of the DNA NW. This structural deformation could disrupt the overlapping of stacked π orbitals of the nucleic acids in the DNA helices by distorting the alignment and angle of each nucleic acid [120]. Electrical conduction in DNA is theorized to occur primarily through the overlapping π orbitals of adjacent nucleic acids, so disruption to the structure of this electrical pathway could be a critical mechanism that affects the electrical conductance of the DNA NW [121], [62]. Preserving the structural integrity of the DNA NW by applying HMDS to the substrate also appears to increase the electrical conductance of the DNA NWs. The electrical measurements and current-voltage (I-V) curves that are shown above for DNA NWs with and without HMDS help to visualize the profound impact that an HMDS surface pre-treatment has on increasing (or preserving) the electrical conductivity of DNA NWs.

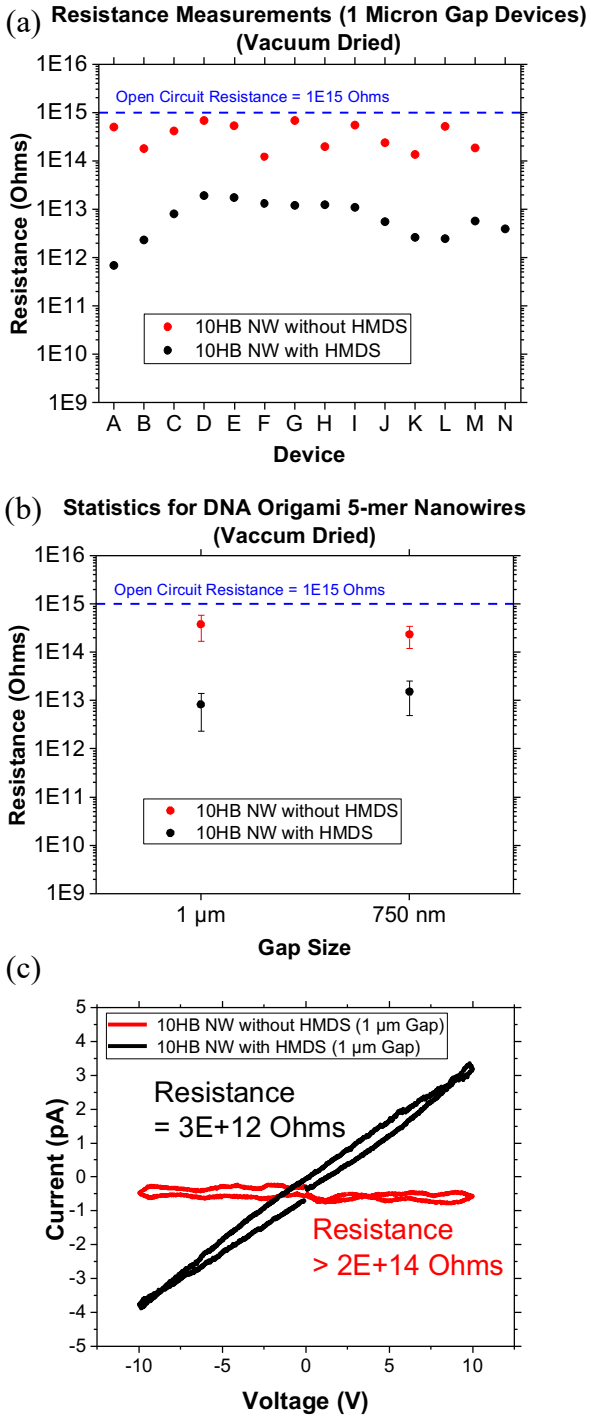

Figure 6.7. Results for Electrical Resistance Measurements of 10HB NWs on EAC without HMDS and with HMDS. a) Individual Resistance Measurement Values for 1 Micron Gap Devices of EAC; b) Statistics for 1 Micron Gap and 750 nm Gap Devices of EAC; c) Current-Voltage Curves for 10HB NWs on 1 Micron Gap Devices of EAC. All Samples are Vacuum Dried. The EAC Substrate Consists of Si_3N_4 with/without HMDS.

Control Experiments:

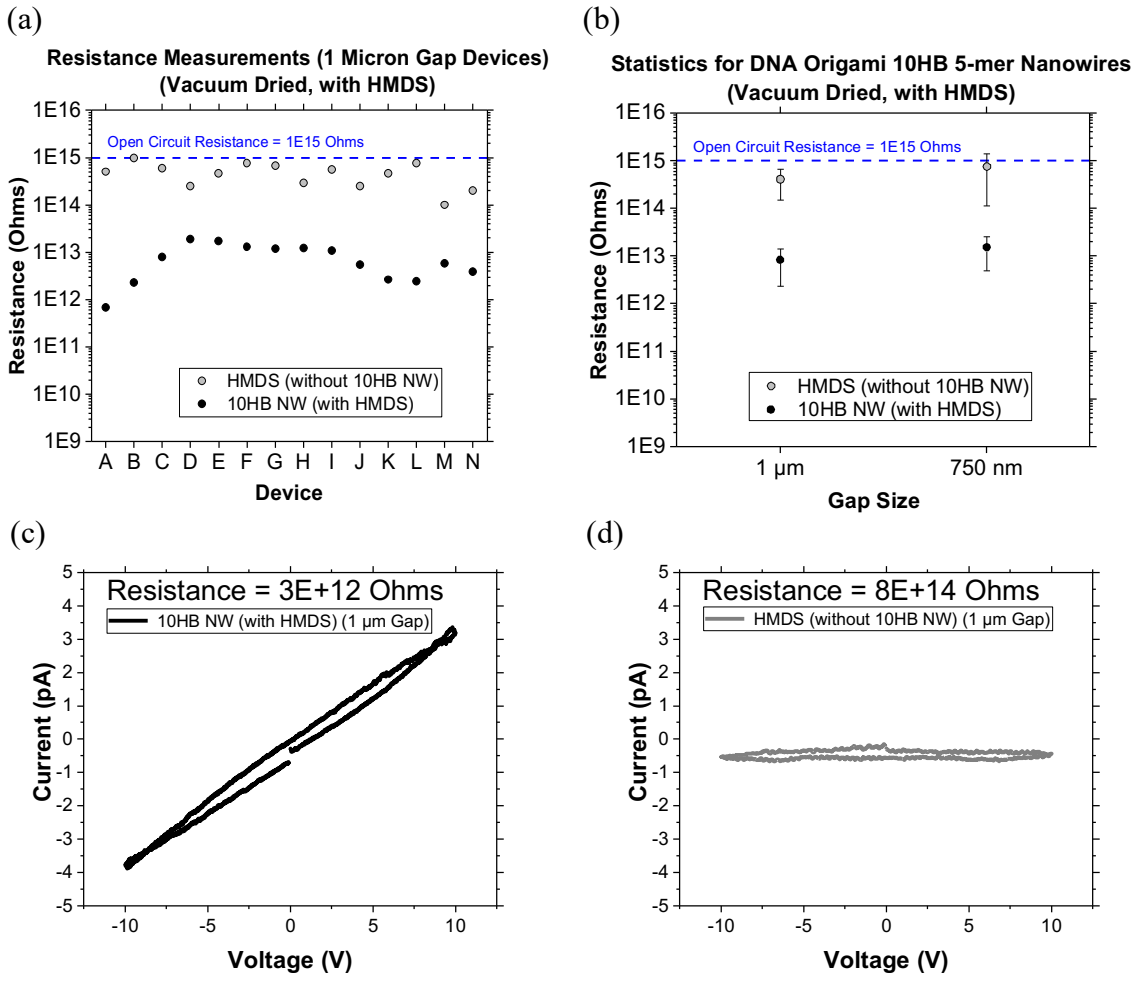

Figure 6.8. Resistance Results for HMDS (without 10HB NWs) and 10HB NWs (with HMDS) on the Electrode Array Chip (Si_3N_4 Substrate, Vacuum Dried). a) Resistance Measurements; b) Statistics; c) Current-Voltage Curve of 10HB NW on Si_3N_4 with HMDS Surface Treatment (Black); d) Current-Voltage Curve of HMDS Treatment on Si_3N_4 without 10HB NW (Gray).

The resistance measurements and current-voltage (I-V) curves shown in **Figure 6.8** indicate that when HMDS is applied to the silicon nitride (Si_3N_4) substrate/chip and then DNA NWs are deposited onto the chip, the 10HB NWs are somewhat electrically conductive (black data, between 10^{12} and 10^{13} ohms). The electrical measurement results are also shown for a Si_3N_4 substrate/chip treated with HMDS before the DNA NWs are deposited onto the chip, which results

in very high electrical resistance (gray data, between 10^{14} and 10^{15} ohms). These combined results indicate that the increased electrical conductance is due to the DNA NWs with HMDS, rather than simply being due to the HMDS alone without the DNA NWs. This demonstrates that the large increase (or preservation) of the electrical conductivity of samples with HMDS-treated substrates is due to enhanced electrical conductivity through the DNA NWs rather than through the HMDS surface treatment. We observe that HMDS-treated substrates without DNA NWs are less electrically conductive than the same HMDS-treated substrates with DNA NWs.

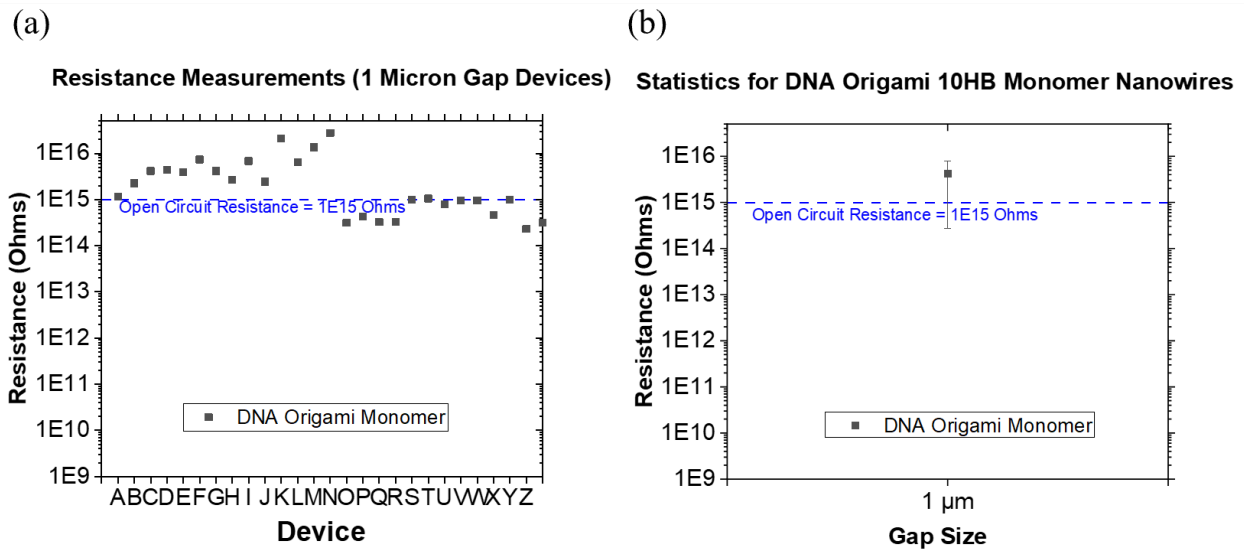

Figure 6.9. Resistance Results for DNA Origami 10HB Monomer Nanowires on the Electrode Array Chip (Si_3N_4 Substrate, Vacuum Dried). a) Resistance Measurements; b) Statistics.

The resistance measurements and statistics shown in **Figure 6.9** were acquired for DNA origami 10HB monomer nanowires on 1 micron gap devices of the Electrode Array Chip (EAC). The length of each DNA origami 10HB monomer nanowire is ~250 nm, while the gap between the gold electrodes is ~1 micron (~1000 nm). Therefore, it is not possible for the DNA origami 10HB monomer nanowire to bridge the silicon nitride insulator gap and make electrical contact with a pair of gold electrodes. The electrical resistance measurements and statistics for the DNA origami 10HB monomer nanowires on 1 micron gap devices of the EAC indicate a resistance between 10^{15} and 10^{16} ohms (equivalent to an open circuit), which indicates that the DNA origami 10HB monomer nanowires are too short to make electrical contact with the gold electrodes. These high resistance electrical measurements also serve as a control experiment upon which to compare the much lower resistance electrical measurements of the >1 micron long DNA origami 10HB 5-mer nanowires, which are long enough to bridge the ~1 micron gaps and contact the gold electrodes.

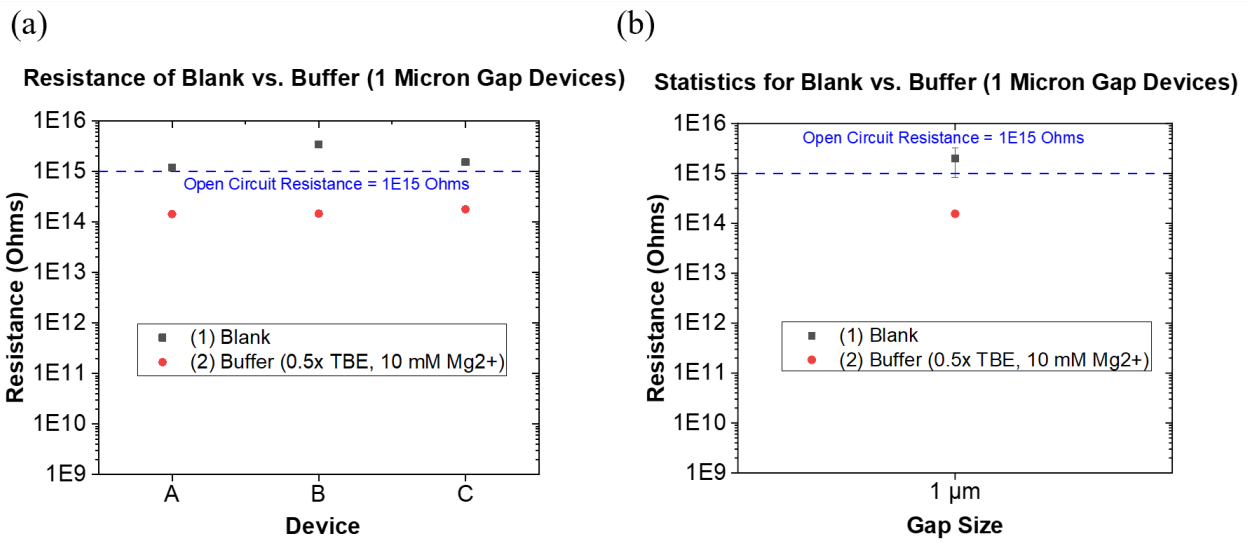

Figure 6.10. Resistance Results for Blank (No Buffer) and Buffer (0.5x TBE, 10 mM Mg^{2+}) on the Electrode Array Chip (Si_3N_4 Substrate, Vacuum Dried). a) Resistance Measurements; b) Statistics.

The resistance measurements and statistics shown in **Figure 6.10** were acquired for the 1 micron gap devices of the Electrode Array Chip (EAC), both for a blank chip (without buffer) and for a chip with buffer (0.5x TBE, 10 mM Mg^{2+}). These electrical resistance measurements and statistics indicate that a blank EAC has a very high electrical resistance between 10^{15} and 10^{16} ohms (equivalent to an open circuit). The electrical measurements and statistics for the buffer (0.5x TBE, 10 mM Mg^{2+}) on the EAC indicate a slightly lower electrical resistance between 10^{14} and 10^{15} ohms. Both the blank EAC and the EAC with buffer have much higher electrical resistance values than the electrical resistance measurements/statistics of the 10HB NWs (between 10^{12} and 10^{13} ohms). Therefore, the blank vs. buffer resistance measurements and statistics serve as a useful control experiment which serve as a resistance baseline for comparison and validation of the more conductive electrical measurement results for the 10HB NWs.

6.3 Conclusion

This work demonstrates that the structural integrity of DNA NWs varies on different substrates with and without a molecular monolayer surface treatment, and that the electrical conductance of the DNA NWs critically depends on these interface-driven structural changes. AFM is used to measure the height of DNA NWs on substrates such as Si_3N_4 and mica, with and without an HMDS surface treatment. The AFM measurements reveal that the HMDS surface treatment increases the height of the DNA NWs by 1.6 +/-0.8 nm. Electrical measurements acquired for DNA NWs on Si_3N_4 substrates with and without HMDS demonstrate that the electrical resistance of the DNA NWs decreases by about an order of magnitude from ~10^{14} ohms to ~10^{13} ohms when the substrate is surface treated with HMDS. The results from this study indicate that the height or structural integrity of DNA NWs and their electrical conductivity critically depend upon the DNA-substrate interaction, which can be mitigated by applying an HMDS surface treatment to the substrate before depositing the DNA NWs. Applying an HMDS surface treatment to Si_3N_4 substrates creates a significant increase in the electrical conductivity and the height of the DNA NWs by mitigating the structural deformation of DNA NWs on Si_3N_4 substrates. These results highlight the potential for DNA NWs to be used in nanoelectronic devices. The microfabricated semiconductor chip with lithographically defined gold electrodes and submicron gaps demonstrates a useful platform for measuring the electrical conductivity of nanoscale electronic materials such as DNA NWs. The demonstrated technique and platform may serve as a foundation for further improving and measuring the electrical conductivity of DNA nanoelectronic devices.

6.4 Experimental Section

Design and Assembly of DNA Origami Nanowires (DNA NWs): The 10-helix bundle (10HB) pentamer (5-mer) nanowire and the 6-helix bundle (6HB) dimer nanowire are designed to have adequate length and rigidity for bridging gold electrodes that are separated by submicron gaps. The design software caDNAno is used to design the staple sequences for the 10HB NW and the 6HB NW. To assemble the DNA NWs with fluorophores for fluorescence imaging, 17 selected staples along the 10HB monomer and 12 staples along the 6HB monomer are modified with 3' handles extending outside the bulk of the DNA origami monomer. These handle sequences are complimentary to DNA strands fluorescently modified with Alexa 488 fluorophores from Integrated DNA Technologies (IDT). The yield of completely intact DNA NWs purified by agarose gel electrophoresis (AGE) is approximately 50%. To assemble the 10HB monomers into a long 5-mer nanowire, five unique sets of sticky ends used to connect the individual monomers end-to-end are designed. For the beginning of the first DNA origami monomer and the end of the last, the sticky ends are designed to capture a thiol-modified DNA strand. Five batches of 10HB origami monomers are first assembled separately – each with their own set of unique sticky ends. For the 6HB dimer, two differently designed 6HB monomers are first assembled and each of them has one end exposed for connector strands. Four connector strands bind with both 6HB monomers and connect them into a dimer nanowire. The other end of both 6HB monomers has sticky ends for thiol-modified DNA strands. The 10HB monomers in each batch are assembled with p8064 DNA scaffold strands (20 nM), DNA staples/sticky ends (100 nM each), Alexa 488 modified DNA (2.5 μM), thiol modified DNA (500 nM) in the first and last DNA origami monomers, and 1X TE buffer consisting of Tris (10 mM) and EDTA (1 mM) supplemented with Mg^{2+} (12.5 mM). A 2-hour annealing protocol is used, starting at 95 °C for 5 minutes, then stepping from 85 °C to 25 °C

for 2 minutes at each degree. Next all 10HB monomers are mixed and incubated at 42 °C for 12 hours to allow the sticky ends to connect the 10HB monomers together to form the 10HB NWs. The 6HB monomer goes through the same protocol with p7308 DNA scaffold strands but without the sticky ends. Instead, the two 6HB monomers are mixed with a 10x higher concentration of the connector strands and incubated at 42 °C for 12 hours to connect the 6HB monomers together to form the 6HB NWs. Later, the DNA NWs are subjected to agarose gel electrophoresis in 0.8% agarose in 0.5X TBE buffer consisting of Tris (45 mM) and boric acid (45 mM) and EDTA (1 mM) supplemented with Mg^{2+} (10 mM). The assembled 10HB NW and 6HB NW DNA bands in the gel are excised and purified with Freeze 'N Squeeze spin columns. Samples can be stored at room temperature for up to a month.

Design and Fabrication of the Electrode Array Chip (EAC): The experimental substrate that is used to electrically measure the DNA origami nanowires (DNA NWs) is a custom-designed microchip referred to as the Electrode Array Chip (EAC). The EAC is designed using a software program called L-Edit. The EAC is microfabricated from a ~300 nm thick low-pressure chemical vapor deposition (LPCVD) silicon nitride (Si_3N_4) film on a silicon (Si) wafer, with arrays of ~50 nm thick gold electrodes that are separated by small (micron or submicron) gaps. Each device on the chip contains 14 pairs of gold electrodes that are separated by these small gaps. There are 5 types of devices, which have different gap sizes: 1 micron, 750 nm, 625 nm, 500 nm, and 250 nm. There are 10 devices of each gap size on the chip, so with the 5 different types/sizes of devices there are a total of 50 devices on each chip. Since each device has 14 pairs of gold electrodes, there are up to 700 pairs of gold electrodes on each chip that can be used for electrical measurements. There are two layers of the EAC that are patterned using photolithography. The first layer consists of the ~50 nm thick gold electrodes on the LPCVD Si_3N_4. On top of the first layer of the chip there

is a second layer of ~100 nm thick Si_3N_4 which is deposited with plasma-enhanced chemical vapor deposition (PECVD). This top Si_3N_4 layer is used to encapsulate and protect most of the area of the gold electrodes from the DNA NW solution that is deposited onto the chip. There are small openings or windows in the ~100 nm thick PECVD Si_3N_4 encapsulation layer that allow the DNA NWs to be deposited onto the device areas, where the DNA NWs are desired to bridge the gold electrodes. The gold contact pads are also exposed to allow for contact with electrical measurement probes.

Surface Treatment of the Substrate with HMDS: The substrate (e.g., Electrode Array Chip, SiO_2, Si_3N_4, sapphire, mica) can be surface treated with a chemical/molecular self-assembled monolayer (SAM). This surface treatment has the effect of passivating the surface of the substrate, as well as insulating the DNA NWs with a molecular barrier between the DNA NWs and the surface of the substrate. For this experimental investigation, the surface treatment of the substrate is accomplished by depositing and spin-coating an HMDS chemical/molecular coating on the surface of the substrate to modify the surface properties of the substrate to make it hydrophobic/hydrophilic and/or change the surface charge/chemistry of the substrate and passivate the substrate. The technique used in this experimental research study to create a passivated surface with an HMDS monolayer is as follows: The substrate is cleaned with a ~1-minute O_2 plasma etch just prior to the surface treatment. The substrate is prebaked at 150 °C for 30 minutes on a hot plate to dehydrate the substrate. The substrate is allowed to cool down to room temperature for 1 minute before applying the HMDS. The HMDS is applied to coat the entire substrate, and any visible bubbles are removed. The substrate with HMDS is spun at 1000 RPM for 45 seconds on a spin coater. The substrate is baked at 110 °C for 1 minute to thermally activate the HMDS.

Depositing DNA NWs onto the Substrate: The DNA NW solution (either 6HB NW or 10HB NW) is prepared by using a micropipette to disperse the DNA NW stock solution by gently pipetting the DNA NW stock solution up and down a few times, and then depositing 5 μL of the ~5 ng μL^{-1} (100 pM – 1 nM) DNA NW stock solution into a new clean microcentrifuge tube. Then 20 μL of ultrapure (18.2 Megaohm-cm) DI water is pipetted into the same microcentrifuge tube. The combined ~1 ng μL^{-1} working solution is pipetted up and down several times to mix it all together. The mixed solution is deposited onto the substrate or chip. The orientation of the DNA NWs can be controlled by gently pipetting the solution across the chip and flowing the DNA NWs over the gold electrodes by repeatedly depositing/removing the solution from opposite edges of the chip. The solution is allowed to incubate on the substrate/chip for 10 minutes – 1 hour to allow the DNA NWs to settle onto the surface of the substrate/chip.

AFM Imaging of DNA NWs on Mica/Si_3N_4: After the DNA NWs are deposited onto substrates such as mica and Si_3N_4 that are optionally surface treated with HMDS, the DNA NWs are then imaged using atomic force microscopy (AFM) with in-air imaging conditions. The AFM software that is used to control the AFM hardware is Phoenix Studio 21 by SPM Labs. The AFM hardware is made by Bruker / Veeco / Digital Instruments (Multi-Mode Atomic Force Microscope, Model MMAFM-1). A soft tapping silicon AFM tip made by Asylum Research Probes / Oxford Instruments is used with a 7 nm radius, frequency f = 70 kHz, spring constant k = 2 N m^{-1} (Tip Model: AC240TS-R3). The AFM imaging settings typically includes a scan size of ~1000 nm (~1 μm), a scan rate of 1.0 Hz, and PID tuning parameters of P = 1000 and I = 1.0.

Fluorescence Microscopy Imaging of DNA NWs on EAC: The substrate used for fluorescence microscopy is the Electrode Array Chip (EAC). The chip is attached to a microscope slide using double-sided copper tape. After the DNA NW solution is deposited onto the chip, a

square coverslip (#1.5H High-Precision, ~0.17 mm thick, 18 mm x 18 mm) is placed on top of the chip and disperses the DNA NW solution to cover the entire chip. The microscope used is a ZEISS Axio Observer inverted fluorescence microscope configured for epifluorescence with a 100x objective with oil immersion. For the fluorescence microscope imaging settings, a gain of 3x and a 5-10 second exposure time is used, and this makes it possible to visualize the DNA NWs with the Alexa 488 fluorophores and/or a fluorescent dye such as ethidium bromide (EtBr).

Electrical Characterization of DNA NWs on EAC: After depositing the DNA NWs onto the EAC and imaging the sample, the chip is vacuum dried to remove water and prevent contamination of the DNA NWs. The chip is vacuum dried 1 day – 1 week before measurement. The DNA NWs are then electrically characterized on the EAC using a probe station to acquire electrical measurements. The purpose of these electrical measurements is to collect IV sweep resistance values of the DNA NWs after the chip is imaged with fluorescence microscopy to identify the locations where the DNA NWs are bridging the gold electrodes. These measurements reveal the conductance/resistance of the DNA NWs, which have Alexa 488 fluorophores and thiols attached to them. Ideally, the DNA NWs should be long enough to bridge most devices on the EAC regardless of the electrode gap size (1 μm gaps, 750 nm gaps, 625 nm gaps, 500 nm gaps, and 250 nm gaps). The data is acquired with a LabVIEW program that controls the output sweep voltage and reads in the input current, which is converted to a voltage by a transimpedance amplifier with a feedback resistor that is used to set the appropriate gain.

Chapter 7: Conductance Enhancement of DNA Origami Nanowires

This chapter contains the introduction, methods, results, discussion, and conclusion for the conductance enhancement of DNA origami nanowires (DNA NWs).

7.1 Introduction

In this chapter, we will discuss some strategies and techniques used to enhance the electrical conductance of DNA NWs, as well as some environmental factors that affect the electrical conductance of DNA NWs. The goal of the research covered in this chapter is to increase the electrical conductivity of DNA NWs. One of the primary strategies to enhance the electrical conductance of DNA NWs is to use DNA intercalators, which are molecules that bind to the DNA. These molecules have the potential to enhance the electrical conductivity of DNA, similar to how chemical dopants such as boron and phosphorus can enhance the electrical conductivity of semiconductors such as silicon. However, as we will explore, environmental conditions such as whether a substrate is native/intrinsic vs. has a surface treatment, or whether a substrate is wet vs. dry, may be more important factors that affect the electrical conductivity of the DNA NWs deposited onto the substrate. This evidence then informs other potential strategies for further enhancing the electrical conductivity of DNA NWs.

7.2 Methods

The experimental design and methods that pertain to the conductance enhancement of DNA NWs are laid out in this section. The first method is pre-intercalation of DNA NWs.

Pre-intercalation of DNA origami nanowires:

The electrical conductance of DNA NWs can be enhanced through a variety of different strategies. One of the methods for enhancing the electrical conductivity of DNA is to bind chemicals such as DNA intercalators onto the DNA. The primary strategy for enhancing the electrical conductivity of the DNA NWs is to pre-intercalate the DNA NWs, by intercalating them before they are deposited onto the Electrode Array Chip. This strategy ensures that the DNA NWs will get properly intercalated because the intercalator is introduced before the DNA NWs are deposited onto the chip, enabling greater degrees of freedom for fluctuations in the molecule and enabling greater intercalator diffusion into the DNA NWs since the DNA NWs are intercalated in the solution and incubated before they are immobilized on the surface of the chip. A post-intercalation (intercalated after deposition) or non-intercalation (not intercalated at all) strategy can be performed on a separate chip to serve as a control experiment in parallel while a pre-intercalation strategy is performed on the primary experimental chip. It is likely that pre-intercalated DNA NWs will become even more electrically conductive than post-intercalated or non-intercalated DNA NWs due to the greater loading of intercalator molecules and fluorescent dyes into/onto the pre-intercalated DNA NWs. The process for pre-intercalating DNA NWs is covered below.

DNA origami nanowire solution pre-intercalation procedure:

15-17 µL of the 1-10 µg/mL intercalator diluted working solution is applied to a new clean 1.5 mL microcentrifuge tube. The DNA origami nanowire stock solution is then gently pipetted up and down several times to disperse it in its own DNA wire stock solution microcentrifuge tube. 3-5 µL of the ~100 pM DNA origami nanowire + Alexa 488 + thiols solution is then applied to the 1.5 mL microcentrifuge tube with the intercalator diluted working solution, and this combined solution is pipetted up and down several times to mix it all together. There should be a total of ~20 µL of combined solution. The microcentrifuge tube with this combined solution is then sealed with parafilm to prevent the solution from evaporating, wrapped with aluminum foil to block out the light, and left upright in a test tube holder in the dark to incubate. The solution is allowed to incubate in the microcentrifuge tube for about 1 day. After the pre-intercalation incubation, this ~20 µL combined solution is deposited onto an Electrode Array Chip (EAC), after the chip is prepared for deposition using the chip preparation procedure. The DNA NW + intercalator solution is then incubated on the chip as would be done for depositing a DNA NW solution without intercalator; and the chip is then washed, imaged, and measured as usual.

Selection of DNA intercalators for enhancing the electrical conductivity of DNA:

An overview of DNA intercalators was covered in the background section on DNA Intercalators. In summary, DNA intercalators can enhance the electrical conductivity of DNA through various mechanisms; such as assisting with the overlap of the base pair π-stack electronic orbitals, acting as donors or acceptors of charge carriers, or simply by changing the morphology or conformation of the DNA. There are clearly a wide variety of DNA intercalators, fluorescent

dyes, and nucleic acid stains that differ in several ways; such as their molecular/chemical makeup, how they bind to DNA (the DNA binding mode), their HOMO energy level, their LUMO energy level, and their HOMO-LUMO energy gap. Another difference is the solubility of these DNA intercalators in different kinds of solutions (e.g., aqueous, solvent). Due to the sensitivity of DNA to its environment, the possibility of DNA changing its shape or morphology in non-aqueous solutions, and the possibility of contaminating the DNA or the chip/substrate with non-aqueous solutions, it is sensible to select DNA intercalators that are soluble in water. Hence, I have selected to study how the following water-soluble DNA intercalators with different DNA binding modes and different HOMO-LUMO gaps affect the electrical conductivity of DNA:

- Acridine Orange (AO) (External Binder) (HOMO-LUMO gap: ~2 eV) [122]
- DAPI (Minor Groove Binder) (HOMO-LUMO gap: ~9 eV) [123]
- Ethidium Bromide (EtBr) (Intercalator) (HOMO-LUMO gap: ~7 eV) [124]
- Propidium Iodide (PI) (Intercalator) (HOMO-LUMO gap: ~2 eV) [125]
- Hoechst 33258 (H 33258) (Minor Groove Binder) (HOMO-LUMO gap: ~1 eV) [126]
- Hoechst 33342 (H 33342) (Minor Groove Binder) (HOMO-LUMO gap: ~3 eV) [126]
- Miami Series (Red, Orange, Yellow, Green) (Intercalator / Groove Binder) (~2-3 eV) [92]
- Anthraquinone-Neomycin Adduct (DPA 561) (Intercalator & Groove Binder) (~4 eV) [127]

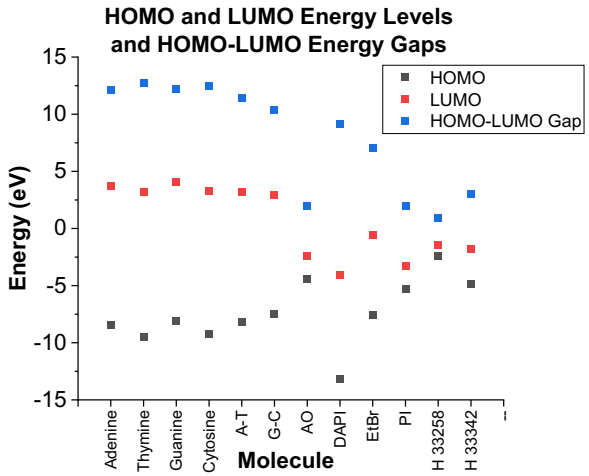

Figure 7.1. HOMO and LUMO Energy Levels and HOMO-LUMO Energy Gaps for DNA and Intercalators

Other mechanisms for enhancing the electrical conductivity of DNA:

While the primary strategy is to enhance the electrical conductivity of DNA NWs by using DNA intercalators, thereby allowing the electrical conductivity of the DNA NW itself to increase, it is possible that such a strategy may not be reliable/consistent or might not yield a sufficient increase in the electrical conductivity of DNA NWs. Therefore, it is prudent to have some alternative strategies for enhancing the electrical conductivity of DNA NWs. For example, the shape, structure, and morphology of the DNA NWs could be modified. A greater number of helix bundles in parallel should increase the number of electrically conductive pathways, thereby increasing the electrical conductivity of the DNA NWs, and shorter DNA NWs should be more conductive than longer DNA NWs. Towards this aim, a 10-helix bundle DNA NW structure (10HB NW) and a 6-helix bundle DNA NW structure (6HB NW) have both been developed, which have different lengths and widths, and which enable the measurement of the electrical conductivity of DNA NWs with different shapes and morphologies. In addition to affecting the electrical

conductivity, the stability and durability of the DNA NW in different environments (e.g., substrates, buffers/solutions) may be affected by the shape and morphology of the DNA NW.

In summary, there are several different strategies that could be used to enhance the electrical conductivity of DNA NWs. DNA intercalation provides perhaps the simplest and most convenient approach, with benefits such as a large repertoire of molecules that are known to bind to DNA, stoichiometric control over the electrical conductivity, and additional imaging capabilities with the fluorescent properties of some DNA intercalators. We will now review the results of some of these strategies for enhancing the electrical conductance of DNA NWs.

7.3 Results

We begin by reviewing the results for the strategy of intercalating the DNA NWs.

Results for Electrical Resistance Measurements of Intercalated DNA Origami 5-mer Nanowires:

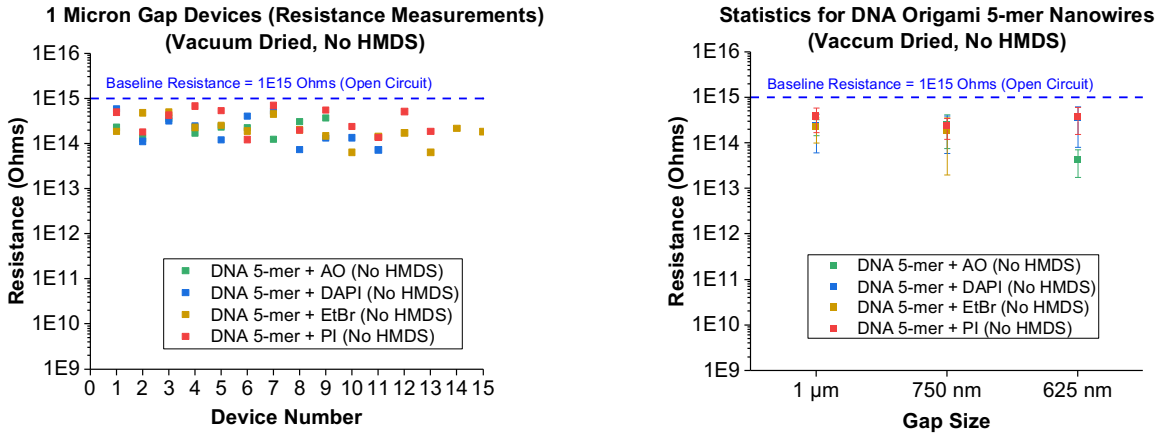

Figure 7.2. Resistance Measurement Values (Left) and Statistics (Right) for Intercalated DNA Origami 5-mer Nanowires

These resistance measurement results show that the electrical resistance of vacuum dried DNA origami 5-mer nanowires (without HMDS on Si_3N_4) does not change much after intercalation. Several different intercalators were tried, including acridine orange (AO), DAPI, ethidium bromide (EtBr), and propidium iodide (PI). In theory, these intercalators should have caused a noticeable decrease in the electrical resistance of the DNA NWs. However, there is an insignificant change in the electrical resistance of the DNA NWs. There appears to be some factor other than DNA intercalation that is greatly affecting the electrical resistivity of the DNA NWs. It's important to highlight that these DNA NW samples were vacuum dried before measurement, and the EAC substrate was not treated with HMDS before DNA NW deposition. The next section helps to explain the most likely cause of the high electrical resistance.

As we saw in the previous chapter, DNA NWs are very sensitive to their environment and interface conditions. It appears that the interface between the DNA and the substrate plays a large role in affecting both the electrical conductivity and the height/thickness of the DNA NWs. The previous chapter demonstrated that both the height and the electrical conductivity of DNA NWs are lower when the DNA NWs are deposited onto a native/untreated Si_3N_4 substrate, while the both the height and the electrical conductivity of DNA NWs are higher when the DNA NWs are deposited onto HMDS-treated Si_3N_4 substrates. An overview of those results is presented below.

Atomic Force Microscopy (AFM) Results for Height of DNA Origami Nanowires on Si_3N_4:

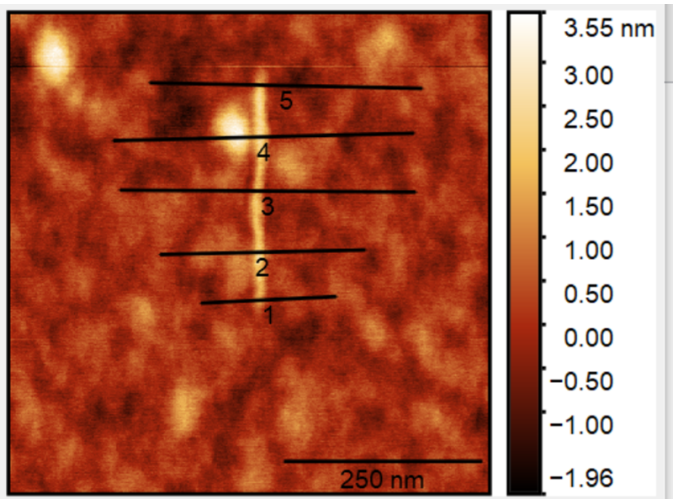

Figure 7.3. AFM Measurement of Height of DNA Origami Nanowire on Si_3N_4 Substrate

The DNA origami 6HB NW has an expected height/thickness of ~5 nm based on its design. However, as the AFM image in Figure 7.3 shows, it has a height/thickness of only ~2 nm when it is deposited onto a native/untreated Si_3N_4 substrate. The DNA NW height/diameter decreases when bound to Si_3N_4 substrates most likely due to DNA-substrate interaction, or a combination of electrostatic and van der Waals forces. This DNA structural deformation on the untreated substrate in turn causes a decrease in electrical conductivity for the DNA NW. However, DNA-substrate interaction can be mitigated by

treating the surface of the substrate with molecular monolayers such as hexamethyldisilazane (HMDS), preventing DNA deformation and somewhat preserving/enhancing the electrical conductivity of the DNA NW.

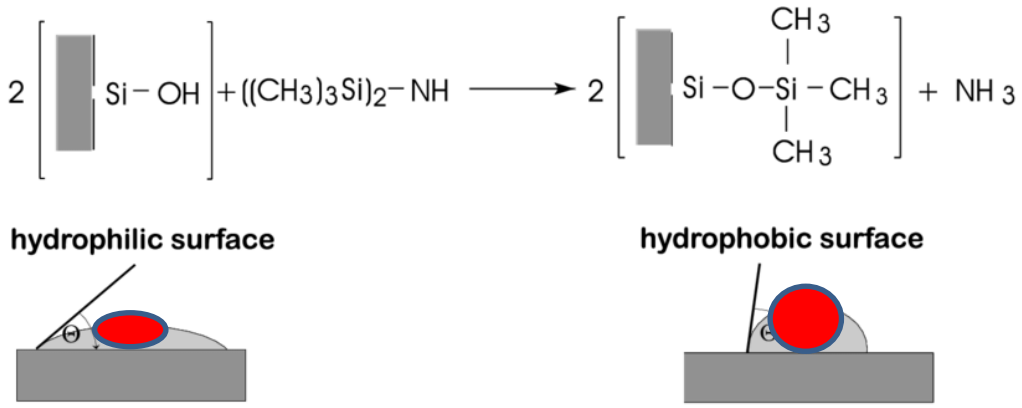

Figure 7.4. Treating Silicon Nitride (Si_3N_4) with HMDS Changes Surface from Hydrophilic to Hydrophobic

Figure 7.4 shows how HMDS radically transforms the surface properties of a silicon/silica substrate from hydrophilic to hydrophobic, altering the chemical and electrostatic properties of the surface. Silicon-based substrates such as SiO_2 and Si_3N_4 are natively hydrophilic, causing water to stick to the surface of the substrate with high surface tension. However, when HMDS is applied to the silicon-based substrate, the surface becomes hydrophobic, causing water to be repelled from the surface of the substrate. It is well-know that DNA is hydrophilic and is typically found in water or a saline buffer solution. Therefore, it is perhaps not surprising that converting a substrate from hydrophilic to hydrophobic with an HMDS surface treatment could affect the properties of the hydrophilic DNA deposited onto the substrate. As the previous chapter demonstrated, the HMDS surface treatment appears to cause the structure/morphology/thickness of the DNA origami nanowire to be preserved, thereby maintaining the good electrical conductivity of the DNA origami nanowire.

Resistance Results for HMDS (No DNA) and DNA Origami 5-mer Nanowires (w/ HMDS):

Current-Voltage Curves for DNA Origami 5-mer Nanowires on Si_3N_4 with/without HMDS:

(Si_3N_4 Substrate, Vacuum Dried)

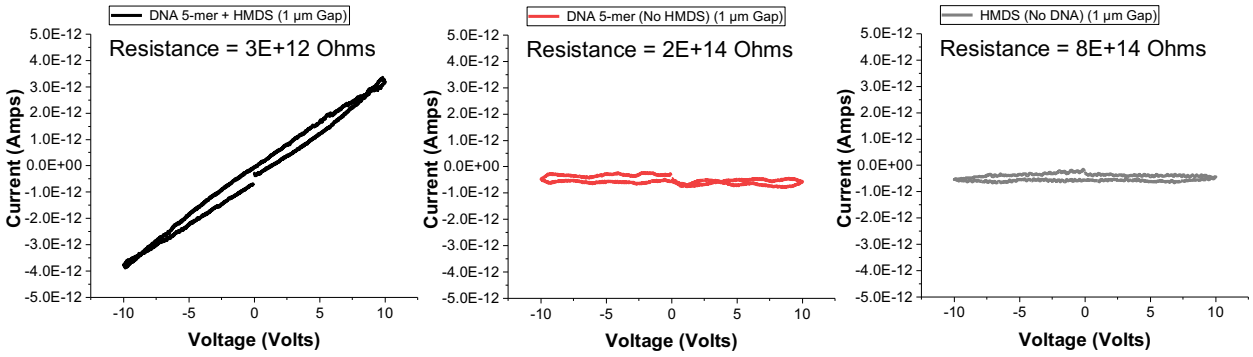

Figure 7.5. Current-Voltage Curves of DNA Origami 5-mer Nanowire on Si_3N_4 with HMDS Surface Treatment (Left) (Black); DNA Origami 5-mer Nanowire on Si_3N_4 without HMDS Treatment (Middle) (Red); HMDS Treatment on Si_3N_4 without DNA Origami 5-mer Nanowire (Right) (Gray)

Some individual current-voltage (I-V) curves are shown above for different experimental conditions to help visualize the profound impact that an HMDS surface pre-treatment has on increasing (or preserving) the electrical conductivity of DNA NWs. These resistance measurements show that the DNA origami 5-mer nanowires are more electrically conductive when HMDS is applied to the silicon nitride (Si_3N_4) substrate/chip and then DNA NWs are deposited onto the chip, thereby preserving the structure and electrical conductance of the DNA NWs. The results also show that the increased electrical conductance is due to the DNA NWs with HMDS and is not simply due to the HMDS alone.

Electrical Conductance of Wet vs. Dry DNA Origami Nanowires:

From the studies on the structure-dependent electrical conductance of DNA NWs as covered in the previous chapter, it seems evident that the surface treatment or environment underneath the DNA NW has a significant effect on its structure and its electrical conductivity. It therefore stands to reason that other environmental factors may also have a significant effect of the electrical conductivity of DNA NWs. The presence of moisture/water/buffer is one such environmental factor that may affect the structure and the electrical conductance of DNA NWs. The DNA NW electrical resistance measurements that were presented so far were of DNA NW samples that were either vacuum dried prior to measurement or were in an ambient environment in which the DNA NW solution had dried out due to evaporation. Those relatively dry DNA NW electrical measurement results had relatively high electrical resistance. We have yet to explore the electrical conductance of DNA NWs in a wet environment of water or buffer. Therefore, this section reviews the electrical conductance of wet vs. dry DNA NWs.

DNA 14HB Dimer + A488 + Thiols in Water on EAC Polaris with HMDS (Wet vs. Dry):

Examples of Device Images and IV Curves:

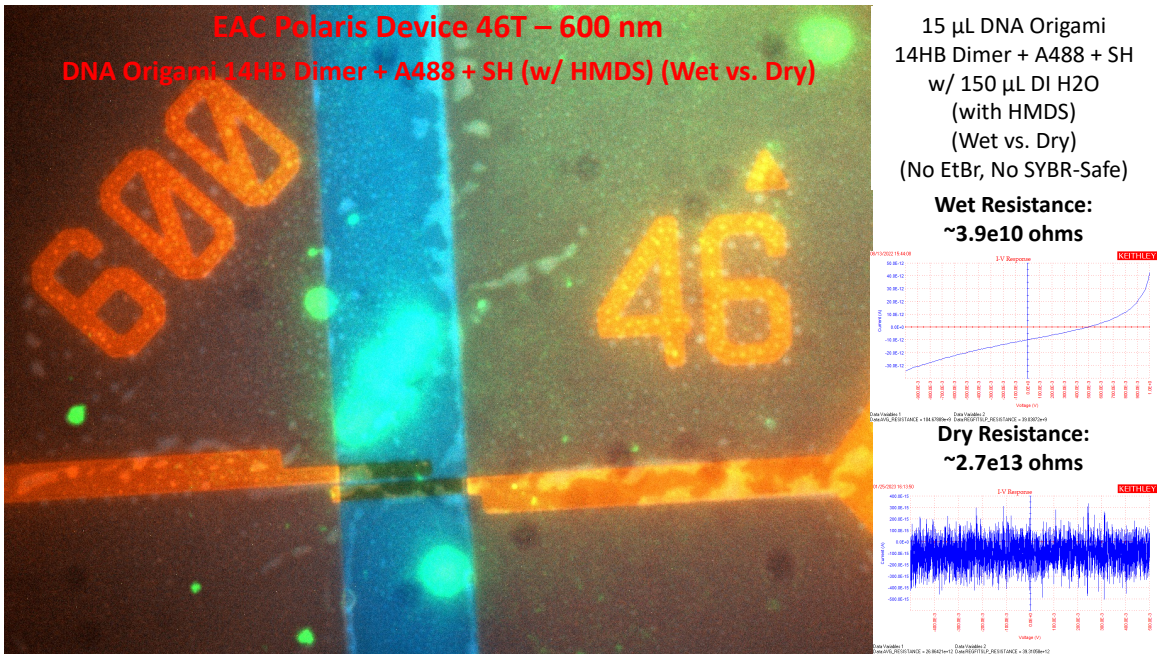

Figure 7.6. EAC Polaris 600 nm Device with DNA Origami 14HB Dimer Nanowires

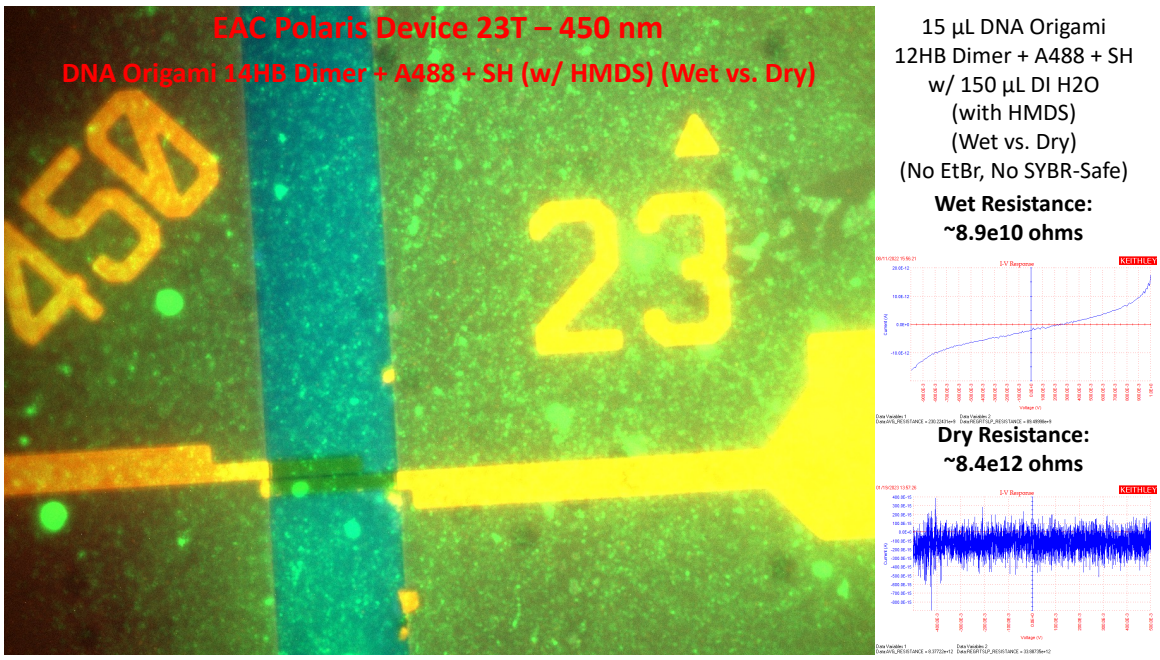

Figure 7.7. EAC Polaris 450 nm Device with DNA Origami 14HB Dimer Nanowires

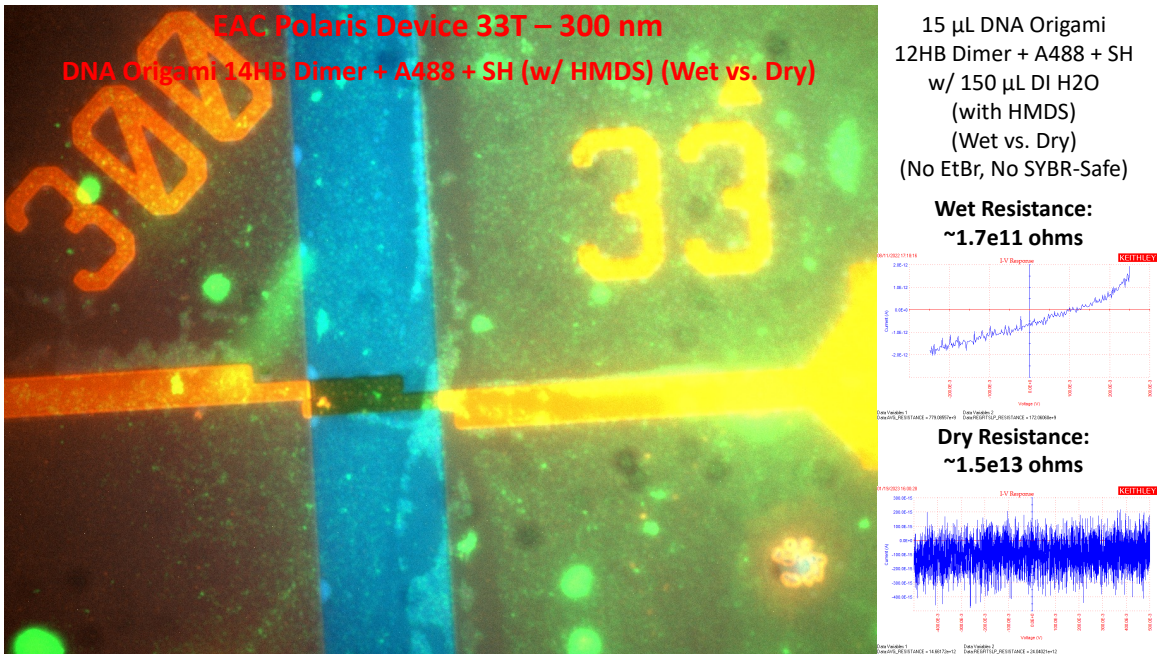

Figure 7.8. EAC Polaris 300 nm Device with DNA Origami 14HB Dimer Nanowires

The figures above show example fluorescence microscopy images, current-voltage (I-V) sweep measurements, and resistance values for wet vs. dry samples of DNA origami 14HB dimer nanowires (14HB NWs). The wet and dry measurements are of the same sample in different environmental conditions (wet vs. dry). The wet measurements are in an environment of ultrapure deionized water (DI H_2O), while the dry measurements are in an environment of ambient air after vacuum-drying the sample. Essentially the only difference between these two environmental states is the presence of water vs. the lack of water on the sample, with the device area being wet vs. dry. As we see from the electrical measurement results, the presence of water appears to increase the electrical conductance of each device by ~100x. It appears that the presence of water is an important factor that greatly affects the electrical conductance of DNA NWs.

Data for DNA 14HB Dimer + A488 + Thiols in Water on EAC Polaris with HMDS (Wet vs. Dry):

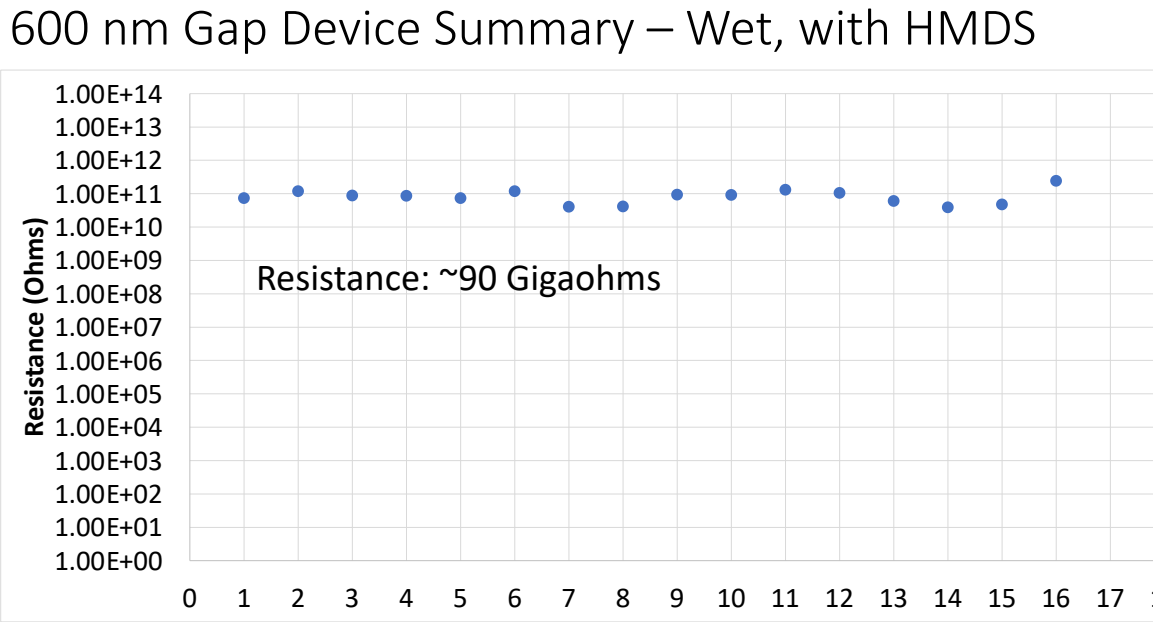

Figure 7.9. Resistance Data for Wet EAC Polaris 600 nm Devices with DNA Origami 14HB NWs

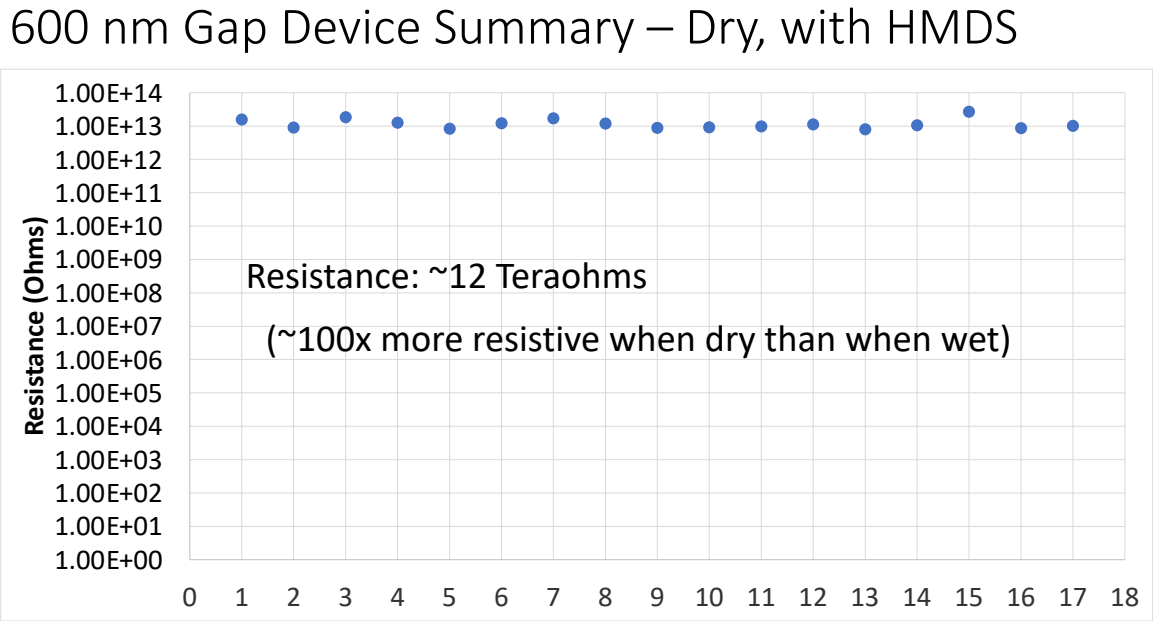

Figure 7.10. Resistance Data for Dry EAC Polaris 600 nm Devices with DNA Origami 14HB NWs

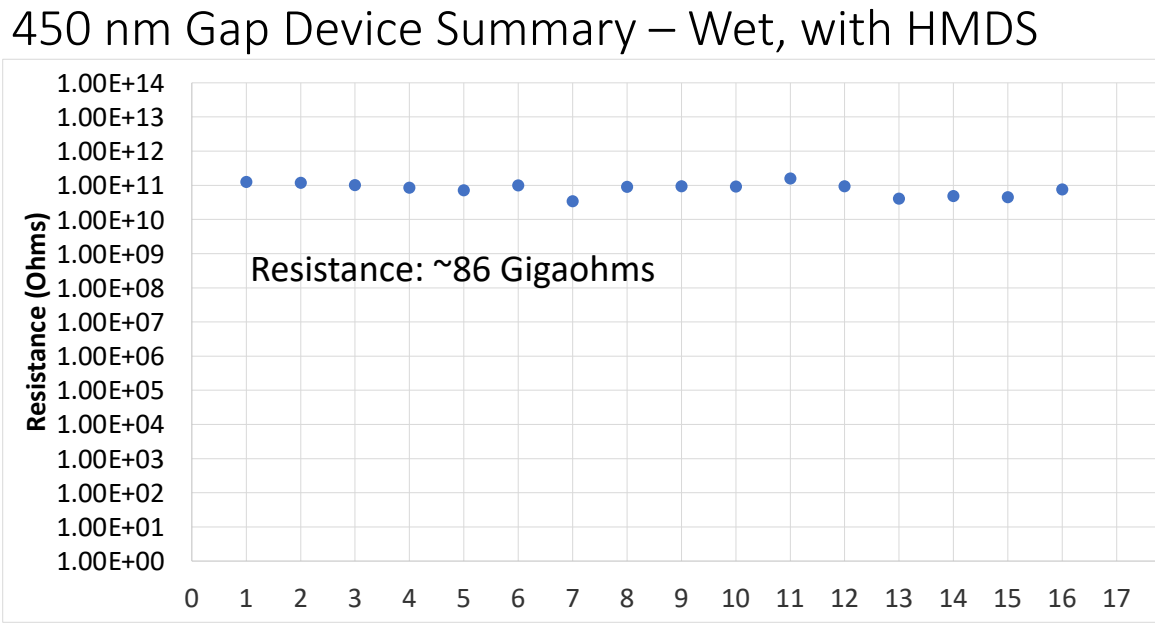

Figure 7.11. Resistance Data for Wet EAC Polaris 450 nm Devices with DNA Origami 14HB NWs

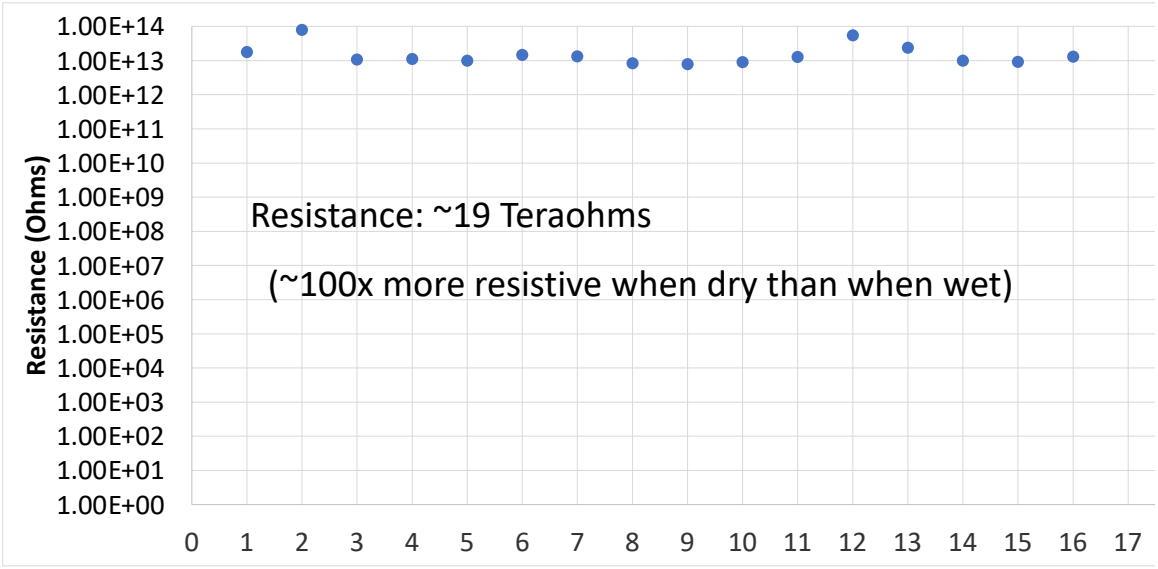

Figure 7.12. Resistance Data for Dry EAC Polaris 450 nm Devices with DNA Origami 14HB NWs

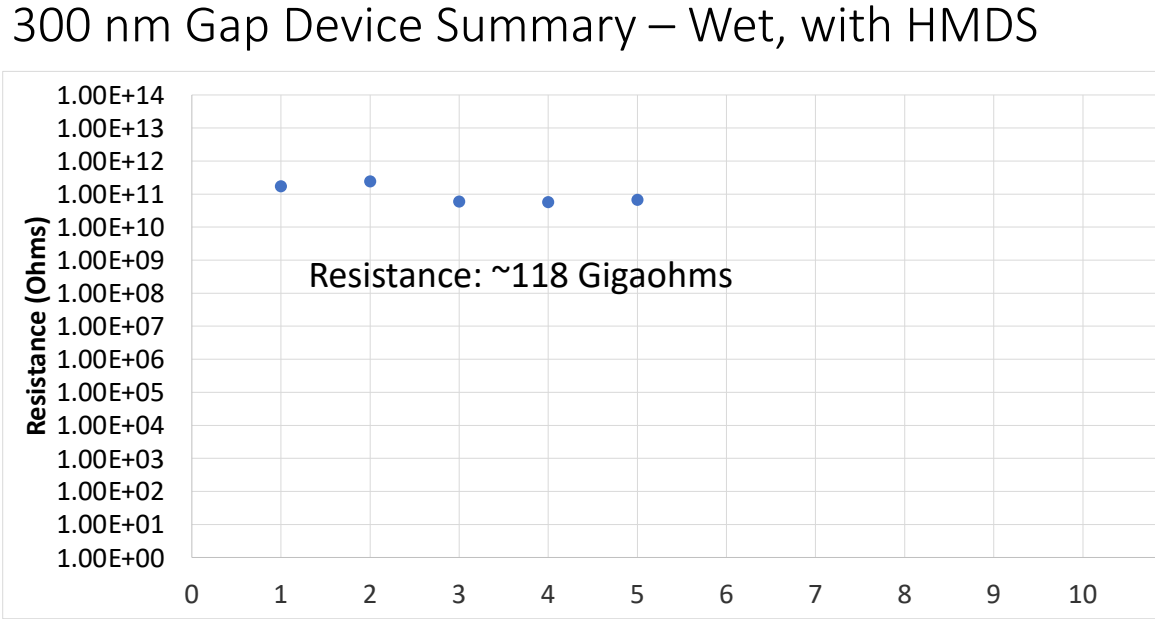

Figure 7.13. Resistance Data for Wet EAC Polaris 300 nm Devices with DNA Origami 14HB NWs

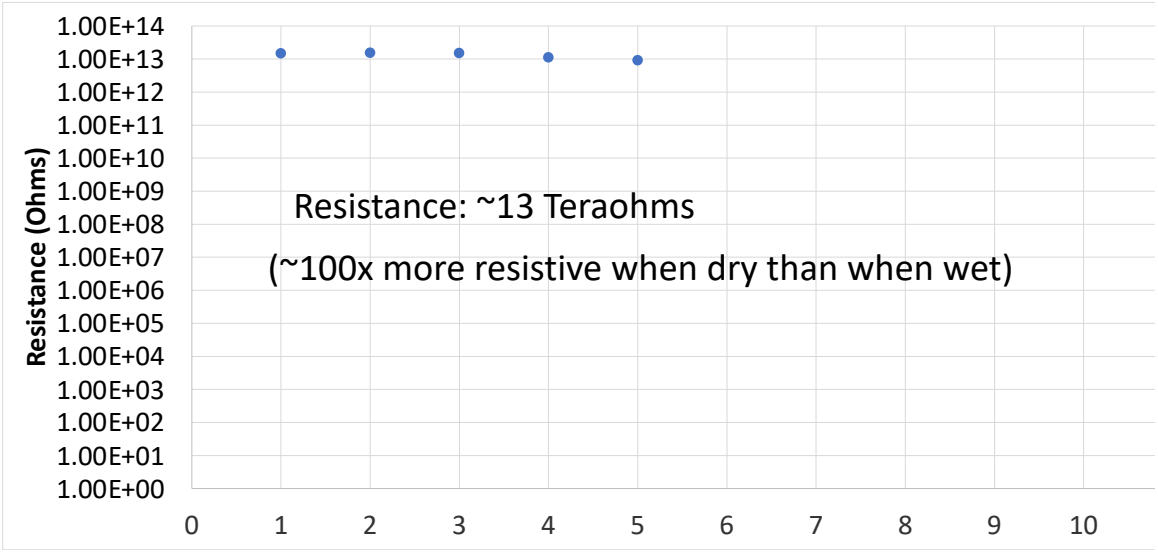

Figure 7.14. Resistance Data for Dry EAC Polaris 300 nm Devices with DNA Origami 14HB NWs

The figures above show resistance data for DNA origami 14HB nanowires (14HB NWs) in deionized water (DI H_2O) for EAC Polaris 300 nm, 450 nm, and 600 nm devices in wet and dry environmental conditions. The current-voltage sweep (IV sweep) data indicates that the 14HB NWs have a relatively low electrical resistance of 86 - 118 gigaohms (~1E11 ohms) when the sample is wet with DI H_2O, and a relatively high electrical resistance of 12 -19 teraohms (~1E13 ohms) when the sample is dry after vacuum drying. This data indicates that the 14HB NWs are ~100x more resistive when they are dry than when they are wet, which suggests that water plays a very important role in the electrical conductance of DNA NWs.

DNA 14HB Dimer + A488 + Thiols in Buffer on EAC Polaris with HMDS (Wet vs. Dry):

Examples of Device Images and IV Curves:

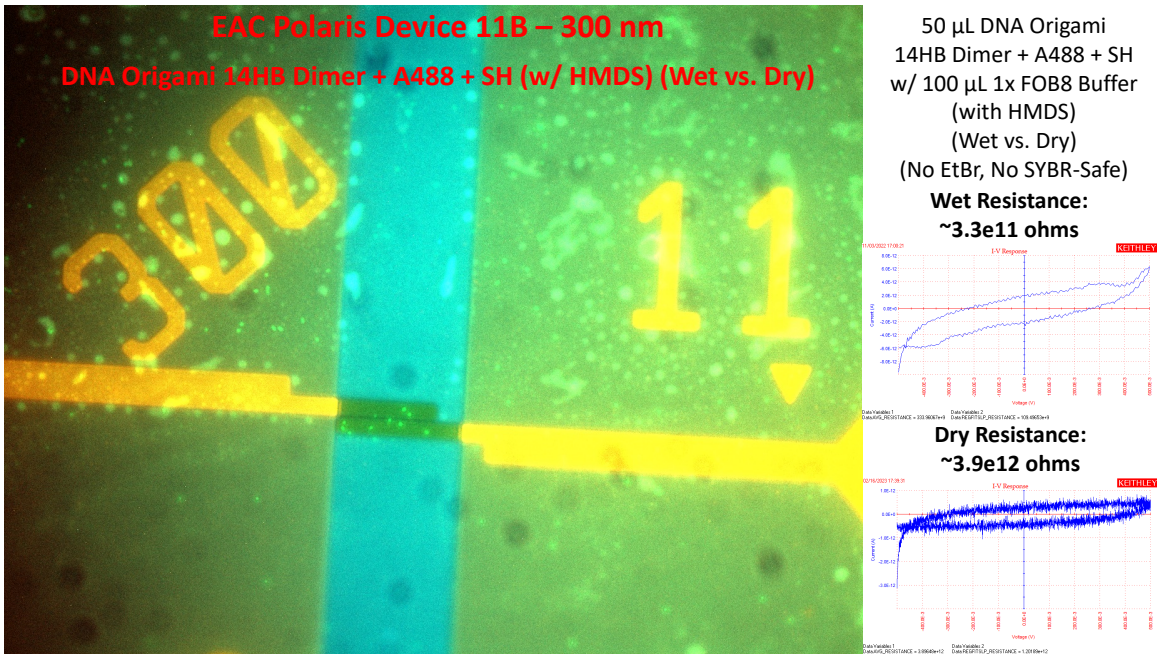

Figure 7.15. EAC Polaris 300 nm Device with DNA Origami 14HB Dimer Nanowires in Buffer

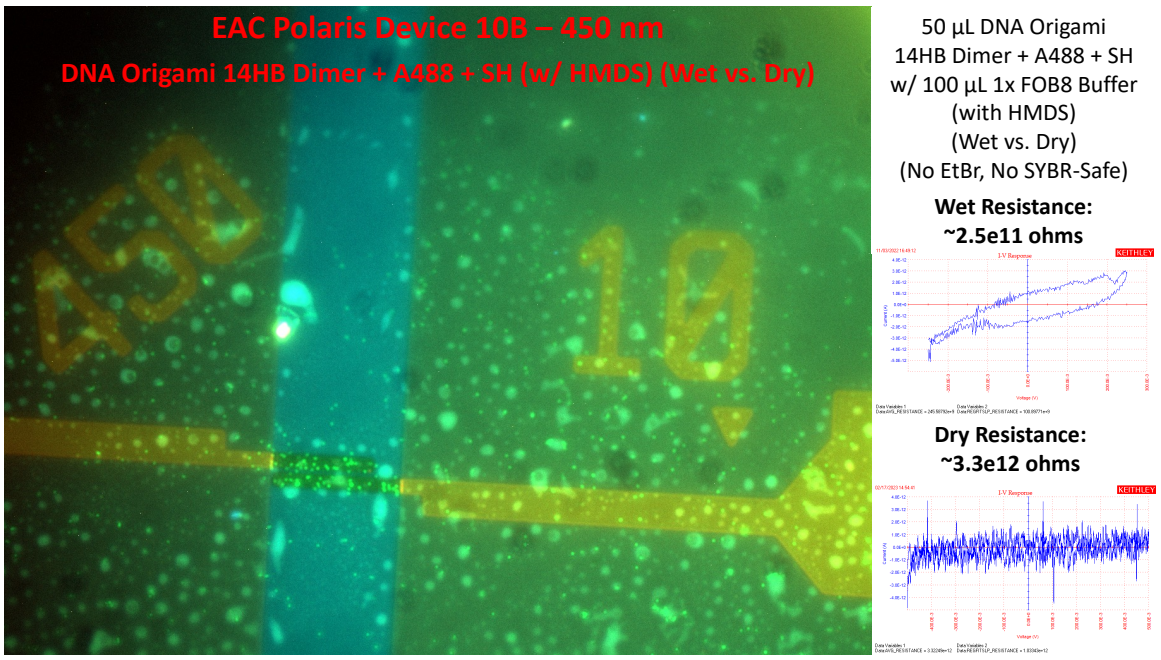

Figure 7.16. EAC Polaris 450 nm Device with DNA Origami 14HB Dimer Nanowires in Buffer

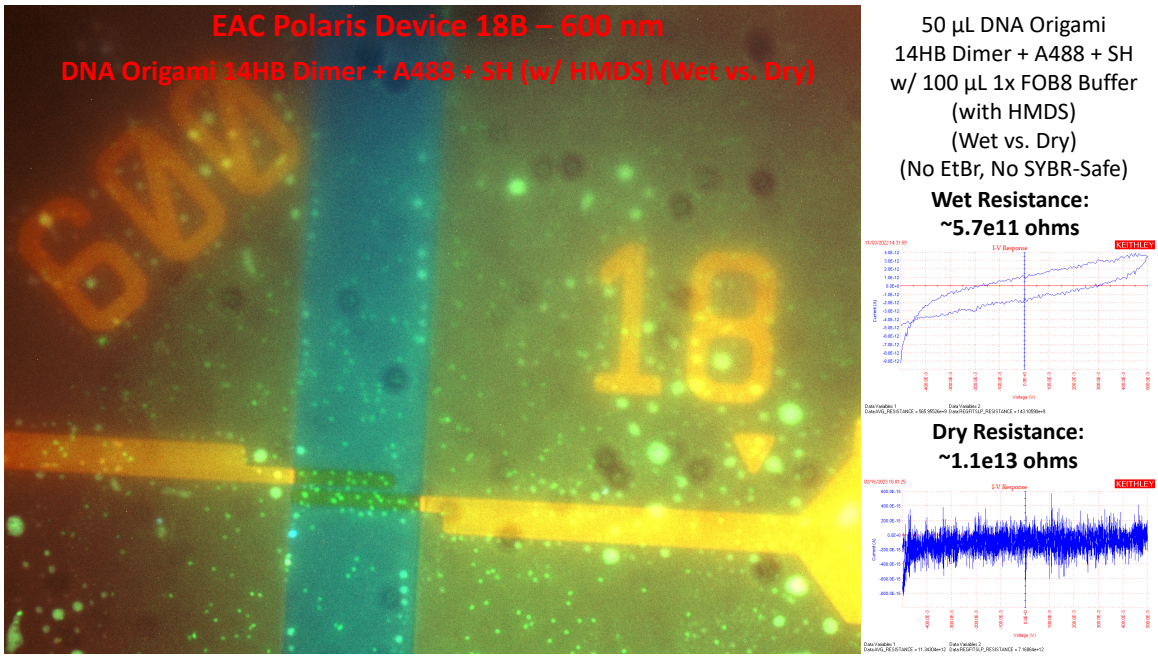

Figure 7.17. EAC Polaris 600 nm Device with DNA Origami 14HB Dimer Nanowires in Buffer

The figures above show example fluorescence microscopy images, current-voltage (I-V) sweep measurements, and resistance values for wet vs. dry samples of DNA origami 14HB dimer nanowires (14HB NWs). The wet and dry measurements are of the same sample in different environmental conditions (wet buffer vs. dry). The wet measurements are in an environment of 1x FOB8 buffer, while the dry measurements are in an environment of ambient air after vacuum-drying the sample. Essentially the only difference between these two environmental states is the presence of buffer (water and salt ions) vs. the lack of buffer on the sample, with the device area being wet vs. dry. Based on the electrical measurement results, the presence of wet buffer appears to increase the electrical conductance of each device by ~10x - ~100x. It appears that the presence of buffer is an important factor that greatly affects the electrical conductance of DNA NWs.

Data for DNA 14HB Dimer + A488 + Thiols in Buffer on EAC Polaris with HMDS (Wet vs. Dry):

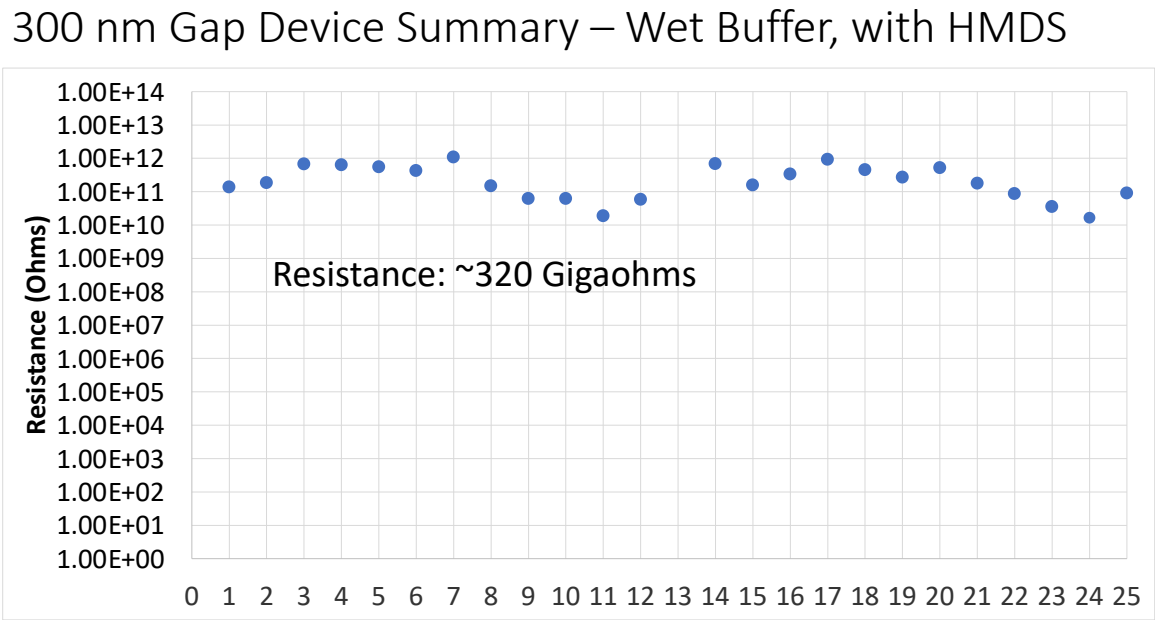

Figure 7.18. Resistance Data for Wet EAC Polaris 300 nm Devices with DNA Origami 14HB NWs in Buffer

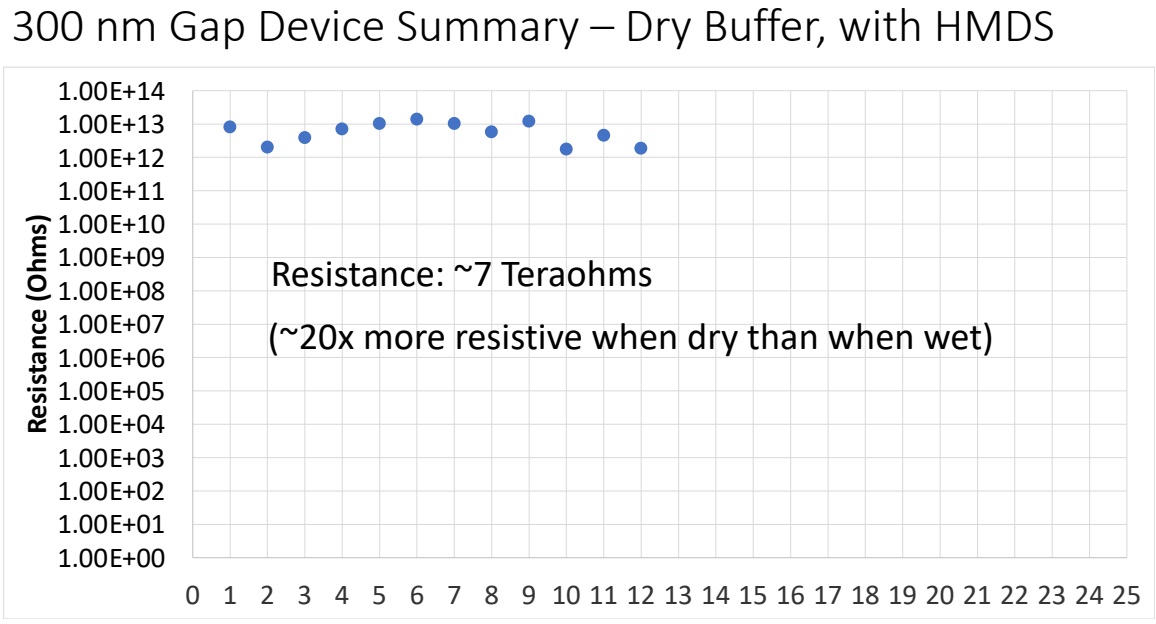

Figure 7.19. Resistance Data for Dry EAC Polaris 300 nm Devices with DNA Origami 14HB NWs in Buffer

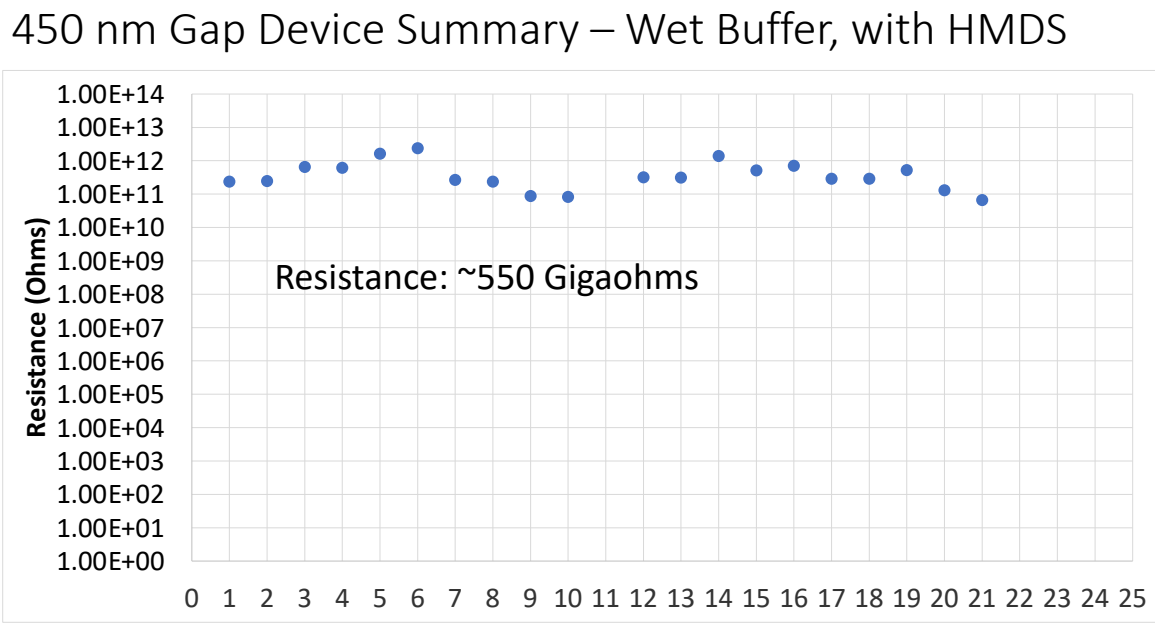

Figure 7.20. Resistance Data for Wet EAC Polaris 450 nm Devices with DNA Origami 14HB NWs in Buffer

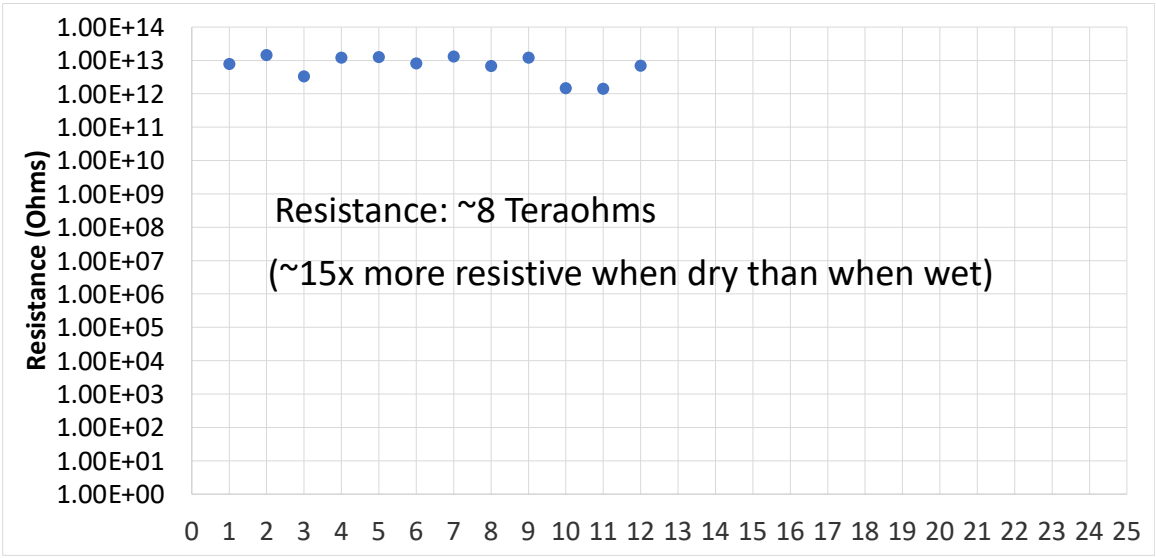

Figure 7.21. Resistance Data for Dry EAC Polaris 450 nm Devices with DNA Origami 14HB NWs in Buffer

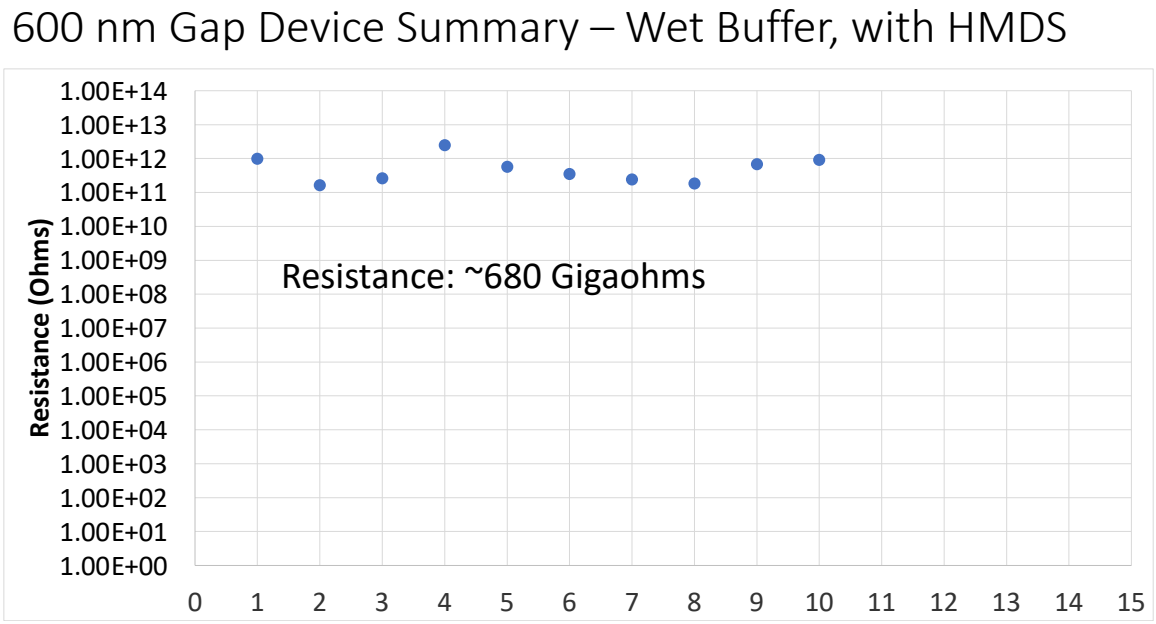

Figure 7.22. Resistance Data for Wet EAC Polaris 600 nm Devices with DNA Origami 14HB NWs in Buffer

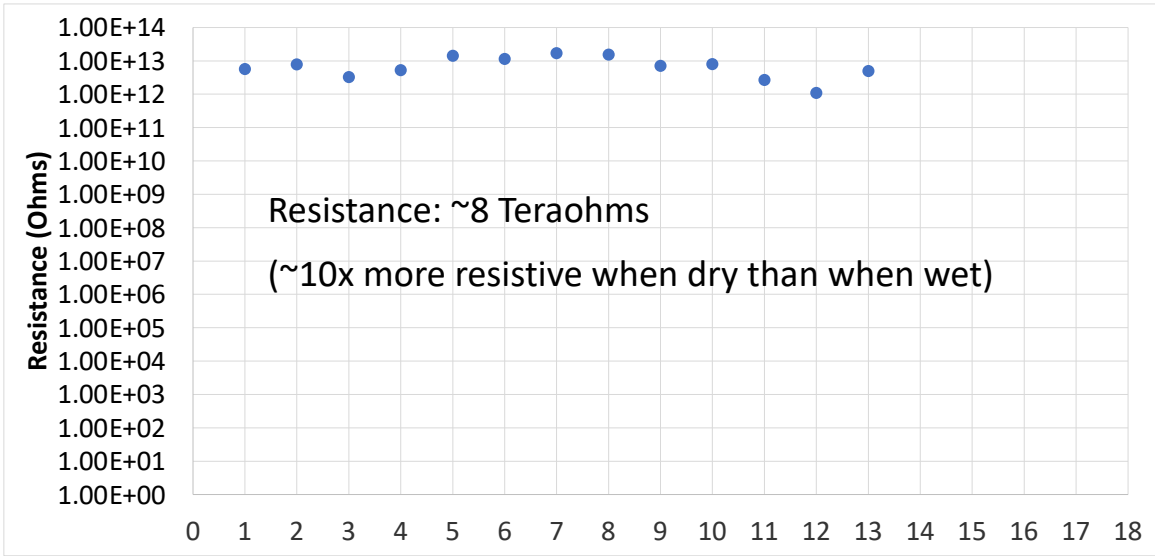

Figure 7.23. Resistance Data for Dry EAC Polaris 600 nm Devices with DNA Origami 14HB NWs in Buffer

The figures above show resistance data for DNA origami 14HB nanowires (14HB NWs) in buffer (1x FOB8) for EAC Polaris 300 nm, 450 nm, and 600 nm devices in wet buffer and dry environmental conditions. The current-voltage sweep (IV sweep) data indicates that the 14HB NWs have a relatively low electrical resistance of 320 - 680 gigaohms (~5E11 ohms) when the sample is wet with 1x FOB8 buffer, and a relatively high electrical resistance of 7 - 8 teraohms (~7E12 ohms) when the sample is dry after vacuum drying. This data indicates that the 14HB NWs are ~10x more resistive when they are dry than when they are wet with buffer, which suggests that buffer (essentially consisting of water and salt ions) plays a very important role in the electrical conductance of DNA NWs.

Control Experiment:

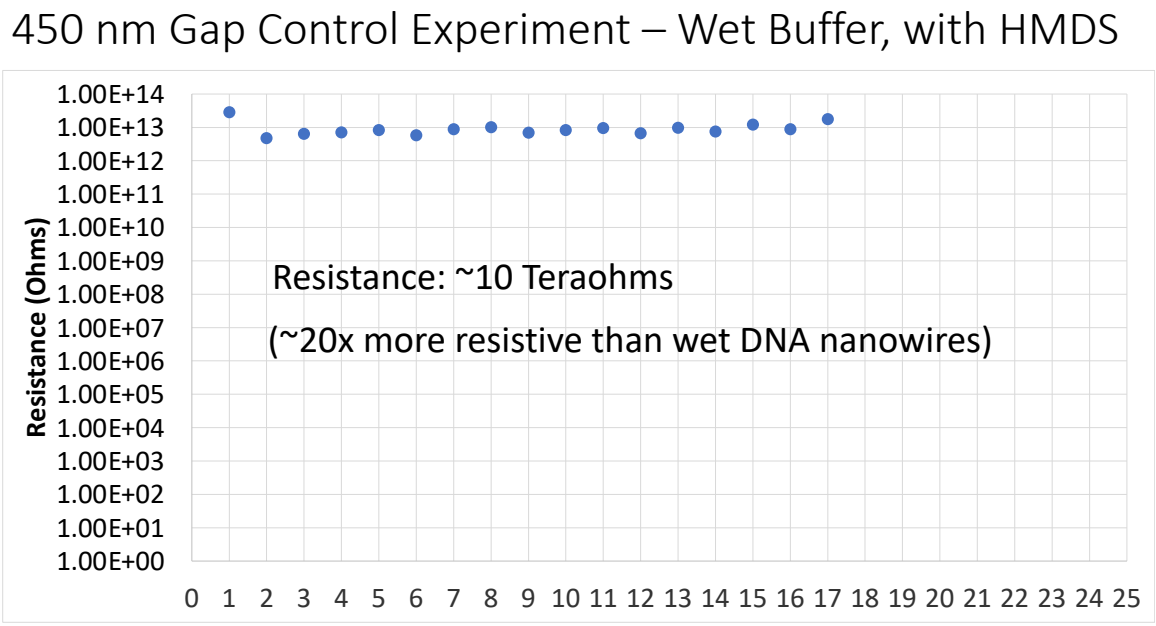

Figure 7.24. Control Experiment Resistance Data for Wet Buffer on EAC Polaris 450 nm Devices without NWs

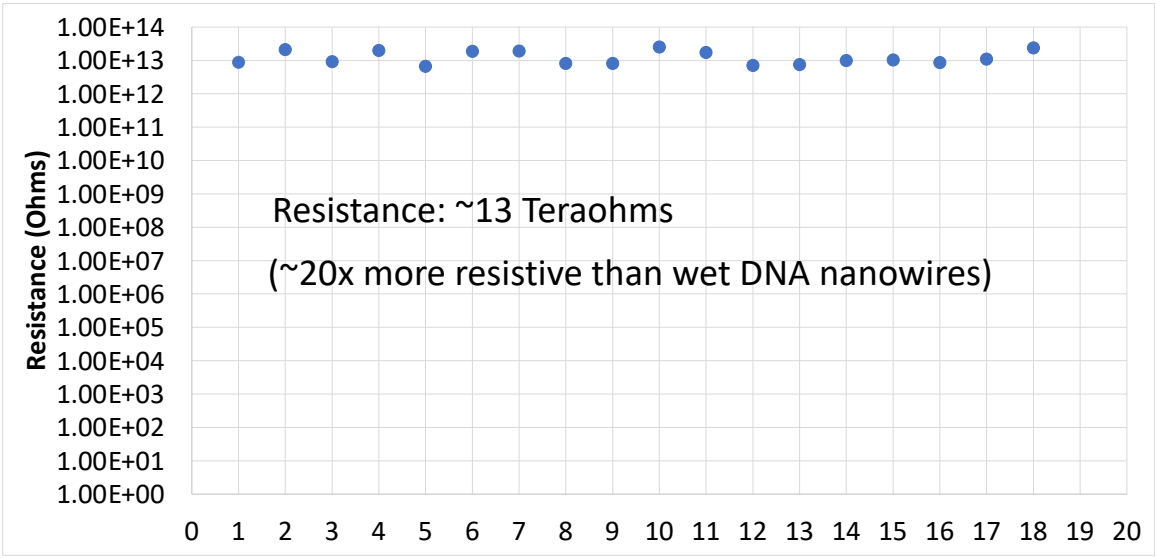

Figure 7.25. Control Experiment Resistance Data for Wet Buffer on EAC Polaris 600 nm Devices without NWs

The figures above show electrical measurement data for control experiments involving the same kind of EAC Polaris chip that was used to collect the electrical measurements for the 14HB NWs. These control experiments were performed in the same experimental/environmental conditions as the 14HB NW experiments, except without the 14HB NWs. Both sets of control experiment data are for an EAC Polaris chip with wet buffer (1x FOB8) without the 14HB NWs. One set of data is for 450 nm gap devices, which indicates an average resistance value of ~10 teraohms (~1E13 ohms). The other set of data is for 600 nm gap devices, which indicates an average resistance value of ~13 teraohms (~1E13 ohms). Both of these resistance values are much greater than the average resistance values of 14HB NWs in 1x FOB8 buffer for 450 nm gap devices (~550 gigaohms, ~6E11 ohms) and 600 nm gap devices (~680 gigaohms, ~7E11 ohms). In fact, the buffer control experiments yield electrical resistance values that are ~20x greater than the electrical resistance values for the experiments of 14HB NWs in buffer. Therefore, we can be confident that the relatively high electrical conductance results of the 14HB NWs experiments are due to the 14HB NWs themselves rather than being attributed to the 1x FOB8 buffer. In essence, it appears that we are measuring the electrical conductance of the 14HB NWs rather than just the buffer surrounding the 14HB NWs.

Given that the preceding results suggest that water and/or buffer play an important role in preserving or increasing the electrical conductance of DNA NWs, it makes sense to measure the electrical conductance of DNA NWs in relatively wet environmental conditions. This can be achieved by not vacuuming drying the sample before electrical measurement and allowing the humidity in the ambient air surrounding the DNA NW sample to provide a source of moisture to keep the DNA NWs relatively wet, aided by the underlying hydrophilic silica substrate.

Resistances for DNA Origami 5-mer Nanowires (SiO_2 Substrate, No HMDS, Not Vacuum Dried):

IV Curves Showing Conductance Enhancement by Anthraquinone-Neomycin Adduct (DPA 561):

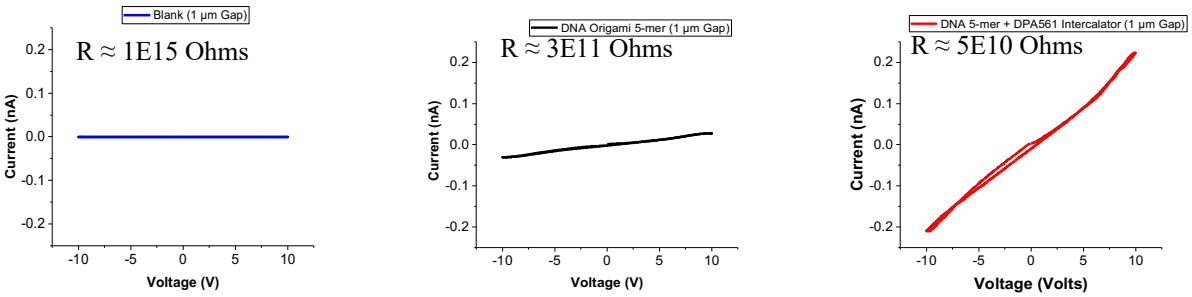

IV Curve of Blank Chip | IV Curve of Initial DNA Structure | IV Curve After DPA 561

Figure 7.26. IV Curves of Conductance Enhancement by Anthraquinone-Neomycin Adduct (DPA 561)

Resistance Measurements for DNA Origami 5-mer Wires (SiO_2, No HMDS, Not Vacuum Dried):

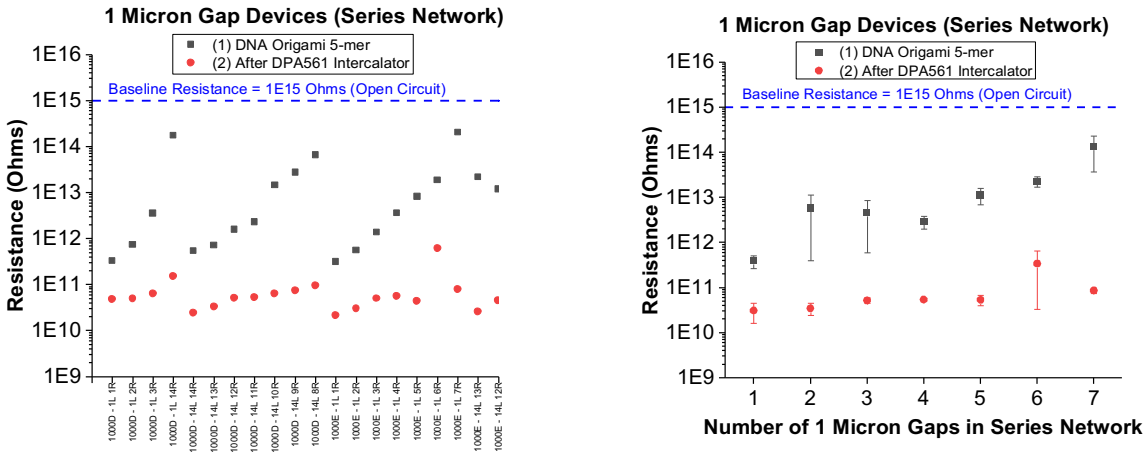

Figure 7.27. Resistance Values and Resistance Statistics for DNA Origami 5-mer Wires

(Series Network of 1 µm Gap Devices)

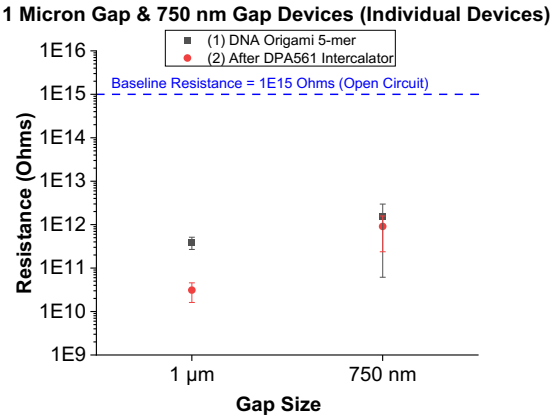

Figure 7.28. Resistance Statistics for DNA Origami 5-mer Wires (Individual 1 µm and 750 nm Gap Devices)

The figure above shows electrical resistance measurements for DNA 10HB 5-mer NWs on an EAC chip that is not vacuum dried and therefore has some moisture due to the ambient humidity and residual water/buffer on the chip. The data in this figure shows lower electrical resistance values for DNA NWs than those that were demonstrated previously for vacuum-dried samples. Therefore, this figure implies that DNA NWs can have relatively high electrical conductivity without an HMDS surface treatment if the sample is somewhat wet/moist. Furthermore, this relatively wet environment may provide enough structural integrity for the DNA so that DNA intercalators may have a slight effect on electrical conductance. In particular, we observe that the resistance of DNA origami 10HB 5-mer nanowires before intercalation is ~1E12 Ohms, and the resistance of DNA origami 10HB 5-mer nanowires after intercalation is ~1E11 Ohms. Therefore, the DPA 561 intercalator increases DNA origami 5-mer nanowire conductance by ~10x. This demonstrates a significant improvement in the electrical conductance of the DNA NW.

7.4 Discussion

The research objective covered in this chapter was to understand the various factors that affect the electrical conductance of DNA NWs, and to further improve their electrical conductivity. From the results, it appears that the structure of the DNA itself plays a primary role in the electrical conductivity of the DNA NWs. Therefore, it is important to preserve the structural integrity of the DNA NWs as much as possible, to enhance or preserve the electrical conductivity of the DNA NWs. In the previous chapter, the structural integrity of DNA NWs was studied to understand the effects of DNA-substrate interaction (e.g., the electrostatic interaction between the DNA NWs and the substrate causing the DNA NWs to become deformed). The previous chapter presented results for atomic force microscopy (AFM), which was used to study the variation or deformation in height/thickness/diameter of DNA NWs on various substrates (e.g., silicon dioxide, silicon nitride, mica) to better understand the extent of DNA-substrate interaction for different substrates, and to identify the substrates and/or surface treatments for preserving the structure and thus the electrical conductivity of the DNA NWs. Essentially, we observed that the DNA-substrate interaction could be mitigated by applying a surface treatment to the substrate before depositing the DNA NWs. Applying an HMDS surface treatment to Si_3N_4 substrates has led to a noticeable increase in the electrical conductivity of DNA NWs by mitigating the structural deformation of DNA NWs on Si_3N_4 substrates. However, in this chapter we explored that there are other environmental factors besides DNA-substrate interaction that could allow for further gains in the electrical conductivity of DNA NWs. The results in this chapter indicate that the presence of water/buffer/humidity may also help to preserve the structural morphology of the DNA NWs and help to preserve/increase the electrical conductivity of DNA NWs. Therefore, it could be beneficial to understand exactly how water/buffer/humidity affects the DNA-substrate interaction and the

height/thickness/diameter of DNA NWs on substrates with/without molecular monolayer surface treatments through further AFM studies. Alternatively, the structure of the DNA NWs could be preserved by connecting the DNA NWs between two raised gold electrodes and suspending the DNA nanowires above the insulating substrate, thereby avoiding the DNA-substrate interaction.

Another strategy for increasing the electrical conductivity of DNA NWs is to attach carbon nanotubes to the DNA NWs. Carbon nanotubes are well known for their very high electrical conductivity. In this case, the electrical conduction would primarily occur through the carbon nanotubes rather than through DNA itself. The DNA NWs would serve as templates or conduits for carrying/holding the attached carbon nanotubes, and the DNA NWs could then be used to place the carbon nanotubes in specific desired locations on substrates with precision and accuracy. This carbon nanotube strategy is very promising, as it may allow for the electrical effects of DNA-substrate interaction to be entirely mitigated or bypassed. My research group has done some preliminary work on the design and synthesis of DNA NWs that are bound with carbon nanotubes (CNT DNA NWs). In this strategy, the DNA NWs could be used to place and locate the carbon nanotubes and make good electrical contact with the gold electrodes with the thiol groups that are attached to the DNA NWs, thereby creating CNT DNA NWs that have very high electrical conductivity. The CNT DNA NWs can be deposited, imaged, and electrically measured on test substrates such as the Electrode Array Chip, just as is done for the DNA NWs.

Aside from the DNA NWs and the CNT DNA NWs, there are some other strategies that could be used to enhance the electrical conductivity of DNA NWs. For example, as discussed in the background section on DNA Nanoelectronics; different base pair or nucleotide sequences should enhance the electrical conductivity of DNA, with G-C rich sequences expected to produce higher electrical conductivity than A-T rich sequences. Therefore, the base pair sequence in the

DNA NWs could be engineered to include many more G-C base pairs than A-T base pairs. Yet other strategies for enhancing the electrical conductivity of DNA NWs include metallization of the DNA NWs (e.g., with gold or silver), attaching graphene nanoribbons to the DNA NWs, and attaching conductive polymers to the DNA NWs. All these strategies may be worthy of further experimentation and development by researchers.

7.5 Conclusion

In summary, this chapter focused on strategies, methods, and results for enhancing the electrical conductance of DNA NWs. There are several different strategies that can be employed to increase the electrical conductivity of DNA NWs. Techniques such as modifying the sequence of base pairs, doping the DNA NWs with intercalators, controlling the interface between the DNA and the substrate, and controlling the ambient environment surrounding the DNA NW (buffer/wet vs. dry) have been explored and shown to affect conductance. It seems the overarching issue is that the structural integrity of the DNA NW is the dominant factor that affects its conductance, and there are a multitude of factors that can affect the structure/morphology of the DNA NW. Therefore, controlling the structure and surrounding environment of the DNA NW will be crucial for enhancing the conductivity of DNA NW. However, the fact that the electrical conductance of DNA NWs is dependent upon their structure and environment illustrates the potential application of DNA NWs being used as sensor devices. Ultimately, much more work remains to be done to achieve optimal performance and higher electrical conductivity, particularly in terms of reproducibility and scalability. Further research in this area has the potential to pave the way for practical applications of DNA NWs in fields such as nanoelectronics and sensing.

Chapter 8: Controlled Deposition of DNA Origami Nanowires

This chapter contains the approach, results, discussion, and conclusion for the objective of controlled deposition of DNA origami nanowires.

8.1 Introduction

In this chapter, we will discuss the techniques and results for achieving controlled deposition of DNA origami nanowires (DNA NWs). For DNA NWs to be effectively used in potential applications such as nanoelectronics, researchers must be able to deposit DNA NWs in targeted locations. Therefore, this chapter will discuss a technique involving an HMDS surface treatment that has been developed to control the deposition of DNA NWs in targeted regions by attracting or repelling the DNA NWs, depending on the surface treatment. This chapter will also discuss the challenges and limitations of this technique, and future directions for research in this field.

8.2 Methods

The goal covered in this chapter is to achieve controlled deposition/delivery of DNA NWs onto test substrates, such as the Electrode Array Chip (EAC). To this end, the experimental design and methods that pertain to this objective are laid out in this section. The approach for controlled deposition of DNA origami nanowires is as follows. The EAC is cleaned with a ~1-minute O_2 plasma etch just prior to surface treatment. Next, the EAC is surface treated to create hydrophobic/hydrophilic surface (e.g., HMDS, APTES). The DNA origami nanowire solution is

then applied to the EAC and allowed to incubate on the chip. Next, the EAC is washed to remove excess salt/buffer solution. DNA NWs are then imaged on the EAC with fluorescence microscopy. After imaging, the EAC is vacuum dried to remove water and prevent contamination of DNA nanowires. The sample may then be electrically measured if desired.

The approach for this objective is very similar to that used previously for electrical characterization of DNA NWs, with the primary difference being the surface treatment of the EAC before the deposition, washing, imaging, and electrical measuring of the DNA NWs on the EAC. The surface treatment of the EAC is accomplished by depositing a chemical/molecular coating on the surface of the chip to make the chip hydrophobic/hydrophilic and/or change the surface charge/chemistry of the chip.

Surface Treatment of Electrode Array Chip (EAC):

The primary strategy for achieving controlled deposition of DNA NWs is to perform a surface treatment of the EAC by depositing and possibly spin-coating a chemical/molecular coating to create a self-assembled monolayer (SAM) on the surface of the chip to modify the surface properties of the chip to make it hydrophobic/hydrophilic and/or change the surface charge of the chip. As discussed in the background section on DNA Origami Deposition; this can be accomplished with several different techniques. Perhaps the most straightforward technique is to create a hydrophobic surface (e.g., with an HMDS monolayer). DNA is hydrophilic with a negatively charged sugar-phosphate backbone. Therefore, DNA is repelled from the hydrophobic HMDS monolayer that is bound to the silicon nitride (Si_3N_4) insulator surface, and DNA instead migrates towards the gold electrodes where the thiols that are attached to the DNA NWs assist with forming a strong electrically conductive covalent bond between the gold and the DNA NWs.

There is evidence (e.g., from AFM studies) that the shape, morphology, and height/thickness of DNA is affected by its interaction with the surfaces of substrates such as silicon dioxide (SiO_2), silicon nitride (Si_3N_4), and mica. This change in the shape, morphology, and height/thickness of DNA affects the electrical conductivity of the DNA. Therefore, passivating the surface of the Si_3N_4 substrate with chemical/molecular monolayers such as HMDS has an additional benefit because it helps to mitigate the interactions between the DNA and the substrate.

If depositing a monolayer of HMDS on the entire surface of the Si_3N_4 substrate is not sufficient for the controlled deposition of DNA NWs, it is possible to remove selective regions of the HMDS monolayer using photolithography with photoresist and an O_2 plasma etch to remove the HMDS in the lithographically patterned areas, and then strip off the photoresist to reveal the remaining HMDS monolayer. When the SiO_2 or Si_3N_4 substrate undergoes an O_2 plasma etch, it creates surface silanols. These surface silanols are negatively charged but can attract and adhere DNA with the proper buffer conditions (e.g., magnesium ion concentration, pH). The concentration of magnesium ions (Mg^{2+}) in the DNA buffer solution can affect the adhesion and mobility of DNA NWs, as an insufficient amount of divalent magnesium cations reduces the number of Mg^{2+} bridges between the DNA NWs and ionized silanols and affects the charge neutralization within the DNA structure. A previous study has revealed that maximum DNA-substrate binding is observed at ~35 mM Mg^{2+}, 110 pM DNA origami, pH 8.35, and a 60-minute incubation time. Therefore, these are desirable DNA origami nanowire deposition conditions that could be used for HMDS-treated substrates where the HMDS has been selectively removed with photolithography and an O_2 plasma etch to create surface silanols on the Si_3N_4 substrate.

However, DNA NWs that are weakly bound to the Si_3N_4 substrate via Mg^{2+} bridges between the DNA and ionized silanols are susceptible to being removed from the substrate during

washing protocols, due to the weak DNA-substrate binding and the high solubility of DNA in water. Therefore, it may be preferable to wash the DNA and substrate with a series of 50% - 90% ethanol-in-water solutions, in which DNA is less soluble but the buffer solution and magnesium ions can still be washed away efficiently, and then the substrate can be allowed to dry under ambient conditions to leave behind the DNA NWs adhered onto the clean and dry Si_3N_4 substrate. It may also be preferable to use another method such as silane chemistry to achieve controlled deposition of DNA NWs. For example, the surface silanols that are created on the Si_3N_4 substrate during the O_2 plasma etch can be converted into positively charged amino groups ($–NH^{3+}$) using a silanization agent such as aminopropyl silatrane or (3-aminopropyl)triethoxysilane (APTES), which make the surface of the SiO_2 substrate positively charged in order to attract the negatively charged sugar-phosphate backbone of the DNA. Aminopropyl silatrane is much less prone to aggregation than APTES, so it if preferable to use aminopropyl silatrane as the silanization agent. In this way, it is possible to achieve DNA NW deposition/adhesion without any magnesium ions (Mg^{2+}), or with a very low magnesium ion concentration. This has the additional benefit of reducing the amount of magnesium ions that remain on the DNA NWs and substrate after deposition and imaging, which reduces the amount of parasitic ionic conduction along the DNA NWs during the electrical conductance measurements.

If the methods and strategies that have already been discussed do not work for some reason, there are other strategies that could either accompany or replace the primary strategies for the controlled deposition of DNA NWs. One of these strategies includes getting DNA NWs to land in certain locations using functionalization of the DNA; which we are already doing to a certain extent with thiol linkers on both ends of the DNA NWs for bonding the DNA to gold, but could be done in an even more targeted approach by using specific DNA hybridization between the DNA

NWs and thiol-linked nucleotide sequences that only match certain ends of a DNA NW, only match certain types of DNA NWs (e.g., intercalated vs. non-intercalated), and/or are only located on some gold electrodes. Furthermore, molecular combing can be used to orient DNA strands and DNA nanowires in particular directions, which is achieved by the flowing or moving of droplets of DNA solution across the substrate (e.g., by gently flowing compressed air or nitrogen at a ~45° angle to blow the droplet across the substrate, by wicking the DNA solution across the substrate with capillary action, or by simply allowing the droplet to evaporate and the meniscus to recede) [128], [129], [130]. Another technique is spray-coating or print-coating, which does not require any surface pre-treatment of the substrate, can be done with low-magnesium or magnesium-free DNA origami solutions, does not require any washing protocols, and a PDMS mask can be used for selective deposition of the DNA origami [131]. Other strategies could include using optical tweezers for alignment of DNA, or a microfluidic platform for selectively flowing the DNA NW solution across only the desired deposition regions.

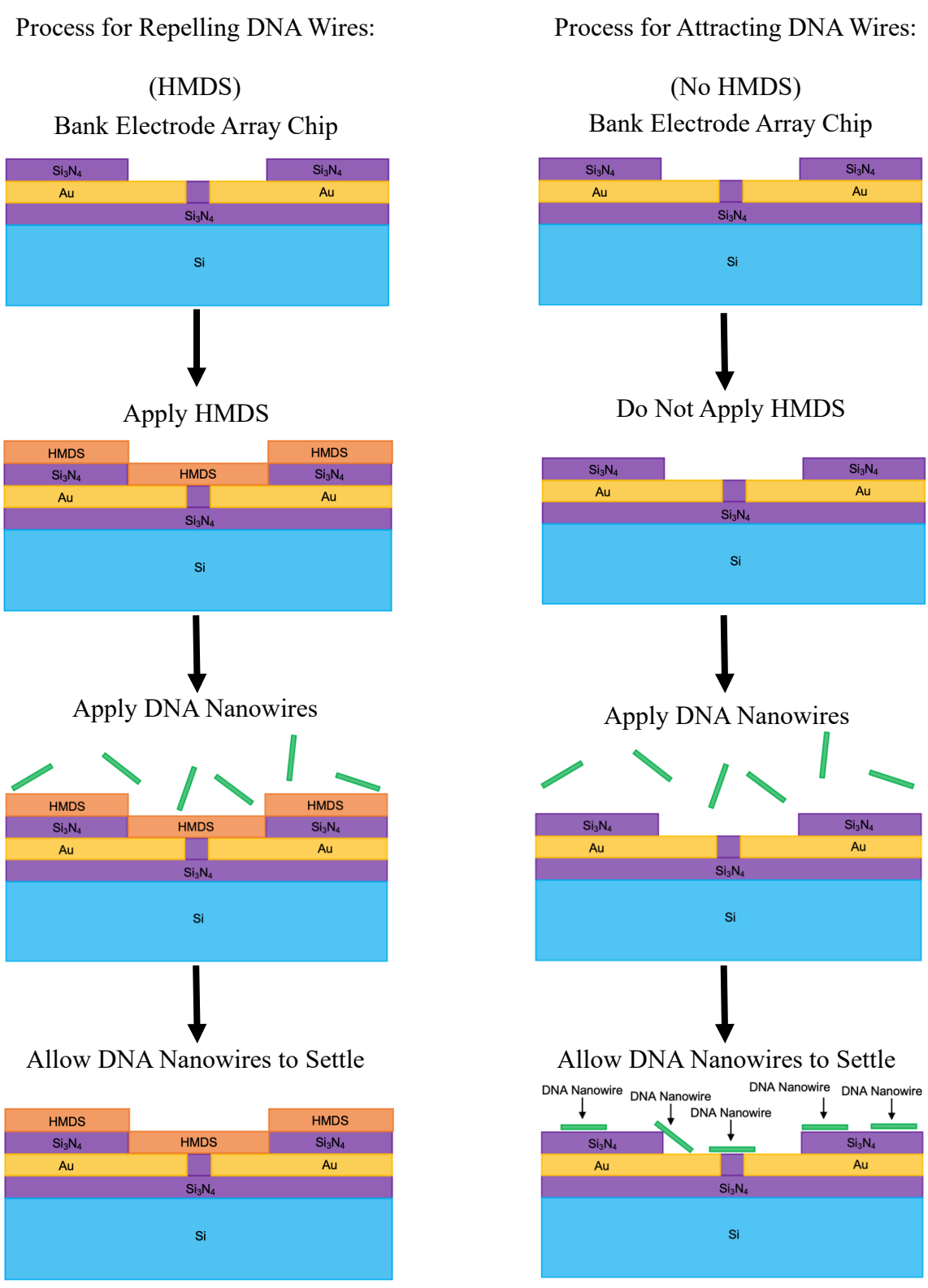

Figure 8.1. Process for Repelling vs. Attracting DNA Origami Nanowires

8.3 Results

Fluorescence Images of HMDS Surface Pre-Treatment vs. No HMDS Surface Pre-Treatment:

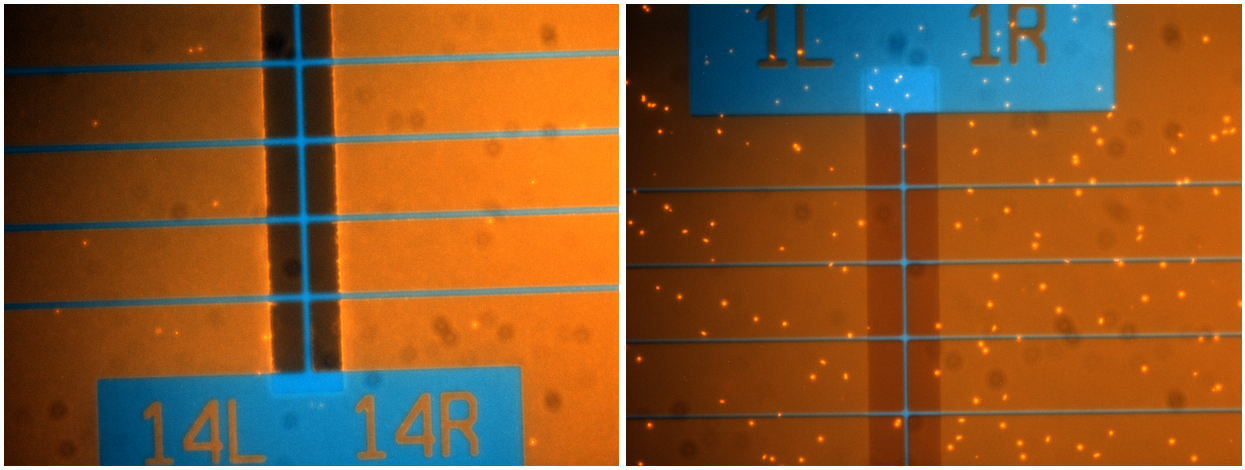

Figure 8.2. Fluorescence Microscopy Images of EAC with HMDS Surface Treatment to Repel DNA Wires (Left) and of EAC with No HMDS Surface Treatment to Attract DNA Wires (Right)

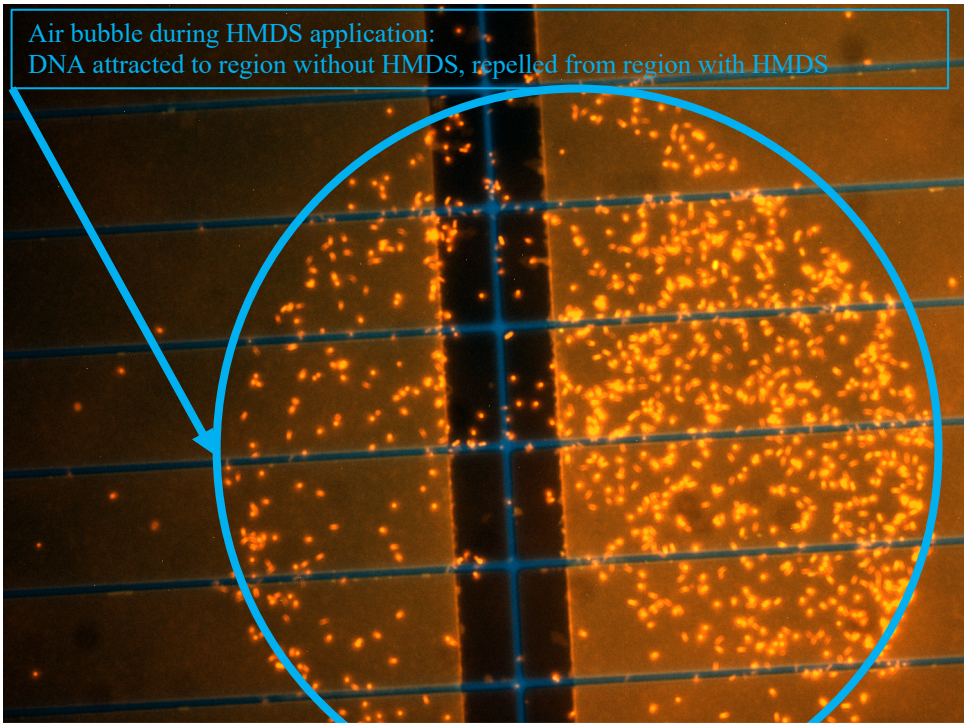

Figure 8.3. Fluorescence Microscopy Image of EAC with and without HMDS Surface Pre-Treatment (Circular Area Has No HMDS Due to Air Bubble During HMDS Application)

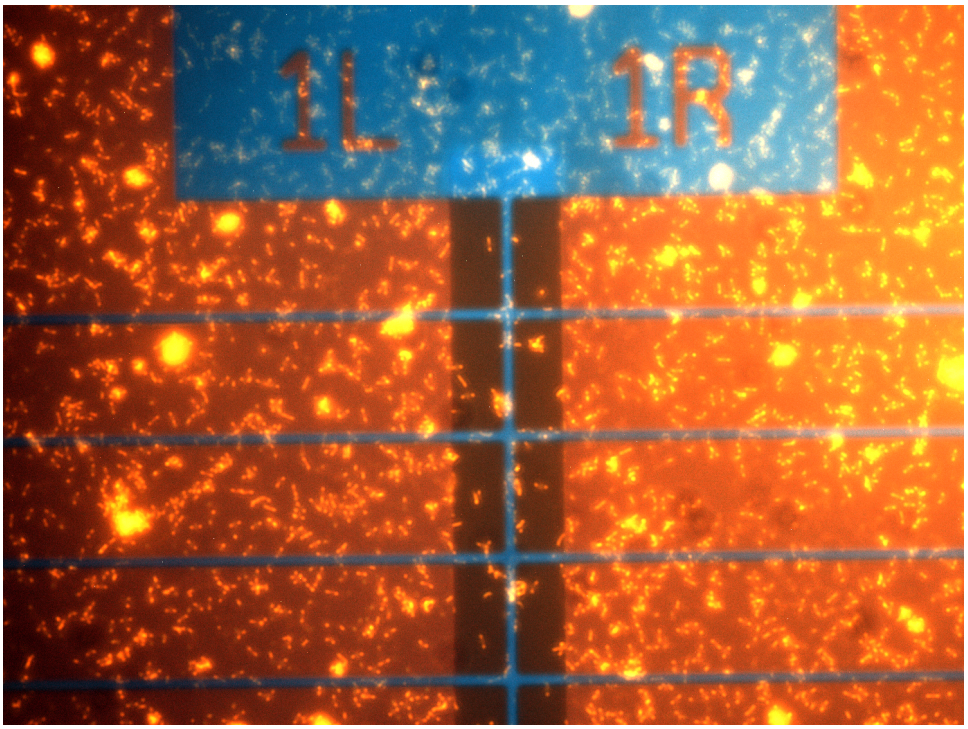

Figure 8.4. Fluorescence Microscopy Image of EAC with HMDS Surface Pre-Treatment (DNA 5-mer Wires)

(DNA 5-mer Wires Have Alexa 488 Fluorophores, Making HMDS Ineffective for Selectivity)

The figures above show fluorescence images that reveal that applying an HMDS surface pre-treatment to the Electrode Array Chip is effective at repelling DNA NWs without Alexa 488 fluorophores away from the Electrode Array Chip, whereas not applying an HMDS surface pre-treatment causes the wires to be deposited and attracted onto the chip. These results prove that HMDS could provide a mechanism or strategy for selective deposition of DNA NWs. However, when the DNA NWs have Alexa 488 fluorophores attached to them, the DNA NWs are not repelled by the HMDS surface treatment, but instead stick to the substrate. Therefore, it appears that selective deposition/repulsion with HMDS only works for DNA NWs without Alexa 488 fluorophores.

8.4 Discussion

One of the outcomes for this objective is a proof of concept or successful demonstration of the controlled deposition of DNA NWs on substrates. This would create a framework for the capability to eventually deposit DNA NWs in targeted locations on substrates. The experimental results are promising for this objective, as the results have yielded a successful demonstration in which DNA NWs that do not have Alexa 488 fluorophores attached to them are selectively repelled from Si_3N_4 substrates that are pre-treated with HMDS, whereas the same DNA NWs without Alexa 488 fluorophores are attracted to Si_3N_4 substrates that are not pre-treated with HMDS. Therefore, the outcome of controlled deposition of DNA NWs could be achieved by patterning substrates such as Si_3N_4 using photoresist and photolithography to add or remove molecular monolayer surface treatments such as HMDS in the patterned regions, thereby causing DNA NWs to be selectively deposited only in the patterned regions. While HMDS repels DNA NWs, there are other molecular monolayers such as APTES that attract DNA NWs, thereby enabling the substrate to be selectively coated with molecular monolayers that either repel or attract the DNA NWs in specific regions on the chip. Using these techniques, it should be possible to trap individual DNA NWs with control over the orientation, position, and location of the DNA NWs on the substrate/chip. This trapping or controlled deposition could be achieved if the size and aspect ratio of the patterned regions of the photoresist are designed appropriately. The best resolution that I have been able to achieve with an optical photolithography process in the university cleanroom is 500 nm – 250 nm. The DNA origami 5-mer nanowires are about 10 nm wide x 1.25 μm long. Therefore, rectangular deposition areas/patterns in the photoresist could be 250 nm wide x 1.5 μm long, or 500 nm wide x 1.5 μm long. This will eventually allow circuit elements to be constructed out of DNA NWs that are placed on substrates to build circuits and devices with DNA NWs on chips.

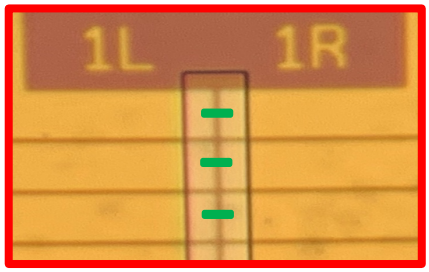

Figure 8.5. Overhead/Top Profile of Targeted Deposition of DNA Origami Nanowires

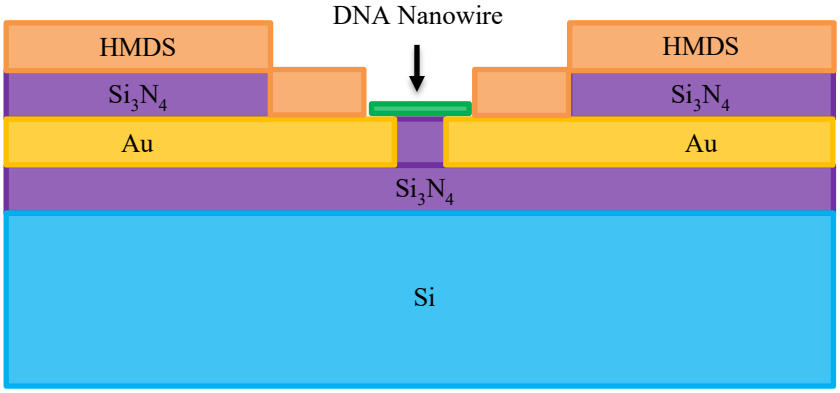

Figure 8.6. Cutaway/Side Profile of Targeted Deposition of DNA Origami Nanowires

The figures shown above depict conceptually how targeted deposition of DNA NWs would work. The top figure shows an overhead perspective of how the DNA NWs (shown in green) could get deposited neatly and reliably across pairs of gold electrodes, with ~1 DNA NW per pair of gold electrodes. This would be an ideal scenario for electrically characterizing DNA NWs and creating reliable and consistent devices. The bottom figure shows a cutaway/side profile of targeted deposition of DNA NWs, with the DNA nanowire shown in green. The DNA NW appears only in the region that is not covered/treated with HMDS.

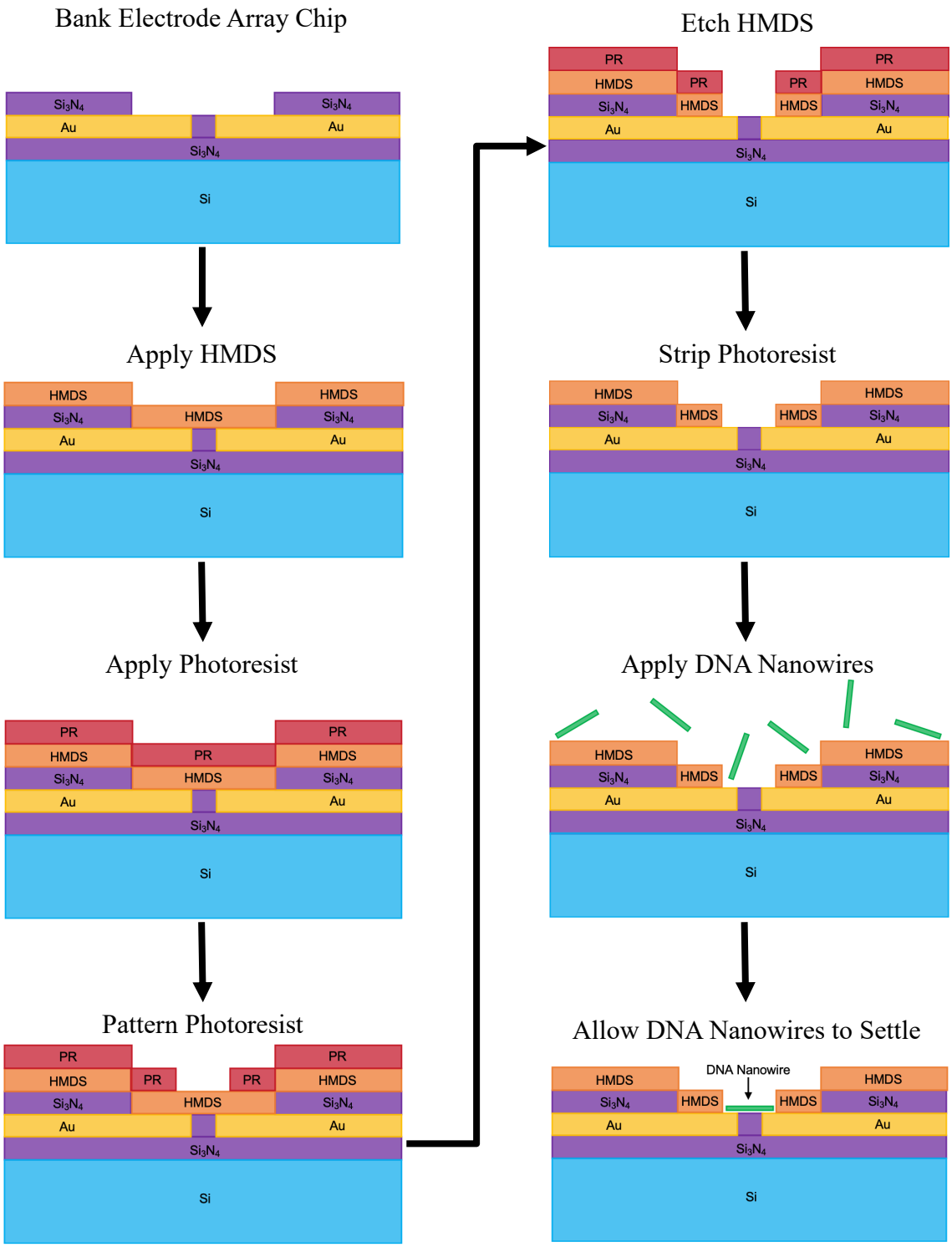

Figure 8.7. Process for Targeted Deposition of DNA Origami Nanowires

8.5 Conclusion

In summary, this chapter covered controlled deposition of DNA NWs. The experimental results from this chapter indicate that HMDS could be used as a potential tool to control the selective deposition of DNA NWs, by repelling DNA in areas with an HMDS surface treatment while attracting DNA in areas without an HMDS surface treatment. However, it appears that the Alexa 488 fluorophores attached to the DNA NW may interfere with the repulsion of DNA NWs from the HMDS surface treatment, potentially making this technique appropriate only for DNA NWs with few/no Alexa 488 fluorophores attached to them. These results successfully demonstrate a proof of concept and a framework that could be extended towards eventually achieving targeted deposition of DNA NWs on substrates. Perhaps the biggest challenge for achieving targeted deposition of DNA NWs is to incrementally improve the yield and the precision of placement for DNA NWs on substrates, as the resolution of photolithography systems in many university cleanrooms is fairly limited with micron-scale resolution. Therefore, a logical next step would be to perform another proof-of-concept experiment using electron-beam (E-beam) lithography to define nanoscale patterns (with ~10 nm or ~100 nm resolution) into the HMDS surface treatment to attract individual nanowires that have similar dimensions as the very small rectangular patterns (e.g., 50 nm x 500 nm) capable of being drawn by an E-beam lithography system. Overall, the research results so far provide a trajectory towards eventually controlling the placement of many different DNA NWs on substrates to form intricate, complex, and useful devices.

Chapter 9: Future Directions

With the objectives of this dissertation being accomplished, the next logical step would be to put the achievement of these goals to practical use by demonstrating the utility of DNA origami nanowires (DNA NWs) for DNA-based electronics by creating an actual functioning prototype of a DNA-based nanoelectronic device. Therefore, one potentially useful nanoelectronic device could be an electrical DNA origami nanowire non-volatile read-only memory (DNA NW ROM) device. Such a DNA NW ROM device would enable non-volatile read-only storage of vast amounts of data, because DNA is only ~2 nm in diameter and is among the smallest practical materials that is known to humankind. DNA is already well-known for reliably and efficiently encoding very sophisticated and important information in very small form factors (e.g., the ~3 billion base pairs of the human genome, which can fit within the ~6 μm diameter nucleus of a cell). Electronically encoding information in a slightly different form factor (e.g., ~100 megabytes/mm^2 for a 2D layout, or ~1 terabyte/mm^3 for a 3D layout) using ~10 nm wide x ~100 nm long DNA NWs would enable unprecedented data storage capabilities and allow such data to be read electronically by computers, which would greatly benefit many existing big data applications and would unlock a myriad of new applications. For example, everyone could walk around with the entire contents of the Library of Congress (~100 terabytes) stored on a single (1 cm x 1 cm x 1 mm) chip within a smartphone or USB flash drive in their pocket, allowing them to access the information without a mobile/internet connection.

While this ultra-high-density data storage capacity may seem unfeasible with contemporary technology, such futuristic applications could well become reality if DNA nanotechnology continues to flourish and advances continue to be made in the field of DNA nanoelectronics. However, the next step towards achieving such lofty goals would be to create

prototypes of DNA NW ROM devices that initially have very little data storage capacity but have increasingly more data storage capacity with each successive generation of the prototype (e.g., 64 bits, 128 bits, 256 bits, …, 1 MB, 1 GB, 1 TB, 100 TB). The initial prototype would have only a 2D layout with discrete DNA NWs connected to pairs of lithographically defined gold electrodes, with each DNA NW forming an individual memory cell, in order to store a limited number of bits (e.g., 64 bits). Those 64 DNA NWs that form 64 individual memory cells or 64 bits would be able to encode a short message such as "UC Davis" comprised of 8 ASCII characters or 8 bytes. This initial prototype would serve as a proof-of-concept to confirm that DNA NWs can be used to create a functioning DNA NW ROM device. The final prototype could eventually have a 3D layout with a network of DNA NWs that are self-assembled into a monolithic DNA NW superstructure, which would be precisely aligned and mounted onto a silicon chip with gold electrodes for electrical readout. Such 3D DNA NW ROM devices could enable unprecedented ultra-high-density storage.

Different strategies could be used to encode digital information in the form of a high electrical conductance "1" or a low electrical conductance "0" in each memory cell, such as selectively depositing electrically conductive DNA NWs only in memory cells that will encode a "1" and not in memory cells that will encode a "0". Another strategy is to deposit DNA NWs in all memory cells, but only intercalate or enhance the electrical conductivity of DNA NWs in the memory cells that will encode a "1" while leaving DNA NWs in the memory cells that will encode a "0" with the natively low electrical conductivity of intrinsic DNA NWs. Alternatively, each DNA NW could have its electrical conductivity enhanced to one of multiple different resistance values (e.g., by exposing some DNA NWs to a higher concentration/dose of intercalators than others).

Chapter 10: Conclusion

DNA origami is a novel technology that has the potential to be utilized as a platform for creating next-generation electronics. There are several advantages that DNA origami provides for building circuits; such as the nanoscale size of DNA origami, its customizability and functionalization, and its ability to be fabricated with a bottom-up rather than a top-down approach. DNA origami is useful for constructing a plethora of different nanoscale structures, including DNA origami nanowires (DNA NWs). Surprisingly, relatively little research has been performed on the electrical properties of DNA origami, strategies for enhancing its electrical conductance, methods for selectively controlling the deposition of DNA origami onto various substrates, and the potential usefulness of DNA origami for constructing electronic circuits. DNA has a relatively high impedance, which from a rudimentary standpoint would seem to preclude DNA from being used in electronic circuits. However, the conductivity of DNA may be controlled or enhanced through a variety of different methodologies; such as doping the DNA with intercalators, functionalizing the DNA with highly conductive nanomaterials, and attaching linkers such as thiols onto the DNA to form strong covalent and electrically conductive bonds with metals such as gold.

If the electrical conductivity of DNA origami can be enhanced to a sufficient extent, then DNA NWs could be used as circuit elements in electronic devices; such as highly resistive or highly conductive memory cells for encoding data. Furthermore, if DNA NWs can be made to be very conductive at longer length scales, then such DNA nanowires could be used not only as circuit elements, but also as wires that route electrical signals between circuit elements. Finally, DNA origami could also be utilized to create templates or scaffolds for fabricating nanoscale circuits and to place electrically conductive nanoscale materials such carbon nanotubes and gold nanoparticles with unprecedented accuracy and precision using a bottom-up fabrication approach.

Ultimately, these DNA origami nanoscale circuits and nanodevices could be integrated with conventional semiconductor technology to be incorporated into semiconductor chips such as ultra-high density read-only memories for everyday electronics.

Chapter 11: References

[1] P. Ye, T. Ernst, and M. V. Khare, "The last silicon transistor: Nanosheet devices could be the final evolutionary step for Moore's Law," *IEEE Spectr.*, vol. 56, no. 8, pp. 30–35, Aug. 2019.

[2] J. M. Shalf and R. Leland, "Computing beyond moore's law," *Computer (Long. Beach. Calif).*, vol. 48, no. 12, pp. 14–23, Dec. 2015.

[3] M. Bathe and P. W. K. Rothemund, "DNA nanotechnology: A foundation for programmable nanoscale materials," *MRS Bull.*, vol. 42, no. 12, pp. 882–888, Dec. 2017.

[4] T. N. Theis and H. S. Philip Wong, "The End of Moore's Law: A New Beginning for Information Technology," *Comput. Sci. Eng.*, vol. 19, no. 2, pp. 41–50, Mar. 2017.

[5] T. Zhang *et al.*, "3D DNA Origami Crystals," *Adv. Mater.*, vol. 30, no. 28, p. 1800273, Jul. 2018.

[6] R. S. Williams, "What's Next?," *Comput. Sci. Eng.*, vol. 19, no. 2, pp. 7–13, Mar. 2017.

[7] G. Whitesides, J. Mathias, and C. Seto, "Molecular self-assembly and nanochemistry: a chemical strategy for the synthesis of nanostructures," *Science*, vol. 254, no. 5036, pp. 1312–1319, Nov. 1991.

[8] S. Nummelin, J. Kommeri, M. A. Kostiainen, and V. Linko, "Evolution of Structural DNA Nanotechnology," *Adv. Mater.*, vol. 30, no. 24, p. 1703721, Jun. 2018.

[9] Y. Ke *et al.*, "DNA brick crystals with prescribed depths," *Nat. Chem.*, vol. 6, no. 11, pp. 994–1002, Nov. 2014.

[10] Y. Hu and C. M. Niemeyer, "From DNA Nanotechnology to Material Systems Engineering," *Adv. Mater.*, vol. 31, no. 26, p. 1806294, Jun. 2019.

[11] G. E. Moore, "Cramming more components onto integrated circuits," *Electronics*, vol. 38, no. 8, pp. 114–117, Apr. 1965.

[12] M. M. Waldrop, "The chips are down for Moore's law," *Nature*, vol. 530, no. 7589, pp. 144–147, Feb. 2016.

[13] R. K. Cavin, P. Lugli, and V. V. Zhirnov, "Science and Engineering Beyond Moore's Law," *Proc. IEEE*, vol. 100, no. Special Centennial Issue, pp. 1720–1749, May 2012.

[14] G. Ferry, "The structure of DNA," *Nature*, vol. 575, no. 7781, pp. 35–36, Nov. 2019.

[15] J. D. Watson and F. H. C. Crick, "Molecular Structure of Nucleic Acids: A Structure for Deoxyribose Nucleic Acid," *Nature*, vol. 171, no. 4356, pp. 737–738, Apr. 1953.

[16] J. C. Venter *et al.*, "The sequence of the human genome," *Science*, vol. 291, no. 5507, pp. 1304–1351, Feb. 2001.

[17] E. S. Lander *et al.*, "Initial sequencing and analysis of the human genome," *Nature*, vol. 409, no. 6822, pp. 860–921, Feb. 2001.

[18] E. Check Hayden, "Technology: The $1,000 genome," *Nature*, vol. 507, no. 7492, pp. 294–295, Mar. 2014.

[19] D. G. Gibson *et al.*, "Creation of a bacterial cell controlled by a chemically synthesized genome," *Science*, vol. 329, no. 5987, pp. 52–56, Jul. 2010.

[20] R. Feynman, "There's Plenty of Room at the Bottom," *Eng. Sci.*, vol. 23, no. 5, pp. 22–36, Feb. 1960.

[21] N. C. Seeman, "Nucleic acid junctions and lattices," *J. Theor. Biol.*, vol. 99, no. 2, pp. 237–247, Nov. 1982.

[22] E. Winfree, F. Liu, L. A. Wenzler, and N. C. Seeman, "Design and self-assembly of two-dimensional DNA crystals," *Nature*, vol. 394, no. 6693, pp. 539–544, Aug. 1998.

[23] N. C. Seeman and H. F. Sleiman, “DNA nanotechnology,” *Nat. Rev. Mater.*, vol. 3, no. 1, p. 17068, Nov. 2017.
[24] V. Linko and H. Dietz, “The enabled state of DNA nanotechnology,” *Curr. Opin. Biotechnol.*, vol. 24, no. 4, pp. 555–561, Aug. 2013.
[25] N. C. Seeman, “DNA in a material world,” *Nature*, vol. 421, no. 6921, pp. 427–431, Jan. 2003.
[26] P. W. K. Rothemund, “Folding DNA to create nanoscale shapes and patterns,” *Nature*, vol. 440, no. 7082, pp. 297–302, Mar. 2006.
[27] F. Hong, F. Zhang, Y. Liu, and H. Yan, “DNA Origami: Scaffolds for Creating Higher Order Structures,” *Chem. Rev.*, vol. 117, no. 20, pp. 12584–12640, Oct. 2017.
[28] S. M. Douglas, H. Dietz, T. Liedl, B. Högberg, F. Graf, and W. M. Shih, “Self-assembly of DNA into nanoscale three-dimensional shapes,” *Nature*, vol. 459, no. 7245, pp. 414–418, May 2009.
[29] H. Dietz, S. M. Douglas, and W. M. Shih, “Folding DNA into twisted and curved nanoscale shapes,” *Science*, vol. 325, no. 5941, pp. 725–30, Aug. 2009.
[30] D. Han, S. Pal, J. Nangreave, Z. Deng, Y. Liu, and H. Yan, “DNA origami with complex curvatures in three-dimensional space,” *Science*, vol. 332, no. 6027, pp. 342–6, Apr. 2011.
[31] P. Wang, T. A. Meyer, V. Pan, P. K. Dutta, and Y. Ke, “The Beauty and Utility of DNA Origami,” *Chem*, vol. 2, no. 3, pp. 359–382, Mar. 2017.
[32] A. Heuer-Jungemann and T. Liedl, “From DNA Tiles to Functional DNA Materials,” *Trends Chem.*, vol. 1, no. 9, pp. 799–814, Dec. 2019.
[33] K. F. Wagenbauer, C. Sigl, and H. Dietz, “Gigadalton-scale shape-programmable DNA assemblies,” *Nature*, vol. 552, no. 7683, pp. 78–83, Dec. 2017.
[34] A. Xu *et al.*, “DNA origami: The bridge from bottom to top,” *MRS Bull.*, vol. 42, no. 12, pp. 943–950, Dec. 2017.
[35] F. Praetorius, B. Kick, K. L. Behler, M. N. Honemann, D. Weuster-Botz, and H. Dietz, “Biotechnological mass production of DNA origami,” *Nature*, vol. 552, no. 7683, pp. 84–87, Dec. 2017.
[36] “Practical DNA,” *Nature*, vol. 531, no. 7594, pp. 276–276, Mar. 2016.
[37] P. L. Xavier and A. R. Chandrasekaran, “DNA-based construction at the nanoscale: emerging trends and applications,” *Nanotechnology*, vol. 29, no. 6, p. 062001, Feb. 2018.
[38] S. Ramakrishnan, H. Ijäs, V. Linko, and A. Keller, “Structural stability of DNA origami nanostructures under application-specific conditions,” *Comput. Struct. Biotechnol. J.*, vol. 16, pp. 342–349, Jan. 2018.
[39] H. Kim, S. P. Surwade, A. Powell, C. O’Donnell, and H. Liu, “Stability of DNA Origami Nanostructure under Diverse Chemical Environments,” *Chem. Mater.*, vol. 26, no. 18, pp. 5265–5273, Sep. 2014.
[40] M. Madsen and K. V. Gothelf, “Chemistries for DNA Nanotechnology,” *Chem. Rev.*, vol. 119, no. 10, pp. 6384–6458, Feb. 2019.
[41] J. Sharma, R. Chhabra, C. S. Andersen, K. V. Gothelf, H. Yan, and Y. Liu, “Toward Reliable Gold Nanoparticle Patterning On Self-Assembled DNA Nanoscaffold,” *J. Am. Chem. Soc.*, vol. 130, no. 25, pp. 7820–7821, Jun. 2008.
[42] T. G. W. Edwardson, K. L. Lau, D. Bousmail, C. J. Serpell, and H. F. Sleiman, “Transfer of molecular recognition information from DNA nanostructures to gold nanoparticles,” *Nat. Chem.*, vol. 8, no. 2, pp. 162–170, Feb. 2016.
[43] Y. Tian, Y. Zhang, T. Wang, H. L. Xin, H. Li, and O. Gang, “Lattice engineering through

nanoparticle–DNA frameworks," *Nat. Mater.*, vol. 15, no. 6, pp. 654–661, Jun. 2016.
[44] R. Schreiber, I. Santiago, A. Ardavan, and A. J. Turberfield, "Ordering Gold Nanoparticles with DNA Origami Nanoflowers," *ACS Nano*, vol. 10, no. 8, pp. 7303–7306, Aug. 2016.
[45] W. Liu, J. Halverson, Y. Tian, A. V. Tkachenko, and O. Gang, "Self-organized architectures from assorted DNA-framed nanoparticles," *Nat. Chem.*, vol. 8, no. 9, pp. 867–873, Sep. 2016.
[46] X. Luo, P. Chidchob, J. F. Rahbani, and H. F. Sleiman, "Encapsulation of Gold Nanoparticles into DNA Minimal Cages for 3D-Anisotropic Functionalization and Assembly," *Small*, vol. 14, no. 5, p. 1702660, Feb. 2018.
[47] M. Taniguchi and T. Kawai, "DNA electronics," *Phys. E Low-Dimensional Syst. Nanostructures*, vol. 33, no. 1, pp. 1–12, Jun. 2006.
[48] S. S. Mallajosyula and S. K. Pati, "Toward DNA conductivity: A theoretical perspective," *J. Phys. Chem. Lett.*, vol. 1, no. 12, pp. 1881–1894, Jun. 2010.
[49] D. D. Eley and D. I. Spivey, "Semiconductivity of organic substances. Part 9. - Nucleic acid in the dry state," *Trans. Faraday Soc.*, vol. 58, pp. 411–415, Jan. 1962.
[50] J. Jortner, M. Bixon, T. Langenbacher, and M. E. Michel-Beyerle, "Charge transfer and transport in DNA," *Proc. Natl. Acad. Sci. U. S. A.*, vol. 95, no. 22, pp. 12759–12765, Oct. 1998.
[51] L. Xiang, J. L. Palma, C. Bruot, V. Mujica, M. A. Ratner, and N. Tao, "Intermediate tunnelling-hopping regime in DNA charge transport," *Nat. Chem.*, vol. 7, no. 3, pp. 221–226, Feb. 2015.
[52] N. Goshi, A. Narenji, C. Bui, J. L. Mokili, and S. Kassegne, "Investigation Into the Effects of Nucleotide Content on the Electrical Characteristics of DNA Plasmid Molecular Wires," *IEEE Trans. Nanobioscience*, vol. 15, no. 6, pp. 585–594, Sep. 2016.
[53] J. C. Genereux and J. K. Barton, "Mechanisms for DNA Charge Transport," *Chem. Rev.*, vol. 110, no. 3, pp. 1642–1662, Mar. 2010.
[54] M. Bixon, B. Giese, S. Wessely, T. Langenbacher, M. E. Michel-Beyerle, and J. Jortner, "Long-range charge hopping in DNA," *Proc. Natl. Acad. Sci. U. S. A.*, vol. 96, no. 21, pp. 11713–11716, Oct. 1999.
[55] E. M. Boon and J. K. Barton, "Charge transport in DNA," *Curr. Opin. Struct. Biol.*, vol. 12, no. 3, pp. 320–329, Jun. 2002.
[56] Y. A. Berlin, A. L. Burin, and M. A. Ratner, "DNA as a molecular wire," *Superlattices Microstruct.*, vol. 28, no. 4, pp. 241–252, Oct. 2000.
[57] J. C. Genereux and J. K. Barton, "Molecular electronics: DNA charges ahead," *Nat. Chem.*, vol. 1, no. 2, pp. 106–107, May 2009.
[58] A. Golkar Narenji *et al.*, "Electrochemical Characterization of Synthetic Hybrid DNA Molecular Wires," *ECS Trans.*, vol. 72, no. 3, pp. 21–27, May 2016.
[59] K. L. Jiménez-Monroy *et al.*, "High Electronic Conductance through Double-Helix DNA Molecules with Fullerene Anchoring Groups," *J. Phys. Chem. A*, vol. 121, no. 6, pp. 1182–1188, Feb. 2017.
[60] Z. G. Yu and X. Song, "Variable range hopping and electrical conductivity along the DNA double helix," *Phys. Rev. Lett.*, vol. 86, no. 26, pp. 6018–6021, Jun. 2001.
[61] Y. S. Jo, Y. Lee, and Y. Roh, "Current-voltage characteristics of λ- and poly-DNA," *Mater. Sci. Eng. C*, vol. 23, no. 6–8, pp. 841–846, Dec. 2003.
[62] T. Heim, D. Deresmes, and D. Vuillaume, "Conductivity of DNA probed by conducting-atomic force microscopy: Effects of contact electrode, DNA structure, and surface

interactions," *J. Appl. Phys.*, vol. 96, no. 5, pp. 2927–2936, Sep. 2004.
[63] R. G. Endres, D. L. Cox, and R. R. P. Singh, "Colloquium: The quest for high-conductance DNA," *Rev. Mod. Phys.*, vol. 76, no. 1, pp. 195–214, Jan. 2004.
[64] A. Y. Kasumov, D. V. Klinov, P. E. Roche, S. Guéron, and H. Bouchiat, "Thickness and low-temperature conductivity of DNA molecules," *Appl. Phys. Lett.*, vol. 84, no. 6, pp. 1007–1009, Feb. 2004.
[65] H. W. Fink and C. Schönenberger, "Electrical conduction through DNA molecules," *Nature*, vol. 398, no. 6726, pp. 407–410, Apr. 1999.
[66] D. Porath, A. Bezryadin, S. De Vries, and C. Dekker, "Direct measurement of electrical transport through DNA molecules," *Nature*, vol. 403, no. 6770, pp. 635–638, Feb. 2000.
[67] J. D. Slinker, N. B. Muren, S. E. Renfrew, and J. K. Barton, "DNA charge transport over 34 nm," *Nat. Chem.*, vol. 3, no. 3, pp. 228–233, Mar. 2011.
[68] D. Porath, N. Lapidot, and J. Gomez-herrero, "Charge transport in DNA-based devices," in *Lecture Notes in Physics*, vol. 680, Springer, Berlin, Heidelberg, 2006, pp. 411–444.
[69] Y. Li *et al.*, "Detection and identification of genetic material via single-molecule conductance," *Nat. Nanotechnol.*, vol. 13, no. 12, pp. 1167–1173, Nov. 2018.
[70] D. Bouilly, "Detecting short RNA sequences of pathogens," *Nat. Nanotechnol.*, vol. 13, no. 12, pp. 1094–1096, Dec. 2018.
[71] Xu, Zhang, Li, and Tao, "Direct Conductance Measurement of Single DNA Molecules in Aqueous Solution," *Nano Lett.*, vol. 4, no. 6, pp. 1105–1108, Jun. 2004.
[72] J. Hihath, B. Xu, P. Zhang, and N. Tao, "Study of single-nucleotide polymorphisms by means of electrical conductance measurements," *Proc. Natl. Acad. Sci. U. S. A.*, vol. 102, no. 47, pp. 16979–16983, Nov. 2005.
[73] J. M. Artés, Y. Li, J. Qi, M. P. Anantram, and J. Hihath, "Conformational gating of DNA conductance," *Nat. Commun.*, vol. 6, no. 1, p. 8870, Dec. 2015.
[74] S. Kassegne *et al.*, "AC electrical characterisation and insight to charge transfer mechanisms in DNA molecular wires through temperature and UV effects," *IET Nanobiotechnology*, vol. 9, no. 3, pp. 153–163, Jun. 2015.
[75] A. G. Narenji, N. Goshi, C. Bui, J. Mokili, and S. Kassegne, "Effect of temperature and UV illumination on charge transport mechanisms in DNA," in *Nanosensors, Biosensors, and Info-Tech Sensors and Systems 2015*, 2015, vol. 9434, p. 94340C.
[76] R. Korol and D. Segal, "From Exhaustive Simulations to Key Principles in DNA Nanoelectronics," *J. Phys. Chem. C*, vol. 122, no. 8, pp. 4206–4216, Mar. 2018.
[77] Y. A. Berlin, A. L. Burin, and M. A. Ratner, "Charge hopping in DNA," *J. Am. Chem. Soc.*, vol. 123, no. 2, pp. 260–268, Jan. 2001.
[78] M. Bixon and J. Jortner, "Charge transport in DNA via thermally induced hopping," *J. Am. Chem. Soc.*, vol. 123, no. 50, pp. 12556–12567, Dec. 2001.
[79] A. D. Bobadilla *et al.*, "DNA origami impedance measurement at room temperature," *J. Chem. Phys.*, vol. 130, no. 17, p. 171101, May 2009.
[80] V. Linko, S.-T. Paasonen, A. Kuzyk, P. Törmä, and J. J. Toppari, "Characterization of the Conductance Mechanisms of DNA Origami by AC Impedance Spectroscopy," *Small*, vol. 5, no. 21, pp. 2382–2386, Nov. 2009.
[81] B. Teschome, S. Facsko, T. Schönherr, J. Kerbusch, A. Keller, and A. Erbe, "Temperature-Dependent Charge Transport through Individually Contacted DNA Origami-Based Au Nanowires," *Langmuir*, vol. 32, no. 40, pp. 10159–10165, Oct. 2016.
[82] E. Braun, Y. Eichen, U. Sivan, and G. Ben-Yoseph, "DNA-templated assembly and

electrode attachment of a conducting silver wire," *Nature*, vol. 391, no. 6669, pp. 775–778, Feb. 1998.
[83] K. Tapio, J. Leppiniemi, B. Shen, V. P. Hytönen, W. Fritzsche, and J. J. Toppari, "Toward Single Electron Nanoelectronics Using Self-Assembled DNA Structure," *Nano Lett.*, vol. 16, no. 11, pp. 6780–6786, Nov. 2016.
[84] I. D. Johnson and M. T. Z. Spence, "Nucleic Acid Detection and Analysis," in *The Molecular Probes Handbook: A Guide to Fluorescent Probes and Labeling Technologies*, 11th ed., Life Technologies, 2010.
[85] B. A. Armitage, "Cyanine Dye–DNA Interactions: Intercalation, Groove Binding, and Aggregation," in *DNA Binders and Related Subjects*, Springer, Berlin, Heidelberg, 2005, pp. 55–76.
[86] P. O. Vardevanyan, A. P. Antonyan, M. A. Parsadanyan, H. G. Davtyan, and A. T. Karapetyan, "The binding of ethidium bromide with DNA: interaction with single- and double-stranded structures," *Exp. Mol. Med.*, vol. 35, no. 6, pp. 527–533, Dec. 2003.
[87] "The 10 Best DNA Dyes and Probes | Biomol Blog | Resources | Biomol GmbH - Life Science Shop." [Online]. Available: https://www.biomol.com/resources/biomol-blog/the-10-best-dna-dyes-and-probes. [Accessed: 05-May-2020].
[88] H. Zipper, H. Brunner, J. Bernhagen, and F. Vitzthum, "Investigations on DNA intercalation and surface binding by SYBR Green I, its structure determination and methodological implications.," *Nucleic Acids Res.*, vol. 32, no. 12, p. e103, Jul. 2004.
[89] F. A. P. Crisafuli, E. B. Ramos, and M. S. Rocha, "Characterizing the interaction between DNA and GelRed fluorescent stain," *Eur. Biophys. J.*, vol. 44, no. 1–2, pp. 1–7, Feb. 2015.
[90] D. Watkins, C. Gong, P. Kellish, and D. P. Arya, "Probing A-form DNA: A fluorescent aminosugar probe and dual recognition by anthraquinone-neomycin conjugates," *Bioorganic Med. Chem.*, vol. 25, no. 4, pp. 1309–1319, Feb. 2017.
[91] D. R. G. Pitter, A. S. Brown, J. D. Baker, and J. N. Wilson, "One probe, two-channel imaging of nuclear and cytosolic compartments with orange and red emissive dyes," *Org. Biomol. Chem.*, vol. 13, no. 36, pp. 9477–9484, Aug. 2015.
[92] D. R. G. Pitter, J. Wigenius, A. S. Brown, J. D. Baker, F. Westerlund, and J. N. Wilson, "Turn-on, fluorescent nuclear stains with live cell compatibility," *Org. Lett.*, vol. 15, no. 6, pp. 1330–1333, Mar. 2013.
[93] J. N. Wilson, J. Wigenius, D. R. G. Pitter, Y. Qiu, M. Abrahamsson, and F. Westerlund, "Base pair sensitivity and enhanced ON/OFF ratios of DNA-binding: Donor-acceptor-donor fluorophores," *J. Phys. Chem. B*, vol. 117, no. 40, pp. 12000–12006, Oct. 2013.
[94] H.-K. Liu and P. J. Sadler, "Metal Complexes as DNA Intercalators," *Acc. Chem. Res.*, vol. 44, no. 5, pp. 349–359, May 2011.
[95] R. E. Holmlin, P. J. Dandliker, and J. K. Barton, "Charge Transfer through the DNA Base Stack," *Angew. Chemie (International Ed. English)*, vol. 36, no. 24, pp. 2714–2730, Jan. 1997.
[96] A. E. Gerdon, S. S. Oh, K. Hsieh, Y. Ke, H. Yan, and H. T. Soh, "Controlled Delivery of DNA Origami on Patterned Surfaces," *Small*, vol. 5, no. 17, pp. 1942–1946, Sep. 2009.
[97] S. Woo and P. W. K. Rothemund, "Self-assembly of two-dimensional DNA origami lattices using cation-controlled surface diffusion," *Nat. Commun.*, vol. 5, no. 4889, pp. 1–11, Dec. 2014.
[98] A. Gopinath and P. W. K. Rothemund, "Optimized Assembly and Covalent Coupling of Single-Molecule DNA Origami Nanoarrays," *ACS Nano*, vol. 8, no. 12, pp. 12030–12040,

Dec. 2014.
[99] C. Kielar *et al.*, "On the Stability of DNA Origami Nanostructures in Low-Magnesium Buffers," *Angew. Chemie*, vol. 130, no. 30, pp. 9614–9618, Jul. 2018.
[100] A. Gopinath, E. Miyazono, A. Faraon, and P. W. K. Rothemund, "Engineering and mapping nanocavity emission via precision placement of DNA origami," *Nature*, vol. 535, no. 7612, pp. 401–405, Jul. 2016.
[101] R. J. Kershner *et al.*, "Placement and orientation of individual DNA shapes on lithographically patterned surfaces," *Nat. Nanotechnol.*, vol. 4, no. 9, pp. 557–561, Sep. 2009.
[102] A. M. Hung, C. M. Micheel, L. D. Bozano, L. W. Osterbur, G. M. Wallraff, and J. N. Cha, "Large-area spatially ordered arrays of gold nanoparticles directed by lithographically confined DNA origami," *Nat. Nanotechnol.*, vol. 5, no. 2, pp. 121–126, Feb. 2010.
[103] B. Gao, K. Sarveswaran, G. H. Bernstein, and M. Lieberman, "Guided Deposition of Individual DNA Nanostructures on Silicon Substrates," *Langmuir*, vol. 26, no. 15, pp. 12680–12683, Aug. 2010.
[104] M. A. Pillers *et al.*, "Preparation of Mica and Silicon Substrates for DNA Origami Analysis and Experimentation," *J. Vis. Exp.*, no. 101, p. e52972, Jul. 2015.
[105] E. Penzo, R. Wang, M. Palma, and S. J. Wind, "Selective placement of DNA origami on substrates patterned by nanoimprint lithography," *J. Vac. Sci. Technol. B, Nanotechnol. Microelectron. Mater. Process. Meas. Phenom.*, vol. 29, no. 6, p. 06F205, Nov. 2011.
[106] A. Kuzyk, B. Yurke, J. J. Toppari, V. Linko, and P. Törmä, "Dielectrophoretic Trapping of DNA Origami," *Small*, vol. 4, no. 4, pp. 447–450, Mar. 2008.
[107] A. C. Pearson, E. Pound, A. T. Woolley, M. R. Linford, J. N. Harb, and R. C. Davis, "Chemical Alignment of DNA Origami to Block Copolymer Patterned Arrays of 5 nm Gold Nanoparticles," *Nano Lett.*, vol. 11, no. 5, pp. 1981–1987, May 2011.
[108] P. Morales *et al.*, "Suspending DNA Origami Between Four Gold Nanodots," *Small*, vol. 12, no. 2, pp. 169–173, Jan. 2016.
[109] M. B. Scheible, G. Pardatscher, A. Kuzyk, and F. C. Simmel, "Single Molecule Characterization of DNA Binding and Strand Displacement Reactions on Lithographic DNA Origami Microarrays," *Nano Lett.*, vol. 14, no. 3, pp. 1627–1633, Mar. 2014.
[110] B. Ding *et al.*, "Interconnecting Gold Islands with DNA Origami Nanotubes," *Nano Lett.*, vol. 10, no. 12, pp. 5065–5069, Dec. 2010.
[111] G. Dekker and M. A. Ratner, "Electronic properties of DNA," *Phys. World*, vol. 14, no. 8, p. 29, Aug. 2001.
[112] Y.-W. Kwon, C. H. Lee, D.-H. Choi, and J.-I. Jin, "Materials science of DNA," *J. Mater. Chem.*, vol. 19, no. 10, pp. 1353–1380, Feb. 2009.
[113] K. Wang, "DNA-Based Single-Molecule Electronics: From Concept to Function," *J. Funct. Biomater.*, vol. 9, no. 1, p. 8, Jan. 2018.
[114] L. D. Williams and L. J. Maher III, "Electrostatic Mechanisms of DNA Deformation," *Annu. Rev. Biophys. Biomol. Struct.*, vol. 29, no. 1, pp. 497–521, Jun. 2000.
[115] M. L. Sushko, A. L. Shluger, and C. Rivetti, "Simple Model for DNA Adsorption onto a Mica Surface in 1:1 and 2:1 Electrolyte Solutions," *Langmuir*, vol. 22, no. 18, pp. 7678–7688, 2006.
[116] D. J. Müller and A. Engel, "The height of biomolecules measured with the atomic force microscope depends on electrostatic interactions," *Biophys. J.*, vol. 73, no. 3, pp. 1633–1644, Sep. 1997.

[117] S. Xiao, H. Zhu, L. Wang, and H. Liang, "DNA conformational flexibility study using phosphate backbone neutralization model," *Soft Matter*, vol. 10, no. 7, pp. 1045–1055, Jan. 2014.
[118] A. Podestà *et al.*, "Positively Charged Surfaces Increase the Flexibility of DNA," *Biophys. J.*, vol. 89, no. 4, pp. 2558–2563, Oct. 2005.
[119] K. J. McConnell and D. L. Beveridge, "DNA Structure: What's in Charge?," *J. Mol. Biol.*, vol. 304, no. 5, pp. 803–820, Dec. 2000.
[120] P. Maragakis, R. L. Barnett, E. Kaxiras, M. Elstner, and T. Frauenheim, "Electronic structure of overstretched DNA," *Phys. Rev. B*, vol. 66, no. 24, p. 241104, Dec. 2002.
[121] E. Scheer, "A DNA that conducts," *Nat. Nanotechnol.*, vol. 9, no. 12, pp. 960–961, Dec. 2014.
[122] I. M. Jauris, S. B. Fagan, M. A. Adebayo, and F. M. Machado, "Adsorption of acridine orange and methylene blue synthetic dyes and anthracene on single wall carbon nanotubes: A first principle approach," *Comput. Theor. Chem.*, vol. 1076, pp. 42–50, Jan. 2016.
[123] D. Řeha *et al.*, "Intercalators. 1. Nature of Stacking Interactions between Intercalators (Ethidium, Daunomycin, Ellipticine, and 4',6-Diaminide-2-phenylindole) and DNA Base Pairs. Ab Initio Quantum Chemical, Density Functional Theory, and Empirical Potential Study," *J. Am. Chem. Soc.*, vol. 124, no. 13, pp. 3366–3376, Apr. 2002.
[124] N. Flores-Holguín, J. Frau, and D. Glossman-Mitnik, "Assessment of the Validity of Some Minnesota Density Functionals for the Prediction of the Chemical Reactivity of the SYBR Green I and Ethidium Bromide Nucleic Acid Stains," in *Density Functional Calculations - Recent Progresses of Theory and Application*, IntechOpen, 2017, pp. 63–76.
[125] T. P. D. De Silva *et al.*, "Influence of Anion Variations on Morphological, Spectral, and Physical Properties of the Propidium Luminophore," *J. Phys. Chem. A*, vol. 123, no. 1, pp. 111–119, Jan. 2019.
[126] J. Frau, F. Munoz, and D. Glossman Mitnik, "Validation of the Koopman's Theorem in DFT by Means of the Calculation of the Conceptual DFT Descriptors of Three Fluorescent DNA Staining Dyes," *Chem. Informatics*, vol. 2, no. 2, p. 7, Nov. 2016.
[127] M. J. Frisch *et al.*, "Gaussian 09, Revision B.01." Gaussian, Inc., Wallingford, CT, 2010.
[128] Z. Deng and C. Mao, "DNA-Templated Fabrication of 1D Parallel and 2D Crossed Metallic Nanowire Arrays," *Nano Lett.*, vol. 3, no. 11, pp. 1545–1548, Nov. 2003.
[129] J. Li *et al.*, "A convenient method of aligning large DNA molecules on bare mica surfaces for atomic force microscopy," *Nucleic Acids Res.*, vol. 26, no. 20, pp. 4785–4786, Oct. 1998.
[130] D. Bensimon, A. J. Simon, V. Croquette, and A. Bensimon, "Stretching DNA with a Receding Meniscus: Experiments and Models," *Phys. Rev. Lett.*, vol. 74, no. 23, pp. 4754–4757, Jun. 1995.
[131] V. Linko, B. Shen, K. Tapio, J. J. Toppari, M. A. Kostiainen, and S. Tuukkanen, "One-step large-scale deposition of salt-free DNA origami nanostructures," *Sci. Rep.*, vol. 5, no. 1, p. 15634, Dec. 2015.

Chapter 12: Appendix

Appendix A: Process Flow for the Fabrication of the Electrode Array Chip (EAC)

Electrode Array Chip (EAC) Process Recipe with KL5302 Hi-Res Broadband Photoresist

Last updated 2020-02-23 (for Electrode Array Chip)

Wafer:
300 nm Stoichiometric LPCVD Silicon Nitride (Si_3N_4) on Silicon (Si)

Electrode Array Chip (EAC) Layer 1 - Metal Electrodes:

Wafer Cleaning:
The wafer should be cleaned properly before beginning the microfabrication process.
If the wafer is visibly dirty/soiled (e.g., due to the wafer being used in previous process attempts), the wafer is cleaned with a Microposit Remover 1165 bath for 5-10 minutes with ultrasound/sonication. The Microposit Remover 1165 bath is heated to ~50 °C for better stripping/cleaning performance.
The wafer is then rinsed with acetone, methanol, and isopropanol (in that order). Two solvent rinse series/cycles are performed to ensure adequate removal of organics and debris.
[New wafers should not need to be cleaned with all the solvents (acetone, methanol, isopropanol), but only need to be rinsed with isopropanol.]
The solvent rinse is always finished with an isopropanol rinse, as isopropanol leaves the least amount of residue behind.
The wafer is then blown dry with the nitrogen gun.
The final cleaning step for the (either new or previously used) wafer is then performed by doing a 1 minute O_2 plasma clean/descum in the PETS RIE plasma etcher tool (7 sccm O_2, 200 W (31%) power, 215 mTorr pressure setpoint).

Prebake (Dehydration Bake):
The wafer is prebaked at 150 °C for 30 minutes on a hot plate to dehydrate the wafer. Prebaking at 150 °C for longer than 30 minutes is better for dehydrating the wafer. (In previous versions of this process recipe, the wafer was prebaked at 110 °C for 10 minutes; however, this lower temperature and duration is not sufficient to completely dehydrate oxide/nitride surfaces, but it is alright for silicon surfaces).
Alternatively, the wafer can be vacuum baked at 150 °C for 3 minutes in the Solitec vacuum oven.
The wafer is allowed to cool down to room temperature for 1 minute before applying the HMDS, and then HMDS is applied immediately after cooling (before the wafer can rehydrate again from the ambient humidity).

HMDS:
HMDS is applied to coat the entire wafer, and any visible bubbles are removed.
If doing photolithography for EAC Layer 1 with a lift-off layer/resist (the preferred method), the LOL1000 spin recipe is used for spin coating the HMDS.

If doing photolithography for EAC Layer 1 without a lift-off layer/resist (not recommended due to poor lift-off results), the KL5302 photoresist spin recipe is used for spin coating the HMDS. [Although a lift-off layer/resist may not be strictly necessary to perform lift-off if the lift-off configuration is used in the CHA E-beam evaporator during metal deposition, better lift-off results are achieved when using a lift-off layer/resist such as LOL1000. Regardless of whether or not a lift-off layer is being used, the lift-off configuration should be used in the CHA E-beam evaporator during metal deposition to ensure better lift-off results.]
If doing photolithography for EAC Layer 2 (without lift-off), the KL5302 photoresist spin recipe is used for spin coating the HMDS.
After spin coating the HMDS, the wafer is baked at 110 °C for 1 minute to thermally activate the HMDS and chemically bond the HMDS to the surface of the wafer.
The wafer is then allowed to cool down to room temperature for 1 minute before applying the LOL1000 and/or photoresist.

Lift-Off Layer/Resist (LOL1000):
If a lift-off layer/resist is desired (for EAC Layer 1), LOL1000 Lift-Off Layer/Resist is used (for gold electrode metal lift-off).

LOL1000 Spin Recipe:
LOL1000 is applied to coat the entire wafer, and any visible bubbles are removed.
Spread: 500 RPM for 15 seconds
Spin: 500 RPM for 45 seconds (for ~150 nm thick LOL layer)

LOL Softbake: 200 °C for 3 minutes. The wafer is allowed to cool down to room temperature for 1 minute before applying photoresist.

KL5302 Hi-Res Photoresist:

~270 nm Thick Photoresist Spin Recipe:
KL5302 Hi-Res Photoresist is applied to coat the entire wafer. Any visible bubbles are removed.
Spread: 5 seconds @ 500 RPM (Spread RPM is not specified in the datasheet, so 500 RPM is chosen empirically.)
Spin Speed: 1000 RPM (for ~270nm thick photoresist)
Spin Duration: 45-60 seconds (45 seconds as specified in the datasheet)

(~270 nm thick photoresist is used to ensure that the photoresist is thick enough to survive any subsequent etch processes.)

Photoresist Softbake: 105 °C for 60 seconds (1 minute)
(90 °C - 105 °C for 60 seconds, as specified in the datasheet)

GCA i-Line Wafer Stepper Recipe: (It may be better to wait at least 1 hour, or overnight, before exposing the photoresist, to allow the photoresist to reabsorb some moisture from the humidity in the air.)

Exposure Recipe for ~270 nm Thick Photoresist:

Exposure: 0.380 second (0.350 second was used previously, but it was underexposed. 0.375 second still seems to be under-exposed. Try using 0.380 second next. If that is still under-exposed, try using a 0.400 second exposure in the future, or possibly even 0.425 second.)
(With an exposure of 0.375 second, ~500 nm lines are reliably achieved, and some ~250 nm lines are achieved after photoresist and lift-off layer development. However, the 1 micron lines appear to be too large, indicating under-exposure.)
Focus offset: 0
Aperture Settings: 10

Post Exposure Bake (PEB): 115 °C for 60 seconds (1 minute)

Development: CD-26 (TMAH)
If using LOL1000 Lift-Off Layer (e.g., EAC Layer 1), then only a short development time of ~15 seconds or less is necessary. LOL1000 gets etched quickly in CD-26 (TMAH), so only ~15 seconds is needed. A 10 second development time may be better than 15 seconds for achieving ~250 nm lines, but this still needs to be verified.
If not using LOL1000 Lift-Off Layer (e.g., EAC Layer 2) then more development time in CD-26 (TMAH) may be used, 15-30 seconds.
It is best to check development after 15 seconds initially, and every 5 seconds or so thereafter to ensure that the wafer is not getting overdeveloped. Gently rinse with DI water and gently blow dry with nitrogen to stop the development process, and inspect the development progress of critical features under the microscope.

O_2 Plasma Etch:
Before etching trenches into the silicon nitride, it is necessary to remove the HMDS and any other organics from the areas of the wafer that were patterned and developed, to uncover the pristine silicon nitride underneath. Ensure that there is no water on the surface of the wafer before the O_2 plasma etch (the wafer should be dried/dehydrated/baked before the O_2 plasma etch if there is still water on the chip; check the wafer for any water residue using the microscope before continuing with the plasma etch). A measurement of the nitride thickness before and after the O_2 plasma etch can be obtained using the Nanometrics Nanospec Reflectometer tool to estimate the film thickness (ensure that the tool is using the Silicon Nitride setting, R.I.: 2.001). The film thickness measurements should be invalid (e.g., 4000-7000 Å) before the O_2 plasma etch, and valid (e.g., ~3000 Å) after the O_2 plasma etch. If the wafer is hard baked before doing the O_2 plasma etch, it may be necessary to do several O_2 plasma etches in 10 second intervals, (e.g., up to a total of 60 seconds) before the HMDS/LOL1000 is completely burned off and the Nanometrics tool reads the correct nitride thickness of ~3000 Å. If you are unsure if the Nanometrics tool is reading the correct nitride thickness, you can remove some photoresist/LOL1000/HMDS from the edge of the wafer by using a cleanroom swab or kimwipe wetted with acetone. The Nanometrics tool should show that this freshly exposed nitride has a film thickness of ~3000 Å.
The typical O_2 plasma etch recipe for wafer descumming is as follows:
Previously, the 10 second O_2 plasma etch was performed in the PETS RIE plasma etch tool (7 cc/min O_2, 200 W (31%) power, 215 mTorr pressure setpoint) to descum the wafer. These results were inconsistent because the tool is controlled manually.
Now, for better consistency, the 10 second O_2 plasma etch should be performed in the Advanced Vacuum Vision 320 RIE plasma etch tool.

Advanced Vacuum Vision 320 RIE - O_2 Plasma Etch/Clean Recipe:

10 minute O_2 plasma clean (empty chamber)

10 second O_2 plasma descum (wafer in chamber) (Recipe: Hihath_Jon_O2_Descum_HMDS_10sec)

(100 sccm O_2, 50 mTorr pressure, 200 W RF power, 10 seconds etch time)

10 minute O_2 plasma clean (empty chamber)

Hard Bake:

Hard bake the wafer at 110 °C for 5 minutes before doing RIE etching, to increase the durability of the photoresist for the plasma etching process for etching trenches into the silicon nitride.

(Previously, the hard bake was done at 115 °C for 3-5 minutes before doing RIE etching, to increase the durability of the photoresist for the plasma etching process for etching trenches into the silicon nitride. This temperature might be slightly too high, resulting in reflow or rounded edges.)

Alternatively, 110 °C for 1 minute (60 seconds) seems to work fine, and may reduce photoresist reflow or rounding of photoresist line edges. A shorter or lower temperature hard bake may produce more vertical sidewalls. A longer hard bake may improve photoresist durability during the plasma etching process.

RIE/ICP Plasma Etch for Silicon Nitride Trenches:

Previous wafer runs of the Electrode Array Chip have used the PETS RIE plasma etcher to etch ~50 nm trenches into the silicon nitride. However, the PETS RIE has been shown to have poor uniformity in the etch profile, as chips near the edge of the wafer get etched more deeply/rapidly than chips in the center of the wafer. Therefore, better results can probably be obtained by using the Plasma-Therm Vision 320 RIE tool instead, and especially by using the Plasma-Therm Apex SLR RIE/ICP tool instead. These etch recipes can be tested with a dummy piece of silicon nitride wafer, or a dummy silicon nitride wafer first. However, the etch rate will vary depending on the size of the sample used and how much silicon nitride is exposed during the etch process. Therefore, it is best to use a full wafer that has been patterned/developed with photoresist. Measure the film thickness with the Nanometrics Nanospec Reflectometer tool before and after the etch.

Plasma-Therm Apex SLR RIE/ICP:

To etch 60-75 nm of LPCVD silicon nitride (Si_3N_4):

10 minute O_2 plasma clean (empty chamber)

5 minute condition (empty chamber)

30 second plasma etch process (wafer in chamber)

30 second etch with 2 O_2 : 100 SF_6 (2 sccm O_2 : 100 sccm SF_6), 100 W RF bias, 500 W RF ICP, 75 mTorr pressure.

It is not necessary to rotate the wafer by 180° half-way through the etch process, as the ICP tool produces a fairly uniform etch profile.

10 minute O_2 plasma clean (empty chamber)

Confirm Etch Depth with Nanometrics Nanospec Reflectometer and Dektak Profilometer:

Before depositing metal, the etch depth should be verified near the edge of the wafer by removing some photoresist (with a swab or kimwipe wetted with acetone), and using the profilometer and Nanometrics tool to measure the height difference of the nitride features to see how deep the nitride

etch was. The Nanometrics Nanospec Reflectometer can be used to confirm the nitride thickness near the center of the wafer, but photoresist should not be removed from the center of the wafer, as this will most likely also damage or distort the photoresist of adjacent chips, greatly decreasing the yield of the wafer. The etch depth and nitride film thickness will be used to determine how much metal should be deposited into the trenches to make the gold electrodes as flush/level as possible with the top surface of the nitride/wafer.

CHA E-Beam Evaporator for Metal Deposition (Ti and Au):
Assuming that the etch depth is 60-75 nm, with an average etch depth of 70 nm, then 5 nm of titanium (Ti) could be deposited followed by 65 nm of gold (Au). This would make the metal electrodes flush or slightly above the nitride for most of the devices.
Therefore, deposit 70 nm of metal (5 nm of Ti and 65 nm of Au).

CHA E-Beam Evaporator Recipe for Depositing 5 nm Ti and 65 nm Au:
CHA E-Beam Evaporator Configuration: Lift-Off
Material 1: Ti (Titanium)
Pocket #: 2
Rate: 0.5 Å/s
Thickness: 5 nm (0.050 kÅ)
Sample Rotation: Yes
Material 2: Au (Gold)
Pocket #: 5
Rate: 1.0 Å/s
Thickness: 65 nm (0.650 kÅ)
Sample Rotation: Yes

Lift-Off:
According to the literature, Microposit Remover 1165 is recommended for use in stripping LOL products, top coat photoresist, and excess deposited metal. For removing metallized liftoff layers, use Remover 1165 at 50 °C for 60 minutes, then switch to a new bath of Remover 1165 at 50 °C for 30 minutes. Use ultrasound/sonication for both baths.
However, through my own experiments, I have found that it is actually better to sonicate the wafer in three separate baths of Microposit Remover 1165 heated at 50 °C for a total of 1:30 (90 minutes), switching to a new bath every 30 minutes. This reduces the amount of residue or particles that can settle on the wafer.
Transfer the wafer immediately from the old bath to the new bath, and don't allow the wafer to dry between baths. The wafer should be constantly sonicated throughout the entire 60-90 minute lift-off process. The gold appears to adhere very well to the silicon nitride due to the titanium adhesion layer, and there seems to be much greater risk of critical features not lifting off well/completely rather than gold electrodes/contacts not adhering to the wafer, so over-sonication is the appropriate strategy. If the wafer is not sonicated immediately and thoroughly when being placed into the lift-off bath, the photoresist or lift-off layer may dissolve without completely lifting off the critical features.
After the final/third bath, rinse the wafer twice with acetone, methanol, and isopropanol (in that order). Blow the wafer dry with nitrogen, rinse once more with isopropanol, then blow dry again

with nitrogen. Inspect the wafer under the microscope, to confirm that lift-off is complete, and that the wafer is clean without particles and residue.

Confirm Height Profile Difference Between Gold Electrodes and Nitride Surface:
After the lift-off process, use the Dektak Profilometer to confirm the height difference between the gold electrodes and the nitride surface at different regions on the wafer (center, mid-way, edge). The gold should be as close/flush to the nitride level as possible; especially mid-way from the center of the wafer to the edge of the wafer, where most of the good chips should be. It's probably better for the gold to be slightly above the nitride than below the nitride. If you observe rabbit ears (spikes sticking up from the edges of the gold electrodes), it may indicate that the photoresist was underexposed or underdeveloped, and thus had a convex shape, causing the thin protruding lip of the photoresist to eventually be etched away during the nitride trench etch, which caused the edge of the nitride trench to be etched less (less than 50 nm) than the rest of the trench.
If a longer exposure time or longer development time doesn't fix this rabbit ears issue, perhaps it could be fixed by using less power during the nitride trench etch (e.g., 50 W instead of 200 W). The best solution is probably to ensure that you use a lift-off layer such as LOL1000 to produce clean smooth metal line edges.

<u>Electrode Array Chip (EAC) Layer 2 - Encapsulation Window:</u>

Isopropanol Rinse and O_2 Plasma Clean:
The wafer could have gotten dirty while it was being measured with the Dektak profilometer, or while it was being stored.
Rinse the wafer with isopropanol, then blow it dry with nitrogen.
Do a 1 minute O_2 plasma etch in the PETS RIE plasma etcher (7 cc/min O_2, 200 W (31%) power, 215 mTorr pressure setpoint) to descum the wafer.

100 nm PECVD Si_3N_4 Deposition with Vision 310 PECVD:
7 minutes and 24 seconds (7:24) should produce 100 nm of PECVD Si_3N_4 on the wafer.
PECVD Process Steps:

- Clean 30 minutes (empty chamber)
- Condition 5 minutes (empty chamber)
- Deposit 7 minutes 24 seconds (wafer in chamber)
  - PECVD Si_3N_4 Deposition Recipe:
    300 °C, 20 sccm SiH_4, 10 sccm NH_3, 1960 sccm N_2, 750 mTorr pressure, 50 W RF power, 7:24 time
- Clean 30 minutes (empty chamber)

Isopropanol Rinse and O_2 Plasma Clean:
The wafer should be cleaned again before starting the next photolithography layer.
Rinse the wafer with isopropanol, then blow it dry with nitrogen.
Do a 1 minute O_2 plasma etch in the PETS RIE plasma etcher (7 cc/min O_2, 200 W (31%) power, 215 mTorr pressure setpoint) to descum the wafer.

Prebake (Dehydration Bake):

The wafer is prebaked at 150 °C for 30 minutes on a hot plate to dehydrate the wafer. Prebaking at 150 °C for longer than 30 minutes is better for dehydrating the wafer. (In previous versions of this process recipe, the wafer was prebaked at 110 °C for 10 minutes; however, this lower temperature and duration is not sufficient to completely dehydrate oxide/nitride surfaces, but it is alright for silicon surfaces).
Alternatively, the wafer can be vacuum baked at 150 °C for 3 minutes in the Solitec vacuum oven.
The wafer is allowed to cool down to room temperature for 1 minute before applying the HMDS, and then HMDS is applied immediately after cooling (before the wafer can rehydrate again from the ambient humidity).

HMDS:
HMDS is applied to coat the entire wafer, and any visible bubbles are removed.
If doing photolithography for EAC Layer 2 (without lift-off), the KL5302 photoresist spin recipe is used for spin coating the HMDS.
After spin coating the HMDS, the wafer is baked at 110 °C for 1 minute to thermally activate the HMDS and chemically bond the HMDS to the surface of the wafer.
The wafer is then allowed to cool down to room temperature for 1 minute before applying the photoresist.

KL5302 Hi-Res Photoresist:

~270 nm Thick Photoresist Spin Recipe:
KL5302 Hi-Res Photoresist is applied to coat the entire wafer. Any visible bubbles are removed.
Spread: 5 seconds @ 500 RPM (Spread RPM is not specified in the datasheet, so 500 RPM is chosen empirically.)
Spin Speed: 1000 RPM (for ~270nm thick photoresist)
Spin Duration: 45-60 seconds (45 seconds as specified in the datasheet)

(~270 nm thick photoresist is used to ensure that the photoresist is thick enough to survive any subsequent etch processes.)

Photoresist Softbake: 105 °C for 60 seconds (1 minute)
(90 °C - 105 °C for 60 seconds, as specified in the datasheet)

GCA i-Line Wafer Stepper Recipe:

Exposure Recipe for ~270 nm Thick Photoresist:
Exposure: 0.380 second (0.350 second was used previously, but it was underexposed. 0.375 second still seems to be under-exposed. Try using 0.380 second next. If that is still under-exposed, try using a 0.400 second exposure in the future, or possibly even 0.425 second.)
(With an exposure of 0.375 second, ~500 nm lines are reliably achieved, and some ~250 nm lines are achieved after photoresist and lift-off layer development. However, the 1 micron lines appear to be too large, indicating under-exposure.)
Focus offset: 0
Aperture Settings: 10

Post Exposure Bake (PEB): 115 °C for 60 seconds (1 minute)

Development: CD-26 (TMAH)
If not using LOL1000 Lift-Off Layer (e.g., EAC Layer 2) then more development time in CD-26 (TMAH) may be used, 15-30 seconds.
It is best to check development after 15 seconds initially, and every 5 seconds or so thereafter to ensure that the wafer is not getting overdeveloped. 30 seconds of development should be sufficient for EAC Layer 2. Gently rinse with DI water and gently blow dry with nitrogen to stop the development process, and inspect the development progress of critical features under the microscope.

O_2 Plasma Etch:
Before etching into the PECVD silicon nitride, it is necessary to remove the HMDS and any other organics from the areas of the wafer that were patterned and developed, to uncover the pristine silicon nitride underneath. Ensure that there is no water on the surface of the wafer before the O_2 plasma etch (the wafer should be dried/dehydrated/baked before the O_2 plasma etch if there is still water on the chip; check the wafer for any water residue using the microscope before continuing with the plasma etch). A measurement of the nitride thickness before and after the O_2 plasma etch can be obtained using the Nanometrics Nanospec Reflectometer tool to estimate the film thickness (ensure that the tool is using the Silicon Nitride setting, R.I.: 2.001). The film thickness measurements should be invalid (e.g., 4000-7000 Å) before the O_2 plasma etch, and valid (e.g., 4000 Å) after the O_2 plasma etch. If the wafer is hard baked before doing the O_2 plasma etch, it may be necessary to do several O_2 plasma etches in 10 second intervals, (e.g., up to a total of 60 seconds) before the HMDS is completely burned off and the Nanometrics tool reads the correct nitride thickness of ~4000 Å. If you are unsure if the Nanometrics tool is reading the correct nitride thickness, you can remove some photoresist/HMDS from the edge of the wafer by using a cleanroom swab or kimwipe wetted with acetone. The Nanometrics tool should show that this freshly exposed nitride has a film thickness of ~4000 Å.
The typical O_2 plasma etch recipe for wafer descumming is as follows:
Previously, the 10 second O_2 plasma etch was performed in the PETS RIE plasma etch tool (7 cc/min O_2, 200 W (31%) power, 215 mTorr pressure setpoint) to descum the wafer. These results were inconsistent because the tool is controlled manually.
Now, for better consistency, the 10 second O_2 plasma etch should be performed in the Advanced Vacuum Vision 320 RIE plasma etch tool.
Advanced Vacuum Vision 320 RIE - O_2 Plasma Etch/Clean Recipe:

10 minute O_2 plasma clean (empty chamber)
10 second O_2 plasma descum (wafer in chamber) (Recipe: Hihath_Jon_O2_Descum_HMDS_10sec)
(100 sccm O_2, 50 mTorr pressure, 200 W RF power, 10 seconds etch time)
10 minute O_2 plasma clean (empty chamber)

Hard Bake:
Hard bake the wafer at 110 °C for 5 minutes before doing RIE etching, to increase the durability of the photoresist for the plasma etching process for etching into the PECVD silicon nitride.
(Previously, the hard bake was done at 115 °C for 3-5 minutes before doing RIE etching, to increase the durability of the photoresist for the plasma etching process for etching trenches into

the silicon nitride. This temperature might be slightly too high, resulting in reflow or rounded edges.)
Alternatively, 110 °C for 1 minute (60 seconds) seems to work fine, and may reduce photoresist reflow or rounding of photoresist line edges. A shorter or lower temperature hard bake may produce more vertical sidewalls. A longer hard bake may improve photoresist durability during the plasma etching process.

~100 nm ICP Plasma Etch for PECVD Silicon Nitride Encapsulation Windows:
The silicon nitride encapsulation windows are formed by etching ~100 nm into the PECVD silicon nitride using the Plasma-Therm Apex SLR RIE/ICP tool. A dummy silicon nitride wafer could be used to get an estimate for the etch rate. However, the etch rate will vary depending on the size of the sample used and how much silicon nitride is exposed during the etch process. Therefore, it is best to use a full wafer that has been patterned/developed with photoresist. Measure the film thickness with the Nanometrics Nanospec Reflectometer tool before and after the etch.

Plasma-Therm Apex SLR RIE/ICP:
To etch 100 nm of PECVD silicon nitride (Si_3N_4):
10 minute O_2 plasma clean (empty chamber)
5 minute condition (empty chamber)
25 second plasma etch process (wafer in chamber)
25 second etch with 45 CF_4 : 5 O_2 (45 sccm CF_4 : 5 sccm O_2), 150 W RF bias, 500 W RF ICP, 100 mTorr pressure, 20 °C temperature.
It is not necessary to rotate the wafer by 180° half-way through the etch process, as the ICP tool produces a fairly uniform etch profile.
10 minute O_2 plasma clean (empty chamber)

Confirm Etch Depth with Nanometrics Nanospec Reflectometer and Dektak Profilometer:
Before stripping/removing all the photoresist, the etch depth should be verified near the edge of the wafer by removing some photoresist (with a swab or kimwipe wetted with acetone), and using the profilometer and Nanometrics tool to measure the height difference of the nitride features to see how deep the silicon nitride etch was. The Nanometrics Nanospec Reflectometer can be used to confirm the silicon nitride thickness near the center of the wafer, but photoresist should not be removed from the center of the wafer, as this will most likely also damage or distort the photoresist of adjacent chips, greatly decreasing the yield of the wafer. The etch depth and silicon nitride film thickness will be used to determine whether the etch process was able to etch through all ~100 nm of the PECVD silicon nitride film.

Photoresist Removal/Stripping and Wafer Cleaning:
The photoresist should be removed/stripped to clean the wafer properly before continuing/finishing the microfabrication process.
For thorough cleaning, the wafer can be cleaned with a Microposit Remover 1165 bath for 5-10 minutes with ultrasound/sonication. The Microposit Remover 1165 bath is heated to ~50 °C for better stripping/cleaning performance.
For a faster photoresist removal/stripping, the wafer can be rinsed with acetone.
The wafer is then rinsed with acetone, methanol, and isopropanol (in that order). Two solvent rinse series/cycles are performed to ensure adequate removal of organics and debris.

The solvent rinse is always finished with an isopropanol rinse, as isopropanol leaves the least amount of residue behind.
The wafer is then blown dry with the nitrogen gun.
The final cleaning step for the wafer is then performed by doing a 1 minute O_2 plasma clean/descum in the PETS RIE plasma etcher tool (7 sccm O_2, 200 W (31%) power, 215 mTorr pressure setpoint).

Electrode Array Chip (EAC) Optional Final Layer - HMDS (and PR) Encapsulation:

Isopropanol Rinse and O_2 Plasma Clean:
The wafer could have gotten dirty while it was being stored, if this part of the fabrication process is being performed on a different day than previous fabrication steps. If so, it is a good idea to clean the wafer before proceeding.
Rinse the wafer with isopropanol, then blow it dry with nitrogen.
Do a 1 minute O_2 plasma etch in the PETS RIE plasma etcher (7 cc/min O_2, 200 W (31%) power, 215 mTorr pressure setpoint) to descum the wafer.

Prebake (Dehydration Bake):
The wafer is prebaked at 150 °C for 30 minutes on a hot plate to dehydrate the wafer. Prebaking at 150 °C for longer than 30 minutes is better for dehydrating the wafer. (In previous versions of this process recipe, the wafer was prebaked at 110 °C for 10 minutes; however, this lower temperature and duration is not sufficient to completely dehydrate oxide/nitride surfaces, but it is alright for silicon surfaces).
Alternatively, the wafer can be vacuum baked at 150 °C for 3 minutes in the Solitec vacuum oven.
The wafer is allowed to cool down to room temperature for 1 minute before applying the HMDS, and then HMDS is applied immediately after cooling (before the wafer can rehydrate again from the ambient humidity).

HMDS:
HMDS is applied to coat the entire wafer, and any visible bubbles are removed.
If doing photolithography for EAC Layer 2 (without lift-off), the KL5302 photoresist spin recipe is used for spin coating the HMDS.
After spin coating the HMDS, the wafer is baked at 110 °C for 1 minute to thermally activate the HMDS and chemically bond the HMDS to the surface of the wafer.
The wafer is then allowed to cool down to room temperature for 1 minute before applying the photoresist.

KL5302 Hi-Res Photoresist:

~270 nm Thick Photoresist Spin Recipe:
KL5302 Hi-Res Photoresist is applied to coat the entire wafer. Any visible bubbles are removed.
Spread: 5 seconds @ 500 RPM (Spread RPM is not specified in the datasheet, so 500 RPM is chosen empirically.)
Spin Speed: 1000 RPM (for ~270nm thick photoresist)
Spin Duration: 45-60 seconds (45 seconds as specified in the datasheet)

(~270 nm thick photoresist is used to ensure that the photoresist is thick enough to survive any subsequent etch processes.)

Photoresist Softbake: 105 °C for 60 seconds (1 minute)
(90 °C - 105 °C for 60 seconds, as specified in the datasheet)

GCA i-Line Wafer Stepper Recipe:

Exposure Recipe for ~270 nm Thick Photoresist:
Exposure: 0.380 second (0.350 second was used previously, but it was underexposed. 0.375 second still seems to be under-exposed. Try using 0.380 second next. If that is still under-exposed, try using a 0.400 second exposure in the future, or possibly even 0.425 second.)
(With an exposure of 0.375 second, ~500 nm lines are reliably achieved, and some ~250 nm lines are achieved after photoresist and lift-off layer development. However, the 1 micron lines appear to be too large, indicating under-exposure.)
Focus offset: 0
Aperture Settings: 10

Post Exposure Bake (PEB): 115 °C for 60 seconds (1 minute)

Development: CD-26 (TMAH)
If not using LOL1000 Lift-Off Layer (e.g., EAC Layer 2) then more development time in CD-26 (TMAH) may be used, 15-30 seconds.
It is best to check development after 15 seconds initially, and every 5 seconds or so thereafter to ensure that the wafer is not getting overdeveloped. 30 seconds of development should be sufficient for EAC Layer 2. Gently rinse with DI water and gently blow dry with nitrogen to stop the development process, and inspect the development progress of critical features under the microscope.

Hard Bake:
Hard bake the wafer at 110 °C for 5 minutes before dicing up and sorting the chips, to increase the durability of the photoresist for future storage and for future experimental procedures.
Alternatively, 110 °C for 1 minute (60 seconds) seems to work fine, and may reduce photoresist reflow or rounding of photoresist line edges. A shorter or lower temperature hard bake may produce more vertical sidewalls. A longer hard bake may improve photoresist durability during the future processes.

Appendix B: Agarose Gel Electrophoresis (AGE)

Agarose Gel Electrophoresis (AGE):

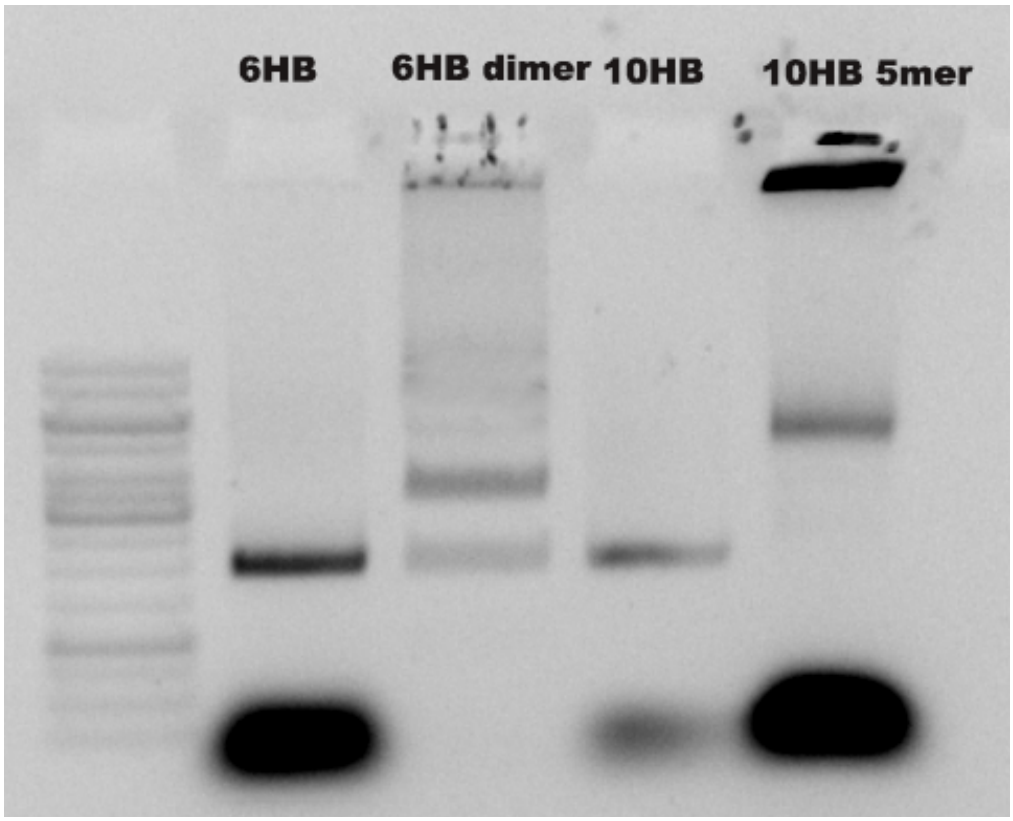

Figure S1. Agarose Gel Electrophoresis (AGE) of DNA NWs. Lane 1: 1kb Ladder; Lane 2: 6HB Monomer; Lane 3: 6HB Dimer (6HB NW); Lane 4: 10HB Monomer; Lane 5: 10HB 5-mer (10HB NW).

Results for the agarose gel electrophoresis (AGE) of the DNA NWs are shown in **Figure S1**. Distinct bands are visible, separated by the different sizes of the DNA monomers and the DNA polymers/NWs. Notice that the 6HB dimer (6HB NW) band is above the 6HB monomer band, and the 10HB 5-mer (10HB NW) band is above the 10HB monomer band, confirming the larger size and proper assembly of the DNA NWs. After running the DNA NWs through the gel, the bands

can be excised and purified with Freeze ‘N Squeeze spin columns to separate the properly assembled DNA NWs from the misassembled/unassembled DNA strands and the supernatant.

Appendix C: DNA Origami Nanowire (DNA NW) Sequence Information

DNA Origami 6HB Dimer Nanowire Sequence Information:

6HB front sequence

H0-1		ACAACAACCATCGCAGGTCGACTCTAGAGCGATTAAGTTGGG
H0-2		AATTTCTTAAACAGGACCGTATACGCATTTCGCTATTACGCC
H0-3		GAGCCTTTAATTGTTACCGAGCTCGAATCAGGCTGCGCAACT
H0-4		ATTTTTTCACGTTGTGTGAAATTGTTATCGCTTCTGGTGCCG
H0-5		AGTGAGAATAGAAACCGGAAGCATAAAGATCGGCCTCAGGAA
H0-6		CTGTATGGGATTTTGCTAACTCACATTAATCGTAACCGTGCA
H0-7		CTAAAGTTTTGTCGAGTCGGGAAACCTGATTGACCGTAATGG
H0-8		CTGTAGCATTCCACAACGCGCGGGGAGACGAGTAACAACCCG
H0-9		TACCGTAACACTGAGTTTTTCTTTTCACCTGGCCTTCCTGTA
H0-10		CACCCTCATTTTCATTCACCGCCTGGCCCATTTTTTAACCAA
H0-11		CCTCAGAACCGCCACTGGTTTGCCCCAGATATTTTGTTAAAA
H0-12		GAATAGGTGTATCACCGAAATCGGCAAAACAGGAAGATTGTA
H0-13		GCGGATAAGTGCCGAGATAGGGTTGAGTCAATCATATGTACC
H0-14	Seam	
Staple		CAAGAGAAGGATTATATTAAAGAACGTGATTCGCCTGATTCGATGAACG
H0-15		TATTATTCTGAAACTCTATCATGGTTGCATACAGTAACAGTA
H0-16		TGCCCGTATAAACATCGTTAGAATCAGATAAAGAAATTGCGT

H0-17	ACTGGTAATAAGTTGGGATTTTAGACAGTAGAACCTACCATA
H0-18	TCCAGTAAGCGTCATTTTTATAATCAGTAATCCTGATTGTTT
H0-19	CATTAAAGCCAGAATCACGCAAATTAACCATCATATTCCTGA
H0-20	GGTCAGACGATTGGATAACATCACTTGCCATTTTGCGGAACA
H0-21	CACCACCAGAGCCGTTGCTGGTAATATCTTGCCCGAACGTTA
H0-22	CGCCACCCTCAGAGACAGGAAAAACGCTTATTAGACTTTACA
H0-23	CACCACCGGAACCGATCGTCTGAAATGGGATTAGAGCCGTCA
H0-24	CGTTTGCCATCTTTACACGACCAGTAATGAAGGTTATCTAAA
H0-25	GCGCGTTTTCATCGGAACCCTTCTGACCATATCTGGTCAGTT
H0-26	CAGTAGCGACAGAAAATATTTTTGAATGAAGCATCACCTTGC
H0-27	CGGAAACGTCACCAAGCCCTAAAACATCCAACAGTGCCACGC
H1-1	CGAAAGACAGCATCGCTCCTTTTGATAAAACTAAAGTACGGT
H1-2	CTTTGAGGACTAAAAAGCAAACTCCAACTGATTCCCAATTCT
H1-3	ACGGGTAAAATACGAATATCGCGTTTTAAGATACATTTCGCA
H1-4	AACGAAAGAGGCAAGGATTGCATCAAAATTCATTTGGGGCGC
H1-5	CCCCCAGCGATTATAAATCAGGTCTTTAAATAGTAGTAGCAT
H1-6	ATTTGTATCATCGCATGCTTTAAACAGTCAAAGAATTAGCAA
H1-7	TGCTCCATGTTACTATACTGCGGAATCGAGCTAAATCGGTTG
H1-8	CATAAGGGAACCGACAGAGGGGGTAATATTTTGCGGGAGAAG
H1-9	AACGGTGTACAGACAAAAACCAAAATAGTTTAGAACCCTCAT
H1-10	AAGAGTAATCTTGATAAGAGCAACACTATGTAGGTAAAGATT
H1-11	AACGTAACAAAGCTCTAATGCAGATACACAAATCACCATCAA
H1-12	ACGAGAAACACCAGTAGAAAGATTCATCATTAATGCCGGAGA

H1-13		TTTAATTTCAACTTCTACGTTAATAAAAGGCTATCAGGTCAT
H1-14	Seam	
Staple		TTAAGAACTTTTTTTGTTTAACGTCAAAAGGCTGAGACTCCT
H1-15		CCTTTACAGAGAGAACAAAATAAACAGCATTCATTTCAATTA
H1-16		ACGGGAGAATTAACCCAACGCTAACGAGCATCAAGAAAACAA
H1-17		ATTGAGCGCTAATAGTTGCTATTTTGCAAATTACCTTTTTTA
H1-18		TAAGCCCAATAATACTCCCGACTTGCGGTGAGTGAATAACCT
H1-19		CTATCTTACCGAAGGGCTTATCCGGTATATTTTCCCTTAGAA
H1-20		CGAACAAAGTTACCGAATCATTACCGCGTAAGACGCTGAGAA
H1-21		ACGGAATACCCAAACACTCATCGAGAACAGGTCTGAGAGACT
H1-22		ACGCAGTATGTTAGCTTTCCTTATCATTTTATATAACTATAT
H1-23		GGCAACATATAAAACCTAATTTACGAGCGACAAAGAACGCGA
H1-24		TATTTTGTCACAATTCAACAATAGATAAATTTCATCTTCTGA
H1-25		GCCAAAGACAAAAGCAATAAACAACATGCGTGTGATAAATAA
H1-26		AGGTAAATATTGACAAAGTACCGACAAACATAATTACTAGAA
H1-27		ACCGTCACCGACTTAATTTAGGCAGAGGACAAATTCTTACCA
H2-1		GAGTACCTTTAATTGGAACGAGGGTAGCTTGCGCCGACAATG
H2-2		GCGAACCAGACCGGGACTTTTTCATGAGTTGCTTTCGAGGTG
H2-3		CCCGAAAGACTTCATAATGCCACTACGAAAAGGCTCCAAAAG
H2-4		GTCAGAAGCAAAGCAAGAATACACTAAAAATTGCGAATAATA
H2-5		TGACCATAAATCAAACCAAGCGCGAAACAACAGTTTCAGCGG
H2-6		TGAATCCCCCTCAACTGATAAATTGTGTAGTAAATGAATTTT
H2-7		CTGGATAGCGTCCATAGCCGGAACGAGGGTTAGCGTAACGAT

H2-8 AAAAGAAGTTTTGCACTGACCAACTTTGACAAACTACAACGC

H2-9 TACCAGACGACGATCAGGCGCATAGGCTAATAGGAACCCATG

H2-10 ATTACGAGGCATAGCAAGAACCGGATATACCCTCAGAGCCAC

H2-11 AATACCACATTCAAGCTCATTCAGTGAATTTAGTACCGCCAC

H2-12 AACATTATTACAGGAACGAGTAGTAAATATAAGTATAGCCCG

H2-13 TTGGGAAGAAAAATTAATCATTGTGAATTTGCTCAGTACCAG

H2-14 - Seam

Staple CAATCCAAAAATCGAGAAACAATAACGGGACTCCAACGTCAA

H2-15 CTAATTTGCCAGTTATAACATAAAAACACCTATTTCGGAACC

H2-16 TATCCTGAATCTTATGAACACCCTGAACGCCTTGAGTAACAG

H2-17 TTAAATCAAGATTATCAGAGAGATAACCTGATACAGGAGTGT

H2-18 GCGTTTTAGCGAACAGAGCAAGAAACAATCTGAATTTACCGT

H2-19 AATCAGATATAGAACCCTTTTTAAGAAAAACAAATAAATCCT

H2-20 TATTTTCATCGTAGAGAAGGAAACCGAGAGGAGGTTGAGGCA

H2-21 TAAACCAAGTACCGAGAACTGGCATGATGCCGCCACCAGAAC

H2-22 CAATAATCGGCTGTCAAACGTAGAAAATGCCACCCTCAGAAC

H2-23 AAATAATATCCCATGAAACGCAAAGACAACCGGAACCAGAGC

H2-24 AACGCGCCTGTTTACAATAGAAAATTCAAGCCCCCTTATTAG

H2-25 TGTCCAGACGACGAGGCGACATTCAACCAGCGTCAGACTGTA

H2-26 TAATAAGAGAATATGGAAATTATTCATTAGCAGCACCGTAAT

H2-27 CAACGCCAACATGTGAGCCATTTGGGAAACCATTAGCAAGGC

H3-1 GTCTGGAAGTTTCAGGATGTGCTGCAAGCCTTTGATAGCGAG

H3-2 GCGAACGAGTAGATTCGGTGCGGGCCTCGGCTAGTACCCGTA

H3-3		AATGGTCAATAACCCGCCATTCGCCATTTCGTAATCATGGTC
H3-4		GAGCTGAAAAGGTGCAGCTTTCCGGCACCCGCTCACAATTCC
H3-5		TAACATCCAATAAAGGGACGACGACAGTTGTAAAGCCTGGGG
H3-6		AATTAAGCAATAAAGTGTAGATGGGCGCATTGCGTTGCGCTC
H3-7		TACCAAAAACATTAGGAACAAACGGCGGTCGTGCCAGCTGCA
H3-8		CCTTTATTTCAACGACATTAAATGTGAGGGCGGTTTGCGTAT
H3-9		ATATTTTAAATGCAAAAATAATTCGCGTCAGTGAGACGGGCA
H3-10		CAAAAGGGTGAGAATTGTTAAATCAGCTCTGAGAGAGTTGCA
H3-11		TATGATATTCAACCAATTGTAAACGTTACAGGCGAAAATCCT
H3-12		GGGTAGCTATTTTTGAAAAGCCCCAAAAATCCCTTATAAATC
H3-13		TGCCTGAGAGTCTGTAAAACTAGCATGTGTTGTTCCAGTTTG
H3-14	Seam	
Staple		AAGTTACAATAAGAAACGAGGCTCATTATACCAGTCAGGACG
H3-15		CCTGAGCAAAAGAAAACGTCAGATGAATTTTGACGAGCACGT
H3-16		AATTAATTACATTTACGTAAAACAGAAAGCGGGAGCTAAACA
H3-17		ATGGAAACAGTACAAATAATGGAAGGGTGAACGGTACGCCAG
H3-18		TGCTTCTGTAAATCCAATTCATCAATATGAGGCCACCGAGTA
H3-19		TCCTTGAAAACATAAGGAGCGGAATTATCGTTGTAGCAATAC
H3-20		GAGTCAATAGTGAATTGAGTAACATTATCTGAGTAGAAGAAC
H3-21		ACCTTTTTAACCTCTCGTATTAAATCCTCAGAACAATATTAC
H3-22		GTAAATGCTGATGCTGAGGATTTAGAAGCATGGAAATACCTA
H3-23		GAAAACTTTTTCAAACTAACAACTAATAATTATTTACATTGG
H3-24		CCTAAATTTAATGGTGAAAGGAATTGAGAAAAGGGACATTCT

H3-25		GGCGTTAAATAAGACAAACCCTCAATCATGAAAGCGTAAGAA
H3-26		AAAGCCTGTTTAGTAAATGAAAAATCTAGCTATTAGTCTTTA
H3-27		GTATAAAGCCAACGATTAACACCGCCTGGCCATTAAAAATAC
H4-1		TAACGCCAGGGTTTTGTTTTAAATATGCGAGGTCATTTTTGC
H4-2		AGCTGGCGAAAGGGTTCCATATAACAGTAGGTCAGGATTAGA
H4-3		GTTGGGAAGGGCGATTAGTTTGACCATTATTCGAGCTTCAAA
H4-4		GAAACCAGGCAAAGTGTTTAGCTATATTAGATTAAGAGGAAG
H4-5		GATCGCACTCCAGCGCATCAATTCTACTCCCTGACTATTATA
H4-6		TCTGCCAGTTTGAGTCATACAGGCAAGGTCAGAAAACGAGAA
H4-7		GATAGGTCACGTTGGCCTCAGAGCATAATCATAAATATTCAT
H4-8		TCGGATTCTCCGTGTGACCCTGTAATACGTAAAATGTTTAGA
H4-9		GCCAGCTTTCATCACAAGGATAAAAATTCGAGAGGCTTTTGC
H4-10		TAGGAACGCCATCAATGCCTGAGTAATGTCATAACCCTCGTT
H4-11		TTCGCATTAAATTTAGGCCGGAGACAGTTAACGCCAAAAGGA
H4-12		TAAGCAAATATTTAGTTCTAGCTGATAAAGTTGAGATTTAGG
H4-13		CCGGTTGATAATCAGAGAGATCTACAAACGAACTAACGGAAC
H4-14	Seam	
Staple		GTAATCGGAGCAAACAAGAGAATGCTTTGAATACC
H4-15		CCTTTTACATCGGGCGCAGAGGCGAATTCATATTATTTATCC
H4-16		AGATTTTCAGGTTTGATGATGAAACAAACGTCTTTCCAGAGC
H4-17		TCAAAATTATTTGCAACAATTTCATTTGCCCAGCTACAATTT
H4-18		GGATTATACTTCTGTAAATCAATATATGGAGGTTTTGAAGCC
H4-19		TTATCAGATGATGGGTCGCTATTAATTATCTAAGAACGCGAG

H4-20		AAGAAACCACCAGAGCGATAGCTTAGATCCCAATAGCAAGCA
H4-21		TTAATTTTAAAAGTTTTATCAAAATCATAAGCAAGCCGTTTT
H4-22		AACAATTCGACAACCGGCTTAGGTTGGGCCAAGAACGGGTAT
H4-23		ATAGATAATACATTAAATCCAATCGCAAATGTAGAAACCAAT
H4-24		ATATCTTTAGGAGCATATATTTTAGTTAGTCCTGAACAAGAA
H4-25		GGCAAATCAACAGTTTTGAAATACCGACTTCAGCTAATGCAG
H4-26		TGAACCTCAAATATATAAACACCGGAATAGGTAAAGTAATTC
H4-27		TGAGAGCCAGCAGCATCATATGCGTTATCATTTTCGAGCCAG
H5-1		GCTTGCATGCCTGCCCACGCATAACCGAGTCACCCTCAGCAG
H5-2		GCAAGTCCGCTAGCCTTGATACCGATAGAACGGCTACAGAGG
H5-3		TAAGGATCCCCGGGATCGGTTTATCAGCGAAGTTTCCATTAA
H5-4		ATAGCTGTTTCCTGAAAATCTCCAAAAAAGGCACCAACCTAA
H5-5		ACACAACATACGAGGGAACAACTAAAGGACACTCATCTTTGA
H5-6		TGCCTAATGAGTGAGCTAAACAACTTTCAAAGTACAACGGAG
H5-7		ACTGCCCGCTTTCCTCTTTCCAGACGTTCGAAATCCGCGACC
H5-8		TTAATGAATCGGCCAGACAGCCCTCATACGCAGACGGTCAAT
H5-9		TGGGCGCCAGGGTGGTTTCGTCACCAGTAAAGAGGACAGATG
H5-10		ACAGCTGATTGCCCGGGATAGCAAGCCCGGCTGACCTTCATC
H5-11		GCAAGCGGTCCACGCCCTCAGAACCGCCTCATTACCCAAATC
H5-12		GTTTGATGGTGGTTCCGTACTCAGGAGGTAAGGCTTGCCCTG
H5-13		AAAAGAATAGCCCGTCGAGAGGGTTGATTGGGCTTGAGATGG
H5-14	Seam	
Staple		GAACAAGAGTCCACGGATTAGCGGGGTTTACCTTATGCGATT

H5-15	AGGGCGAAAAACCGATGAAAGTATTAAGAATGAAAATAGCAG
H5-16	ATAACGTGCTTTCCGTTAATGCCCCCTGGGGAAGCGCATTAG
H5-17	GGAGGCCGATTAAATTAACGGGGTCAGTAAAGTCAGAGGGTA
H5-18	AATCCTGAGAAGTGTACATGGCTTTTGACACAAGAATTGAGT
H5-19	AAAGAGTCTGTCCATGGAAAGCGCAGTCTGAAATAGCAATAG
H5-20	TTCTTTGATTAGTACCTTGATATTCACAAGTAAGCAGATAGC
H5-21	TCAAACTATCGGCCCCGCCAGCATTGACGAAACGCAATAATA
H5-22	CGCCAGCCATTGCACCACCACCCTCAGATAAGACTCCTTATT
H5-23	CATTTTGACGCTCACCTCCCTCAGAGCCACATACATAAAGGT
H5-24	CAGATTCACCAGTCTCATAATCAAAATCCCACGGAATAAGTT
H5-25	GGCCAACAGAGATAGCATTTTCGGTCATTATGGTTTACCAGC
H5-26	TACGTGGCACAGACTCAAGTTTGCCTTTGATTGAGGGAGGGA
H5-27	ATGCGCGAACTGATATGAAACCATCGATAAAGGTGAATTATC

6HB rear sequence

H0-1	CCTGCAACAGTGCCTCATCGGCATTTTCCAATGAAACCATCG
H0-2	GCAGAAGATAAAACATCTTTTCATAATCCACCAGTAGCACCA
H0-3	AGCCCTAAAACATCGAACCGCCTCCCTCCGTCACCGACTTGA
H0-4	AATATTTTTGAATGTCAGAGCCACCACCGTAAATATTGACGG
H0-5	GAACCCTTCTGACCGAGCCGCCGCCAGCCAAAGACAAAAGGG

H0-6		ACACGACCAGTAATGATTGGCCTTGATATTTTGTCACAATCA
H0-7		ATCGTCTGAAATGGCCAGAATGGAAAGCCAACATATAAAAGA
H0-8		ACAGGAAAAACGCTGCGTCATACATGGCGCAGTATGTTAGCA
H0-9		TTGCTGGTAATATCTAAGTTTTAACGGGGGAATACCCAAAAG
H0-10		ATAACATCACTTGCTAAACAGTTAATGCAACAAAGTTACCAG
H0-11		TCACGCAAATTAACTGAAACATGAAAGTATCTTACCGAAGCC
H0-12		TTTTTATAATCAGTGGATTAGGATTAGCAGCCCAATAATAAG
H0-13		GGGATTTTAGACAGGTGCCGTCGAGAGGTGAGCGCTAATATC
H0-14	(Seam)	TCGTTAGAATCAGAGTATCACCGTACTCGGTAGAAAGATTTGAACACCC
H0-15		TCTATCATGGTTGCCCGCCACCCTCAGAATCTACGTTAATAA
H0-16		TATTAAAGAACGTGTTTTCAGGGATAGCAAGAACTGGCTCAT
H0-17		AGATAGGGTTGAGTCACTGAGTTTCGTCTAATTTCAACTTTA
H0-18		CCGAAATCGGCAAATTCCACAGACAGCCGAGAAACACCAGAA
H0-19		CTGGTTTGCCCCAGTTGTCGTCTTTCCACGTAACAAAGCTGC
H0-20		TTCACCGCCTGGCCGATTTTGCTAAACAGAGTAATCTTGACA
H0-21		GTTTTTCTTTTCACTAGAAAGGAACAACCGGTGTACAGACCA
H0-22		AACGCGCGGGGAGAACGTTGAAAATCTCTAAGGGAACCGAAC
H0-23		AGTCGGGAAACCTGAATTGTATCGGTTTCTCCATGTTACTTA
H0-24		GCTAACTCACATTAAAACAGCTTGATACTTGTATCATCGCCT
H0-25		CCGGAAGCATAAAGCATCGCCCACGCATCCCAGCGATTATAC
H0-26		TGTGAAATTGTTATCAGGGAGTTAAAGGCGAAAGAGGCAAAA
H0-27		TACCGAGCTCGAATAGCGAAAGACAGCAGGGTAAAATACGTA
H1-1		GGTCAGTTGGCAAATAGGCAGAGGCATTAACATGTTCAGCTA

H1-2		TATCTAAAATATCTTTAATTGAGAATCGAGATAAGTCCTGAA
H1-3		AGCCGTCAATAGATACAAATTCTTACCAACGAGCATGTAGAA
H1-4		ACTTTACAAACAATCATAATTACTAGAAATCATTCCAAGAAC
H1-5		GAACGTTATTAATTCGTGTGATAAATAAGAGAACAAGCAAGC
H1-6		GCGGAACAAAGAAAATTTCATCTTCTGAACCGCGCCCAATAG
H1-7		ATTCCTGATTATCAGACAAAGAACGCGACGGTATTCTAAGAA
H1-8		GATTGTTTGGATTATTATATAACTATATTTGCGGGAGGTTTT
H1-9		CTACCATATCAAAAAGGTCTGAGAGACTTTTGCACCCAGCTA
H1-10		AATTGCGTAGATTTTAAGACGCTGAGAAAACGAGCGTCTTTC
H1-11		TAACAGTACCTTTTATTTTCCCTTAGAAAACAGCCATATTAT
H1-12		CTGATTGCTTTGAATGAGTGAATAACCTTTTGTTTAACGTCA
H1-13		AATTATTCATTTCAAATTACCTTTTTTAGAATAACATAAAAA
H1-14	(Seam)	CAAACATCAAAGCAAATATTTAAATTGTATAACGTGCTTTCC
H1-15		TGTTAAAATTCGCATACCCCGGTTGATAGATACATAACGCCA
H1-16		TTAACCAATAGGAAATCGATGAACGGTAACACTATCATAACC
H1-17		TTCCTGTAGCCAGCGGCTATCAGGTCATAAATAGCGAGAGGC
H1-18		ACAACCCGTCGGATATTAATGCCGGAGAGTAATAGTAAAATG
H1-19		CGTAATGGGATAGGCAAATCACCATCAAGAATCGTCATAAAT
H1-20		ACCGTGCATCTGCCTGTAGGTAAAGATTAACAGTTCAGAAAA
H1-21		CTCAGGAAGATCGCTTTAGAACCCTCATTCTTTACCCTGACT
H1-22		TGGTGCCGGAAACCTTTTGCGGGAGAAGTCAAAAAGATTAAG
H1-23		GCGCAACTGTTGGGAGCTAAATCGGTTGGTTTTAATTCGAGC
H1-24		ATTACGCCAGCTGGCAAAGAATTAGCAATCCAACAGGTCAGG

H1-25		AAGTTGGGTAACGCAATAGTAGTAGCATTGATAAGAGGTCAT
H1-26		AACGACGGCCAGTGTTCATTTGGGGCGCTGAATATAATGCTG
H1-27		TAGACCTTTGATAGAGATACATTTCGCAAAAGTACGGTGTCT
H2-1		GCCAACATGTAATTTCAACAGTTGAAAGCAGTATTAACACCG
H2-2		CTCAACAGTAGGGCTTAGGAGCACTAACCGAACGAACCACCA
H2-3		ATCATATGCGTTATAATACATTTGAGGAATGCGCGAACTGAT
H2-4		ATAAACACCGGAATTCGACAACTCGTATTACGTGGCACAGAC
H2-5		TTTGAAATACCGACTTAAAAGTTTGAGTGGCCAACAGAGATA
H2-6		ATATATTTTAGTTACCACCAGAAGGAGCCAGATTCACCAGTC
H2-7		AAATCCAATCGCAAGATGATGGCAATTCCATTTTGACGCTCA
H2-8		CGGCTTAGGTTGGGTACTTCTGAATAATCGCCAGCCATTGCA
H2-9		TTTATCAAAATCATTTATTTGCACGTAATCAAACTATCGGCC
H2-10		GCGATAGCTTAGATTCAGGTTTAACGTCTTCTTTGATTAGTA
H2-11		GTCGCTATTAATTAACATCGGGAGAAACAAAGAGTCTGTCCA
H2-12		TAAATCAATATATGTACCAAGTTACAAAAATCCTGAGAAGTG
H2-13		AACAATTTCATTTGATTACCTGAGCAAAGGAGGCCGATTAAA
H2-14	(Seam)	AAAAACAATACCACACAACATTATTACAAGGAGGTTTAGTAC
H2-15		ATGTCAATCATATGTTAAATTTTTGTTAAGGGCGAAAAACCG
H2-16		GAGCAAACAAGAGACGCCATCAAAAATAGAACAAGAGTCCAC
H2-17		GAGAGATCTACAAATTTCATCAACATTAAAAAGAATAGCCCG
H2-18		GTTCTAGCTGATAATCTCCGTGGGAACAGTTTGATGGTGGTT
H2-19		AGGCCGGAGACAGTTCACGTTGGTGTAGGCAAGCGGTCCACG
H2-20		ATGCCTGAGTAATGAGTTTGAGGGGACGACAGCTGATTGCCC

H2-21		CAAGGATAAAAATTACTCCAGCCAGCTTTGGGCGCCAGGGTG
H2-22		TGACCCTGTAATACAGGCAAAGCGCCATTTAATGAATCGGCC
H2-23		GCCTCAGAGCATAAAAGGGCGATCGGTGACTGCCCGCTTTCC
H2-24		TCATACAGGCAAGGCGAAAGGGGGATGTTGCCTAATGAGTGA
H2-25		GCATCAATTCTACTCAGGGTTTTCCCAGACACAACATACGAG
H2-26		TGTTTAGCTATATTCCAAGCTTGCATGCATAGCTGTTTCCTG
H2-27		TTAGTTTGACCATTCGAGGCAAGTCCGCTAAGGATCCCCGGG
H3-1		ATGCAGAACGCGCCGCCGGAAACGTCACGGTCATAGCCCCCT
H3-2		CAAGAAAAATAATAAGAGCCAGCAAAATAAAATCACCGGAAC
H3-3		ACCAATCAATAATCAGGTGAATTATCACAGAGCCGCCACCCT
H3-4		GGGTATTAAACCAATTGAGGGAGGGAAGCTCAGAGCCGCCAC
H3-5		CGTTTTTATTTTCATGGTTTACCAGCGCATTGACAGGAGGTT
H3-6		CAAGCAAATCAGATACGGAATAAGTTTATTCACAAACAAATA
H3-7		CGCGAGGCGTTTTAATACATAAAGGTGGGCAGTCTCTGAATT
H3-8		GAAGCCTTAAATCAAGACTCCTTATTACTTTTGATGATACAG
H3-9		CAATTTTATCCTGAAACGCAATAATAACGTCAGTGCCTTGAG
H3-10		CAGAGCCTAATTTGTAAGCAGATAGCCGCCCCTGCCTATTTC
H3-11		TTATCCCAATCCAAAAATAGCAATAGCTATTAAGAGGCTGAG
H3-12		AAAATGAAAATAGCCAAGAATTGAGTTAGGGGTTTTGCTCAG
H3-13		CAGGGAAGCGCATTAGTCAGAGGGTAATGTTGATATAAGTAT
H3-14	(Seam)	TTTAGGAGGAAGATTGTATAGAAAACAAAATTAATTACATTT
H3-15		AAAGGAATTACGAGCGTTGGGAAGAAAAACCGCCACCCTCAG
H3-16		CTCGTTTACCAGACCCTTATGCGATTTTAAGCCCAATAGGAA

H3-17	TTTTGCAAAAGAAGGGCTTGAGATGGTTACCAGTACAAACTA
H3-18	TTTAGACTGGATAGAGGCTTGCCCTGACCTCATAGTTAGCGT
H3-19	ATTCATTGAATCCCATTACCCAAATCAAGACGTTAGTAAATG
H3-20	CGAGAATGACCATACTGACCTTCATCAAACTTTCAACAGTTT
H3-21	ATTATAGTCAGAAGAGAGGACAGATGAATAAAGGAATTGCGA
H3-22	AGGAAGCCCGAAAGCAGACGGTCAATCACAAAAAAAAGGCTC
H3-23	TTCAAAGCGAACCAAAATCCGCGACCTGATCAGCTTGCTTTC
H3-24	ATTAGAGAGTACCTAGTACAACGGAGATCGATAGTTGCGCCG
H3-25	TTTTGCGGATGGCTACTCATCTTTGACCAACCGATATATTCG
H3-26	TAGCTCAACATGTTGCACCAACCTAAAACCGCTTTTGCGGGA
H3-27	GGAAGTTTCATTCCAGTTTCCATTAAACTCGGAACGAGGGTA
H4-1	ATAGCAGCACCGTACGACGACAATAAACTTCGAGCCAGTAAT
H4-2	TTACCATTAGCAAGTGTTTATCAACAATCCATATTTAACAAC
H4-3	GCCATTTGGGAATTTCCCATCCTAATTTGTATAAAGCCAACG
H4-4	AAATTATTCATTAAGGCTGTCTTTCCTTAAAGCCTGTTTAGT
H4-5	CGACATTCAACCGAGTACCGCACTCATCGGCGTTAAATAAGA
H4-6	ATAGAAAATTCATATCGTAGGAATCATTCCTAAATTTAATGG
H4-7	AACGCAAAGACACCATAGAAGGCTTATCGAAAACTTTTTCAA
H4-8	AACGTAGAAAATACGCGAACCTCCCGACGTAAATGCTGATGC
H4-9	AACTGGCATGATTAAGATTAGTTGCTATACCTTTTTAACCTC
H4-10	AAGGAAACCGAGGAATCTTACCAACGCTGAGTCAATAGTGAA
H4-11	CTTTTTAAGAAAAGCCAGTTACAAAATATCCTTGAAAACATA
H4-12	AGCAAGAAACAATGATAAGAAACGATTTTGCTTCTGTAAATC

H4-13		AGAGAGATAACCCAAGCCTTTACAGAGAATGGAAACAGTACA
H4-14	(Seam)	TGAACAAAGACGGGAGAATTAACCATCAGTTGAGA
H4-15		AACGAACTAACGGAATTCAACTAATGCAATCAGAAAAGCCCC
H4-16		TATACCAGTCAGGAGCATAGTAAGAGCAATCGTAAAACTAGC
H4-17		ATCATTGTGAATTAGACGATAAAAACCATGCCTGAGAGTCTG
H4-18		CGAGTAGTAAATTGTTTTGCCAGAGGGGGGGTAGCTATTTTT
H4-19		TCATTCAGTGAATACGTCCAATACTGCGTATGATATTCAACC
H4-20		AGAACCGGATATTCCCTCAAATGCTTTACAAAAGGGTGAGAA
H4-21		GGCGCATAGGCTGGAATCAAAAATCAGGATATTTTAAATGCA
H4-22		TGACCAACTTTGAACAAAGCGGATTGCACCTTTATTTCAACG
H4-23		GCCGGAACGAGGCGACTTCAAATATCGCTACCAAAAACATTA
H4-24		GATAAATTGTGTCGGACCGGAAGCAAACAATTAAGCAATAAA
H4-25		CAAGCGCGAAACAATTAATTGCTCCTTTTAACATCCAATAAA
H4-26		GAATACACTAAAACTAGAGCTTAATTGCGAGCTGAAAAGGTG
H4-27		ATGCCACTACGAAGTTAAATATGCAACTAATGGTCAATAACC
H5-1		ACTGTAGCGCGTTTACGCTGAGAGCCAGCTCAATCAATATCT
H5-2		TATTAGCGTTTGCCAGAGGTGAGGCGGTGAATTGAGGAAGGT
H5-3		CAGAGCCACCACCGGCCATTAAAAATACAACTAATAGATTAG
H5-4		CAGAACCGCCACCCGCTATTAGTCTTTATTTAGAAGTATTAG
H5-5		CAGAACCACCACCATGAAAGCGTAAGAATAAATCCTTTGCCC
H5-6		GAGGCAGGTCAGACAAAAGGGACATTCTAACATTATCATTTT
H5-7		AATCCTCATTAAAGATTATTTACATTGGGGAATTATCATCAT
H5-8		TACCGTTCCAGTAACATGGAAATACCTAATCAATATAATCCT

H5-9		GAGTGTACTGGTAACAGAACAATATTACGGAAGGGTTAGAAC
H5-10		TAACAGTGCCCGTACTGAGTAGAAGAACAACAGAAATAAAGA
H5-11		GGAACCTATTATTCCGTTGTAGCAATACAGATGAATATACAG
H5-12		ACTCCTCAAGAGAAGAGGCCACCGAGTAAATAACGGATTCGC
H5-13		TACCAGGCGGATAAGAACGGTACGCCAGATCGCGCAGAGGCG
H5-14	(Seam)	AGCCCGGAATAGGTGCGGGAGCTAAACAAGAAGATGATGAAA
H5-15		CGCCACCCTCAGAATTTGACGAGCACGTAAACGTTAATATTT
H5-16		AGCCACCACCCTCAGACTCCAACGTCAAAATCAGCTCATTTT
H5-17		CCCATGTACCGTAAGTTGTTCCAGTTTGATTCGCGTCTGGCC
H5-18		CAACGCCTGTAGCAATCCCTTATAAATCAATGTGAGCGAGTA
H5-19		AACGATCTAAAGTTCAGGCGAAAATCCTAACGGCGGATTGAC
H5-20		AATTTTCTGTATGGCTGAGAGAGTTGCAATGGGCGCATCGTA
H5-21		CAGCGGAGTGAGAACAGTGAGACGGGCAACGACAGTATCGGC
H5-22		ATAATAATTTTTTCGGCGGTTTGCGTATTCCGGCACCGCTTC
H5-23		CAAAAGGAGCCTTTTCGTGCCAGCTGCATCGCCATTCAGGCT
H5-24		GAGGTGAATTTCTTATTGCGTTGCGCTCCGGGCCTCTTCGCT
H5-25		ACAATGACAACAACTGTAAAGCCTGGGGGCTGCAAGGCGATT
H5-26		GTCGCTGAGGCTTGCCGCTCACAATTCCTCACGACGTTGTAA
H5-27		TCGTCACCCTCAGCTCGTAATCATGGTCCTGCAGGTCGACTC

6HB connecting strands

Connector 1	TCTAAAGCATCACAGCAGAAGATAGTTTAATCAAAAACAGAG
Connector 2	ATCCTTGCTGAACCTACCGACAATGAGATTAATAAGGTAAAG
Connector 3	AAGAGAATATAAAGTCAAATATCAAACCCAGCAAATGAAAAA
Connector 4	TAATTCTGTCCAGAATCAGTAGCGACAGGCCTTTAGCGTCAG

DNA Origami 10HB 5-mer Nanowire Sequence Information:

10HB sequence

B1 1	GTTGGTGTCCTCATGCAGCACCGTCGGTAGTTTGAGGCATCA
B1 2	GAGCACATAGATGGATAAATTAATGCCGGAGAGGGAGGTCAC
B1 3	CAAGAATGCCAACGAACGGAACGTGCCGATGGGATTAGCTAT
B1 4	TCGCAAATGGGGCGCTCATCTTTGACCCAACGGAGTAAACAG
B1 5	ATTCTACCTAGCTGGCGCATCGTAACCGGCAGCCTTCCCACG
B1 6	AATACACCTGATAATTGAATCCCCCTCAAGAAGCAATACATT
B1 7	TCATCGCTAAAACACGAGCTGAAAAGGTCCATTAGAAGCGGA
B1 8	TTCAGAATTTACCCTGACTATTATAGTCAATGCTTATTTGTA
B1 9	TTGCATCATATTCAATTGTGTCGAAATCGAAAGAGGCAAAAG
B2 0	AACCGTTTAATAGTGAACGAGTAGATTTGGTGCCACCGGCCA
B2 1	TGAGGGGCGTTTTTCTGGAGGTGTCCAGCCATATAATCATAC
B2 2	CGCGGTCACGACGACAGTCAAATCACCATCAATATGCCAGTT
B2 3	CAACCAGCTTACGGTCGTCTCGTCGCTGTGCATCTGATATTC
B2 4	ATTCTGCAGTAGCACACCAACCTAAAACCGCGACCCGGAATC

B2 5	AGGCAAGCCGGAGACAGTATCGGCCTCAGCCGTTCGGGGTCA
B2 6	TGCCACTTAGCCGGACTGGATAGCGTCCGAAAGACATTCCCA
B2 7	TGTTACTACGAAGGTTAACATCCAATAAACAGTTGTTCAAAT
B2 8	GTCATAAAAAAAGATTAAGAGGAAGCCCAATACTGTGCTCCA
B2 9	ATCGCGTTGTTTAGAACGAGGCGCAGACGGTAAAATACGTAA
B3 0	AGAAAGGGCAAAGACTGGAAGTTTCATTCATCAGCCGGCAAA
B3 1	CAGCCAGTAAAGTTGCACTCAATCCGCCTTTTAAAAGCCTCA
B3 2	TGAAGGGCTTTCCGAATGTGTAGGTAAAGATTCAACGCACTC
B3 3	TTGCAGGCGCTTTCAAACGATGCTGATTGGAAGATAAGGGTG
B3 4	ACGGTGTATTAGCAGTTTCCATTAAACGGGTCAATGGGTAAT
B3 5	GAGCATACCTGAGTGCACCGCTTCTGGTGCGGCCTGTTGCGG
B3 6	TTTTTCAACTGACCCAAAAGAAGTTTTGAACCAGACTAAAGT
B3 7	GAACCGATGAGGAAAAATTAAGCAATAATATGCAACCGGAAG
B3 8	AGTAAAATTTAATTCGAGCTTCAAAGCGCCAGAGGCATAAGG
B3 9	CAAACTCGCTTTTGAACTTTGAAAGAGGTGAGGACTAAAGAC
B4 0	TGCAATGAAGCTAATGTAGCTCAACATGGGGCGCGTTAGTGA
B4 1	AAAGCGCCCCGTAACTGTTGCCCTGCGGCTTAGAGATGACCC
B4 2	AAAAAATCATTCGCAATTTTTAGAACCCTCATATAACCAGGC
B4 3	TATGAGCCGGGTCAAAAAAGCCGCACAGGCCGGAATTTTAAA
B4 4	ATAATGCATCGGTTGGCTACAGAGGCTTACAGATGCAAAATA
B4 5	TGTAATAGGATAAACATTCAGGCTGCGCTGTACATTGGGTAA
B4 6	ACGAGGGCAGGCGCTTACCAGACGACGATACCTTTGCTGAAT
B4 7	TACAGACTAGCAACGTACCAAAAACATTCTTAATTAATTGCT

B4 8 GCGAGAGCAACAGGTCAGGATTAGAGAGTAAAAACAACGGTG

B4 9 CCTTTTGCCCTCGTATAGGCTGGCTGACAAGACAGCATCGGA

B5 0 AACGCAACTTTTGCTATTTTGCGGATGGCTGGTAACGACATA

B5 1 GCGATCGCCGCCAGGTCATAAACATCCCAAGCATATCATAGT

B5 2 TCATTTGGTGCGGGTACAACGCCTGTAGCATTCCTGGGAAGG

B5 3 AGGTTTCTTTGCTCCAGTTGGGCGGTTGAACTGTTTTATTTC

B5 4 GGGTGCCGGGAGAAACCCTCAGCAGCGACTTCATCCAACACT

B5 5 TAGCGTATACAAACCCTCTTCGCTATTAACTTAAAGGTGTGT

B5 6 TTTGCGGCAAGAACAATTACGAGGCATACTAACTCAAGCCTG

B5 7 ATCTTGAGATCGTCGCCACAGACAGCCCAAGTGTAACATTAA

B5 8 ATCATAAATAAGAGGTCATATGAGTGAGGTAAGAGAAGAGTA

B5 9 TTGCGTTCAAAAGGCGGATATTCATTACAGTTAAAGGCCGCT

B6 0 TCACCAGACGATCTAACATACGAGCCGGTTACACTTTTCTGC

B6 1 AGGGGGAGACGCAGACGGCATCAGATGCAAATTGTACGTTAG

B6 2 AAAAAGATGTGCTGAACCCATGTACCGTAACACTGTGGCGAA

B6 3 TCAGCAAATCGTTAAAACAGCGGATCAACGCCAGCAGTTTCG

B6 4 TCCACACAAAGTTTTGAGGCTTGCAGGGCCAAATCCAGATAC

B6 5 TAAATGACAATAGGCAAGGCGATTAAGTGATAGCTCCTGCAG

B6 6 ATATATTGCTCATTGAATACCACATTCAGTCGGGATCACAAT

B6 7 CAAAGCTCGGTCGCTGTCGTCTTTCCAGTATCCGCAACCTGT

B6 8 ATAACGCGCGCTCACTGCCCGCTTTCCAACTAATGAACGTAA

B6 9 CGTGCCAGATTTAGCAGTGAATAAGGCTCCCACGCATAACCG

B7 0 GCAAGCCATTTTCTCTGTTTCCTGTGTGCGGGTTACTCACGG

B7 1 GTTTTCCAGACTTTGCCCCCTGCATCAGGAGCTCGCTTTCAA

B7 2 GAGAGATCAGTCACAGAGCCACCACCCTCATTTTCCGCCAGG

B7 3 CCAGCGGTGCCGGTCTCCGTGGTGAAGGTGGGTAAAGGGATA

B7 4 GTCATAGGTATGGGGACAACAACCATCGTGCCCTGGATTCAT

B7 5 CAGTTTCCACCCTCGACGTTGTAAAACGGTCCCGGAGCGCAG

B7 6 GTTGCGCAACGAGTCAACATTATTACAGACGCGCGAATCATG

B7 7 ACACCAGCGACAATATTTTGCTAAACAAAATTCGTGGGAGAG

B7 8 CAGTTGAGCTGCATTAATGAATCGGCCAGTAGAAAACGAGAA

B7 9 GCGGTTTAACGGAAAGTAAATTGGGCTTGCTTGATACCGATA

B8 0 GAACCGCAGCGGAGGATCCCCGGGTACCACGATCCAATTTGT

B8 1 GCTTTCACGTACAGTGTGCACTCTGTGGCGCGTCCAAAGGAA

B8 2 GGCGAAAGAGGTGGACCGCCACCCTCAGAACCGCCGTGCCAA

B8 3 TGTCACTGCGCGCCCGCCATGTTTACCAACGGCCAACCCTCA

B8 4 AGTTGAGTGAGAATGAATTTCTTAAACAGAGATGGTAATAAA

B8 5 TTGCGAAGTTTAGTAGCCGCCACGGGAACACCGGAGCCAGAA

B8 6 CTTGCTTTAATCATGTTGGGAAGAAAAATTTTTCTTCCTCAC

B8 7 TCAACTTTCGAGGTAGAAAGGAACAACTGTGAGCCTTTCACC

B8 8 ACGAACTGCGTATTGGGCGCCAGGGTGGTCTACGTTTTAATT

B8 9 AGTGAGATCAGGACTGTGAATTACCTTATATCGGTTTATCAG

B9 0 TCAGGAGTAATAATGCGTGCCTGTTCTTTGCTGCGAACAATC

B9 1 ATATCAAAAAGCATTTCACGGTCGGAGCTAAAGATAAACAAA

B9 2 AAAATCTACCCTCAATAGCCCGGAATAGGTGTATCACCTCAA

B9 3 TGCGGCGGGCCGTTCACCTTGCTAACCTCGGATGAACCGTAC

B9 4	CCAGCACTTTTTCAGGAGCCTTTAATTGTGCGATTGCTCATT
B9 5	CAAATAATATAAGTATCAATATCTGGTCCCAGCAGTTAGAGC
B9 6	AAAAGGCTCAGAGAGTCAGAGGGTAATTTCACCGCGTTTCTG
B9 7	GCTAATATCCAAAACGTTGAAAATCTCCACCGGGGCTGGCCC
B9 8	ATACCAGCGGGCAACAGCTGATTGCCCTGAAACTGTTAAGGC
B9 9	TGAGAGAGAACAAAGATAACCCACAAGAGCCTTGATATTCAA
B10 0	GGGTTGAATCCTCACTAAATCGGAACCCCCCCGATCAAATGA
B10 1	CAGTTGAGCAACAGCGGCGAACGTGGCGTTTTTTGCAGTCTC
B10 2	ACCGCCTAAGGAATAGTACCAGGCGGATAAGTGCCAAATCAA
B10 3	TTGACGGGGAAAGCTGCCACGCTGAGAGAGTTGGCGTCGAGA
B10 4	TAAAGCATTAAAGCAGGTCAGACGATTGATTGAGTTAACTGA
B10 5	TGAATTTTTTGCTCTGAGGAAGGTTATCCGGTCAGAAGGGAA
B10 6	CAGGAGGAGAGCAAAAGCGCATTAGACGTGGTTTGGGTGCCG
B10 7	AATAATATTGAGGCCAGAATGGAAAGCGGGGTCGACCCCAGC
B10 8	ACACCCTGTTGCAGCAAGCGGTCCACGCGGAGAATTAAGCCC
B10 9	AGGCGAAAACAGGGGAAACAATGAAATAGCCGCCAGCATTGA
B11 0	GCGGGGTACCGTTCTCACCCAAATCAAGAGAAAGGTATTAAC
B11 1	GAGCACTGAAGATACGGGCGCTAGGGCGTCAGGGCTTTGATG
B11 2	ACCAGCAAACAACTAGACTCCTCAAGAGAAGGATTTCTTTAG
B11 3	GAAAGCGAAAGGAGAAACAGAGGTGAGGTAAAATAAGGATTA
B11 4	TGAACCACAGTAAGCCACCACCAGAGCCGCAATAGGAGAATA
B11 5	ATACAGGGAGGCTGAATAGATTAGAGCCATACCGAGTGTAGC
B11 6	AGCCGCCCCCTTTTGAAAATAGCAGCCTCGAAATCCACTACG

B11 7 ACCGAAGACCAGAACGTCATACATGGCTGATGGCCGGCAAAA

B11 8 ACATAAAAATCCTGTTTGATGGTGGTTCTTACAGACTATCTT

B11 9 TCCCTTACAAAAATTAAGAAAAGTAAGCGCCACCACCCTCAG

B12 0 GTATTAAAGTGTACCGAAAAACCGTCTACTGGCAAACGAACC

B12 1 CATTTGACCTAAAATAACCACCACACCCAAAGAACTCAGTGC

B12 2 TGATAGCGGATTTATCGGAACCTATTATTCTGAAAGATAATA

B12 3 GGTCACGCTGCGCGCATCGCCATTAAAAGTCAATACATGAAA

B12 4 CAAAGGGTGGTAATCCGCCACCCTCAGAAGATAGCTTTTTGT

B12 5 CTTGAGTGCCTATTGAAGTATTAGACTTTTTAATGTTAATGC

B12 6 CGCCACCAGAAGGACCAATCCAAATAAGGATAGGGCCAACGT

B12 7 AGTTACCCTCAGAAAAGTTTTAACGGGGGTGGACTTTGAGTG

B12 8 TTAACGTTAAATCAAAAGAATAGCCCGAAAACGATCGAACAA

B12 9 TTGTTCCATTTATCAACCGAGGAAACGCGCCTCCCTCAGAGC

B13 0 GCCCCCTAACAGTGCGGAGTCCACTATTGCCGCGCCGCGAAC

B13 1 CAACTCGATTTTTGCGTACTATGGTTGCCAACATGATAAATC

B13 2 AGACAATTATTAAATTTGAATTACCTTTTTTAAACAATTCGA

B13 3 GCCGCTACAGGGCGAATGGCTATTAGTCTACAAACAGTTAAT

B13 4 GCATTTTCCCGTATCCACCACCGGAACCAATAATATAAACAG

B13 5 AATATATAATTTCATCCTTTGCCCGAACAGAATACAGCACGT

B13 6 CACCGGAAGAACTGCCTAATTTGCCAGTTAAGAGAGGCAGAG

B13 7 ACCCAAAACCAGAGAATGGAAACAGTACTAATTTAATATAAA

B13 8 CCATATTAGTTTGGAACAAAGCCAGTAATACAAAAACGGAAT

B13 9 GTACCGATCCAGAGGCATGATTAAGACTTTCATAATCAAAAT

B14 0 ATTTAACGTGAGTGATATTTAACAACGCTTTGACGGTGGCAC

B14 1 AAGTTTGCCCTTCTTCGTTAGAATCAGACAACAGTCGTCGCT

B14 2 GATAGAAAGTAACACAAACATCAAGAAAACAAAATATTTTAA

B14 3 ATAACGTGCTTTCCGACCTGAAAGCGTAGTTATTATAATTAC

B14 4 AATCGCCAATAACCGCGTTTGCCATCTTCCTTATTCTAACGA

B14 5 ATTAATTGATGAAATTATCATTTTGCGGTTCTGGCCTAAACA

B14 6 TAGCCCCCAAACGTTTATCCTGAATCTTCCAGACGAATTGAG

B14 7 ATGTTAGCTTATTATTGCTTCTGTAAATAGGGCTTACGACAA

B14 8 GCGTCTTCAAAAGGTAAAGTAATTCTGTACCAACGACGCAGT

B14 9 TAAACAATACAATTAGAAAATACATACAGGCATTTTCGGTCA

B15 0 AGAAGATAATTTTCATAAAGCCAACGCTGCGGGAGCAACAGA

B15 1 CAGAAGGCGACCAGGGGATTTTAGACAGCATATGCAGCGATA

B15 2 AGTCACAAGCGGAAAATTATTCATTTCAATTACCTAAACCAC

B15 3 GGAGGCCGATTAAATAATAAAAGGGACAAACAAAGGAGCAAA

B15 4 TACCAGTCCTTAGAAGCGCGTTTTCATCTAAAGGTATTTTGC

B15 5 GCTTAGAAGAGGCGTTATCATCATATTCTTGGCAGACGCCAG

B15 6 TAGCGTCGAAACGCCTTAAATCAAGATTGCGCCTGAAATTCT

B15 7 TATAAAAAGACTGTATCCTTGAAAACATGTTATACTTTATCA

B15 8 ACCCAGCCATGTTCAGCTAATGCAGAACAGTTGCTGGCAACA

B15 9 ACAATAGTTGAAGCAAAGACACCACGGAATCAAGTTTGCCTT

B16 0 ATCGCGCTTAAGACAGCCTGTTTAGTATGAACGGTATTCACC

B16 1 ATGGCAAGTCTGAATTTTTATAATCAGTAAACACCATTTATC

B16 2 CTCAATCTTCATCACTGATTGCTTTGAATACCAAGTCAGATG

B16 3 AATCCTGAGAAGTGATGGATTATTTACACTGATTATTACAAA

B16 4 TAGAAAAGCTGAGATCAGTAGCGACAGAATAAGTTACTTGCG

B16 5 AAAATCAGATTCGCATATAATCCTGATTCCTACATCCGAGTA

B16 6 TAGCAGCCAATAGAGGCGTTTTAGCGAATAATATCTAATTAC

B16 7 TCACAATACCGTAAAGAGTCAATAGTGAGGAATCACCATCCT

B16 8 GGAGGTTATAAGTCCTGAACAAGAAAAACCTCCCGTATTTTG

B16 9 AATTTACAACGCGAAAATTCATATGGTTAATGAAACCATCGA

B17 0 AATAACGTAGGTCTCGTTAAATAAGAATGAGGCCATTTGACG

B17 1 TCTGAATGGAAAAATCACGCAAATTAACTGAAATACCGGCTT

B17 2 TGCAACAAATGGAATAACAGTACCTTTTACATCGGTTATACT

B17 3 AAAGAGTCTGTCCACGCTCATGGAAATAGTTTGGAGAGAAAC

B17 4 AATAAGGGAGAGACCCGGAAACGTCACCTACCAGCTCCGGTA

B17 5 AGGTTGGTATACAGGGGTTAGAACCTACTTACCGCGCAATAC

B17 6 TACCATTGGCGACAAAATCAGATATAGATAATCGGTGTGATA

B17 7 ACAAAAGAGCAAGGTACCTTTTTAACCTCCGACCGCTGTCTT

B17 8 TTCTAAGGAGCATGTAGAAACCAATCAAAGGCTTAGCCAAAG

B17 9 TCCTTATAGCAAGCTTCAACCGATTGAGACCAGTAGCACCAT

10HB 5mer sticky ends

SE_A_1 ACCAAGTACCGCACTCATCGAGAACATTGTACATAGG

SE_A_2 GGAAATTATTCATTAAAGGTGAATTATTAGGTCGTAC

SE_A_3 CAAATCCAATCGCAAGACAAAGAACGATGCAATAGGT

SE_A_4 ATAACATCACTTGCCTGAGTAGAAGAGGTGAGATTGA

SE_A_5 AAATTATTTGCACGTAAAACAGAAATACAAGAAACTT

SE_A_6 AGATTGGAATCAGCAAGCCGTTTTTATTTTCATCGTA

SE_A_7 GATGGTGTAATTCACCGTCACCGACTTGAGCCATTTG

SE_A_8 TTTATGCTGCACGAGAAAACTTTTTCAAATATATTTT

SE_A_9 GCTAACCAAGGACTCAAACTATCGGCCTTGCTGGTAA

SE_A_10 GAAGCTCATAGAAAGAAATTGCGTAGATTTTCAGGTT

SE_A*_1 ACAACCCGTCGGATTCCCTATGTACAA

SE_A*_2 AGAACGTCAGCGTGGTGTACGACCTAA

SE_A*_3 TGGTCAATAACCTGTTACCTATTGCAT

SE_A*_4 CCAGCGATTATACCAATCAATCTCACC

SE_A*_5 AACGAGAATGACCATAAAGTTTCTTGT

SE_A*_6 GATTCCAATCTTCCGTGGGAACAAACG

SE_A*_7 ATTACACCATCGCTGGTCTGGTCAGCA

SE_A*_8 TGCAGCATAAATAGCTATATTTTCATT

SE_A*_9 CCTTGGTTAGCGCGCGAAACAAAGTAC

SE_A*_10 CTATGAGCTTCAATCAAAAATCAGGTC

SE_B_1 ACCAAGTACCGCACTCATCGAGAACATTCTTACACTA

SE_B_2 GGAAATTATTCATTAAAGGTGAATTACTATCAATAAT

SE_B_3 CAAATCCAATCGCAAGACAAAGAACGAAGTCGTGCTA

SE_B_4 ATAACATCACTTGCCTGAGTAGAAGAATCGTAGTTCG

SE_B_5 AAATTATTTGCACGTAAAACAGAAATATTGGTGGATT

SE_B_6 CACTGATTGGTAGCAAGCCGTTTTTATTTTCATCGTA

SE_B_7 GTCTGGTTACGTCACCGTCACCGACTTGAGCCATTTG

SE_B_8 CTGAAGGAGCTCGAGAAAACTTTTTCAAATATATTTT

SE_B_9 TGAACGTGGAAACTCAAACTATCGGCCTTGCTGGTAA

SE_B_10 CGTTTAATTCTAAAGAAATTGCGTAGATTTTCAGGTT

SE_B*_1 ACAACCCGTCGGATTCTAGTGTAAGAA

SE_B*_2 AGAACGTCAGCGTGGTATTATTGATAG

SE_B*_3 TGGTCAATAACCTGTTTAGCACGACTT

SE_B*_4 CCAGCGATTATACCAACGAACTACGAT

SE_B*_5 AACGAGAATGACCATAAATCCACCAAT

SE_B*_6 ACCAATCAGTGTCCGTGGGAACAAACG

SE_B*_7 CGTAACCAGACGCTGGTCTGGTCAGCA

SE_B*_8 AGCTCCTTCAGTAGCTATATTTTCATT

SE_B*_9 TTCCACGTTCAGCGCGAAACAAAGTAC

SE_B*_10 AGAATTAAACGAATCAAAAATCAGGTC

SE_C_1 ACCAAGTACCGCACTCATCGAGAACACGTGTCCTTAT

SE_C_2 GGAAATTATTCATTAAAGGTGAATTACAGCATCTTGC

SE_C_3 CAAATCCAATCGCAAGACAAAGAACGGGATAAGTCCT

SE_C_4 ATAACATCACTTGCCTGAGTAGAAGACACGTGCTGCT

SE_C_5 AAATTATTTGCACGTAAAACAGAAATGTGGTGGTCTA

SE_C_6 GTCCTGCTACAAGCAAGCCGTTTTTATTTTCATCGTA

SE_C_7 GGAACAGGTCTTCACCGTCACCGACTTGAGCCATTTG

SE_C_8 GTTATCTCATTCGAGAAAACTTTTTCAAATATATTTT

SE_C_9 CTGCTCCTAGAACTCAAACTATCGGCCTTGCTGGTAA

SE_C_10 GGTCAGCTGGAAAAGAAATTGCGTAGATTTTCAGGTT

SE_C*_1 ACAACCCGTCGGATTCATAAGGACACG

SE_C*_2 AGAACGTCAGCGTGGTGCAAGATGCTG

SE_C*_3 TGGTCAATAACCTGTTAGGACTTATCC

SE_C*_4 CCAGCGATTATACCAAAGCAGCACGTG

SE_C*_5 AACGAGAATGACCATATAGACCACCAC

SE_C*_6 TGTAGCAGGACTCCGTGGGAACAAACG

SE_C*_7 AGACCTGTTCCGCTGGTCTGGTCAGCA

SE_C*_8 AATGAGATAACTAGCTATATTTTCATT

SE_C*_9 TCTAGGAGCAGGCGCGAAACAAAGTAC

SE_C*_10 TCCAGCTGACCAATCAAAAATCAGGTC

SE_D_1 ACCAAGTACCGCACTCATCGAGAACACATTCCTTCGA

SE_D_2 GGAAATTATTCATTAAAGGTGAATTATGTCGACGAGA

SE_D_3 CAAATCCAATCGCAAGACAAAGAACGCTGAGCTGGTT

SE_D_4 ATAACATCACTTGCCTGAGTAGAAGACCTATCGTCGT

SE_D_5 AAATTATTTGCACGTAAAACAGAAATCTCTGGAGGAC

SE_D_6 TCCTTGTCCTGAGCAAGCCGTTTTTATTTTCATCGTA

SE_D_7 ACAAGCATTTATCACCGTCACCGACTTGAGCCATTTG

SE_D_8 GATCGAAGTGTCGAGAAAACTTTTTCAAATATATTTT

SE_D_9 CGTCCTAGCAGACTCAAACTATCGGCCTTGCTGGTAA

SE_D_10 GTCGTATTGGTAAAGAAATTGCGTAGATTTTCAGGTT

SE_D*_1 ACAACCCGTCGGATTCTCGAAGGAATG

SE_D*_2 AGAACGTCAGCGTGGTTCTCGTCGACA

SE_D*_3 TGGTCAATAACCTGTTAACCAGCTCAG

SE_D*_4 CCAGCGATTATACCAAACGACGATAGG

SE_D*_5 AACGAGAATGACCATAGTCCTCCAGAG

SE_D*_6 CAGGACAAGGATCCGTGGGAACAAACG

SE_D*_7 TAAATGCTTGTGCTGGTCTGGTCAGCA

SE_D*_8 ACACTTCGATCTAGCTATATTTTCATT

SE_D*_9 CTGCTAGGACGGCGCGAAACAAAGTAC

SE_D*_10 ACCAATACGACAATCAAAAATCAGGTC

SE_E_1 ACCAAGTACCGCACTCATCGAGAACACAGCTCTTCGT

SE_E_2 GGAAATTATTCATTAAAGGTGAATTAAGACTTTACGT

SE_E_3 CAAATCCAATCGCAAGACAAAGAACGGAGCTTTGCAG

SE_E_4 ATAACATCACTTGCCTGAGTAGAAGATCAAGCTGATC

SE_E_5 AAATTATTTGCACGTAAAACAGAAATGAAGGTTCAAT

SE_E_6 TCGTGGTCACAAGCAAGCCGTTTTTATTTTCATCGTA

SE_E_7 AATTTATAAGTTCACCGTCACCGACTTGAGCCATTTG

SE_E_8 GAGCATAGAGTCGAGAAAACTTTTTCAAATATATTTT

SE_E_9 GAGCACAGCTGACTCAAACTATCGGCCTTGCTGGTAA

SE_E_10 GCACGAGATTCAAAGAAATTGCGTAGATTTTCAGGTT

SE_E*_1 ACAACCCGTCGGATTCACGAAGAGCTG

SE_E*_2 AGAACGTCAGCGTGGTACGTAAAGTCT

SE_E*_3 TGGTCAATAACCTGTTCTGCAAAGCTC

SE_E*_4 CCAGCGATTATACCAAGATCAGCTTGA

SE_E*_5 AACGAGAATGACCATAATTGAACCTTC

SE_E*_6 TGTGACCACGATCCGTGGGAACAAACG

SE_E*_7 ACTTATAAATTGCTGGTCTGGTCAGCA

SE_E*_8 ACTCTATGCTCTAGCTATATTTTCATT

SE_E*_9 CAGCTGTGCTCGCGCGAAACAAAGTAC

SE_E*_10 GAATCTCGTGCAATCAAAAATCAGGTC